Durham E-Theses

Photophysical evaluation of substituted zinc phthalocyanines as sensitisers for photodynamic therapy

Stanley, Claire Frances

How to cite:

Stanley, Claire Frances (1997) *Photophysical evaluation of substituted zinc phthalocyanines as sensitisers for photodynamic therapy*, Durham theses, Durham University. Available at Durham E-Theses Online: http://etheses.dur.ac.uk/4681/

Use policy

PHOTOPHYSICAL EVALUATION OF SUBSTITUTED ZINC PHTHALOCYANINES AS SENSITISERS FOR PHOTODYNAMIC THERAPY

Claire Frances Stanley

Department of Chemistry, University of Durham, Durham.

Submitted in partial fulfilment of the requirements for the degree of Doctor of Philosophy, University of Durham.

September 1997.

─ 3 APR 1998

DECLARATION

The work described in this thesis was carried out in the Chemistry Department of the University of Durham between September 1994 and August 1997. This thesis is the work of the author except where acknowledged by reference, and has not been submitted for any other degree.

STATEMENT OF COPYRIGHT

ABSTRACT

Zinc phthalocyanines (ZnPc) are currently being investigated in relation to their use as sensitisers for Photodynamic Therapy (PDT). In particular, the photophysical properties of these dyes are of interest since their ability to generate the cytotoxic species, singlet oxygen ($^1O_2$), is believed to be central to their role in causing tumour necrosis. In this study, a detailed investigation of the photophysical properties of substituted zinc phthalocyanines under various conditions is described.

Two novel β-tetra substituted zinc phthalocyanines have been synthesised, $ZnPc(CMe(CO_2Me)_2)_4$ and $ZnPc(CHMeCO_2H)_4$. The nature of peripheral substituents has little effect on triplet state or singlet oxygen production by ZnPc, however, $ZnPc(CHMeCO_2H)_4$ displays a remarkable sensitivity to the ionic strength of non-aqueous solutions. Ion concentrations below 10^{-4} mol dm^{-3} induce dimerisation whilst concentrations greater than this promote monomerisation. This behaviour is attributed to ion pairing effects. Photophysical properties of substituted zinc phthalocyanines in heterogenous media and on solid substrates are also described.

The temperature and pH of solvent media greatly influence the photophysical properties of phthalocyanines. Octadecyl zinc phthalocyanine (C10) aggregates upon cooling to 77 K in ether-pentane-alcohol (5:5:2) solution. Additional structure in the absorption spectrum is observed, accompanied by the appearance of a fluorescence emission band at 760 nm. Aluminium phthalocyanine chloride in methanol dimerises upon addition of 2.5 x 10^{-5} mol dm^{-3} fluoride ions. Dimer species are characterised by a blue shifted peak in the absorption spectrum and are non-fluorescent. These results are ascribed to different aggregate geometries and discussed in terms of exciton theory. Low pH induces stepwise protonation of the azomethine bridges of the phthalocyanine ring, Pc + nH$^+$ $\rightleftharpoons$ PcH$_n^{n+}$, where n = 0 to 4. Protonation results in significant changes in absorption, fluorescence and triplet state properties of the phthalocyanine. A dramatic decrease in singlet oxygen generation by the phthalocyanine (Φ_Δ (n = 0) = 0.54, Φ_Δ (n = 1) = 0.075) is reported, and occurs under surprisingly mild conditions (pK_a of ZnPcS$_2$ in 1% Triton X-100/H$_2$O = 4.4).

The propensity of ZnPc's to bind to serum protein and to participate in electron transfer reactions with potential electron donors is discussed.

CONTENTS

Chapter One Introduction

Chapter Two Experimental Techniques

Chapter Three Properties of Novel Phthalocyanine Sensitisers

Chapter Four Dimerisation of Phthalocyanines

LIST OF FIGURES

10

11

Chapter 6	*Title of Figure*	*Page*

COMMON ABBREVIATIONS

Abbreviation	*Description*

Phthalocyanines

AlPcCl	Aluminium phthalocyanine chloride
$AlPcS_2$	Disulfonated aluminium phthalocyanine
$(BuO)_8ZnPc$	1,4,8,11,15,18,22,25 octa-butoxy zinc phthalocyanine
C5	1,4,8,11,15,18,22,25 octa-pentyl zinc phthalocyanine
C10	1,4,8,11,15,18,22,25 octa-decyl zinc phthalocyanine
ZnC16	2,3,9,10,16,17,23,24 octa-hexadecyl zinc phthalocyanine
HpD	Haematoporphyrin derivative
P	Porphyrin
Pc	Phthalocyanine
$^{t}Bu_4ZnPc$	β-tetra-tertbutyl zinc phthalocyanine
$ZnPc(CHMeCO_2H)_4$	β-tetra-1-carboxyethyl zinc phthalocyanine
$ZnPc(CMe(CO_2Me)_2)_4$	β-tetra-1,1-di(methoxycarbonyl)ethyl zinc phthalocyanine
$ZnPcS_2$	Disulfonated zinc phthalocyanine

Solvents

1% pyr/tol	1% Pyridine in toluene (v/v)
1% TX/PBS	1% Triton X-100 in phosphate buffered saline (w/v)
1%TX/H_2O	1% Triton X-100 in distilled water (w/v)
CTAB	Hexadecyl trimethylammonium bromide
DMF	N, N-Dimethylformamide
DMSO	Dimethylsulfoxide
EPA	Ether-isopentane-alcohol (5:5:2)
Et_2O	Diethylether
EtOH	Ethanol
IP	Isopentane
MeOH	Methanol
MeTHF	2-Methyl tetrahydrofuran
PBS	Phosphate buffered saline
THF	Tetrahydrofuran
TX	Triton X-100
TXR	Triton X-100 reduced

Others

AA	Ascorbic acid
AAP	Acsorbic acid palmitate
bipy	4,4'-bipyridine
BSA	Bovine serum albumin
DABCO	1,4 diazabicyclo [2,2,2] octane
DMA	N, N dimethylaniline
DMB	1,4 dimethoxybenzene
DiPE	Trans 1,2-dipyridyl ethylene
FWHM	Full Width at Half Maximum
HOMO	Highest Occupied Molecular Orbital
ldl	Low density lipoprotein
LUMO	Lowest Unoccupied Molecular Orbital
PDT	Photodynamic Therapy
TMPD	1,4-N,N,N',N'-tetramethylphenylenediamine

Symbols

ε	Extinction coefficient, $dm^3 \, mol^{-1} \, cm^{-1}$
τ^o	Intrinsic fluorescence lifetime, ns
τ_Δ	Singlet oxygen lifetime, μs
Φ_Δ	Yield of singlet oxygen formation
λ_{em}	Emission wavelength, nm
λ_{ex}	Excitation wavelength, nm
Φ_F	Fluorescence quantum yield
τ_F	Measured fluorescence lifetime, ns
Φ_{IC}	Yield of internal conversion
λ_{max}	Wavelength of maximum absorbance, nm
λ_{Probe}	Probe wavelength in flash photolysis, nm
Φ_T	Triplet quantum yield
τ_T	Triplet state lifetime, μs
$(^1\Delta_g)O_2$	Singlet state molecular oxygen
$(^1\Sigma_g^+)O_2$	Singlet state molecular oxygen
$(^3\Sigma_g^-)O_2$	Ground state molecular oxygen
k_f	Rate of fluorescence, s^{-1}
k_{ic}	Rate of internal conversion, s^{-1}
k_{isc}	Rate of intersystem crossing, s^{-1}
r_{av}	Measured steady state fluorescence anisotropy
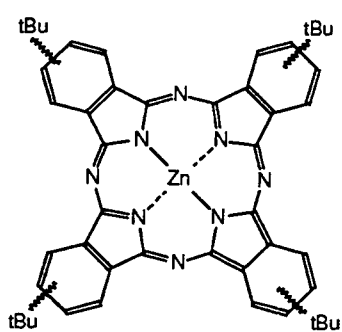
tBu$_4$ZnPc
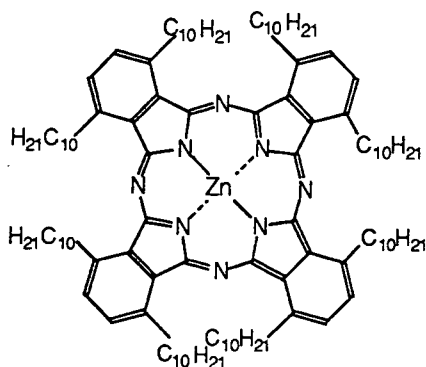
C10
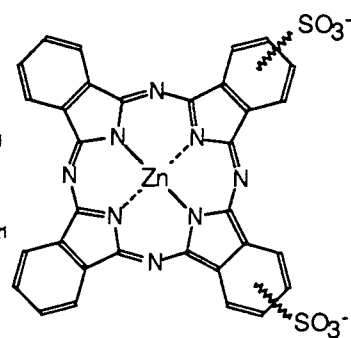
ZnPcS$_2$
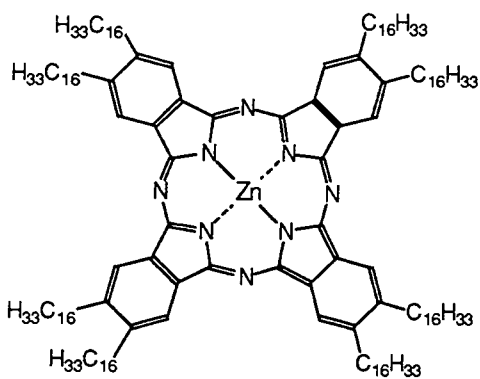
ZnC16
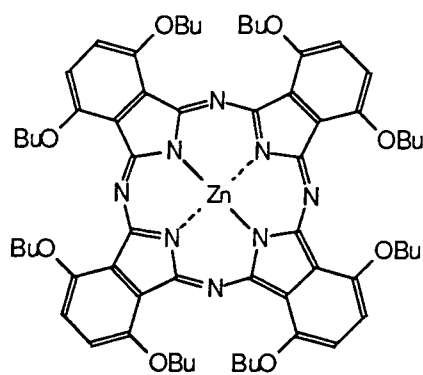
(BuO)$_8$ZnPc
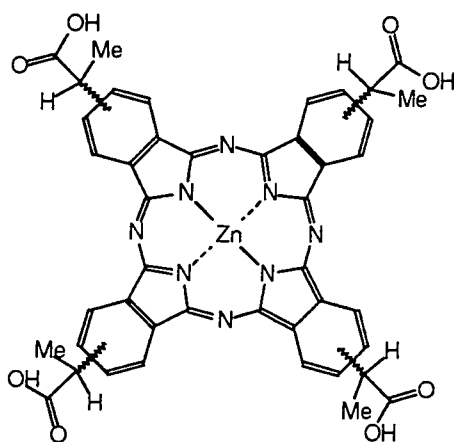
ZnPc(CHMeCO$_2$H)$_4$

ZnPc(CMe(CO$_2$Me)$_2$)$_4$

19
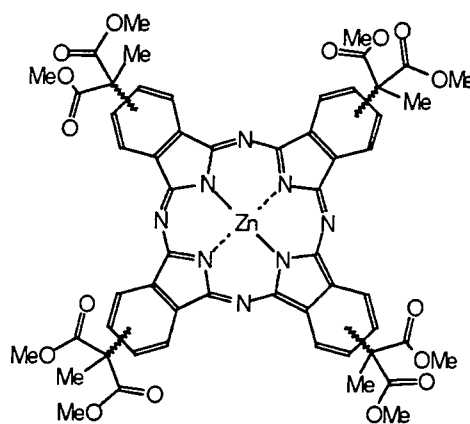
CHAPTER 1

INTRODUCTION

1.1 Background

Photodynamic Therapy, or PDT, is an alternative treatment for cancer which is currently undergoing clinical trials. The principle on which it is based has been known for almost one hundred years. Around that time, Meyer-Betz self administered haematoporphyrin to determine its biological effect[1] and Von Tapiener's laboratory[2] in Munich reported the destruction of skin tumours by the use of topical eosin and light. Progress was slow in the early years, the only major breakthrough coming in 1948 when Figge and co-workers[3] noticed that porphyrins and metalloporphyrins have a tendency to accumulate in neoplastic, traumatised and embryonic tissue. The build-up of porphyrins can be recognised by their characteristic red fluorescence upon irradiation by light. This principle was seized by Figge[4] in 1955 and again by Lipson[5] in 1961, to show that porphyrins could be used to aid in the detection of malignant growths. Lipson and his group were also responsible for the development of HpD[6], one of the first compounds to be clinically tested as a photosensitiser for PDT. HpD is a haematoporphyrin derivative which was shown to exhibit greater localisation than the original porphyrin. Throughout the 1970's the destruction of various types of tumour such as bladder[7], leukaemic[8], breast[9], lung[10] and colon cancers[11], using HpD as a photosensitiser, was reported and it was suggested that singlet oxygen may be an important intermediate in the cytotoxic process[12],[13]. Studies on HpD, including its chemical composition[14] and mechanisms for its transport and distribution throughout the body continued throughout the 1980's and complications associated with using HpD were realised[15]. In 1985 Ben-Hur[16] proposed phthalocyanines as a second generation class of sensitisers in an attempt to overcome these problems. Studies of both the biological and photophysical properties of this class of drugs have proved promising and research continues to increase understanding of the mechanism of cell destruction and sensitiser localisation.

1.2 Principle of PDT[17],[18]

The basic principle of PDT is very simple. The treatment involves the use of a light activated drug, known as a photosensitiser, and a light source such as a laser. The photosensitiser is injected intravenously and, after a period of 48 - 72 hours, the drug is observed to be preferentially located within malignant tissue (Figure 1.1). The photosensitiser is activated by directing light at the tumour, usually from a laser source -

red light is used to allow maximum tissue penetration. It is important to realise that the laser is not being used as an alternative for a scalpel but as a source of monochromatic, collimated light which can be directed down an optic fibre to allow access to internal tumours whilst still retaining intensity. The excited sensitiser is believed to interact with surrounding oxygen to produce cytotoxic species such as singlet oxygen and superoxide, leading to cell destruction.

Sensitiser
Injection

24-72hrs later:
Red light irradiation

Tumour cell
death
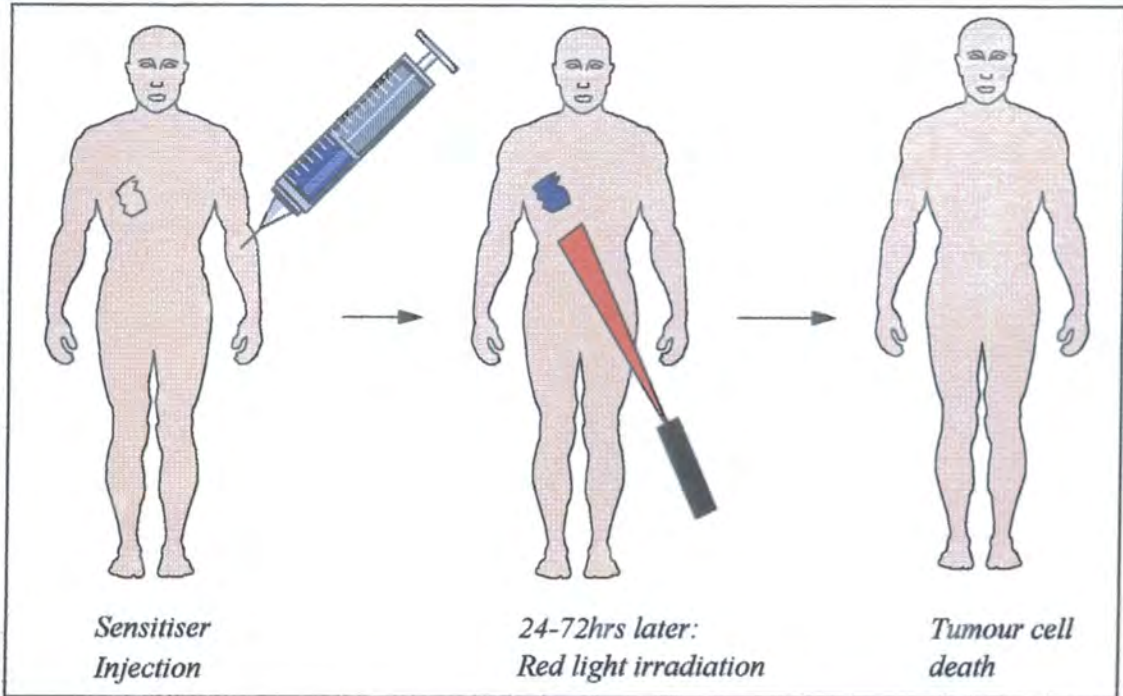
Figure 1.1. The principle of PDT.

The exact mechanism by which PDT operates has been the subject of much debate. Upon absorbing laser radiation, the photosensitiser is excited from its ground state, S_0, to a higher energy singlet state, S_n^*. Rapid conversion to the first excited singlet state, S_1^*, occurs via internal conversion and loss of vibrational energy. Deactivation to the ground state proceeds by a variety of mechanisms (Figure 1.2).
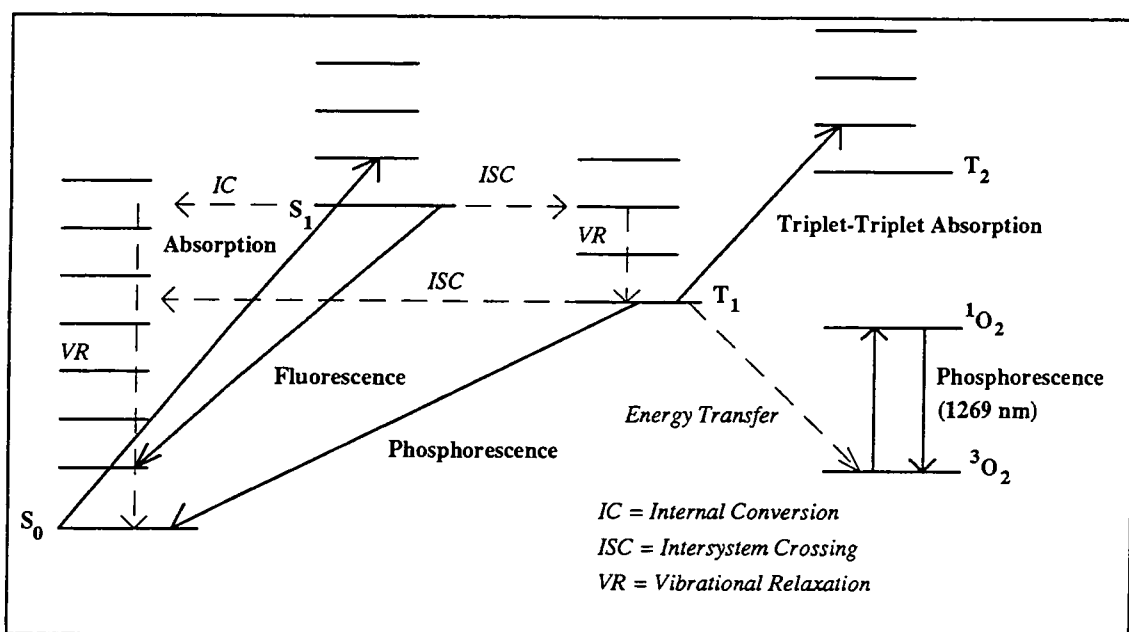
Figure 1.2.
Jablonski diagram showing absorption and deactivation processes of sensitisers.

In the absence of quenchers, these include radiative emission (fluorescence), internal conversion (when the states involved are of the same spin multiplicity) and intersystem crossing. Intersystem crossing involves a transition between states of different multiplicity, $S_1 \rightarrow T_1$ or $T_1 \rightarrow S_0$, and is a prerequisite for population of the triplet state (T_1). This process is forbidden by the zero order approximation[19]; however, the influence of spin-orbit perturbations render the pathway viable. It is the properties of the T_1 state that are of importance in the mechanism of PDT. In the absence of oxygen and other quenching species, triplet species decay via phosphorescence emission or by spin forbidden intersystem crossing to the ground state, S_0. However, in a biological environment, there are generally believed to be two types of reaction which may occur, Type I and Type II (Figure 1.3). The Type I mechanism involves interaction of the sensitiser triplet state with solvent molecules or biological substrates to produce radicals or radical ions by hydrogen atom or electron transfer. These radicals react with oxygen to produce the cytotoxic superoxide radical anion. Alternatively, the triplet state can interact directly with ground state oxygen in an energy transfer reaction to produce singlet oxygen, $(^1\Delta_g) O_2$, $^1O_2$.

Dye

$\downarrow$ hν

Radicals and radical ions $\xleftarrow{\text{Substrate}}$ ${}^3\text{Dye}^{*}$ $\xrightarrow{{}^3O_2}$ ${}^1O_2$

${}^3O_2 \downarrow$ [Type I] $\qquad$ Substrate $\downarrow$ [Type II]

Oxidation Products $\qquad\qquad$ Oxidation Products
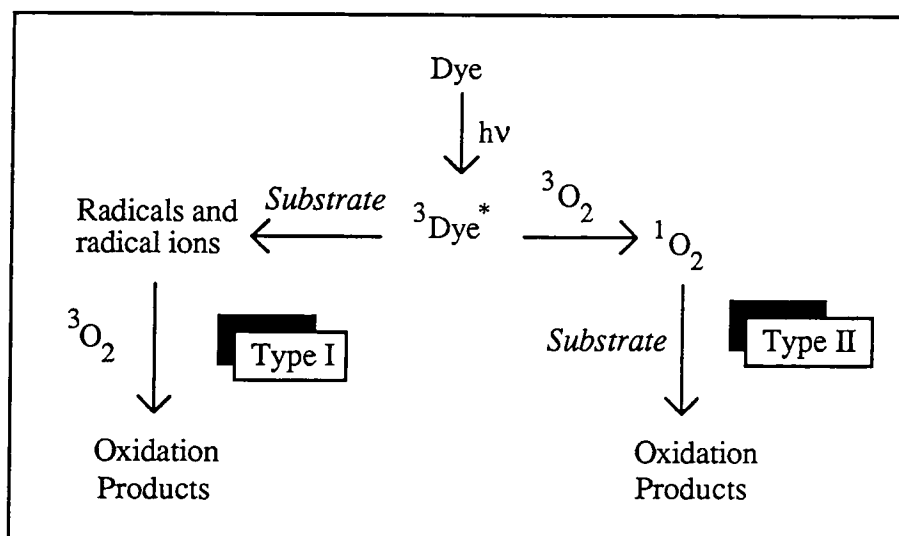
Figure 1.3. Destructive pathways of PDT.

The formation of ${}^1O_2$ has been discussed in detail in a review by Kearns[20]. Production is believed to occur via an energy transfer mechanism from excited singlet (Equation 1.1) or triplet (Equation 1.2) sensitiser states to ground state molecular oxygen.

$$ {}^1Sens^{*} + {}^3O_2 \longrightarrow {}^3Sens^{*} + {}^1O_2 \qquad\qquad (1.1) $$

$$ {}^3Sens^{*} + {}^3O_2 \xrightarrow{k_d} {}^1(Sens..O_2) \longrightarrow O_2({}^1\Delta_g) + {}^1Sens_0 \qquad (a) $$

$$ {}^1(Sens..O_2) \longrightarrow O_2({}^1\Sigma_g^{+}) + {}^1Sens_0 \qquad (b) $$

$$ {}^3(Sens..O_2) \longrightarrow O_2({}^3\Sigma_g^{-}) + {}^1Sens_0 \qquad (c) $$

$$ {}^5(Sens..O_2) \qquad (d) $$

(1.2)
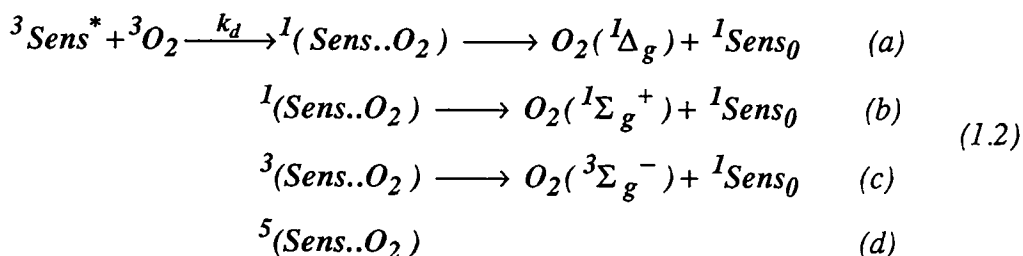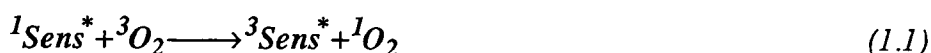
where k_d represents the diffusion controlled rate constant. In practice, singlet state quenching is rarely observed due to the short lifetime of these states with respect to the diffusion rate of molecules through solution, i.e. the number of ${}^1Sens^{*}$ and ${}^3O_2$ collisions is small. It can be seen from Equations 1.2a to 1.2d above, that singlet oxygen species result from only one out of nine possible collision complexes. This leads to a theoretical triplet state quenching constant, k_{O_2}, of 1/9 k_d. Experimentally[21], values of k_{O_2} an order of magnitude lower than k_d were obtained, lending credence to this theory. Molecular orbital schemes for the formation of ${}^1\Delta_g$ and ${}^1\Sigma_g^{+}$ are depicted in Figure 1.4.
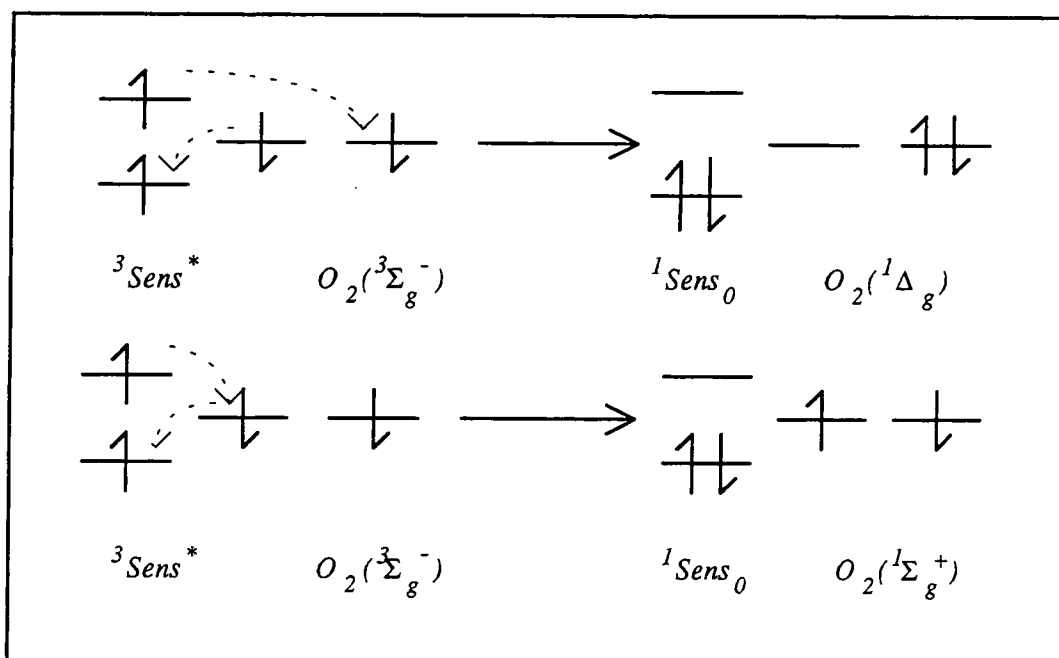
Figure 1.4. Formation of singlet oxygen.

$^1\Sigma_g^+$ and $^1\Delta_g$ excited states of O_2 occur at 13121 cm^{-1} and 7882 cm^{-1} above the ground state respectively. The ratio of each state formed is dependent on the triplet state energy, E_T, of the sensitiser. For E_T values of ~ 160 kJ mol^{-1} (~ 13350 cm^{-1}) or less, $^1\Delta_g$ is the major product.

Both superoxide radical species and singlet oxygen cause oxidative destruction of tissue and hence may perform a vital role in the mechanism of PDT. However, it is generally believed that $^1O_2$ is the major intermediate responsible for photodynamic action although confirmation is prevented by lack of data regarding *in vivo* detection. Detection is difficult due to rapid quenching of $^1O_2$ in an *in vivo* environment, indeed, it has been shown that singlet oxygen phosphorescence generated by sensitisers incorporated into cells[22] is of greatly reduced intensity and shorter lifetime with respect to that in a homogeneous environment. A summary of the competing processes is given below:

$S_0 + h\nu \rightarrow S_1^*$	Absorption	I_a
$S_1^* \rightarrow S_0 + h\nu$	Fluorescence	$k_f[S_1]$
$S_1^* \rightarrow S_0 + heat$	Internal Conversion	$k_{ic}[S_1]$
$S_1^* \rightarrow T_1^*$	Intersystem crossing	$k_{isc}[S_1]$
$T_1^* \rightarrow S_0 + h\nu$	Phosphorescence	$k_p[T_1]$
$T_1^* \rightarrow S_0 + heat$	Intersystem crossing	$k_{isc}[T_1]$
$T_1^* + Subs \rightarrow Sens^{\pm \cdot} + Subs^{\pm \cdot}$	Electron transfer	$k_I[T_1][Subs]$
$T_1^* + O_2(^3\Sigma_g^-) \rightarrow M + O_2(^1\Delta_g)$	Energy Transfer	$k_{II}[T_1][O_2]$

The properties of the drug administered are extremely important and, whilst it is easy to specify those which make an ideal sensitiser, in real terms it is much more difficult due to the many biological factors which may have an influence. To avoid destruction of healthy tissue, a sensitiser should be retained solely by neoplastic tissue[23]. It should absorb in the red region of the spectrum with little or no absorption in the ultraviolet region in order to minimise sensitisation to sunlight after intravenous administration of high concentrations of dye and allow optimum penetration of tissue. It should have a defined chemical composition and, perhaps most important, are the photophysics of the sensitiser and its ability to generate high concentrations of cytotoxic intermediates such as singlet oxygen. There have been large amounts of work carried out in order to develop photosensitisers which fulfil the criteria listed above.

Porphyrins, specifically a water soluble haematoporphyrin derivative and its purified form, marketed as Photofrin II[R], were the first compounds recognised to have potential as PDT sensitisers[6]. These were shown to be clinically effective in many cases using both animal and human subjects[24],[25] however, a number of problems were encountered. Dealing with a complex mixture of compounds made it difficult to replicate the exact formula. Storage times and synthetic routes both affected the composition and the extent of aggregation. Variations[26],[27] such as these lead to reduced biological efficiency in certain environments and different distributions between malignant and healthy tissue. The strong absorption band of porphyrins in the ultraviolet region of the spectrum also introduced a serious side effect to PDT treatment[15]. Retention of significant amounts of porphyrin in the skin led to the patient becoming sensitised to sunlight in the period following treatment, thus risking the development of skin cancer. This was compounded by the low extinction coefficient of porphyrins at 630 nm which made it necessary to inject high concentrations in order to obtain a satisfactory response.

As a result of these problems, a series of second generation sensitisers has been proposed. These include chlorins[28], purpurins[29], phenylporphyrins[30] and phthalocyanines[31]. It is the phthalocyanines (Pc) that are of interest in this study and detailed reviews of these and other sensitisers can be found elsewhere[32],[33],[34]. Phthalocyanines are derivatives of the porphyrin family in which the methine bridges have been replaced by nitrogen and the pyrrole moieties are extended by conjugation with extra benzene rings (Section 1.3). These modifications lead to a remarkably different absorption spectrum with a sharp peak at ~ 670 nm and no absorption between 400 nm and 600 nm. The large extinction coefficients of Pc's in the red region of the spectrum and their transparency at shorter wavelengths give them an immediate advantage over

porphyrins as much lower doses are required and the risk of photosensitisation is substantially reduced. Coordination of certain metals to the Pc ligand has been shown[35] to create a more efficient PDT agent. In general, diamagnetic metals, e.g. Al, Ga and Zn, are the most suitable[36] (τ_T of ZnPc[37] = 270 μs) due to modifications of the photophysical properties which result in long triplet lifetimes and high quantum yields and therefore a greater ability to generate $^1O_2$. Paramagnetic metals such as Cu, Ni, Fe, Cr and Pd increase the rate of intersystem crossing ($T_1 \rightarrow S_0$) and substantially reduce the lifetime of the triplet state (τ_T of CuPc[38] = 0.04 μs). Sulphonated aluminium phthalocyanines have been the subject of many studies[39],[40],[41] and shown to have great promise as future sensitisers. Incorporation of sulphonate groups onto the phthalocyanine ring renders the molecule soluble in aqueous media, useful for intravenous administration, however the efficacy has been shown to depend on the degree on sulphonation[42]. This leads to complications, as separation of the various isomers produced during AlPcS$_n$ synthesis is a formidable task. Alternative methods of controlling the hydrophilicity and lipophilicity of sensitiser macrocycles through the use of axial ligands on chemically pure phthalocyanines such as silicon phthalocyanine[43] and ruthenium naphthalocyanine[44] have also shown promise.

1.3 Electronic Structure of Phthalocyanines

A typical absorption spectrum of a monomeric metallophthalocyanine (ZnPc in 1% pyridine/toluene solution) is depicted in Figure 1.5. Two major bands can be observed at ~ 350 nm and ~ 670 nm, termed the Soret and Q bands respectively. Many theoretical investigations have been performed to assign the transitions responsible for these bands[45],[46],[47],[48].
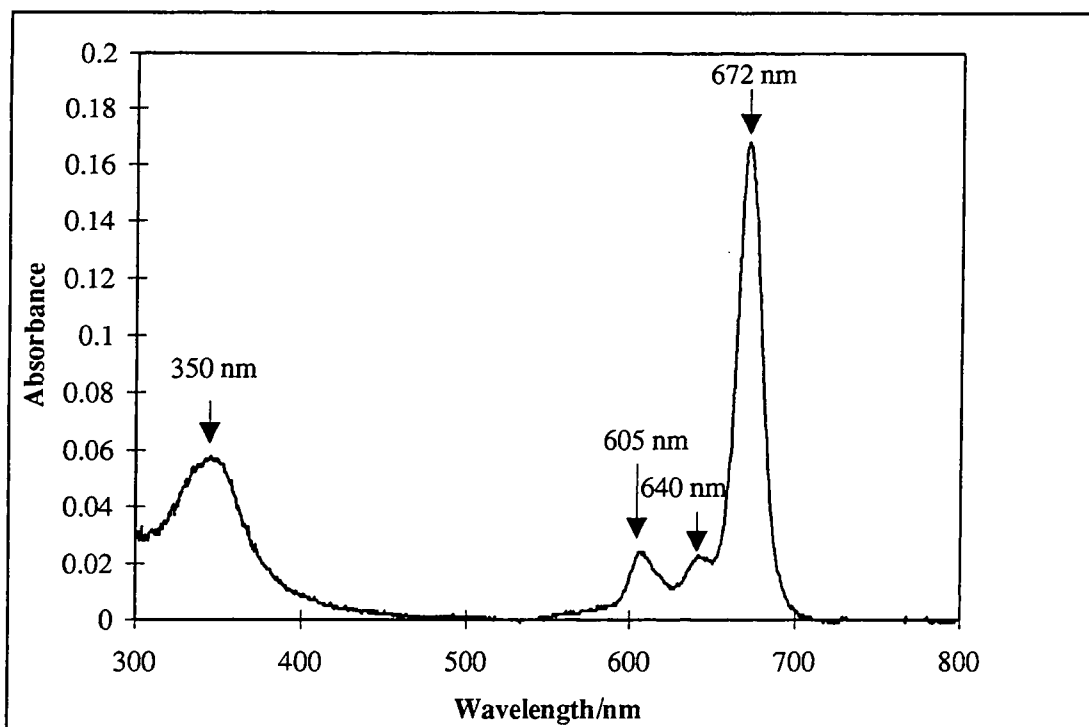
Figure 1.5. UV/Visible absorption spectrum of ZnPc in 1% pyridine/toluene solution.

Absorption is dominated by phthalocyanine ligand electronic structure and it is generally agreed that the Q band arises from a $\pi\pi^*$ ($e_g \leftarrow a_{1u}$) transition from the highest occupied molecular orbital, HOMO, to the lowest unoccupied molecular orbital, LUMO (Figure 1.7). Peaks at ~ 605 nm and ~ 640 nm are assigned to vibrational modes of the first excited state[49]. These hypotheses are supported by fluorescence emission with a 'mirror image' band structure and a small Stokes shift of ca. 10 nm. Transitions are sharp with narrow bandwidths due to rigidity of the planar macrocycle. The HOMO of metal substituted phthalocyanines consists of two degenerate energy levels, corresponding to transitions polarised along the x and y directions[50]. In metal free phthalocyanines, degeneracy of the S_1 state is lifted and splitting of the main Q band occurs, resulting in two transitions separated by ~ 880 cm^{-1}. By convention, the lower energy transition is referred to as Q_x and the $S_2 \leftarrow S_0$ transition as Q_y. Q_x is believed to be polarised along the H-H axis, as depicted in Figure 1.6.
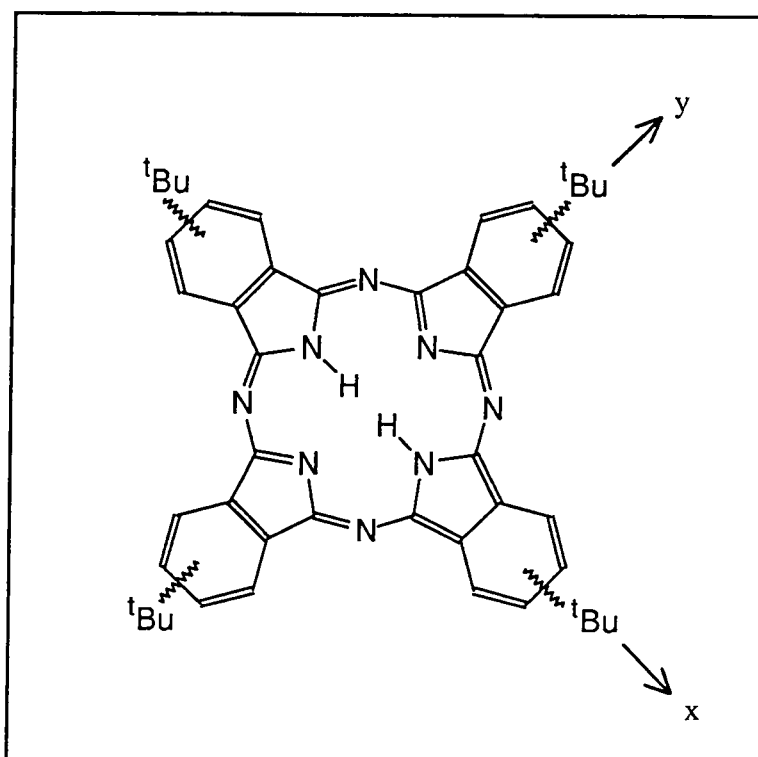
Figure 1.6. Structure of tetra ^{t}butyl metal free phthalocyanine.

Transitions responsible for Soret band absorption are more difficult to identify. Gouterman suggested the main absorption was a $\pi\pi^*$ transition of $e_g \leftarrow a_{2u}$ symmetry, i.e. HOMO-1 to LUMO (Figure 1.7), which was broadened by $n\pi^*$ transitions of comparable energy.
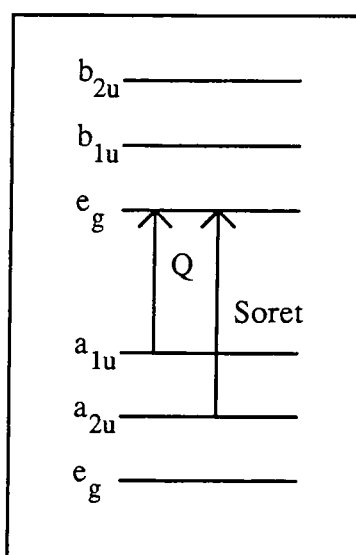
Figure 1.7. Energy level transitions of Q and Soret bands.

This has since been confirmed through absorption and x-ray photoelectron spectroscopy experimental studies performed by Nyokong[51] and Khalib[52]. Rosa[50] performed

28

density functional calculations on the electronic states of several metallophthalocyanines and concluded that the Soret band consists of a mixture of several $\pi\pi*$ and $n\pi*$ transitions. Morley et al.[53] have calculated the position and magnitude of electron density in the HOMO, HOMO-1 and LUMO of zinc phthalocyanine (Figure 1.8). Q band absorption involves large changes in the electron distribution of the excited state with respect to the ground state. Density shifts from inner ring carbon atoms to nitrogen atoms. By contrast, Soret band absorption (HOMO-1 to LUMO) results in minimal changes in the electronic distribution.
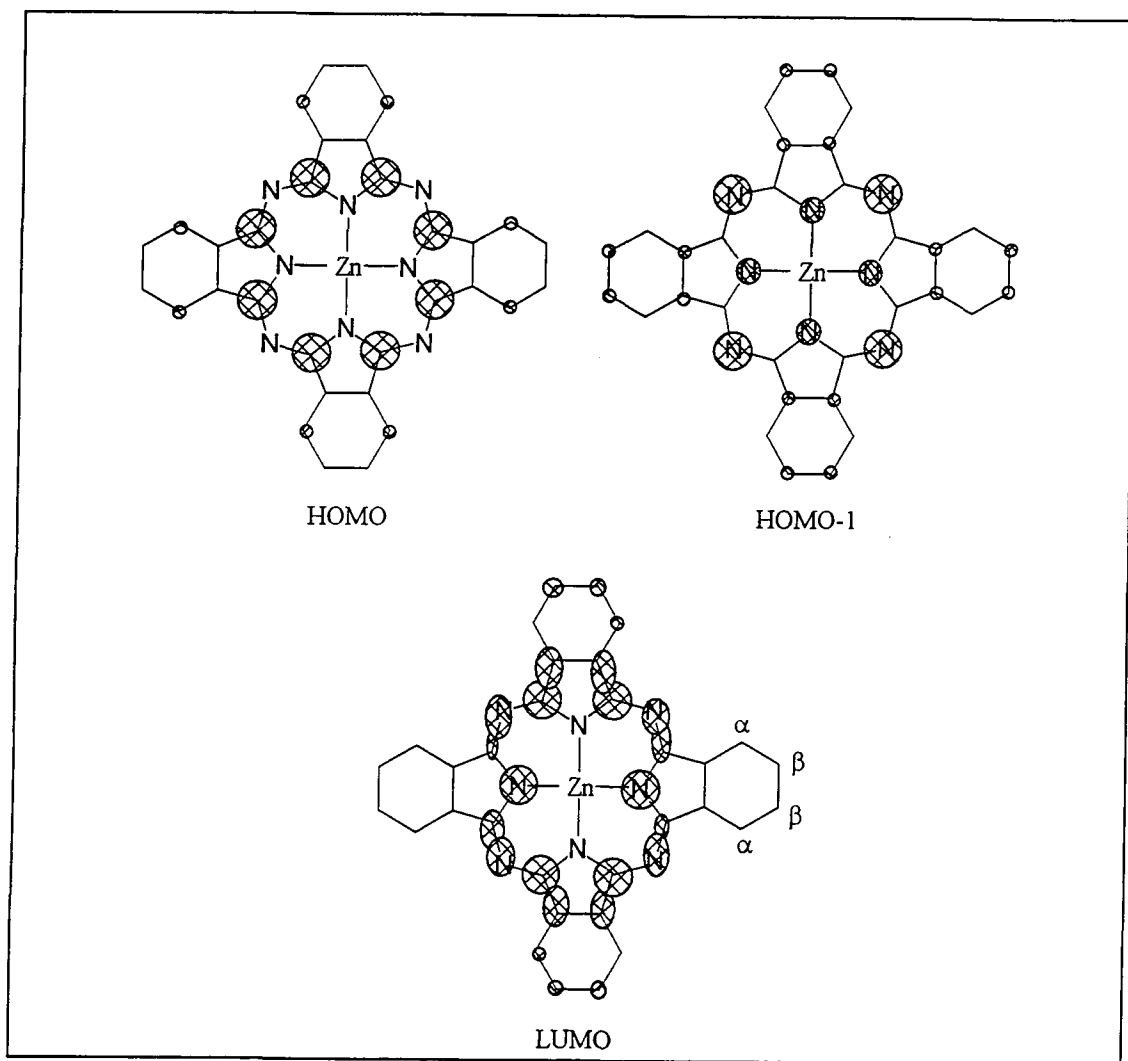
HOMO

HOMO-1

LUMO

**Figure 1.8.** _**Electron density of the HOMO, HOMO-1 and LUMO of ZnPc.**_

1.4 Transport and Delivery Systems

One method of introducing photosensitisers *in vivo* is to use delivery systems[54] such as liposomes, oil emulsions, proteins or antibodies. In this way, hydrophobic sensitisers such as zinc phthalocyanine may be administered intravenously. There have been many studies investigating the suitability of potential vehicles and their effect on the transport mechanism and localisation of sensitisers. Schieweck[55] and Jori[56] have shown that ZnPc may be incorporated into liposomes of various types in its monomeric form, retaining its phototoxic properties. For germanium phthalocyanines, Cremophor EL has been demonstrated to be most suitable since aggregation was observed in liposomal solution[57]. Liposomes and oil emulsions such as Cremophor EL are by far the most common methods chosen for solubilisation of hydrophobic dyes, however, delivery via *in vitro* binding to low density lipoprotein[58] (ldl) or monoclonal antibodies[59] has also been demonstrated. After injection into the bloodstream, sensitiser molecules are believed to interact with human serum proteins[60]. Human serum protein has many different components including albumin, low density lipoprotein (ldl), high density lipoprotein (hdl) and very low density lipoprotein (vldl). The affinity of many different sensitisers for individual components depends on their hydrophilic / lipophilic character. For example, it has been shown that the more hydrophilic dyes such as $AlPcS_n$[61] bind to albumin, whilst those of lipophilic character, e.g. ZnPc, will interact with low density lipoproteins[62],[63],[64]. Protoporphyrin shows evidence of binding to ldl[65], chlorin E6 demonstrates binding to albumin and hdl but not ldl[66] and haematoporphyrin associates with albumin[67], thus, it is clear that binding is highly sensitive to the nature of the chosen sensitiser. The mechanism by which liposomes are incorporated into ldl has been investigated by Rensen *et al.*[68] who have shown that neither aggregation nor fusion of particles are involved. However, the exact mechanism has yet to be elucidated. Distribution to proteins is also affected by the nature of the delivery system. Work by Kessel[69] has demonstrated that Cremophor EL promotes binding of tin etiopurpurin to ldl whilst Polo[70] and Jori[71] have found that the nature of liposomal formulations also has an effect on the transport mode, e.g., 1,2-dipalmitoyl-sn-glycero-3-phosphocholine (DPPC) and 1-palmitoyl-2-oleoyl-sn-glycero-3-phosphocholine (POPC) liposomes encourage release to lipoproteins whilst 1,2-dimiristoyl-sn-glycero-3-phosphocholine (DMPC) allows delivery to both albumin and lipoprotein fractions.

1.5 Retention and Localisation

An understanding of the factors which influence and control the localisation and retention of photosensitisers within neoplastic tissue is an important area for development of photodynamic therapy. There has been a large body of work carried out in this area and many theories have been proposed. However, *in vivo* processes are complex and further study is necessary. Hypotheses concerning retention and localisation may be grouped loosely into two categories, one regarding the physical/biological properties of neoplastic tissue and the other concerning sensitiser characteristics such as its hydrophilicity (Figure 1.9).
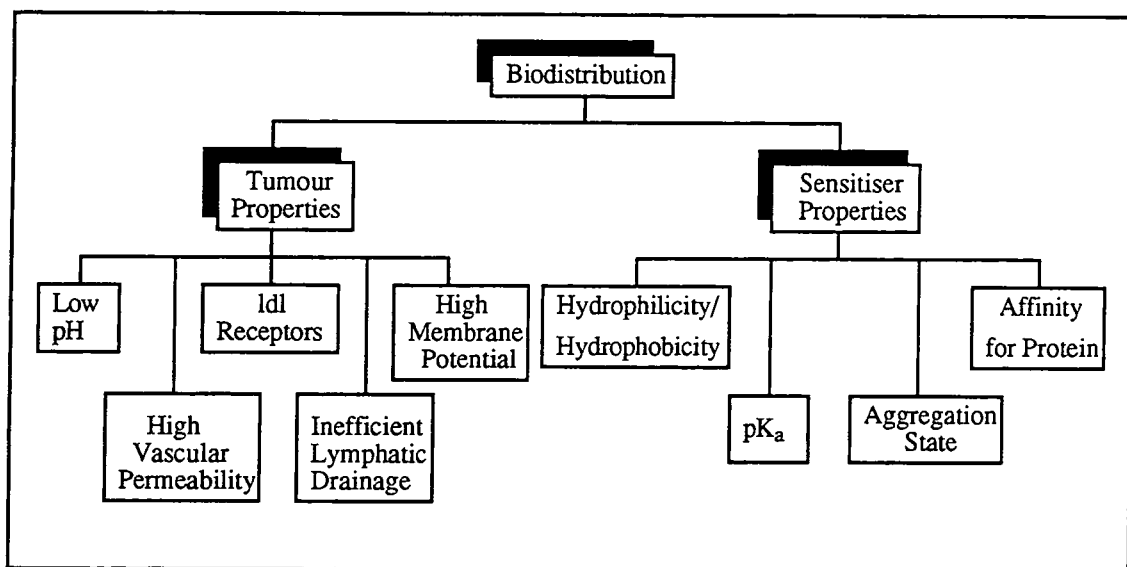
Figure 1.9. Factors affecting retention of sensitisers in a tumour.

A tumour may be divided into five main areas[72]: Vasculature, which provides blood supply and nutrients to the growth; Necrotic or dead areas, prevalent in inner regions of the tumour where blood supply is poor; Immune cells, in particular macrophage cells capable of engulfing and destroying foreign particles; Stromal areas, which are composed largely of proteins such as collagen and elastin and form the tissues that make up the framework of a growth and, of course, malignant tumour cells. A detailed description of the composition of a cell may be found in any standard biology publication, such as 'Molecular Biology of the Cell' by Alberts *et al.*[73]. For the purposes of this text, however, a simple model may be considered (Figure 1.10).
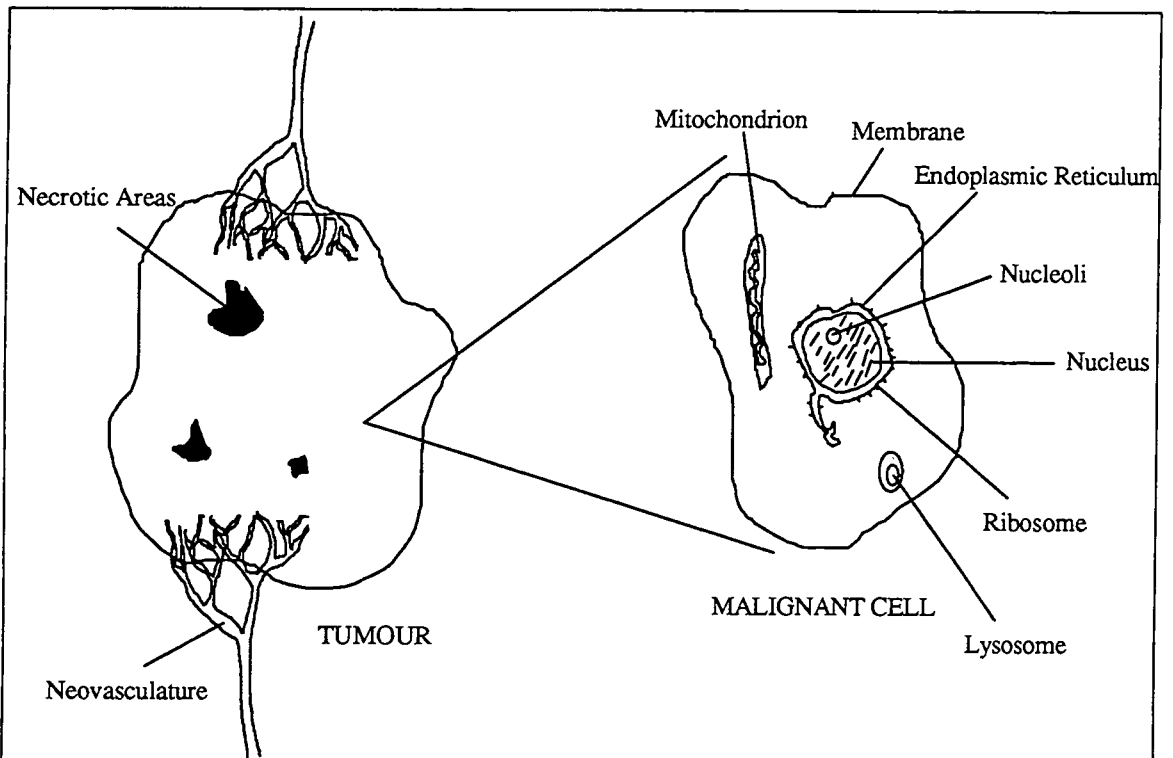
Endoplasmic Reticulum: Forms a link between the cell and the nuclear membrane.

Interstitial Space: Space in between cells.

Lymphatic System: Drains molecules that are too large to pass into blood capillaries.

Lysosome: Organelle which degrades molecules which have been transported into a cell.

Macrophage: Large cell that is able to engulf and destroy foreign particles.

Membrane: Sheet-like tissue that lines cells. Consists of lipid bilayer and is permeable to water and fat soluble substances but impermeable to polar complexes such as sugars.

Mitochondria: Structures which carry out aerobic respiration and contain many enzymes of the cell. Known as the "power house" of the cell.

Necrotic Areas: Dead areas within the tumour, inaccessible to oxygen.

Nucleoli: Contained within the nucleus, nucleoli play an important role in ribosome manufacture.

Nucleus: Control centre of the cell, contains genetic information.

Ribosome: Attached to the endoplasmic reticulum, ribosomes are involved in protein synthesis.

Stroma: Tissue that forms the framework of a growth.

Vasculature: Network of vessels for circulating fluids.

__Figure 1.10. Schematic representation and glossary of a tumour and cell.__

32

The vascular system of tumour growths has been shown to have a greater permeability to plasma proteins than that of healthy tissue[74]. This, in combination with a poor lymphatic drainage system[75] leads to an accumulation of hydrophilic sensitisers in interstitial regions[76]. Intratumoral pH is low with respect to healthy tissue[77] due to production of lactic acid and carbon dioxide by anaerobic glycolysis[78]. Bech and Pottier have both considered the importance of pH. Bech[79] studied the effect of pH on the production of protoporphyrin IX from 5-aminolevulinic acid (ALA) whilst Pottier[80] has shown that the biodistribution of haematoporphyrin is affected by pH. Tumours require a greater amount of cholesterol than healthy cells and, therefore, possess a higher concentration of low density lipoprotein (ldl) receptors[81] possibly encouraging retention of hydrophobic sensitisers. Finally, the membrane potential of malignant cells is higher than that of healthy cells. This promotes transport of hydrophobic sensitisers through the cell membrane[82], in particular cationic dye species, which have been observed to accumulate in mitochondria[83] of the cell. Species which hyperpolarise the cell membrane, such as nigercin, have been shown to increase the efficiency of photodynamic action[84],[85], probably due to an increased uptake of the dye. For cell bound sensitisers, photodynamic action acts to destroy neoplastic growth directly. It is already clear that the site of localisation of sensitiser molecules varies according to the hydrophilicity. In general, hydrophilic sensitisers localise in the vascular stroma[86] since negative peripheral substituents prevent transport across cell membranes. Cell death is achieved as a result of damage to the blood vessels which supply the malignant growth[87].

The aggregation state, ionic distribution and pK_a of sensitisers are also important. Bellnier and Lin[88] suggest that porphyrin molecules are trapped in intracellular sites due to aggregate formation that prevents exit through the cell membrane. Work carried out by Wood and co-workers[89] has demonstrated the importance of ionic charge of photosensitisers. In their study, cellular uptake of cationic ZnPc sensitisers was far greater than that of anionic or neutral species. The site of retention also differed. Cationic and anionic species initially resided in lysosomes whilst neutral molecules located in the plasma membrane. After irradiation, charged species redistributed to nucleoli of the cell. In addition, Johnson et al.[90] have shown that only positively charged rhodamine dyes are capable of crossing the negatively charged cell membrane to reside in the mitochondria of the cell. It follows that pK_a values of sensitisers will have extreme importance in controlling localisation properties. Protonation will alter the ionic state of the molecule and hence the propensity to cross the cell membrane.

Localisation is also affected by the delivery mechanism employed. Kessel has shown[69] that although tin etiopurpurin is efficiently delivered to cells when injected in an ethanolic

solution, cytotoxicity was enhanced when a vehicle such as Cremophor EL was utilised. This implies different mechanisms of retention. Reddi[54] observed a two fold increase in tumour:normal tissue retention ratio in MS2 fibrosarcoma when ldl was used as delivery vehicle as opposed to liposomes. The kinetics and accumulation rate of a silicon naphthalocyanine sensitiser in urothelial cell carcinoma were also observed to depend on the mode of delivery[91]. It is clear that generalisations regarding transport mechanisms, localisation phenomena and cytotoxic pathways should be regarded with caution. Indeed, Peavy and co-workers[92] have shown that the biodistribution of AlPcS varied with tumour type, e.g. distribution throughout tumour tissue was observed in fibrosarcoma, however, in squamous cell carcinoma, sensitiser species were limited to the vascular stroma. It is important to improve understanding in this area of PDT since a knowledge of localisation and retention mechanisms would allow sensitisers to be tailored to provide the optimum conditions for effective treatment of cancer.

1.6 Aim

The aim of this study was to investigate the photophysical properties of substituted zinc phthalocyanines under a range of conditions. The effect of ring modifications such as peripheral substitution by acid, ester or alkyl groups has been considered. In addition, the influence of environmental factors such as medium, temperature and pH has been determined. The propensity of zinc phthalocyanine to interact with biological substrates such as bovine serum albumin or DNA via binding or electron transfer reactions was also of interest. In this way it was hoped to develop an understanding of the photoproperties of zinc phthalocyanine in relation to its use as a sensitiser for photodynamic therapy.

A brief summary of chapters two to six is given below:

Chapter 2: Describes the photophysical techniques used throughout this work including background theory necessary for a basic understanding of the principles involved. Synthesis of two novel, substituted zinc phthalocyanines, $ZnPc(CMe(CO_2Me)_2)_4$ and $ZnPc(CHMeCO_2H)_4$ is also reported.

Chapter 3: Discusses the solution state and photophysical properties of $ZnPc(CMe(CO_2Me)_2)_4$ and $ZnPc(CHMeCO_2H)_4$. The effect of peripheral ligand substitution and the nature of the surrounding medium (homogeneous, heterogeneous or solid state) on the photophysical properties of substituted ZnPc's are also considered.

Chapter 4:   Dimerisation of phthalocyanines is investigated. The photophysical properties of a novel, fluorescent dimer / aggregate of C10 are reported and compared with those of a face-to-face dimer of aluminium phthalocyanine. The properties of both species are discussed in terms of exciton theory. Chapter 4 also describes the steady state fluorescence anisotropy of phthalocyanines and how it may be used to study the nature of excited states.

Chapter 5:   A complete photophysical evaluation of mono to tetra protonated species of $^tBu_4ZnPc$ in ethanol is given. The tendency of $ZnPcS_2$ to protonate in micellar media and on solid state substrates is also described.

Chapter 6:   Discusses the propensity of substituted zinc phthalocyanines to bind to biological substrates such as protein and DNA. Their ability to participate in electron transfer reactions is also studied.

1.7 References

[1]   Meyer-Betz F., Investigations on the biological (photodynamic) action of haematoporphyrin and other derivatives of blood and bile pigments., *Deut. Arch. Klin. Med.*, **112**, 476-503, 1913.

[2]   Von Tapiener H. and Jesionek A., *Therapeutische Versuche mit fluoreszierenden Stoffen*, Muenchener Medizinische Wochenschrift, **50**, 2042-2051, 1903.

[3]   Figge F.J., Weiland G.S. and Manganiello L.O.J., Cancer detection and therapy. Affinity of neoplastic, embryonic and traumatised tissue for porphyrins and metalloporphyrins., *Proc. of the Soc. Exp. Biol. and Med.*, **68**, 640-641, 1948.

[4]   Rasmussen D.S., Ward G.S. and Figge F.H.J., Fluorescence of human lymphatic and cancer tissues following high doses of intravenous hematoporphyrin., *Surgical Forum*, 619-623, 1955.

[5]   Lipson R.L., Baldes E.J. and Olsen A.M., Hematoporphyrin derivative: a new aid for endoscopic detection of malignant disease., *J. Thoracic and Cardiovascular Surgery*, **42**, 623-629, 1961.

[6]   Lipson R.L., Baldes E.J. and Olsen A.M., The use of a derivative of hematoporphyrin in tumour detection., *J. Nat. Cancer Inst.*, **26**, 1-11, 1961.

[7]   Kelly J.F., Snell M.E. and Berenbaum M.C., Photodynamic destruction of human bladder carcinoma., *Br. J. Cancer*, **31**, 237-244, 1975.

[8]   Kessel D., Effects of photoactivated porphyrins at the cell surfaces of leukaemia L1210 cells., *Biochem.*, **16**, 3443-3449, 1977.

[9]   Dougherty T.J., Lawrence G., Kaufman J.E., Boyle D., Weishaupt K.R. and Goldfarb A., Photoradiation in the treatment of recurrent breast cancer with hematoporphyrin derivative therapy., *J. Nat. Cancer Inst.*, **62**, 231 -237, 1979.

[10]   Cortese A.A. and Kinsey J.H., Endoscopic management of lung cancer with hematoporphyrin derivative phototherapy., *Mayo Clinic Proc.*, **57**, 543-547, 1982.

[11]   Dougherty T.J., Lawrence G., Kaufman J.E., Weishaupt K.R., Goldfarb A. and Mittleman A., Photoradiation therapy for the treatment of malignant tumours., *Cancer Res.*, **38**, 2628-2635, 1978.

[12]   Weishaupt K.R., Gromer C.J. and Dougherty T.J., Identification of singlet oxygen as the cytotoxic agent in photo-inactivation of a murine tumor., *Cancer Res.*, **36**, 2326, 1976.

[13]   Parker J.G., The importance of singlet delta oxygen in cancer photoradiation therapy., *John Hopkins APL Technical Digest*, **5**, 48-50, 1984.

[14]   Andreoni A., Cubeddu R., De Silvestri S., Laporta P., Jori G. and Reddi E., Hematoporphyrin derivative: Experimental evidence for aggregated species., *Chem. Phys. Lett.*, **88**, 33-36, 1982.

[15]   Dougherty T.J., Studies on the structure of porphyrins contained in Photofrin II., *Photochem. Photobiol.*, **45**, 879-889, 1987.

[16]   Ben-Hur E. and Rosenthal I., Photochemical generation of superoxide radical and the cytotoxicity of phthalocyanines., *Int. J. Rad. Biol.*, **47**, 145-147, 1985.

[17]   Bensasson R.V., Land E.J. and Truscott T.G., *Excited States and Free Radicals in Biology and Medicine*, p322, Oxford University Press, New York, 1993.

[18]   Ochsner M., Photophysical and photobiological processes in the photodynamic therapy of tumours., *J. Photochem. Photobiol.*, **39**, 1, 1997.

[19]   Turro N.J., *Modern Molecular Photochemistry*, University Science Books, California, p164, 1991.

[20]   Kearns D.R., Physical and chemical properties of singlet molecular oxygen., *Chem. Rev.*, **71**, 395, 1973.

[21]   Gijzeman O.L.J., Kaulman F. and Porter G., Oxygen quenching of aromatic triplet states in solution., *J. Chem. Soc. Faraday Trans. II*, **69**, 708, 1973.

[22]   Oelckers S., Sczepan M., Hanke T. and Roder B., Time resolved detection of singlet oxygen luminescence in red cell ghost suspensions., *J. Photochem. Photobiol. B:Biol.*, **39**, 219, 1997.

[23]   MacRobert A.J. and Phillips D., Photodynamic Therapy, *Chemistry and Industry*, **17**, 1992.

[24]   Dougherty T.J., Grindey G.B., Fiel R., Weishaupt K.R. and   Bryle D.G., Photoradiation therapy II. Cure of animal tumors with hematoporphyrin and light., *J. Nat. Cancer Inst.*, **55**, 115-121, 1975.

[25]   Forbes I.J., Cowled P.A., Leong A.S.Y., Ward A.D., Black R.B., Blake R.B. and Jacka F.J., Phototherapy of human tumours using haematoporphyrin derivative., *Med. J. Australia*, **2**, 489-493, 1980.

[26]   Kessel D., Hematoporphyrin and HpD - Photophysics, photochemistry and phototherapy., *Photochem. Photobiol.*, **39**, 851-859, 1984.

[27]   Moan J., Porphyrin photosensitisation and phototherapy., *Photochem. Photobiol.*, **43**, 681-690, 1986.

[28]   Truscott T.G., The photochemistry of haematoporphyrin and some related species., *J. Chem. Soc. Faraday Trans. 2*, **82**, 2177-2181, 1986.

[29]   Borland C.F., McGarvey D.J., Morgan A.R. and Truscott T.G., Laser flash photolysis of purpurins, more potential photosensitisers of interest in photodynamic therapy., *J. Photochem. Photobiol. B:Biol.*, **2**, 427-434, 1988.

[30]   Bonnett R. and Berenbaum M., *Ciba Foundation Symposium*, 14 Wiley Interscience Publ., Chichester, pp40-59, 1989.

[31]   Bonnett R., Photosensitisers of the porphyrin and phthalocyanine series for PDT., *Chem. Soc. Rev.*, 19-33, 1995.

[32]   Phillips D. and MacRobert A., Spectroscopic studies of photosensitisers and selectivity in photodynamic therapy., *Highlights Modern Biochemistry*, **2**, 1517-1525, 1989.

[33]   Jori G., Far red absorbing photosensitisers - their use in the photodynamic therapy of tumours., *J. Photochem. Photobiol. A:Chem.*, 371-378, 1992.

[34]   Rosenthal I., Phthalocyanines as photodynamic sensitisers., *Photochem. Photobiol.*, **53**, 859-870, 1991.

[35]   Ford W.E., Rihter B.D., Kenney M.E. and Rodgers M.A.J., Photoproperties of alkoxy substituted phthalocyanines with deep red optical absorbance., *Photochem. Photobiol.*, **50**, 277-282, 1989.

[36]   Chan W.S., Marshal J.F., Svensen R., Phillips. and Hart I.R., Photosensitising activity of phthalocyanine dyes screened against tissue culture cells., *Photochem. Photobiol.*, **45**, 757-761, 1987.

[37]   Murov S.L., Carmichael I. and Hug G.L., *Handbook of Photochemistry*, 2nd Edn., p40, Marcel Dekker Inc., New York, 1993.

[38]   McVie J., Sinclair R.S. and Truscott T.G., Triplet states of copper and metal free phthalocyanine., *J. Chem. Soc. Faraday Trans II*, **74**, 1870, 1978.

[39]   Ben-Hur E. and Rosenthal I., Photosensitisation of Chinese hamster cells by water soluble phthalocyanines., *Photochem. Photobiol.*, **43**, 615-619, 1986.

[40]   Ambroz M., MacRobert A.J., Morgan J., Rumbles G., Foley M.S.C. and Philips D., Time resolved fluorescence spectroscopy and intracellular imaging of aluminium phthalocyanine., *J. Photochem. Photobiol. B:Biol.*, **27**, 105-117, 1994.

[41]   Marshall J.F., Chan W.S. and Hart I.R., Effect of photodynamic therapy on anti-tumour immune defences: Comparison of the photosensitisers hematoporphyrin derivative and chloroaluminium sulphonated phthalocyanine., *Photochem. Photobiol.*, **49**, 627-632, 1989.

[42]   Moan J., Berg K., Bommer J. and Western A., Action spectrum of phthalocyanines with respect to photosensitisation of cells., *Photochem. Photobiol.*, **56**, 171-175, 1992.

[43]   He J., Larkin H.E., Li Y.S., Rihter B.D., Zaidi S.I.A., Rodgers M.A.J., Mukhtar H., Kenney M.E. and Oleinick N.L., The synthesis, photophysical and photobiological properties and in vitro structure activity relationships of a set of silicon phthalocyanine PDT photosensitisers., *Photochem. Photobiol.*, **65**, 581, 1991.

[44]   Vollano J.F., Bossard G.E., Martellucci S.A., Darkes M.C., Abrams M.J. and Brooks R.C., The synthesis and in vitro photodynamic activity of a series of novel ruthenium 2, 3 naphthalocyanines., *J. Photochem. Photobiol. B:Biol.*, **37**, 230, 1997.

[45]   Schaffer A.M., Gouterman M. and Davidson E.R., Porphyrins XXVII. Extended Huckel calculations on metal phthalocyanines and tetraazaporphins., *Theoret. Chim. Acta*, **30**, 9, 1973.

[46]   Gouterman M., Spectra of Porphyrins, *J. Mol. Spec.*, **6**, 138, 1961.

[47]   Orti E. and Bredas J.L., Electronic structure of metal free phthalocyanine: A valence effective Hamiltonian theoretical study., *J. Chem. Phys.*, **89**, 1009, 1988.

[48]   Orti E., Bredas J.L. and Clarisse C., Electronic structure of phthalocyanines. Theoretical investigation of the optical properties of phthalocyanine monomers, dimers and crystals., *J. Chem. Phys.*, **92**, 1228, 1990.

[49]   Sevchenko A.N., Solov'ev K.N., Gradyushko A.T. and Shkirman S.F., Narrow-band electronic spectra of metal derivatives of tetrabenzoporphine and phthalocyanine., *Soviet Physics-Doklady*, **11**, 587, 1967.

[50]   Rosa A. and Baerends E.J., Metal-macrocycle interaction in phthalocyanines. Density functional calculations of ground and excited states., *Inorg. Chem.*, **33**, 584, 1994.

[51]   Nyokong T., Gasyna Z. and Stillman M., Analysis of the absorption and magnetic circular dichroism spectra of zinc phthalocyanine and the π cation radical species [ZnPc(-1)]·+., *Inorg. Chem.*, **26**, 1087, 1987.

[52]   Khalib N., Boudjema B., Maitrot M., Chermette H. and Porte L., Electronic structure of zinc phthalocyanine., *Can. J. Chem.*, **66**, 2313, 1988.

[53] Morley J.O. and Charlton M.H., Theoretical investigation of the structure and spectra of zinc phthalocyanines., *J. Phys. Chem.*, **99**, 1928, 1995.

[54] Reddi E., Role of delivery vehicles for photosensitisers in the photodynamic therapy of tumours., *J. Photochem. Photobiol. B:Biol.*, **37**, 189, 1997.

[55] Schieweck K., Caparo H.G., Isele U., Van Hoogevest P., Ochsner M., Maurer T. and Balt E., CGP 55847 liposome delivered Zn(II) phthalocyanine as a phototherapeutic agent for tumours., *S.P.I.E.*, **2078**, 107, 1994.

[56] Valduga G., Reddi E., Jori G., Cubeddu R., Taroni P. and Valentini G., Steady state and time resolved spectroscopic studies on Zn(II) phthalocyanine in liposomes., *J. Photochem. Photobiol. B:Biol.*, **16**, 331, 1992.

[57] Soncin M., Polo L., Reddi E., Jori G., Kenney M.G., Chang G. and Rodgers M.A.J., Effect of axial ligation and delivery system on the tumour localising and photosensitising properties of Ge(IV) octabutoxyphthalocyanines., *Br. J. Cancer*, **71**, 727-732, 1995.

[58] Reddi E., Zhou C., Biolo R., Menegaldo E. and Jori G., Liposome or ldl administered Zn(II) phthalocyanine as a photodynamic agent for tumours. I Pharmacokinetic properties and phototherapeutic efficiency., *Br. J. Cancer*, **61**, 407, 1990.

[59] Mew D., Wat C.K., Towers G.H.N. and Levy J.G., Photoimmunotherapy: Treatment of animal tumours with tumour specific monoclonal antibody - haematoporphyrin conjugate., *J. Immunol.*, **130**, 1473, 1983.

[60] Jori G., *In vivo* transport and pharmacokinetic behaviour of tumor photosensitisers., *Ciba Foundation Symposium*, Wiley Chich., **146**, 78-94, 1989.

[61] Reddi E., Transport modalities of photodynamic agents for tumors., *S.P.I.E.*, **2078**, 246, 1994.

[62] Polo L., Reddi E., Garbo G.M., Morgan A.R. and Jori G., The distribution of the tumour photosensitisers Zn(II) phthalocyanine and Sn(IV) etiopurpurin among rabbit plasma proteins., *Cancer Lett.*, **66**, 217, 1992.

[63] Love W.G., Havenaar E.C., Lowe P.J. and Taylor P.W., Uptake of Zn(II) phthalocyanine by HepG2 cells expressing the low density lipoprotein receptor: studies with the liposomal formulation CGP55847., *S.P.I.E.*, **2078**, 381, 1994.

[64] Versluis A.J., Rensen P.C.N., Kuipers M.E., Love W.G. and Taylor P.W., Interaction between Zn(II) phthalocyanine containing liposomes and human low density lipoprotein., *J. Photochem. Photobiol. B:Biol.*, **23**, 141-148, 1994.

[65] Reyftmann J.P., Morliere P., Goldstein S., Santus R., Dubertriet L. and Lagrange D., Interaction of human serum low density lipoproteins with porphyrins: A spectroscopic and photochemical study., *Photochem. Photobiol.*, **40**, 721, 1984.

[66]   Kessel D., Whitcomb K.L. and Schulz V., Lipoprotein-mediated distribution of N-aspartyl chlorin-E6 in the mouse., *Photochem. Photobiol.*, **56**, 51, 1992.

[67]   Grossweiner L.I and Goyad G.C., Binding of hematoporphyrin derivative to HSA., *Photochem. Photobiol.*, **40**, 1, 1984.

[68]   Rensen P.C.N., Love W.G. and Taylor P.W., *In vitro* interaction of zinc(II)-phthalocyanine-containing liposomes and plasma lipoproteins., *J. Photochem. Photobiol. B:Biol.*, **26**, 29, 1994.

[69]   Kessel D., Morgan A. and Garbo G.M., Sites and efficacy of photodamage by tin etiopurpurin in vitro using different delivery systems., *Photochem Photobiol.*, **54**, 193, 1991.

[70]   Polo L., Bianco G., Reddi E. and Jori G., The effect of liposomal formulations on the interaction of Zn(II) phthalocyanine with isolated low and high density lipoproteins., *Int. J. Biochem. Cell Biol.*, **27**, 1249, 1995.

[71]   Jori G., Tumour photosensitisers: approaches to enhance the selectivity and efficiency of photodynamic therapy., *J. Photochem. Photobiol. B:Biol.*, **36**, 87, 1996.

[72]   Kessel D., *PDT of Neoplastic Disease*, CRC Press, Boston, 1990.

[73]   Alberts B., Bray D., Lewis J., Raff M., Roberts K. and Watson J.D., *Molecular Biology of the Cell*, 2nd Edn., Garland Publishing, London, 1989.

[74]   Ackerman N.B. and Hechmer P.A., Failure of histamine type mediators to enhance vascular permeability in experimental liver metastases., *Surg. Gynecol. Obstet.*, **146**, 884, 1978.

[75]   Feldman G.B., Knapp R.C., Order S.E., and Hellman S., The role of lymphatic obstruction in the formation of ascites in a murine ovarian carcinoma., *Cancer Res.*, **32**, 1663, 1972.

[76]   Roberts W.G. and Hasan T., Role of neovasculature and vascular permeability on the tumour retention of photodynamic agents., *Cancer Res.*, **52**, 924-930, 1992.

[77]   Waddel W.J. and Bates R.G., Intracellular pH., *Physiol. Rev.*, **49**, 285, 1969.

[78]   Albers C., Vanden Kerkhoff W., Vaupel P. and Muller Klieser W., Non-bicarbonate buffering of ascites tumor cells in the rat as titrated by strong acids., *Res. Physiol.*, **45**, 273, 1981.

[79]   Bech O., Berg K. and Moan J., The pH dependency of protoporphyria IX formulation in cells incubated with 5-aminolevulinic acid., *Cancer Lett.*, **113**, 25, 1997.

[80]   Pottier B. and Kennedy J.C., New trends in photobiology. The possible role of ionic species in selective biodistribution of photochemotherapeutic agents toward neoplastic tissue., *J. Photochem. Photobiol. B:Biol.*, **8**, 1, 1990.

[81]   Milanesi C., Zhou C., Biolo R. and Jori G., Zn(II) phthalocyanine as a photodynamic agent for tumours. Studies on the mechanism of photosensitised tumour necrosis., *Br. J. Cancer*, **61**, 846-850, 1990.

[82]   Margaron P., Gregoire M.J., Scasnar V., Ali H., Van Lier V.E., Structure-photodynamic activity relationships of a series of 4-substituted zinc phthalocyanines., *Photochem. Photobiol.*, **63**, 217, 1996.

[83]   Johnson L.V., Summerhayes I.C. and Chen L.B., Decreased uptake and retention of Rhodamine 123 by mitochondria in feline sarcoma virus-transformed mink cells., *Cell*, **28**, 7, 1982.

[84]   Lin C.W. and Shulok J.R., Enhancement of Nile Blue derivative induced photocytotoxicity by nigericin and low cytoplasmic pH., *Photochem. Photobiol.*, **60**, 143, 1994.

[85]   Varnes M.E., Bayne M.T. and Bright G.R., Reduction of the intracellular pH is not the mechanism for the synergistic interaction between photodynamic therapy and Nigericin., *Photochem. Photobiol.*, **64**, 853, 1996.

[86]   Kessel D., Thompson P., Saatio I.C. and Nuntun K.D., Tumour localisation and photosensitisation by sulphonated derivatives of tetraphenylporphine., *Photochem. Photobiol.*, **45**, 787, 1987.

[87]   Selman S.H., Kreimerbirnbaum M., Chaudhuri K., Garbo G.M., Seaman D.A., Keck R.W., Ben-Hur E. and Rosenthal I., Photodynamic treatment of transplantable bladder tumors in rodents after pretreatment with chloroaluminium tetrasulfophthalocyanine., *J. Urol.*, **136**, 141, 1986.

[88]   Bellnier D.A. and Lin C.W., Photodynamic destruction of cultured human bladder tumor cells by haematoporphyrin derivative: effect of porphyrin molecular aggregation., *Photobiochem. Photobiophys.*, **6**, 357, 1983.

[89]   Wood S.R., Holroyd J.A. and Brown S.B., The subcellular localisation of Zn(II) phthalocyanines and their redistribution on exposure to light., *Photochem. Photobiol.*, **65**, 397, 1997.

[90]   Johnson L.V., Summerhays I.C. and Chen L.B., Decreased retention of Rhodamine 123 by mitochondria in feline sarcoma virus transformed mink cells., *Cell*, **28**, 7, 1982.

[91]   Zuk M.M., Rihter B.D., Kenney .E., Rodgers M.A.J. and Kreimer-Birnbaum M., Effect of delivery system on the pharmacokinetics and tissue distribution of bis(Di-isoutyl octadecylsiloxy)silicon 2,3-naphthalocyanine (isoBOCINC), a photosensitiser for tumor therapy., *Photochem. Photobiol.*, **63**, 132-140, 1996.

[92]   Peavy G.M., Krasieva T.B., Tromberg B.J., Eusantos E.D., Berns M.W., Variation in the distribution of a phthalocyanine photosensitiser in naturally occurring tumors of animals., *J. Photochem. Photobiol. B:Biol.*, **27**, 271-277, 1995.

CHAPTER 2

EXPERIMENTAL TECHNIQUES

In this work, photophysical techniques were employed to investigate the properties of phthalocyanines under various conditions. A brief description of experimental methods and relevant theory follows. Where further detail is required, the reader is referred to comprehensive texts referenced throughout. The synthesis of β -tetra-1,1-di(methoxycarbonyl)ethyl zinc phthalocyanine, $ZnPc(CMe(CO_2Me)_2)_4$, and β -tetra-1-carboxyethyl zinc phthalocyanine, $ZnPc(CHMeCO_2H)_4$ is described. Modification of metal free phthalocyanines to produce the zinc metallated derivatives is also included.

2.1 Photophysical Measurements

2.1.1 UV/Visible Absorption Spectroscopy

UV/Visible absorption spectra were carried out with an ATI Unicam UV2-100 spectrometer. Spectra were performed using quartz cuvettes, pathlength = 10 mm, over an appropriate wavelength range (usually 300 nm to 800 nm). A baseline was obtained using a suitable solvent prior to use. Molar extinction coefficients (ε, dm^3 mol^{-1} cm^{-1}) were determined using the Beer-Lambert law,

$$A = \varepsilon c l = log_{10} \frac{I_0}{I} \qquad (2.1)$$

where A is the absorbance at the wavelength of interest, c is the concentration of solution (mol dm^{-3}), l is the pathlength of the cuvette (cm), I_0 is the intensity of incident radiation and I is the intensity of radiation after passing through the sample.

2.2.2 Fluorescence Spectroscopy
2.1.2.1 Spectra

Fluorescence emission and excitation spectra were recorded using a Perkin Elmer LS50B luminescence spectrometer fitted with a red sensitive, Hamamatsu R928 photomultiplier tube (PMT). The optical bench was controlled by FL-Winlab 3.0 running on an Elonex P90 computer. In order to minimise inner filter effects[1], samples were prepared such

that their maximum absorbance was < 0.05. Emission spectra were generated by exciting at 610 nm or 630 nm and recorded over the range 640 nm - 850 nm. To maximise resolution, a scan speed of 120 nm min^{-1} and slits of 10 nm and 2.5 nm for the excitation and emission slits respectively were used. Where necessary, emission spectra were corrected for wavelength dependent sensitivity of the photomultiplier using a correction curve supplied by Perkin Elmer. Excitation spectra were recorded by monitoring fluorescence emission at 760 nm. These spectra were corrected internally for variation in the excitation intensity using a built in Rhodamine dye quantum counter.

In certain cases, for example, the emission and excitation spectra of protonated phthalocyanines (Chapter 5), the LS50B was unsuitable for measurements. This was due to a combination of low sensitivity of the detector in the near IR region of the spectrum and low output of the xenon lamp excitation source at wavelengths > 700 nm. For these samples the arrangement depicted in Figure 2.1 was employed to measured emission.
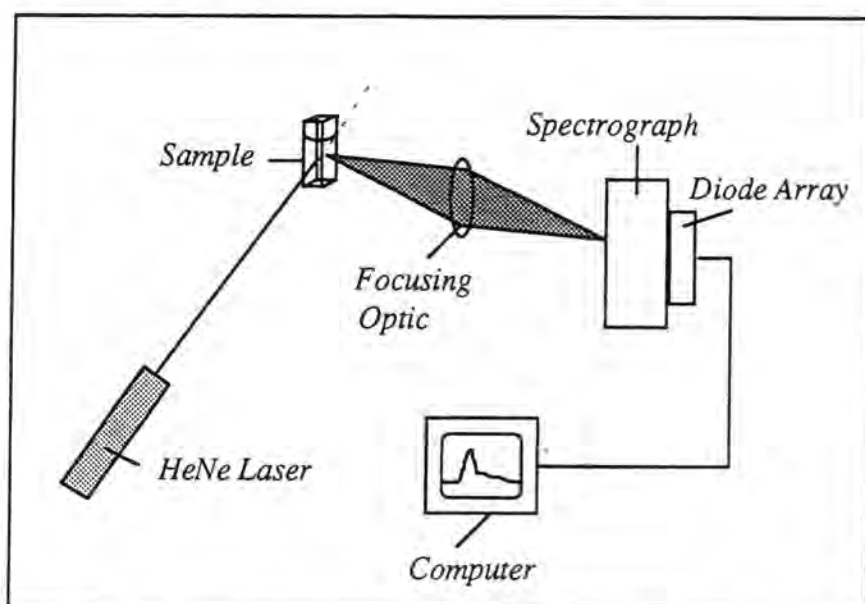
Figure 2.1. Experimental arrangement for recording emission spectra from phthalocyanine species emitting in the near-IR.

A continuous wave HeNe laser (Melles Griot, 632.8 nm, power ~ 5 mW) was used to excite the sample. Emission was collected at 90° to irradiation and focused into a spectrograph (Bentham TM300V) equipped with a diode array detector (EG & G 1453a). The diode array was calibrated using the emission lines of an argon ion laser. Spectra were corrected for wavelength dependent sensitivity of the diode using a correction curve generated using a standard tungsten lamp. Excitation spectra of samples emitting in the near IR were recorded on a SPEX FluoroMax fluorimeter at Imperial College, London.

43

2.1.2.2 Fluorescence Quantum Yields

The fluorescence quantum yield is defined as the number of photons emitted as fluorescence as a ratio of the number of photons absorbed. This can be expressed in terms of competing decay processes by assuming steady state conditions, i.e. the rate of formation of singlet state equals the rate of decay.

Process	Rate
$S_0 + hv \rightarrow S_1$	I_a
$S_1 \rightarrow S_0 + hv$	$k_f[S_1]$
$S_1 \rightarrow S_0 + heat$	$k_{ic}[S_1]$
$S_1 \rightarrow T_1$	$k_{isc}[S_1]$

Using the steady state approximation:

$$I_a = k_f [S_1] + k_{ic} [S_1] + k_{isc} [S_1] \tag{2.2}$$

$$\Rightarrow \qquad \Phi_F = \frac{k_f}{k_f + k_{ic} + k_{isc}} \tag{2.3}$$

Fluorescence quantum yields determined in this work were obtained using the comparative method of Williams et al.[2] in which the quantum yield is expressed as

$$\Phi_x = \Phi_{std} \cdot \frac{A_{std}}{A_x} \cdot \frac{I_x}{I_{std}} \cdot \frac{n_x^2}{n_{std}^2} \tag{2.4}$$

where Φ_x and Φ_{std} are the quantum yields of the unknown and standard respectively. A is the absorbance of the solution at the excitation wavelength, I is the integrated area of fluorescence emission and n is the refractive index of the solvent. Stock solutions of the unknown and standards were prepared with absorbances below 0.05 to minimise excitation and emission inner filter effects. Measurements were performed using several dilutions of each sample to ensure that concentration had no effect on the fluorescence yield. Chlorophyll a in ether (Φ_F[3] = 0.32) and zinc phthalocyanine in 1 % pyridine / toluene (Φ_F[4] = 0.3) were used as standards (maximum concentration = 3 x 10^{-7} mol dm^{-3}). Fluorescence emission was corrected for the wavelength dependent sensitivity of the detector and then integrated to obtain the area of emission, I. Manipulations of data points were carried out using Microsoft Excel.

2.1.2.3 Fluorescence Anisotropy

Fluorescence anisotropy is a valuable analytical technique which may be used to obtain information regarding the size, shape and rotational motion of a fluorophore, the lifetime and nature of its emissive state and the temperature/viscosity of the surrounding solvent. The technique is based on the principle that when a fluorophore emits, the total emission intensity is composed of the sum of components polarised in the x, y and z directions (I_x, I_y and I_z). When the exciting radiation is vertically polarised and oriented perpendicular to the direction of detection, $I_x = I_y$, so the total intensity may be expressed by, $I = I_z + 2I_y$ or $I = I_{VV} + 2I_{VH}$, where the subscripts refer to the direction of polarisation of the incident and emitted radiation respectively (V, vertical and H, horizontal). Anisotropy is defined as the difference in vertically and horizontally polarised emission relative to the total emission intensity, $I_{VV} - I_{VH}/I$ and can be expressed by Equation 2.5.

$$r_{av} = \frac{I_{VV} - GI_{VH}}{I_{VV} + 2GI_{VH}} \qquad (2.5)$$

where $G = I_{HV}/I_{HH}$ is a correction factor for the polarisation dependence of the apparatus.

Fluorescence anisotropy measurements were carried out using a Perkin Elmer LS50B luminescence spectrometer, with built in vertical and horizontal polarising filters to orientate incident and emitted radiation (Figure 2.2). Four scans were performed to obtain r; $I_{VV}(\lambda)$, $I_{VH}(\lambda)$, $I_{HV}(\lambda)$ and $I_{HH}(\lambda)$. Data obtained from each scan was substituted into Equation 2.5 and analysed using Microsoft Excel to calculate r_{av}, the steady state fluorescence anisotropy.
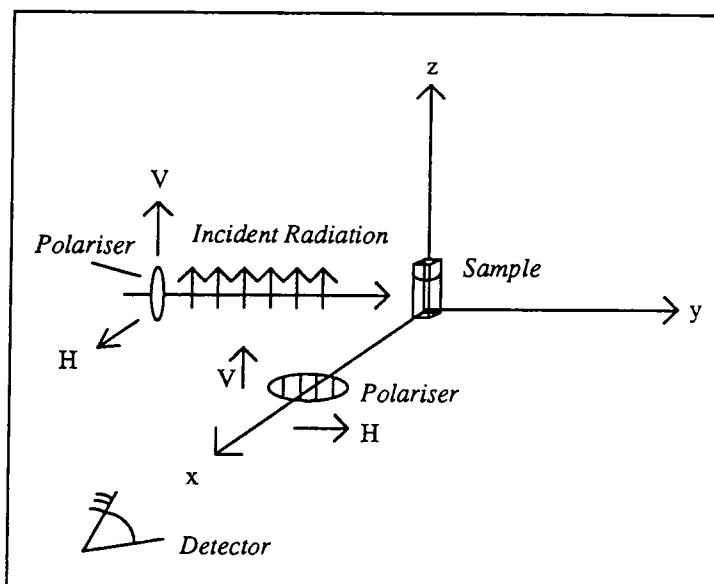
Figure 2.2. Experimental arrangement for measurement of fluorescence anisotropy.

2.1.3 Time Correlated Single Photon Counting

2.1.3.1 Introduction to Measuring Fluorescence Lifetimes

The theory of time correlated single photon counting (TCSPC) is described in detail in several texts[5],[6] and only a brief outline will be given here. The decay of fluorescence from a fluorophore usually occurs via a first order process and may be represented by a single exponential decay. If more than one species is present then the decay may be described by a sum of exponential terms (Equation 2.6), in which A_n represents the intensity at time zero, τ_n is the characteristic lifetime and $I(t)$ is the intensity at time, t.

$$I(t) = A_1 e^{-t/\tau_1} + A_2 e^{-t/\tau_2} \ldots A_n e^{-t/\tau_n} \qquad (2.6)$$

The number of terms required is governed by the number of emitting species present in the sample. Contributions of each component to the overall decay are represented by the yield, as defined by Equation 2.7.

$$Yield = \int_0^\infty A_i e^{-t/\tau_i} = A_i \tau_i \qquad (2.7)$$

Decays are recorded using a sub-nanosecond pulsed excitation source (such as a laser or flashlamp) to excite the sample repeatedly. The time, t, taken for a single photon to be detected is recorded for each event and a histogram of number of photons ($I(t)$) vs time, t, built up. The histogram is based on the probability of detecting a photon. A short time

after excitation, the probability is greater than at large time intervals when the fluorescence has decayed. The time, t, is measured using a time to amplitude converter which may be started by the excitation pulse and stopped on detection of a photon, or vice versa. The latter case is only feasible when a highly regular excitation source such as a mode locked laser is employed. The measured decay consists of a convolution of the time response of the excitation source, the electronics of the apparatus and the true fluorescence decay. On analysis, the true fluorescence decay may be determined using a process termed 'iterative re-convolution'. The instrument response function is re-convolved with an exponential function with estimate values for A and τ. These are varied until the best fit - as judged by non-linear least squares analysis - is obtained. The quality of a calculated fit is judged by statistical parameters such as the reduced χ^2, the Durbin-Watson parameter, random residuals and the correlation function.

2.1.3.2 Experimental Arrangement

Fluorescence lifetime measurements were carried out using the time correlated single photon counting equipment at Imperial College, London (Figure 2.3). The apparatus is described in detail elsewhere[7]. In brief, the experiment used a frequency doubled, mode locked Nd:YAG laser (Coherent, Antares 76S) to pump a cavity dumped dye laser (Coherent 701 dye laser & 7220 cavity dumper). DCM was used as the gain medium. This provided an excitation wavelength of 638 nm with a pulse duration of < 10 ps. Fluorescence was detected at $90°$ to the excitation beam using a microchannel plate photomultiplier (PHOTEK 413 LJ), discriminator (Ortec 584) and time to amplitude converter (Ortec 547). A double monochromator (Instruments SA 1602) was employed to select the desired wavelength of fluorescence emission. An intensity vs. time distribution was built up using a multichannel analyser (Canberra Series 35) which consisted of 512 channels with a chosen time interval of 36 ps per channel. Decays were recorded to 20000 counts in the peak channel. Samples were prepared such that their maximum absorbance did not exceed 0.05. The instrument response function was recorded by replacing the fluorophore with a scattering medium and monitoring the resulting signal at the wavelength of excitation. Decays were transferred to a computer and analysed using a non-linear least squares fitting program (Glife, Imperial College). The fitting function was judged to be acceptable when $0.8 < \chi^2 > 1.4$, residual plots appeared random and the Durbin-Watson parameter had a value between 1.7 and 2.2.

47
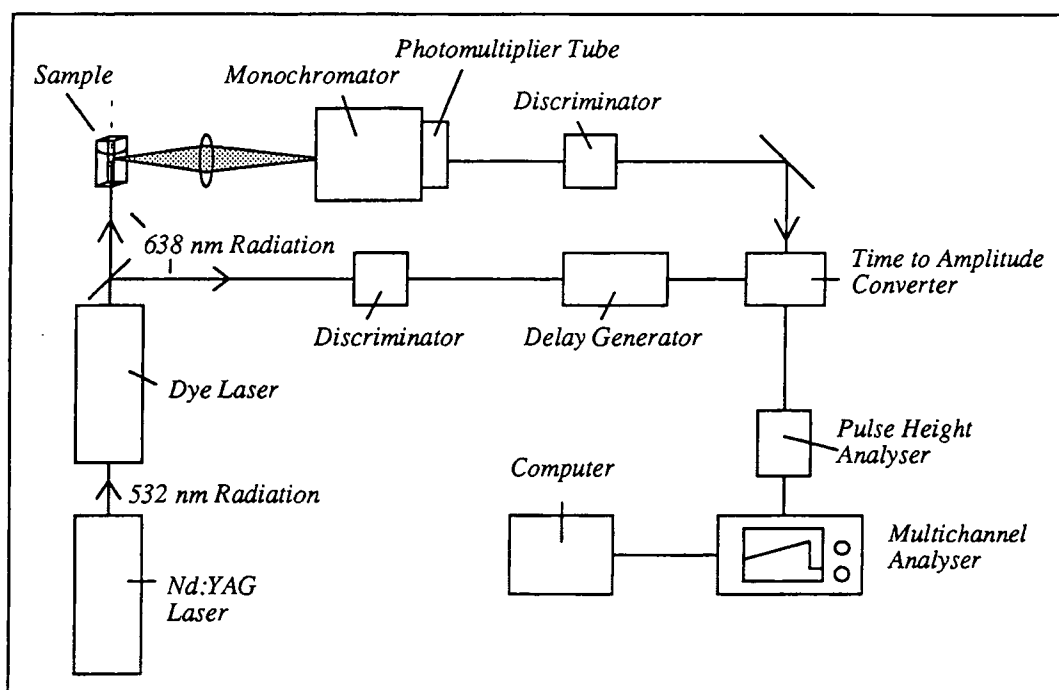
Figure 2.3. Time correlated single photon counting setup.

2.1.4 Nanosecond Laser Flash Photolysis

2.1.4.1 Introduction to Flash Photolysis

The technique of flash photolysis was developed by Lord Porter who first observed that light of high intensity could induce chemical reactions[8]. The technique may be applied to any photochemically activated system in which a transient species with a lifetime in the nanosecond to millisecond timescale is produced[9]. For example, the transient species produced by sunscreens upon absorption of ultraviolet radiation may be studied[10], electron transfer processes may be initiated and followed[11] and energy transfer processes examined[12].

In this study, the photophysical properties of phthalocyanines are of paramount interest. In these systems, a sample is irradiated using a laser to produce the first excited singlet state, S_1. S_1 decays via several mechanisms such as fluorescence, internal conversion and intersystem crossing to produce a triplet state, T_1 (Figure 1.2). White light is then used as a probe (Figure 2.4) to gain information about the triplet state such as its lifetime and quantum yield.

48
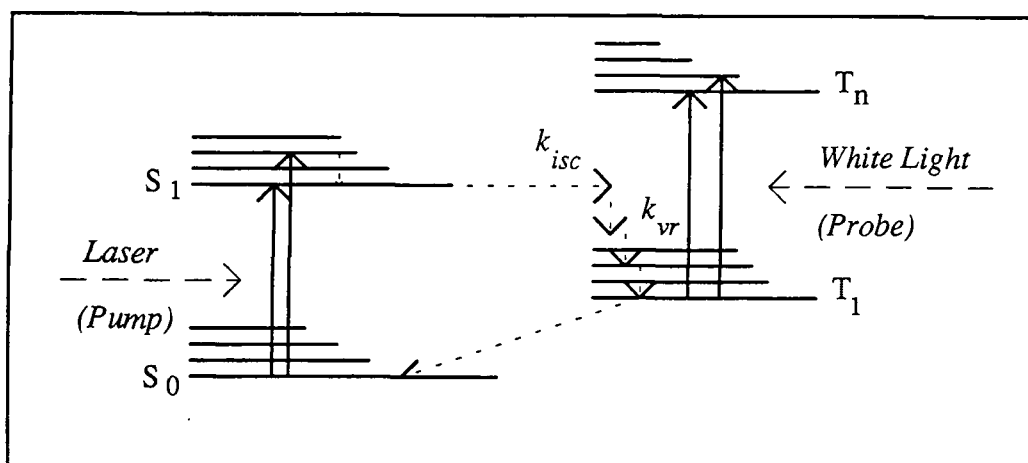
Figure 2.4. Principle of flash photolysis.

The probe light pumps the T_1 state into higher triplet states allowing the concentration of T_1 to be followed by monitoring changes in the intensity of the probe light with time (Figure 2.5). I_a represents the intensity of probe light absorbed by transient species, I_t is the transmitted radiation and I_0 is the intensity of incident probe irradiation.
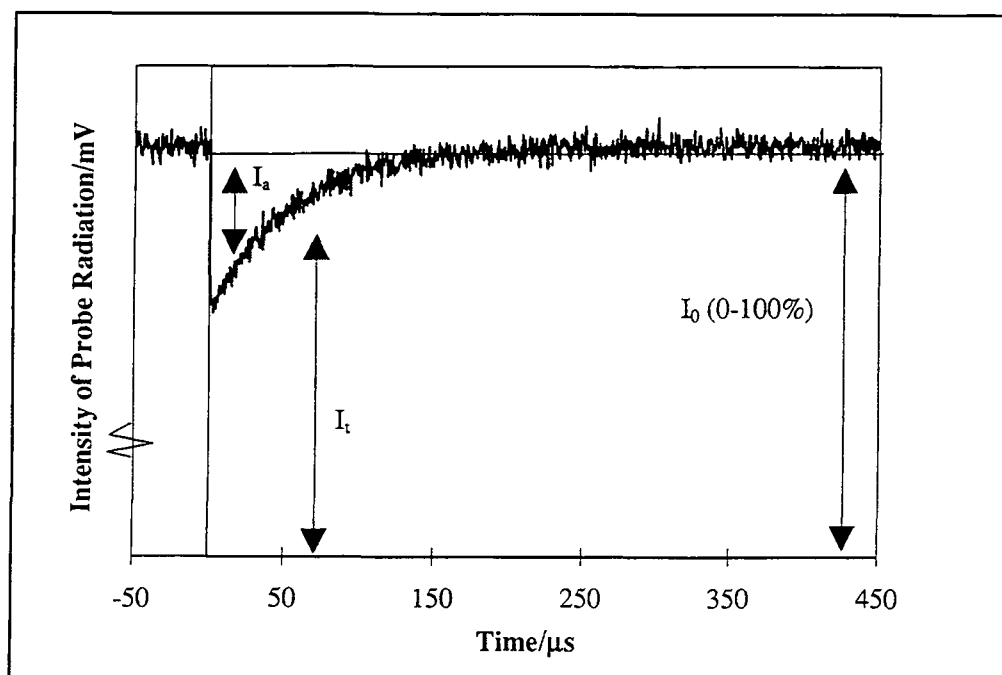
Figure 2.5. Typical transient decay.

The absorbance of the transient species can be calculated using Equation 2.8, where I_a is positive when the intensity of probe radiation decreases upon irradiation (i.e. an absorbing species is formed) and negative when an increase is observed (i.e. bleaching of the ground state occurs).

49

$$\Delta A = log_{10}\left(\frac{I_0}{I_0 - I_a}\right) \qquad\qquad (2.8)$$

As Figure 2.6 demonstrates, it is possible to build up a three dimensional data set of the new absorbing species by varying the wavelength at which measurements are taken, enabling kinetic and spectral information about the triplet state to be extracted.
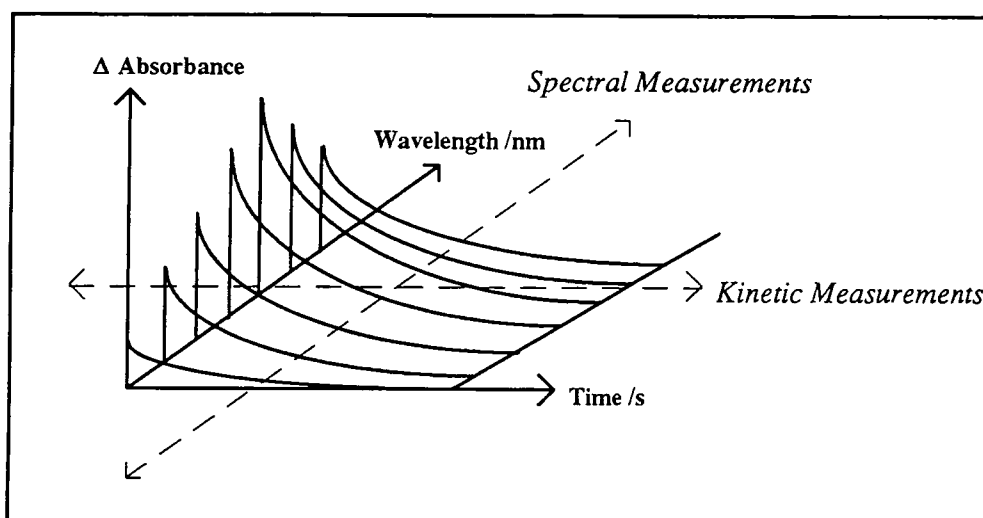
Figure 2.6. Three dimensional flash photolysis measurements.

Using three parameters - absorbance, wavelength and time - spectra can be plotted to show the spectrum of the transient species and how it develops over time. Determination of the triplet state lifetime, extinction coefficient and quantum yield are described in more detail in Sections 2.1.4.3, 2.1.4.4 and 2.1.4.6 respectively.

2.1.4.2 Experimental Setup

Studies of phthalocyanine triplet states were performed using a nanosecond laser flash photolysis system assembled in Durham. The apparatus (Figure 2.7) consisted of a Q switched Nd:YAG laser (Spectra Physics, Quanta Ray GCR-150-10). This laser produced a 10Hz train of pulses with a FWHM of ca. 8 ns and was frequency doubled to produce 532 nm radiation (typically < 200 mJ pp) which was used to pump a dye laser (Lambda Physik FL 2002). DCM or Pyridine 1 laser dyes (Lambda Physik) were used as gain media to obtain light of wavelengths 630 nm to 700 nm. An excitation wavelength of 355 nm was achieved via third harmonic generation of 1064 nm emission from the Nd:YAG laser. A 5 mm diameter liquid light guide was used to deliver light to the sample (absorbance ~ 0.3 at the excitation wavelength). Pulse energies were measured using a calibrated pyroelectric energy meter (Gentek, ED 100, 133 mV/mJ) and were

50

typically < 0.5 mJ. A tungsten-halogen lamp (100 W) was used to probe the transient species produced upon laser excitation. The probe beam was focused into the sample (irradiated volume 0.8 cm x 0.8 cm x 0.3 cm) using quartz lenses (100 mm focal length) and subsequently into a monochromator (Bentham TM300). The monochromator had a resolution of 2 nm per millimetre of slit width and was computer controlled.
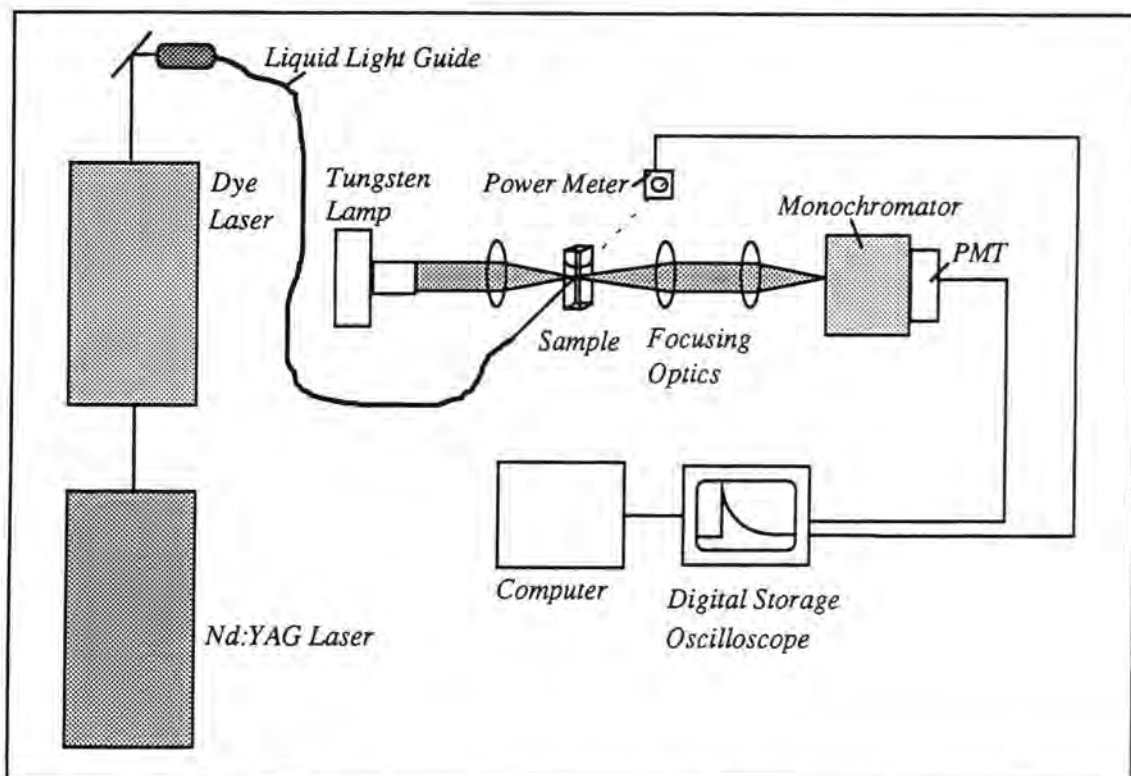
Figure 2.7. Experimental arrangement of flash photolysis apparatus.

The intensity of light detected at a given wavelength was measured by a photomultiplier tube (Hamamatsu R928) with a 250 Ω termination resistor. Transient decays were averaged over at least 32 laser pulses and displayed as voltage readings by a digital storage oscilloscope, DSO (Tektronix TDS 320). The oscilloscope was triggered externally by a signal from a photodiode as the laser was fired. Decays were transferred to a computer where data were converted into absorbance units using Equation 2.8 and analysed using Microsoft Excel and Grafit.

2.1.4.3 Triplet Lifetime Measurements

The rate of decay of triplet state species in solution is given by Equation 2.9, in which k_p represents the rate of phosphorescence emission, k_0, is the intrinsic rate of non-radiative decay of triplet species, $k_{TT}[T_1]$ and $k_{Pc}[Pc]$ are triplet-triplet annihilation and self

quenching terms respectively and the final term accounts for bimolecular quenching by quencher molecules.

$$k_T = k_p + k_0 + k_{TT} [T] + k_{Pc} [Pc] + \sum_i k_Q [Q_i] \qquad (2.9)$$

At room temperature, phosphorescence is negligible and decay is dominated by radiationless deactivation pathways, i.e. terms 2 to 5. By careful control of experimental conditions it is possible to eliminate the third and fifth terms. Triplet-triplet annihilation[13],[14] occurs at high triplet state concentrations and introduces a second order reaction into the decay ($^3Pc^* + {}^3Pc^* \rightarrow {}^1(PcPc^*)$). This phenomenon is caused by high conversion of ground state (S_0) molecules into T_1 states and can be avoided by the use of low laser powers (< 0.5 mJ/pulse) and dilute samples. Samples were thoroughly degassed using the freeze-pump-thaw technique to remove oxygen, the major quenching impurity in phthalocyanine solutions. Thus, term 5, deactivation by extrinsic quenchers, can be ignored. Equation 2.9 is reduced to:

$$k_T = k_0 + k_{Pc} [Pc] \qquad (2.10)$$

It follows that, at any given concentration of phthalocyanine, triplet state deactivation will follow first order kinetics and the rate of decay of T_1 may be determined from a monoexponential fit to experimental data (absorbance vs time). This yields the experimental, or observed, lifetime, τ_T ($\tau_T = 1/k_T$). At high concentrations of phthalocyanine, τ_T may be reduced due to self quenching of triplet species by ground state molecules ($^3Pc^* + Pc_0 \rightarrow Pc_0 + Pc_0 + $ heat). The self quenching rate constant, k_{Pc}, can be determined by measuring the lifetime, τ_T, at various concentrations of phthalocyanine. In this work, reported values of τ_T are uncorrected for self quenching.

Quenching of phthalocyanine triplet states by extrinsic quencher molecules such as oxygen or tetrathiafulvalene (TTF) (Chapter 6) is represented by Equation 2.11 if $[^3Pc]$ $<<$ $[Pc_0]$, i.e. triplet-triplet annihilation can be ignored. The concentration of phthalocyanine was held constant for all samples, thus term 4 of Equation 2.9 may be incorporated into the decay constant, k_0.

$$\frac{1}{\tau_T} = k_T = k_0 + k_Q [Q] \qquad (2.11)$$

The quenching rate constant, k_Q, was determined by monitoring τ_T as a function of quencher concentration, [Q]. k_Q can therefore be calculated from the gradient of a plot of $1/\tau_T$ vs [Q], whilst the intercept gives the triplet lifetime in the absence of quencher molecules.

2.1.4.4 Triplet Extinction Coefficients

At any given wavelength, the observed transient decay is a mixture of two components; triplet state absorption and ground state bleaching. If it is assumed that the concentration of S_0 species bleached upon excitation is equal to the concentration of T_1 species formed, then the observed change in absorbance may be given by Equation 2.12,

$$\Delta A(\lambda) = (\varepsilon_T^*(\lambda) - \varepsilon_s(\lambda))[T_1]l \qquad (2.12)$$

where ε_T^* and ε_s are the triplet and ground state extinction coefficients respectively, [T] is the triplet state concentration and l is the path length (in cm). In this work, triplet state extinction coefficients were determined using the singlet depletion method[15]. It was assumed that at the wavelength of maximum ground state absorption (i.e. 674 nm for $^tBu_4ZnPc$ in MeOH), ε_T was zero and ε_s[16] was 1.8×10^5 mol^{-1} dm^3 cm^{-1}. ΔA may be described by Equation 2.13 and [T_1] calculated.

$$\Delta A_{\lambda_{max}} = -\varepsilon_s [T_1]l \qquad (2.13)$$

For the majority of phthalocyanines the triplet state absorption band lies in a spectral region where ground state absorption is negligible (400 nm - 600 nm) and hence ε_T may be calculated from Equation 2.12.

2.1.4.5 Transient Absorption Spectra

Transient absorption spectra were recorded by measuring ΔA at 5 nm wavelength intervals over the range 400 nm to 800 nm. Decays were analysed using a suitable exponential decay function (either mono- or bi- exponential fits were sufficient). ΔA at t_0, the moment of excitation, and at a time delay, Δt, after excitation was noted. In this way, a transient spectrum, ΔA vs. λ, could be generated and its temporal characteristics determined. Transient spectra were corrected for ground state absorption by adding a fraction of the UV/Visible absorption spectrum of the sample to the measured 'triplet minus singlet' spectrum.

2.1.4.6 Triplet Quantum Yields

Triplet quantum yields were determined using the comparative method[17]. Solutions of the unknown and standard were prepared such that they were optically matched at the excitation wavelength. The quantum yield is defined in Equation 2.14.

$$\Phi_T = \frac{No.\ of\ triplet\ state\ molecules\ formed}{No.\ of\ photons\ absorbed} \qquad (2.14)$$

The unknown and standard solutions have the same optical density, i.e. the number of photons absorbed will be equal, therefore,

$$No.\ of\ Photons\ absorbed \propto \frac{[T]_x}{\Phi_{T_x}} = \frac{[T]_{std}}{\Phi_{T_{std}}} \qquad (2.15)$$

where Φ_T represents the quantum yield of triplet state formation, [T], is the concentration of triplet formed, and x and std refer to the unknown and standard respectively. Rearranging,

$$\Phi_{T_x} = \Phi_{T_{std}} \frac{[T]_x}{[T]_{std}} \qquad (2.16)$$

Using the Beer-Lambert law (Equation 2.1), the final equation, where ε is the extinction coefficient of the excited state and A is the transient absorbance, is obtained (Equation 2.17).

$$\Phi_{T_x} = \Phi_{T_{std}} \frac{A_x \ \varepsilon_{Tstd}}{\varepsilon_{Tx} \ A_{std}} \qquad (2.17)$$

In this study, laser irradiation was carried out at 355 nm, 638 nm or 700 nm using pulse energies of < 0.5 mJ. Benzophenone in acetonitrile (λ_{Tmax} = 525 nm, Φ_T = 1, ε_T = 6250)[3], disulfonated aluminium phthalocyanine in methanol (λ_{Tmax} = 490 nm, Φ_T = 0.22, ε_T = 36000)[18] and zinc phthalocyanine in 1 % pyr/tol (λ_{Tmax} = 490 nm, Φ_T =

0.58, $\varepsilon_T = 36000$)[19] were used as standards. For each sample the power was varied and the change in absorbance of the sample determined by probing at λ_{Tmax}. A_x and A_{std} were obtained from the gradient of a graph of laser power vs ΔA (calculated using Equation 2.8) and substituted into Equation 2.17 to find Φ_T. For samples where large overlap between transient and ground state absorption occurred, e.g. tri and tetra protonated phthalocyanines, Φ_T was measured by monitoring ground state bleaching in preference to triplet state formation. Equation 2.17 was applied, however ε_T was replaced with the singlet extinction coefficient, ε_s.

2.1.5 Singlet Oxygen Phosphorescence Detection
2.1.5.1 Introduction to Singlet Oxygen

Singlet oxygen, $(^1\Delta_g)O_2$, $(^1O_2)$ is generated from phthalocyanine molecules almost exclusively through triplet state quenching by ground state oxygen, $(^3\Sigma_g^-)O_2$, via an encounter complex[20]. $^1\Delta_g$ is assumed to be the only reactive state in solution. This state is far more stable than $^1\Sigma_g^+$ and in gaseous media may have a lifetime of minutes due to the spin forbidden nature of the transition $(^1\Delta_g \rightarrow {}^3\Sigma_g^-)$[21]. Equation 2.18 depicts the expression for the quantum yield of singlet oxygen formation, Φ_Δ.

$$\Phi_\Delta = \Phi_T \frac{k_{\Delta O_2}[O_2]}{(k_{\Delta O_2} + k_{\Sigma O_2})[O_2] + k_{nr} + k_r} \qquad (2.18)$$

where Φ_T is the quantum yield of triplet state formation, $k_{\Delta O_2}$ is the rate of quenching by O_2 to $O_2(^1\Delta_g)$, $k_{\Sigma O_2}$ is the rate of quenching by O_2 to give $O_2(^3\Sigma_g^-)$ and k_{nr} & k_r represent non-radiative and radiative deactivation pathways of T_1 respectively. In most systems quenching by oxygen is very rapid and $(k_{\Delta O_2}+k_{\Sigma O_2}) \gg k_{nr} + k_r$, hence, Equation 2.18 may be simplified to yield Equation 2.19.

$$\Phi_\Delta = \Phi_T \left(\frac{k_{\Delta O_2}}{k_{\Delta O_2} + k_{\Sigma O_2}} \right) \qquad (2.19)$$

The rate terms in brackets represent the fraction of triplet state molecules quenched by ground state oxygen to yield singlet oxygen and is generally represented by S_Δ. Therefore,

$$\Phi_\Delta = \Phi_T S_\Delta \qquad (2.20)$$

Deactivation of singlet oxygen in solution occurs via two pathways: non-radiative decay by transfer of vibrational energy to solvent molecules, and radiative decay in the form of phosphorescence emission at 1269 nm (7882 cm^{-1}). The quantum efficiency of $^1O_2$ phosphorescence emission is generally extremely small ($\Phi_{\Delta r} \sim 10^{-3}$)[22] and deactivation is dominated by non-radiative processes. Both the non-radiative deactivation rate, k_{nr}, and the radiative rate constant, k_r, have been shown to be affected by the chosen solvent. Non-radiative decay pathways are controlled by the ability of surrounding solvent molecules to act as energy sinks by accepting electronic energy from excited oxygen molecules as vibrational energy. Hence, the lifetime of $^1O_2$, τ_Δ, is vastly different in protiated and deuterated solvents[23], e.g. τ_Δ (H_2O) = 4 μs and $\tau_\Delta(D_2O)$ = 68 μs. The lifetime of emission, τ_Δ, is determined by k_r, k_{nr} and molecular quenching rates, k_Q, thus,

$$\frac{1}{\tau_\Delta} = k_r + k_{nr} + \Sigma k_Q [Q] \qquad (2.21)$$

For phthalocyanine dyes, the term $k_Q[Q]$ has been found to be negligible, therefore, $1/\tau_\Delta$ = k_D, where k_D is the sum of radiative and non-radiative decay pathways. The quantum yield of singlet oxygen phosphorescence is given by Equation 2.22.

$$\Phi_{\Delta r} = \Phi_\Delta \left(\frac{k_{\Delta r}}{k_{\Delta r} + k_{\Delta nr}} \right) \qquad (2.22)$$

$^1O_2(^1\Delta_g)$ may be detected using chemical traps or quenchers such as tryptophan or cholesterol[24]; however, complications can arise due to lack of solubility in the system under study or reaction between the added species and sensitiser molecules. Around 1979, direct detection of the phosphorescence from singlet oxygen ($^1\Delta_g \rightarrow {}^3\Sigma_g^-$) at 1270 nm was made possible through the use of a highly sensitive, large area germanium photodiode coupled to a transient digitiser[25]. This provides a convenient and reliable method for measuring the properties of $^1O_2$ and is the method adopted in this study.

2.1.5.2 Experimental Methods

Singlet oxygen lifetimes and yields were determined using the experimental arrangement depicted in Figure 2.8. A frequency tripled Nd:YAG laser was used as an excitation source (λ = 355 nm, 10 ns pulse, < 1 mJ per pulse). Luminescence at 1270 nm was detected using a germanium photodiode (North Coast E0-817P) and amplifier combination. A spherical mirror (Comar Instruments, 50 mm diameter, 50 mm focal length) was used to maximise luminescence reaching the detector. To reduce noise, the detector was cooled to 77 K with liquid nitrogen. Radiation from the sample was passed

through a 1% bandpass interference filter (1270 nm) before reaching the Ge detector. Electronic signals were passed into a digital storage oscilloscope (Tektronix TDS 320) and averaged over 16 laser shots. A typical signal is shown in Figure 2.9.
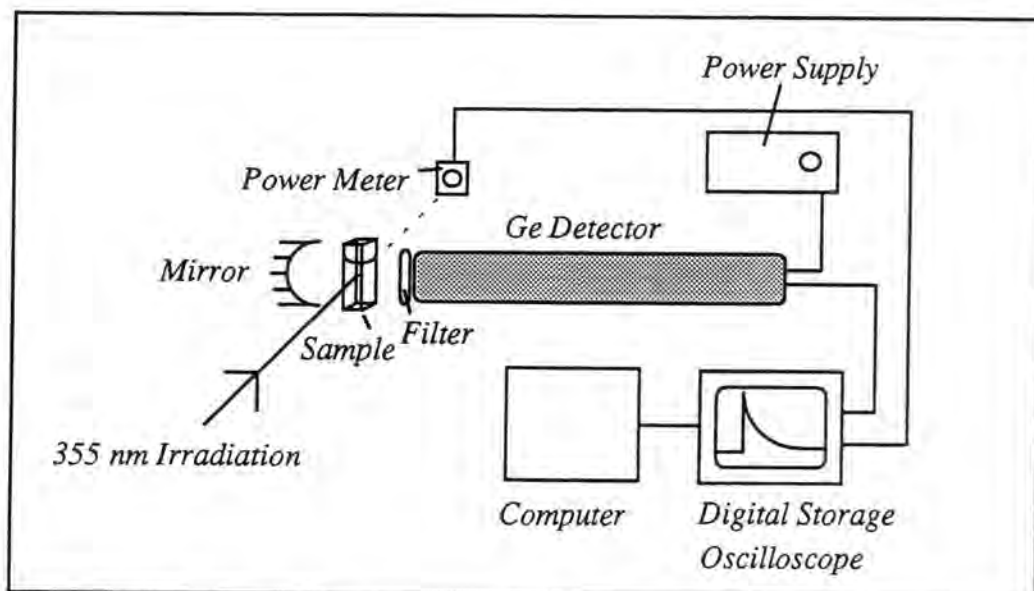
Figure 2.8. Experimental arrangement for singlet oxygen measurements.
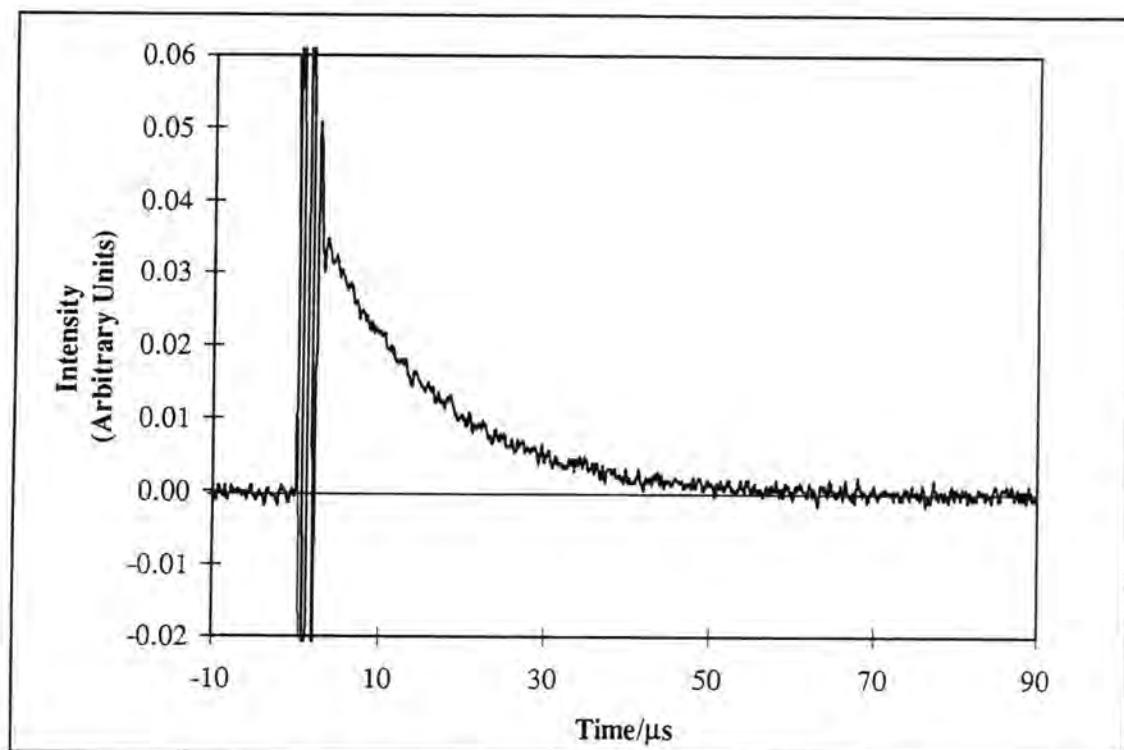
Figure 2.9. Typical $^1O_2$ decay (Sensitiser: ZnPc(CHMeCO$_2$H)$_4$, Solvent: EtOH).

The large spike at the start of the trace has been shown to be sensitiser fluorescence transmitted by the filter used to select 1269 nm light[26]. This is particularly important for

red emitting dyes such as phthalocyanines and, under certain experimental conditions, may cause saturation of the DSO amplifier (See Appendix A and Reference 26). An electronic switch has been developed to eliminate these effects[27]. This problem was not so acute when a Tektronix TDS 320 oscilloscope was employed, therefore, in this work, use of the switch was not required. Data was transferred to a computer and manipulated using a curve fitting package (Grafit). The lifetime of emission could be found directly by fitting a single exponential decay to the data (rate of decay (k) equals $1/\tau_\Delta$). Quantum yields were determined by comparison with reference compounds. Samples of the unknown and standard were prepared such that the absorbance at the excitation wavelength was similar (~ 0.3). In this work, Rose Bengal in EtOH ($\Phi_\Delta = 0.86$), MeOH or 1% Triton X-100/phosphate buffer saline ($\Phi_\Delta = 0.75$) and tetraphenylporphyrin in 1% pyridine/toluene solution ($\Phi_\Delta = 0.8$) or chloroform ($\Phi_\Delta = 0.55$) were used as standards[28]. The intensity of the emission was measured as a function of laser power for the unknown and the standard, and the gradients, I, compared using Equation 2.23.

$$\Phi_{\Delta_x} = \Phi_{\Delta_{std}} \frac{A_{std}}{A_x} \frac{I_x}{I_{std}} \qquad (2.23)$$

A is the absorbance of the solution at the excitation wavelength and std and x refer to the standard and unknown respectively. It is important that the unknown and reference compound are used in the same solvent due to the large dependence of k_{nr} and k_r solvent properties.

2.1.6 Low Temperature Measurements

Low temperature measurements were performed in ether-pentane-alcohol 5:5:2 (EPA) solution or 100 % ethanol, cooled to 77 K using a liquid nitrogen cooled cryostat (Oxford Instruments, DN 1704). Intermediate temperatures were obtained using a temperature controller (Oxford Instruments, Intelligent Instrument Controller, ITC 4). Samples were allowed to equilibrate for at least 30 minutes at each temperature. UV/Visible, fluorescence and flash photolysis spectrometers were adapted to accommodate the cryostat.

2.1.7 Diffuse Reflectance Spectroscopy[29],[30]
2.1.7.1 Theory
2.1.7.1.1 Reflection

Diffuse reflectance spectroscopy has been used since the early 1920's as a means of measuring the optical properties of heterogeneous and solid samples. Due to the inherent opacity of these substances, transmission measurements are impractical, thus techniques have been developed to obtain information via detection of radiation scattered from the surface of the sample. Reflection from matt surfaces has been shown to consist of two components, specular or regular reflection, and diffuse reflection. Specular reflection is well known and occurs from highly polished or mirrored surfaces. Its behaviour is governed by Snell's Law (Equation 2.24), which defines the <u>direction</u> of reflected and transmitted beams of radiation, and Fresnel's equations[31] from which Equations 2.25 and 2.26 are obtained. These determine the <u>relative intensities</u> of each polarised component of reflected light.

$$\text{Snell's Law:} \qquad sin\theta_i = sin\theta_r \ \ and \ \ n_1 \, sin\theta_i = n_2 \, sin\theta_t \qquad (2.24)$$

where n_1 and n_2 are the refractive index values of each medium, θ_i is the angle of incidence, θ_t is the angle of the transmitted beam and θ_r is the angle of the reflected radiation.

$$R_{II} = \left[\frac{n^2 \, cos\theta_i - [\, n^2 - sin^2\theta_i \,]^{1/2}}{n^2 \, cos\theta_i + [\, n^2 - sin^2\theta_i \,]^{1/2}} \right]^2 \qquad (2.25)$$

$$R_\perp = \left[\frac{cos\theta_i - [\, n^2 - sin^2\theta_i \,]^{1/2}}{cos\theta_i + [\, n^2 - sin^2\theta_i \,]^{1/2}} \right]^2 \qquad (2.26)$$

where R_{II} is the intensity of reflected parallel polarised light, $R_\perp$ is the intensity of reflected perpendicularly polarised light and n is the relative index of refraction (n_2/n_1).

It should be noted that the proportion of specular reflection depends on both the angle of incidence, θ_i, and on the polarisation of the incident radiation. Reflected radiation retains the polarisation characteristics of the incident beam and is detected at a defined angle, θ_r, equal to θ_i (Figure 2.10). For natural light, the total reflected radiation is given by R_{Spec} = $(R_{II} + R_\perp)/2$ which, in the case of normal incidence, yields

$$R_{Spec} = \left[\frac{n-1}{n+1}\right]^2 \qquad (2.27)$$

If the reflecting surface absorbs at the wavelength of irradiation, attenuation occurs according to Lamberts law (Equation 2.28).

$$I = I_0 e^{-\alpha x} \qquad (2.28)$$

where α, the absorption coefficient, is related to the absorption index of the medium, κ by:

$$\alpha = \frac{4\pi\kappa}{\lambda} \qquad (2.29)$$

Equation 2.27 now becomes[29]:

$$R_{spec} = \frac{(n-1)^2 + (n\kappa)^2}{(n+1)^2 + (n\kappa)^2} \qquad (2.30)$$

which predicts that as the absorbance increases, the yield of specular reflection will also increase.
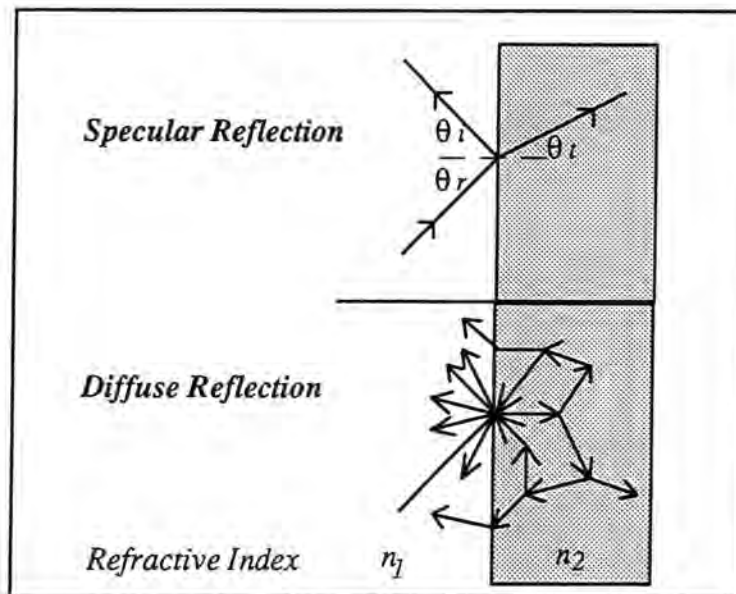
Figure 2.10. Specular and diffuse reflection.

Diffuse reflection occurs as a result of multiple scattering and absorption of an incident beam by individual sample particles. In contrast to specular reflection, diffuse reflection is unpolarised, isotropically distributed at all angles of observation, and independent of the angle of incidence or polarisation of the incident light (Figure 10). It has been observed to be affected by the particle size and absorbing power of a reflecting sample. Several theories have been proposed to account for these phenomena, however, the most commonly adopted is that proposed by Kubelka and Munk based on differential equations[29].
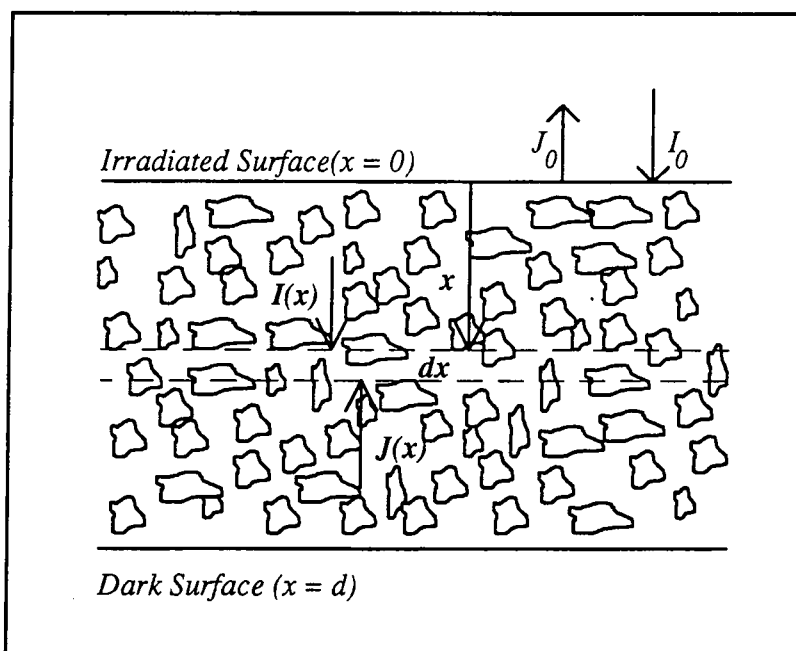
Figure 2.11. Parameters for Kubelka-Munk theory.

If one considers light of intensity, I_0, falling on a sample of randomly distributed absorbers (Figure 2.11), the flux intensity will decrease as the radiation passes a distance, x, through the medium (Equation 2.31). By comparison, the intensity of the reflected light flux, J, will increase as further scattering occurs (Equation 2.32).

$$dI(x) = -I(x)(K+S)dx + J(x)Sdx \qquad (2.31)$$

$$dJ(x) = J(x)(K+S)dx - I(x)Sdx \qquad (2.32)$$

K and S are the absorption and scattering coefficients respectively of the medium with units cm^{-1}. For an ideal diffuser, $K = \alpha = 2\varepsilon c$, where ε is the Naperian extinction coefficient (mol dm^{-3} cm^{-1}) and c is the concentration (mol dm^{-3}). The factor 2 accounts for the increased average distance travelled by light due to scattering. Equations 2.31 and 2.32 consider only the case where irradiation is perpendicular to the surface,

however, the error introduced by this approximation is small when compared with the overall assumption of ideal diffuse reflection. In addition, these equations hold strictly only for samples irradiated by diffuse light. In practise, many experimental arrangements use a directed light source and the theory remains valid for an incident angle of 60°. Using Equation 2.33 for the diffuse reflectance, R, and the integral solutions of Equations 2.31 and 2.32 for a layer of thickness d, it can be shown (References 29 and 30) that the diffuse reflectance is given by Equation 2.34.

$$R = \frac{J_0}{I_0} \qquad (2.33)$$

$$R = \frac{\sinh(bS_d)}{a\sinh(bS_d) + b\cosh(bS_d)} \text{ where } a = \frac{K+S}{S} \text{ and } b = (a^2-1)^{1/2}$$
$$(2.34)$$

In the special case of infinite layer thickness or 'optically thick' samples, $d \rightarrow \infty$, and the diffuse reflectance is given by the more useful Equation 2.35.

$$F(R) = \frac{K}{S} = \frac{(1-R_\infty)^2}{2R_\infty} \qquad (2.35)$$

For a sample whose scattering coefficient is independent of wavelength, F(R) is termed the remission function and represents the absorption spectrum determined by transmission spectroscopy. In practise, many differences may occur due to the assumptions made by Kubelka-Munk theory. The over-riding assumption of this theory is that of ideal diffuse reflection. Samples are supposed to consist of randomly distributed absorbers with a particle size far smaller than the thickness of the layer and to have infinite lateral dimension in order that edge effects may be neglected. Contributions due to specular reflection are ignored and though this is acceptable (but not strictly true) for weakly absorbing samples, as the absorbance (κ and K) increases, contributions due to specular reflection increase (Equation 2.30) whilst those due to diffuse reflection decrease (Equation 2.34). Therefore, for strongly absorbing samples it becomes unrealistic to discount specular reflection. Remission functions measured under these conditions will underestimate the absorbance of a sample. Indeed, a paradoxical situation may occur where concentrated solutions will appear to absorb less than their dilute partners. This is a consequence of differences in the mean depth, d, travelled by radiation through the medium. Light incident on a sample of weakly absorbing molecules will penetrate deeply and, hence, may be absorbed more efficiently than in a

62

concentrated sample where the penetration depth is small and large quantities of specular reflection occur. In addition, derivation of Equation 2.35 assumes that K and S are independent of x. This is true for a homogeneous sample of absorbers, however, when the concentration or absorbance of molecules changes with penetration depth a different analysis is required. This is discussed below for the case of transient formation upon laser excitation.

2.1.7.1.2 Diffuse Reflectance Flash Photolysis

Diffuse reflectance flash photolysis has been pioneered by Frank Wilkinson and his group at Loughborough[32],[33]. The group recognised that the concentration of transient species produced by flash photolysis will decrease as incident radiation is absorbed on travelling through the sample. Therefore, the assumption of Kubelka-Munk theory that K is independent of x is no longer valid. It can be shown that the concentration of species produced by laser excitation falls off exponentially with penetration depth[34]. Modifications to Kubelka-Munk theory are therefore required. Lin and Kan[35] have solved Equations 2.31 and 2.32 for the case where K varies exponentially with x at an analysing wavelength, a (Equation 2.36).

$$R^a = R_B^a \left[\frac{1 + \frac{\gamma}{\delta}u + \frac{\gamma(\gamma+1)u^2}{\delta(\delta+1)2!} + \dots}{1 + \frac{\gamma+1}{\delta}u + \frac{(\gamma+1)(\gamma+2)u^2}{\delta(\delta+1)2!} + \dots} \right] \qquad (2.36)$$

where R^a_B is the background reflectance at the analysing wavelength, $\gamma = (b_e R_B^a)^{-1}$,

$\delta = \frac{(\gamma + 1 - R_B^a)}{b_e}$, $u = \frac{2K^a_T(0)}{b_e S}$ where K^a_T is the absorption coefficient of the

transient species at the analysing wavelength, and $b_e = \frac{[K_e^2 + 2K_e S]^{1/2}}{S}$ where K_e is

the absorption coefficient of the ground state at the excitation wavelength.

In diffuse reflectance flash photolysis experiments, the measured quantity is given by Equation 2.37.

$$\frac{[R_B^a - R^a(t)]}{R_B^a} = 1 - R_T^a \qquad (2.37)$$

where R^a_B and $R^a(t)$ represent the reflectance before and after excitation respectively and R^a_T is the relative transient reflectance. Kessler et al. have shown[36] by substitution of typical values of S (5 - 500 cm^{-1}), R^a_B (0.7 - 0.95) and K^a_T (0.1 - 10 cm^{-1}) into Equation 2.36 that for 1-R^a_T < 0.1, 1-R^a_T is linearly dependent on [T]. Assuming a unimolecular reaction, decay lifetimes may be determined by fitting a monoexponential curve to 1-R^a_T vs time. In bimolecular reactions, for example, triplet-triplet annihilation, no simple kinetic analysis is possible.

For the purposes of this study it was assumed that an exponential decrease of triplet species occurred within the sample, i.e. 1 - R^a_T α [T]. If the sample concentration is low, or the laser power is high, complete sample conversion may occur at the surface. For this situation, the plug model must be considered. Under these conditions, Equation 2.35 is valid and hence, 1-R_T is proportional to [T]$^{1/2}$. This will not be discussed in detail here and the reader is referred to Reference 34 for more information.

2.1.7.2 Experimental
2.1.7.2.1 Sample Preparation

Substrates (cellulose, filter paper or silica) were dried for 24 h in an oven at 100 °C prior to use. Bovine serum albumin was used as received. Solutions of phthalocyanine in ether, ethanol or methanol were mixed thoroughly with a known weight of substrate. Solvent was removed under vacuum with intermittent stirring of the sample until completely dry. A phthalocyanine/substrate weighting of ~ 50 μg g^{-1} for remission function and transient absorption measurements and ~ 6 μg g^{-1} for fluorescence measurements was used.

2.1.7.2.2 Remission Function Measurements

The remission function, F(R), was determined using an adapted Perkin Elmer LS50B spectrometer. The optimum arrangement permitted the sample to be irradiated at 60° as required by Kubelka-Munk theory and enabled maximum collection of diffuse reflection whilst minimising contributions due to specular reflection. Reflectance spectra were recorded by performing an average of ten synchronous scans over the wavelength range 300 nm to 750 nm. Spectra were performed for substrate (R$_{substrate}$) and sample

(R_{sample}) and executed using a neutral density filter in the emission beam and 5 nm slit widths.

F(R) was calculated using Equation 2.35 where,

$$R_\infty = \frac{R_{sample}}{R_{substrate}} \qquad (2.38)$$

Calculation of the remission function using clean substrate as a reference compensates for any effects that the substrate may have on contributions to the signal resulting from specular reflection.

2.1.7.2.3 Fluorescence Measurements

Fluorescence measurements were carried out using the sample arrangement employed for remission function measurements. Emission scans were performed using slit widths of 10 nm and 5 nm for excitation and emission monochromators respectively, a scan speed of 120 nm min^{-1} and an excitation wavelength of 610 nm. Excitation spectra were obtained by monitoring emission at 760 nm (Slits: 5 nm and 10 nm (excitation and emission respectively), Scan speed: 60 nm min^{-1}).

2.1.7.2.4 Flash Photolysis

Diffuse reflectance flash photolysis was carried out using the experimental arrangement depicted in Figure 2.12. 355 nm radiation from a frequency tripled Nd:YAG laser (Spectra Physics, Quanta Ray GCR-150-10, 10 ns pulse, < 1 mJ per pulse) was used to excite the sample at 60° to the normal. In this way, focusing of specular reflection into the collection optics was avoided. A xenon lamp (Bentham 605) and filter combination (420 nm cutoff filter (Schott glass-GG420, Comar Instruments, UK) and VO^{2+}(aq) chemical filter) was used as a probe beam. Diffuse reflection from the sample was focused into a monochromator (Bentham TM300) and detected using a photomultiplier tube, PMT (Hamamatsu R928). Decays were recorded using a digital storage oscilloscope (Tektronix TDS 320) and transferred to a computer for analysis. Decays were fitted to exponential kinetics using, Grafit, a curve fitting package.
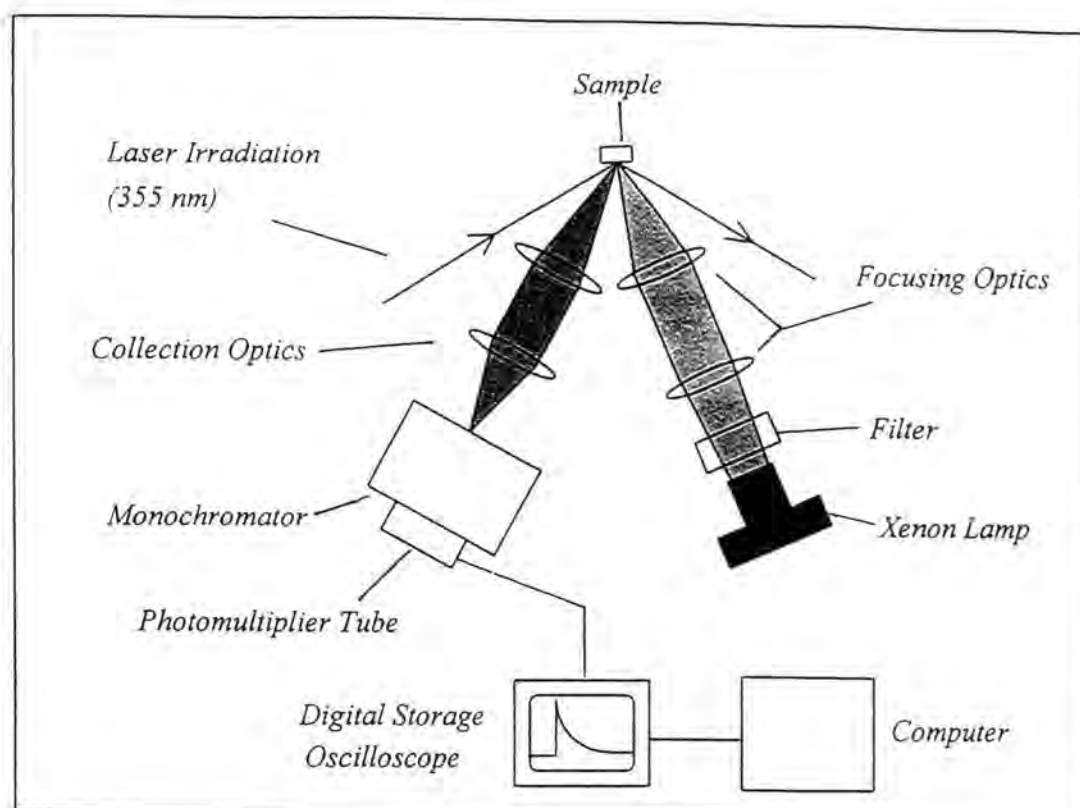
Figure 2.12. Diffuse reflectance flash photolysis: Experimental arrangement.

2.2 Synthesis

2.2.1 Synthesis of Substituted Zinc Phthalocyanines

Figure 2.13 shows the synthetic scheme followed in the preparation of $ZnPc(CMe(CO_2Me)_2)_4$ and $ZnPc(CHMeCO_2H)_4$. Compounds **2**, **3** and **4** were prepared following the literature method of Roze *et al.*[37].

i) **Dimethyl 3,4 dicyanophenylmalonate (2)**[37]. Nitrophthalonitrile, **1** (Acros, 7.53 g), K_2CO_3 (Fison, purity 99%, 3.76 g), tetrabutylammonium bromide (Kodak, 1.04 g) and dimethylmalonate (Aldrich, purity 97%, 10.06 ml) were placed in a round bottom flask with a magnetic flea. Dimethylformamide (DMF - Aldrich, HPLC Grade, 80 ml) was added with stirring and the flask purged with nitrogen. The solution was stirred at 50 °C for 24 hr. Further aliquots of K_2CO_3 (5 g) were added at six and twelve hour intervals. The resulting mixture was then poured onto ice, and the precipitate obtained separated and dried. Purification was achieved by chromatography using a silica column with dichloromethane (CH_2Cl_2 - BDH, Analar Grade) as eluent and drying under high vacuum - yield = 69 %.

$IR(v_{max} /cm^{-1})$: 1730 and 1749 (C=O), 2239 (CN), 2956 (CH).

δ_H(250 MHz; CDCl$_3$): 3.79 (s, 6H, CO$_2$CH$_3$), 4.74 (s, 1H, CH), 7.81-7.91 (m, 3H, ArH)
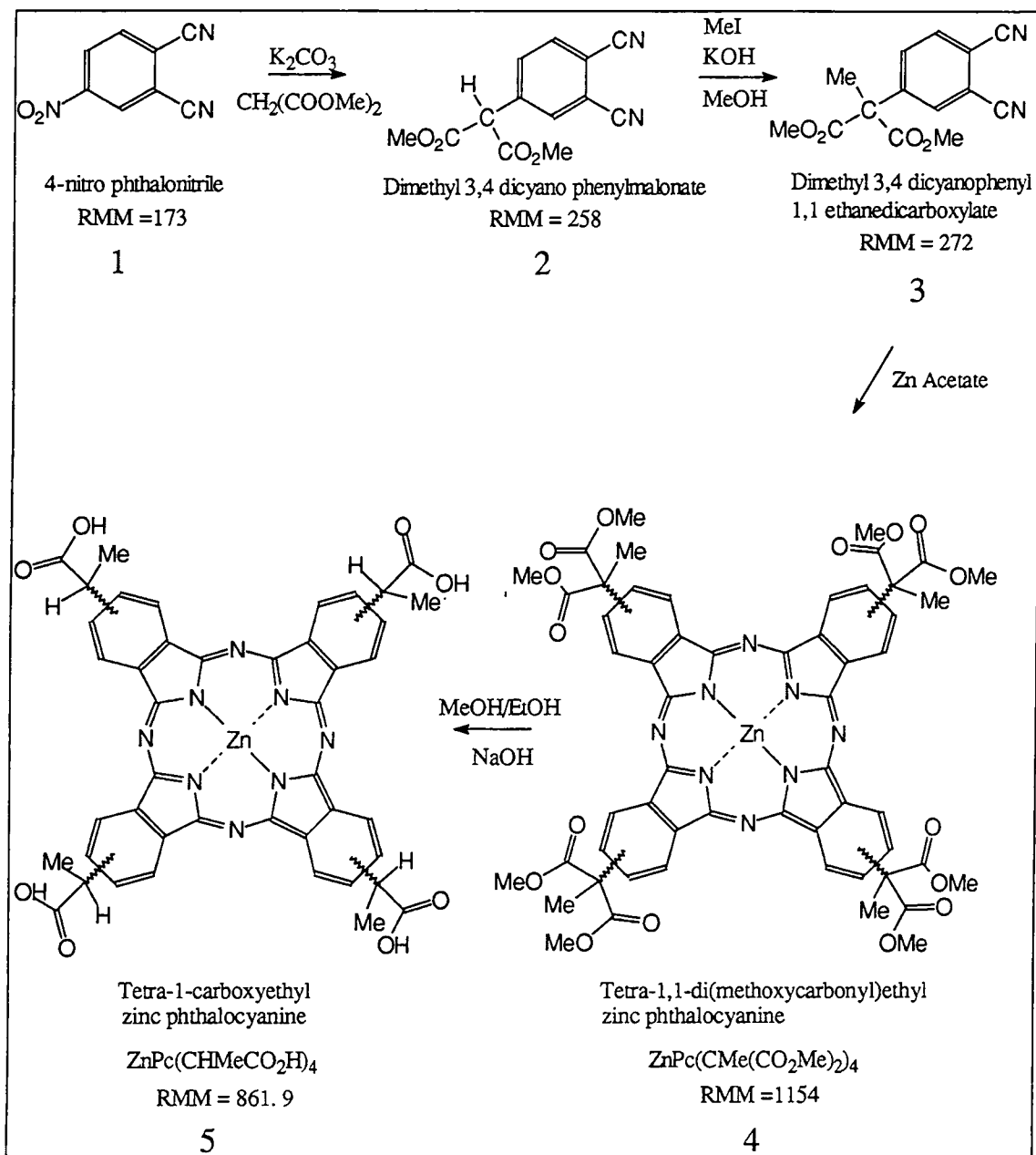
Figure 2.13. Synthetic scheme for production of acid and ester substituted zinc phthalocyanine.

ii) Dimethyl 3,4 dicyanophenyl 1,1 ethane dicarboxylate (3)[37]. Compound 2 (2.15 g), KOH (0.47 g) and MeI (Aldrich, 10 ml) were refluxed in methanol (50 ml) at 50 °C for three hours. Additional aliquots of KOH (0.24 g) and MeI (10 ml) were added and the solution refluxed for a further hour. Following this, the condenser was removed and heating was continued for one hour to remove excess MeI. MeOH was removed in vacuo and crude product separated by solvent extraction from water into CH$_2$Cl$_2$ (3 x 50

ml), to yield an oil which was purified by column chromatography on silica using CH_2Cl_2 as eluent. **3** was obtained as an oily solid after evaporation. Yield = 49 %.

IR(v_{max} /cm^{-1}): 1727 (C=O), 2237 (CN), 2954 and 2997 (CH).

δ_H(250 MHz; CDCl$_3$): 1.90 (s, 3H, C$\underline{H}_3$), 3.80 (s, 6H, CO$_2$C$\underline{H}_3$), 7.76-7.87 (m, 3H, Ar$\underline{H}$)

iii) Tetra-1,1-di(methoxycarbonyl)ethyl zinc phthalocyanine (4)[37].

Compound **3** (250 mg) was crushed with zinc acetate (Aldrich, purity 99.99 %, 250 mg) and heated under an inert atmosphere to 200 °C for six hours. Product was purified by chromatography on silica using 3 % MeOH:CH$_2$Cl$_2$ as eluent and dried in a desiccator under vacuum. Yield = 30 %.

IR (v_{max} /cm^{-1}): 1721 (C=O)

Elemental Analysis: Found %: C, 58.03; H, 4.14; N, 9.41; Zn, 4.19. Calculated %: C, 58.3; H, 4.2; N, 9.7; Zn, 5.66.

UV/Vis (CHCl$_3$, λ_{max} /nm (log ε)): 347 (4.78), 611 (4.37), 677 (5.16)

iv) Tetra-1-carboxyethyl zinc phthalocyanine (5).

Compound **4** was converted into the tetra acid substituted phthalocyanine (**5**) using the method of Kahl and Li[38]. **4** was dissolved in MeOH (20 ml), sodium hydroxide (NaOH) in ethanol (20 ml, ~ 0.15 mol dm^{-3}) was added and the reactants heated under reflux for six hours. The solution was concentrated under vacuum, dissolved in water and filtered to remove insoluble particles. Acidification using hydrochloric acid (HCl, 0.1 mol dm^{-3}), yielded a precipitate which was separated by centrifugation and washed with distilled water (3 x 20 ml). The product was dried under vacuum to yield a blue solid. Yield = 79 %.

IR (v_{max} /cm^{-1}): 2900 (OH), 1700 (C=O)

δ_H(250 MHz; DMSO) 1.90 (d, 3H, C$\underline{H}_3$), 4.45-4.49 (m, 1H, C$\underline{H}$), 8.18-8.22 (m, 1H, Ar$\underline{H}$), 9.24-9.27 (m, 2H, Ar$\underline{H}$).

Elemental Analysis: Found %: C, 55.94; H, 3.68; N, 11.35; Zn, 5.63. Calculated %: C, 61; H, 3.72; N, 12.93; Zn, 7.55.

UV/Vis (CHCl$_3$, λ_{max} /nm (log ε)): 349 (4.65), 610 (4.38), 673 (5.15)

2.2.2 Metallation of $H_2(BuO)_8Pc$ and $H_2(C_{16}H_{34})_8Pc$

Zinc derivatives of $H_2(BuO)_8Pc$ and $H_2(C_{16}H_{34})_8Pc$ were prepared by refluxing with excess zinc acetate in 1% pyridine/toluene solution for six hours[39]. Aqueous HCl was added to remove unreacted zinc acetate. The aqueous phase was removed and the organic layer washed with distilled water several times. The organic fraction was retained, dried with MgSO$_4$ and filtered. Solvent was removed under reduced pressure,

the product passed through a silica column using dichloromethane as eluent and dried under vacuum.

2.3 References

[1]   Dhami S., De Mello A.J., Rumbles G., Bishop S.M., Phillips D. and Beeby A., Phthalocyanine fluorescence at high concentration: Dimers or reabsorption effect?, *Photochem. Photobiol.*, **61**, 341-346, 1995.

[2]   Williams A.T.R., Winfield S.A. and Miller J.N., Relative fluorescence quantum yields using a computer controlled luminescence spectrometer., *Analyst*, **108**, 1067-1071, 1983.

[3]   Murov S.L., Carmichael I. and Hug G.L., *Handbook of Photochemistry*, Marcel Dekker, Inc., 2nd Edn., New York, 1993.

[4]   Vincett P.S., Voight E.M., Rieckhoff K.E., Phosphorescence and fluorescence of phthalocyanines., *J. Chem. Phys.*, **55**, 4131, 1971.

[5]   O'Connor D.V. and Phillips D., *Time Correlated Single Photon Counting*, Academic Press, London, 1984.

[6]   Birch D.J.S. and Imhof R.E. in *Topics in Fluorescence Spectroscopy*, Vol. 1: Techniques, Ed. Lakowicz J.R., Plenum Press, New York, pp1-95, 1991.

[7]   Janot J.M., Beeby A., Bayley P.M. and Phillips D., Preparative, analytical and fluorescence spectroscopic studies of sulphonated aluminum phthalocyanine sensitisers., *Biophys. Chem.*, **41**, 272, 1991.

[8]   Porter G. and Norrish R.G.W., Chemical reactions produced by very high light intensities., *Nature*, **154**, 658, 1949.

[9]   Patterson L. and Porter G., Lasers in photochemical kinetics., *Chem. Br.*, **6**, 246, 1970.

[10]   Andrae I., Bringhen A., Bohm F., Gonzenbach H., Hill T., Mulroy L and Truscott T.G., A UVA filter (4-tert-butyl-4'-methoxydibenzoylmethane): photoprotection reflects photophysical properties., *J. Photochem. Photobiol. B:Biol.*, **37**, 147, 1997.

[11]   De la Tosa F.F., Laser flash photolysis studies of electron transfer in Complex III from yeast mitochondria., *J. Photochem. Photobiol. B:Biol.*, **38**, 184, 1997.

[12]   Boch R., Mohtat N., Lear Y., Arnason J.T., Durst T. and Scaiano J.C., Study of photoinduced energy and electron transfer in α-terthienyl-bovine serum albumin conjugates: A laser flash photolysis study., *Photochem. Photobiol.*, **64**, 92, 1996.

[13]   Frink M.E. and Ferraudi G.J., Excimer formation in triplet-triplet annihilation reactions of the lowest lying triplet excited state in aluminum(III), silicon(IV) and metal-free phthalocyanines - medium and magnetic field effects on the rate of reaction., *Chem. Phys. Lett.*, **124**, 576-578, 1986.

[14]   Ohno T., Kato S., Yamada A. and Tanno T., Electron transfer reactions of the photoexcited triplet state of chloroaluminium phthalocyanine with aromatic amines, benzoquinones and coordination compounds of iron(II) and iron(III)., *J. Phys. Chem.*, **87**, 775-781, 1983.

[15]   Carmichael I. and Hug G.L., Triplet-triplet absorption spectra of organic molecules in condensed phases., *J. Phys. Chem. Ref. Data*, **15**, 1, 1986.

[16]   Simpson M.S.C., Beeby A., Bishop S.M., MacRobert A.J., Parker A.W. and Phillips D., Time resolved laser spectroscopy in biochemistry III., *S.P.I.E.*, **1640**, 520, 1992.

[17]   Amand B. and Bensasson R., Determination of triplet quantum yields by laser flash absorption spectroscopy., *Chem. Phys. Lett.*, **34**, 44, 1975.

[18]   Foley M.S.C., The photophysics of sulphonated aluminium phthalocyanines as sensitisers for photodynamic therapy., *PhD Thesis*, Imperial College, London, 1994.

[19]   Dhami S., Photophysics of phthalocyanines in microheterogeneous systems., p58, *PhD Thesis*, Imperial College, London, 1996.

[20]   Turro N.J., *Modern Molecular Photochemistry*, p583, University Science Press, California, 1991.

[21]   Badger R.M., Wright A.C. and Whitlock R.F., Absolute intensities of the discrete and continuous absorption bands of oxygen gas at 1.26 and 1.065μ and the radiative lifetime of the $^1\Delta_g$ state of oxygen., *J. Phys. Chem.*, **43**, 4345, 1965.

[22]   Krasnovsky A.A., Quantum yield of photosensitised luminescence and radiative lifetime of singlet ($^1\Delta_g$) molecular oxygen in solution., *Chem. Phys. Lett.*, **81**, 443, 1981.

[23]   Losev A.P., Nichiporovich I.N., Byteva I.M., Drozdov N.N. and Aljghgami I.F., The perturbing effect of solvents on the luminescence rate constant of singlet molecular oxygen., *Chem. Phys. Lett.*, **181**, 45, 1991.

[24]   Bensasson R.V., Land E.J. and Truscott T.G., *Excited States and Free Radicals in Biology and Medicine.*, p118, Oxford University Press, New York, 1993.

[25]   Byteva I.M. and Gurinovich G.P., Sensitised luminescence of oxygen in solutions., *J. Lumin.*, **21**, 17, 1979.

[26]   Oldham T.C., Spectroscopic investigations of photodynamic mechanisms in cell cultures., p85, *PhD Thesis*, Imperial College, 1996.

[27]   Beeby A., Parker A.W. and Stanley C.F., Elimination of fluorescence contributions to singlet oxygen measurements using a novel electronic switch., *J. Photochem. Photobiol. B:Biol.*, **37**, 267, 1997.

[28]   Wilkinson F., Helman W.P., Ross A.B., Quantum yields for the photosensitised formation of the lowest electronically excited singlet state of molecular oxygen in solution., *J. Phys. Chem. Ref. Data*, **22**, 113, 1993.

[29]   Wendlandt W.W.M. and Hecht H.G., *Reflectance Spectroscopy*, John Wiley and Sons, New York, 1966.

[30]   Wilkinson F. and Kelly G., Diffuse Reflectance Flash Photolysis in Scaiano J.C., *Handbook of Organic Photochemistry*, CRC Press, Florida, **1**, p293, 1989.

[31]   Harrick N.J., Total internal reflection and its application to surface studies., *Ann. N.Y. Acad. Sci.*, **101**, 928, 1963.

[32]   Kessler R.W. and Wilkinson F., Diffuse reflectance triplet-triplet absorption spectroscopy of aromatic hydrocarbons chemisorbed on γ-alumina., *J. Chem. Soc. Faraday Trans. 1*, **77**, 309, 1981.

[33]   Wilkinson F., Leicester P.A., Ferreira L.F.V. and Freire V.M.M.R., Photochemistry on surfaces: triplet-triplet energy transfer on microcrystalline cellulose studied by diffuse reflectance transient absorption and emission spectroscopy., *Photochem. Photobiol.*, **54**, 599, 1991.

[34]   Oelkrug D., Honnen W., Wilkinson F. and Willsher C.J., Modelling of transient production and decay following laser excitation of opaque materials., *J. Chem. Soc., Faraday Trans. 2.*, **83**, 2081, 1987.

[35]   Lin T. and Kan H.K.A., Calculation of reflectance of a light diffuser with non-uniform absorption., *J. Opt. Soc. Am.*, **38**, 448, 1948.

[36]   Kessler R.W., Krabichler G., Uhl S., Oelkrug D., Hagen W.P., Hyslop J. and Wilkinson F., Transient decay following pulse excitation of diffuse scattering samples., *Opt. Acta*, **30**, 1099, 1983.

[37]   Roze M.P., Berzin'sh E.L. and Neiland O.Y., Synthesis of 3,4 Dicyanophenylmalonic esters and their use in the production of soluble phthalocyanines., *Z. Org. Khim.*, **28**, 827, 1992.

[38]   Kahl S.B. and Li J., Synthesis and characterisation of a boronated metallocyanine for boron neutron capture theory., *Inorg. Chem.*, **35**, 3878, 1996.

[39]   Cook M.J., Chambrier I., Cracknell S.J., Mayes D.A. and Russel D.A., Octaalkyl zinc phthalocyanines: Potential photosensitisers for use in the photodynamic therapy of cancer., *Photochem. Photobiol.*, **62**, 542, 1995.

CHAPTER 3
PROPERTIES OF NOVEL PHTHALOCYANINE
SENSITISERS

3.1 Introduction

Zinc phthalocyanine (ZnPc) has proved to be an efficient sensitiser for photodynamic therapy[1]. Use of zinc as the central metal ion results in high quantum yields of triplet state[2] and singlet oxygen formation. It has been shown to be effective at destroying neoplastic cells in mice[3] and exhibits a high uptake by tumours[4]. One of the drawbacks of unsubstituted ZnPc, however, is very low solubility in both aqueous and organic solvents. This precludes direct injection of therapeutic quantities into the bloodstream and hinders both *in vitro* and *in vivo* studies.

One method used to improve the solubility of phthalocyanines is to incorporate substituents onto the peripheral benzene rings[5]. Pendant groups such as alkyl chains[6], esters[7], ethers[8], amides[9] and alkoxy[10] substituents have been shown to render phthalocyanines soluble in many organic solvents whilst hydrophilic sulfonic acid substituents[11] allow aqueous solutions to be prepared. In addition to improving solubility, the nature of peripheral substitution affects the cytotoxicity and selectivity of the sensitiser. Ben-Hur[12] and Allen[13] found that anti-viral activity of ZnPc was inversely proportional to the number of sulfonate substituents whilst a study by Zimmermann[14] revealed that cationic side chains such as trimethylammonium (Me_3N^+) groups induce selective photosensitisation of mitochondria. Rosenthal *et al.*[15] have shown that sulfonate groups have no effect on the photophysical properties of ZnPc. Similarly, although the absorption spectrum of 1,4,8,11,15,18,22,25-octabutoxy zinc phthalocyanine was red shifted with respect to the parent molecule[16], the yield of triplet state formation was essentially unaffected. Interestingly, although 1,4,8,11,15,18,22,25-octadecyl zinc phthalocyanine exhibits a smaller shift in the $S_1 \leftarrow S_0$ transition than the octabutoxy substituted phthalocyanine, $C_{10}H_{21}-$ chains induce significant changes in the triplet yield relative to unsubstituted zinc phthalocyanine[17]. Clearly, control over substituents of the phthalocyanine ring is an important means of influencing both the photophysical and physiological properties of phthalocyanines *in vitro* and *in vivo*.

As an alternative to modification of the phthalocyanine ring, hydrophobic sensitisers may be incorporated into delivery vehicles such as liposomes[18]. These allow systemic injection to the bloodstream where association with proteins is believed to occur[19]. The proteins act as carriers to deliver sensitisers to lipophilic sites in tumour tissue, where they accumulate. It is therefore important to determine the effect of micellar and solid state media on the photophysics of any potential sensitisers.

The photophysical properties of a sensitiser are the core of photodynamic therapy and determine its ability to generate cytotoxic species (See Section 1.2). The measurement of photophysical parameters such as Φ_F, Φ_T and Φ_Δ is therefore extremely important when evaluating the potential efficacy of a dye. One of the aims of this study was to synthesise a novel, water soluble phthalocyanine and to investigate its solution state properties in homogeneous and heterogeneous media. The influence of peripheral substitution has also been investigated.

3.2 Materials and Methods
3.2.1 Materials

The synthesis and purification of β-tetra-1,1-di(methoxycarbonyl)ethyl zinc phthalocyanine ($ZnPc(CMe(CO_2Me)_2)_4$) and β-tetra-1-carboxyethyl zinc phthalocyanine ($ZnPc(CHMeCO_2H)_4$) was described in Chapter 2. Tetra tertbutyl zinc phthalocyanine ($^tBu_4ZnPc$) and disulfonated zinc phthalocyanine ($ZnPcS_2$) were prepared by Dr. A. Beeby and used as received[20]. 1,4,8,11,15,18,22,25-octadecyl zinc phthalocyanine (C10) was a gift from Prof. M. J. Cook, University of East Anglia[21]. Solvents were Analar grade or better and were used without further purification. Phosphate buffer saline (PBS) was purchased from Sigma and prepared using distilled water. Triton X-100, Triton X-100 reduced and hexadecyl trimethylammonium bromide (CTAB - $CH_3(CH_2)_{15}N(CH_3)_3Br$) were purchased from Aldrich and used as received. Ether-pentane-alcohol (5:5:2) solution was prepared from diethyl ether, isopentane (IP) and ethanol.

3.2.2 Methods

Dimerisation constants were calculated by measuring absorbance at the wavelength of maximum monomer absorption (λ_{max}) for a range of phthalocyanine concentrations. Two analytical methods were employed, that of Tai et al.[22] and that suggested by Fernandez et al.[23]. Tai assumed a one step equilibrium between monomeric and dimeric phthalocyanine and also made the important assumption that the extinction coefficient of

dimer, ε_D << the extinction coefficient of the monomer, ε_S at the monitored wavelength. This yielded Equation 3.1,

$$log[C_t(1-\frac{\varepsilon}{\varepsilon_S})] = log(nK) + nlog[C_t(\frac{\varepsilon}{\varepsilon_S})] \qquad (3.1)$$

where C_t is the total phthalocyanine concentration, ε is the observed extinction coefficient, ε_S is the monomer extinction coefficient (assumed to be 180000 dm^3 mol^{-1} cm^{-1} at λ_{max}[24]), n is the average aggregation number and K is the dimerisation constant. Plots of log $[C_t(1-\varepsilon/\varepsilon_S)]$ vs log $[C_t(\varepsilon/\varepsilon_S)]$ yielded linear fits from which n may be determined from the gradient and K estimated from the intercept. Equation 3.2 gives the formula employed by Fernandez[23].

$$A = \frac{\varepsilon_S}{4K}[(1+8KC_t)^{1/2}-1] + \frac{\varepsilon_D}{2}[C_t - \frac{(1+8KC_t)^{1/2}-1}{4K}] \qquad (3.2)$$

C_t, K and ε_S have the same meaning as above and ε_D is the extinction coefficient of dimeric species. The dimerisation constant was determined by fitting this equation to experimental data using a curve fitting package (Grafit). C_t and ε_S were treated as constants while ε_D and K were allowed to vary until the best fit was achieved.

Stock micellar solutions of $^tBu_4ZnPc$ and $ZnPc(CMe(CO_2Me)_2)_4$ were prepared by sonicating phthalocyanine in Triton X-100 (TX) or Triton X-100 reduced (TXR) followed by dilution to 1% w/v surfactant solution (1.5 x 10^{-3} mol dm^{-3}) using phosphate buffered saline (PBS). Micellar solutions of C10 were prepared by evaporation of toluene from a toluene/1% TX/PBS emulsion. C10 was dissolved in toluene and thoroughly mixed with the surfactant solution. Toluene was removed by stirring and blowing argon over the solution to assist evaporation. Water soluble phthalocyanines ($ZnPcS_2$ and $ZnPc(CHMeCO_2H)_4$) were added directly to 1% TX/PBS solution and sonicated to achieve solubilisation. All surfactant solutions were prepared immediately prior to use.

UV/Visible absorption spectra, fluorescence measurements, triplet state data and singlet oxygen quantum yields were determined using the apparatus and sample conditions described in Chapter 2 (pp 42-71).

3.3 Results and Discussion

3.3.1 Synthesis

Two novel substituted zinc phthalocyanines, $ZnPc(CMe(CO_2Me)_2)_4$ (**4**) and $ZnPc(CHMeCO_2H)_4$ (**5**), have been prepared and characterised (Figure 2.13). The copper complex of **4** is already known[25], however the zinc complex has not been previously reported. Compound **5** differs from known phthalocyanines in the nature of the carboxylic acid substituents[26] - synthesis of a phthalocyanine with carboxylic acid substituents separated from the phthalocyanine ring by an alkyl group (-CHMe-) is reported for the first time. Water solubility of **5** was achieved through hydrolysis of peripheral methyl ester groups of **4**. The synthetic scheme followed to prepare these phthalocyanines is depicted in Figure 2.13. Synthesis of dimethyldicyanophenyl malonate (**2**) and dimethyl 3,4-dicyanophenyl-1,1-ethane dicarboxylate (**3**) was readily accomplished following the method of Roze et al.[25]. A yield of 69% for **2** was comparable to that reported by Roze, whilst the yield of **3** was somewhat improved (49%, c.f. 33%). IR and NMR data for both compounds were in good agreement with literature values. Cyclisation of **3** to produce the tetra ester substituted zinc phthalocyanine, **4**, was carried out by heating to high temperature (200 °C) under a nitrogen atmosphere in the presence of zinc acetate. Following chromatographic purification, a 30% yield of **4** was obtained. This relatively low yield is typical of condensation reactions of this type and is comparable to that obtained by both Roze and Kahl[27]. Compound **4** was characterised by spectroscopic data and elemental analysis. The infra red spectrum exhibited a strong carbonyl absorption at 1721 cm^{-1} whilst the UV/Visible absorption spectrum was characteristic of monomeric phthalocyanine with absorption maxima at 347 nm and 677 nm in $CHCl_3$. A molecular ion was observed in the mass spectrum at m/z = 1153.65, corresponding to the parent ion (RMM = 1153.9).

Hydrolysis of **4** to **5** was accomplished by refluxing **4** with NaOH in methanolic solution for several hours. A good yield (80%) was achieved for this reaction. Compound **5** was well characterised by IR and NMR data. A carbonyl stretch at 1700 cm^{-1}, shifted to lower energy than that of **5** ($v = 1721$ cm^{-1}), was recorded. This is consistent with the behaviour generally observed for acid and ester compounds[28]. The NMR spectrum displayed a clear doublet at 1.9 ppm, characteristic of splitting of methyl hydrogens by the single C-H. UV/Visible absorption data was typical of monomeric phthalocyanine, absorption maxima being observed at 349 nm and 673 nm. Using the Beer-Lambert law (Equation 2.1), an average extinction coefficient at λ_{max}, ε_{Pc}, of 1.4×10^5 mol dm^{-3} cm^{-1} was determined. Assuming[24] ε_s to be 180000 mol dm^{-3} cm^{-1}, it can be concluded that $ZnPc(CHMeCO_2H)_4$ has a purity of $\sim$ 80%. This may explain why the elemental analysis was inconsistent with calculated values.

Synthesis of **4** and **5** was successfully repeated on a larger scale (X3). Product yields were similar. Phthalocyanines **4** and **5** are expected to exist as a mixture of isomers with a statistical mixture of arrangements of the peripheral substituents. Perhaps not surprisingly, it was not possible to separate these by thin layer or column chromatography.

3.3.2 Properties in Homogeneous Solution
3.3.2.2 Results
3.3.2.2.1 Solution State Properties

$ZnPc(CMe(CO_2Me)_2)_4$ and $ZnPc(CHMeCO_2H)_4$ displayed very different solubilities. Ester groups rendered the phthalocyanine soluble in non polar organic solvents such as chloroform and toluene as well as methanol, THF and ethanol. In chloroform, $ZnPc(CMe(CO_2Me)_2)_4$ was remarkably monomeric in character (Figure 3.1a), adhering to the Beer-Lambert law (Equation 2.1) up to concentrations of 2×10^{-4} mol dm^{-3}. Table 3.1 gives the dimerisation constants, K, calculated in various solvents using Equations 3.1 and 3.2. Clearly a large discrepancy exists between each method of analysis, however, the trend was consistent.

Solvent	K^a	K^b	Dielectric Constant, ε
MeOH	$51 \pm d$	22500 ± 2000	33
Toluene	$108 \pm d$	34000 ± 3000	2.38
CH_2Cl_2	$0.49 \pm d$	3100 ± 500	9.08
$CHCl_3$	$\_c$	$\_c$	4.81

a) Calculated using Equation 3.1, b) Calculated using Fernandez method c) Monomeric in concentration range studied, d) Errors incurred using this equation were large: values quoted may vary by as much as an order of magnitude.

Table 3.1. Dimerisation constants of $ZnPc(CMe(CO_2Me)_2)_4$.

$CHCl_3$ and CH_2Cl_2 were the most suitable solvents. $ZnPc(CMe(CO_2Me)_2)_4$ was monomeric in solutions of $CHCl_3$ up to the detection limit of the spectrometer (1×10^{-4} mol dm^{-3}), whilst in CH_2Cl_2, a K value of 0.49^a (3100^b) was obtained. In methanol and toluene, a greater tendency to aggregate was observed, dimer species being characterised[29] by the appearance of an absorption peak at 633 nm (Figure 3.1b). Figure 3.1c shows the calculated absorption spectrum of pure dimer.
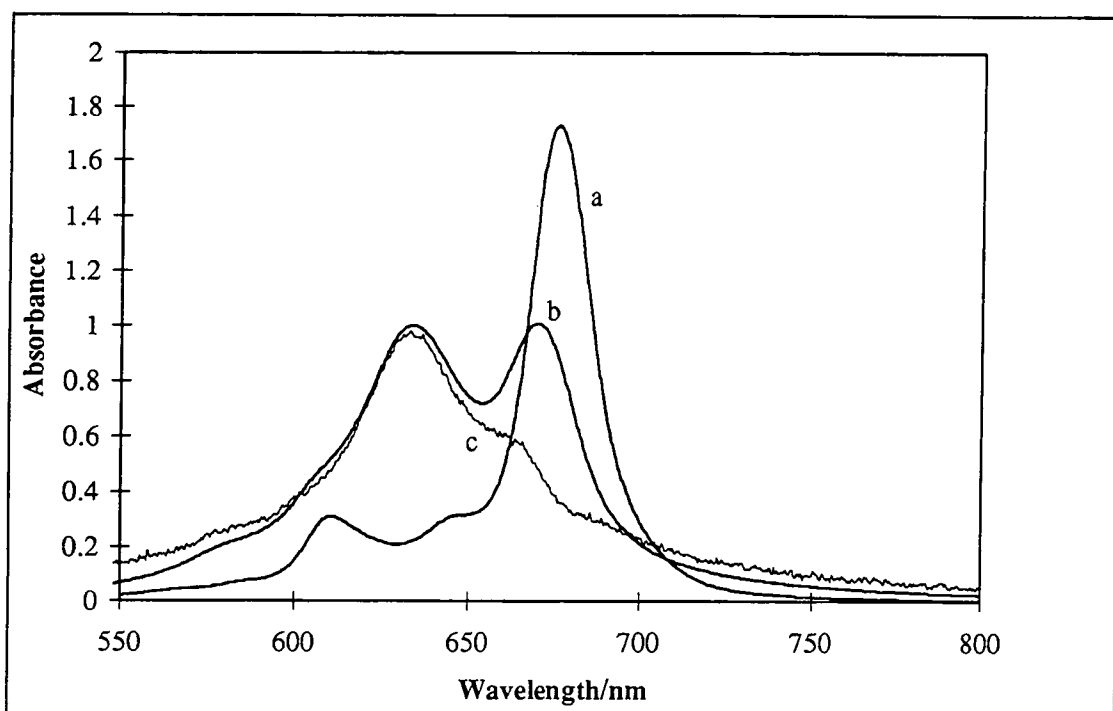
Figure 3.1. Absorption spectra of ZnPc(CMe(CO₂Me)₂)₄, 1 mm pathlength. a)
CHCl₃ (9.6 x 10⁻⁵ mol dm⁻³), b) MeOH (2 x 10⁻⁴ mol dm⁻³), c) Calculated dimer
spectrum.

The acid functionality has hydrophilic properties, thus $ZnPc(CHMeCO_2H)_4$ was soluble in polar solvents such as THF, methanol and ethanol but insoluble in dichloromethane and toluene. Dimerisation in ethanol was found to be extremely sensitive to the ionic strength of the solution. Addition of NaCl, zinc acetate, $Ca(ClO_4)_2$, HCl or NaOH (0 < [ions] < 10^{-4} mol dm⁻³) was found to induce aggregation of $ZnPc(CHMeCO_2H)_4$ in EtOH (Figure 3.2A), whilst high ion concentrations (>10^{-3} mol dm⁻³) caused *monomerisation* (Figure 3.2B). For samples with high ionic strength, the proportion of dimer species was found to increase as any particular solution was diluted due to a reduction in the ionic strength of the solution. This contradicts the general behaviour of phthalocyanines which predicts a decreasing proportion of dimer as concentration decreases[30]. Under the same conditions, the spectra obtained from $ZnPcS_2$ were consistent and predominantly monomeric in character.
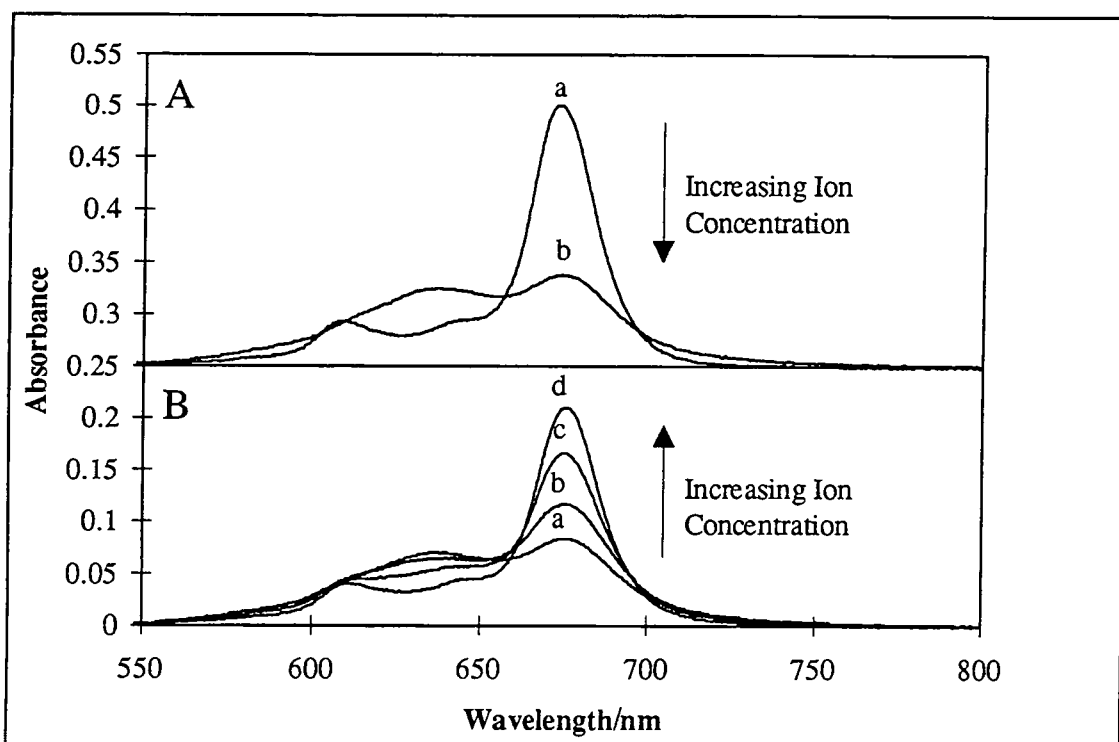
Figure 3.2. A. Aggregation of ZnPc(CHMeCO₂H)₄ in EtOH induced by potassium acetate. a. ~0 mol dm⁻³ b. 10⁻⁴ mol dm⁻³.

B. Disaggregation at high ionic strength a. 10⁻⁴ mol dm⁻³ b. 5 x 10⁻⁴ mol dm⁻³ c. 6 x 10⁻⁴ mol dm⁻³ d. 10⁻³ mol dm⁻³.

Low concentrations of tetrabutylammonium salts were found to promote aggregation but at high concentrations monomerisation did not occur. In addition to dimer species at 633 nm, concentrated solutions of $ZnPc(CHMeCO_2H)_4$ in THF showed an absorption band at 704 nm, red shifted with respect to the main absorption peak. This disappeared upon dilution of the phthalocyanine and by analogy to results described in Chapter 5 (pp 160-184) was ascribed to protonation of the phthalocyanine ring by H^+ ions released from the carboxylic acid functionalities.

Both phthalocyanines were insoluble in distilled water. However, $ZnPc(CHMeCO_2H)_4$ was soluble in phosphate buffered saline (PBS), pH = 7.4, in an aggregated form. Clearly, since the ionic strength of PBS is high (140 mmol dm⁻³ Na/KCl), ions do not promote monomerisation in an analogous manner to the situation in organic solvents. However, disaggregation could be induced by addition of 0.02 mmol dm⁻³ hexadecyl trimethylammonium bromide (CTAB). This concentration is well below the critical micelle concentration[31] (0.9 mmol dm⁻³) of this surfactant. Alkaline conditions had no effect on the state of aggregation of $ZnPc(CHMeCO_2H)_4$ whilst PBS acidified with HCl to pH = 2 caused further aggregation (Figure 3.3).
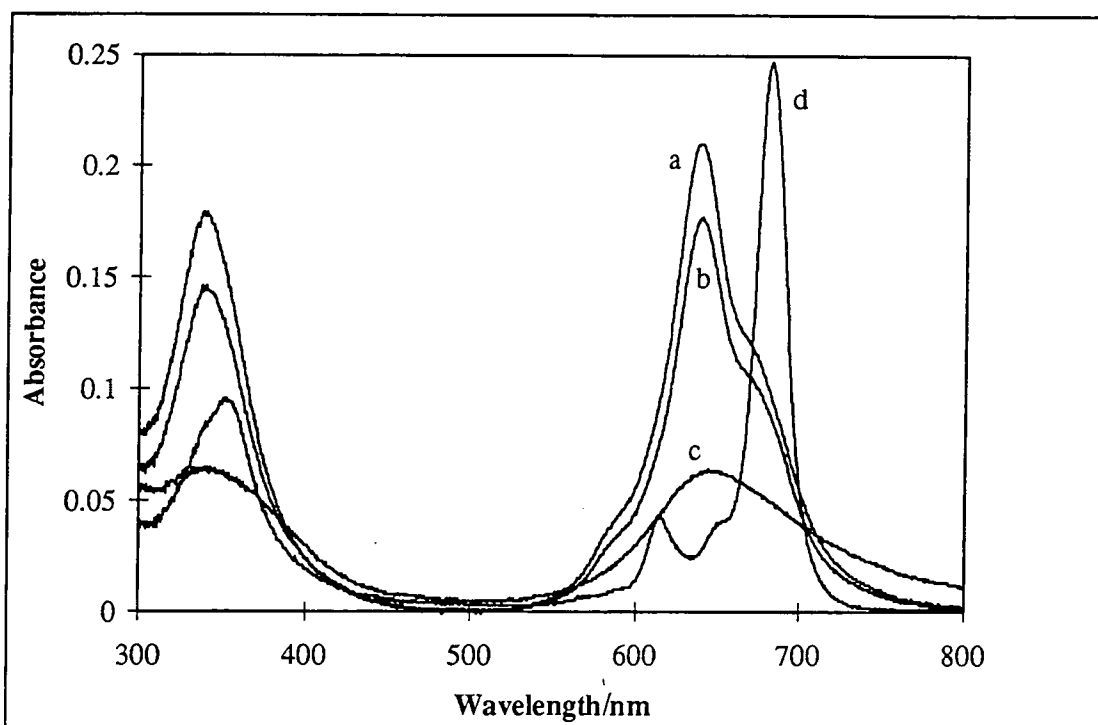
Figure 3.3. UV/Vis spectra of ZnPc(CHMeCO₂H)₄ in PBS.
a. pH = 7.4 b. pH = 11 c. pH = 2 d. pH = 7.4 (0.02 mmol dm⁻³ CTAB).

3.3.2.2.2 Photophysical Properties

The energy of the $S_1 \leftarrow S_0$ transition of $^tBu_4ZnPc$ was found to vary with solvent. Figure 3.4 shows the position of the absorption maximum (λ_{max}) of $^tBu_4ZnPc$ in a variety of solvents as a function of dielectric constant, ε, dipole moment, μ, donor number, DN and refractive index, n_D. No correlation was observed between the polarity or dipole moment of the solvent and λ_{max}. A tentative link between the donor number of the solvent and λ_{max} may be implied, while a reasonably clear linear dependency on the refractive index was observed.
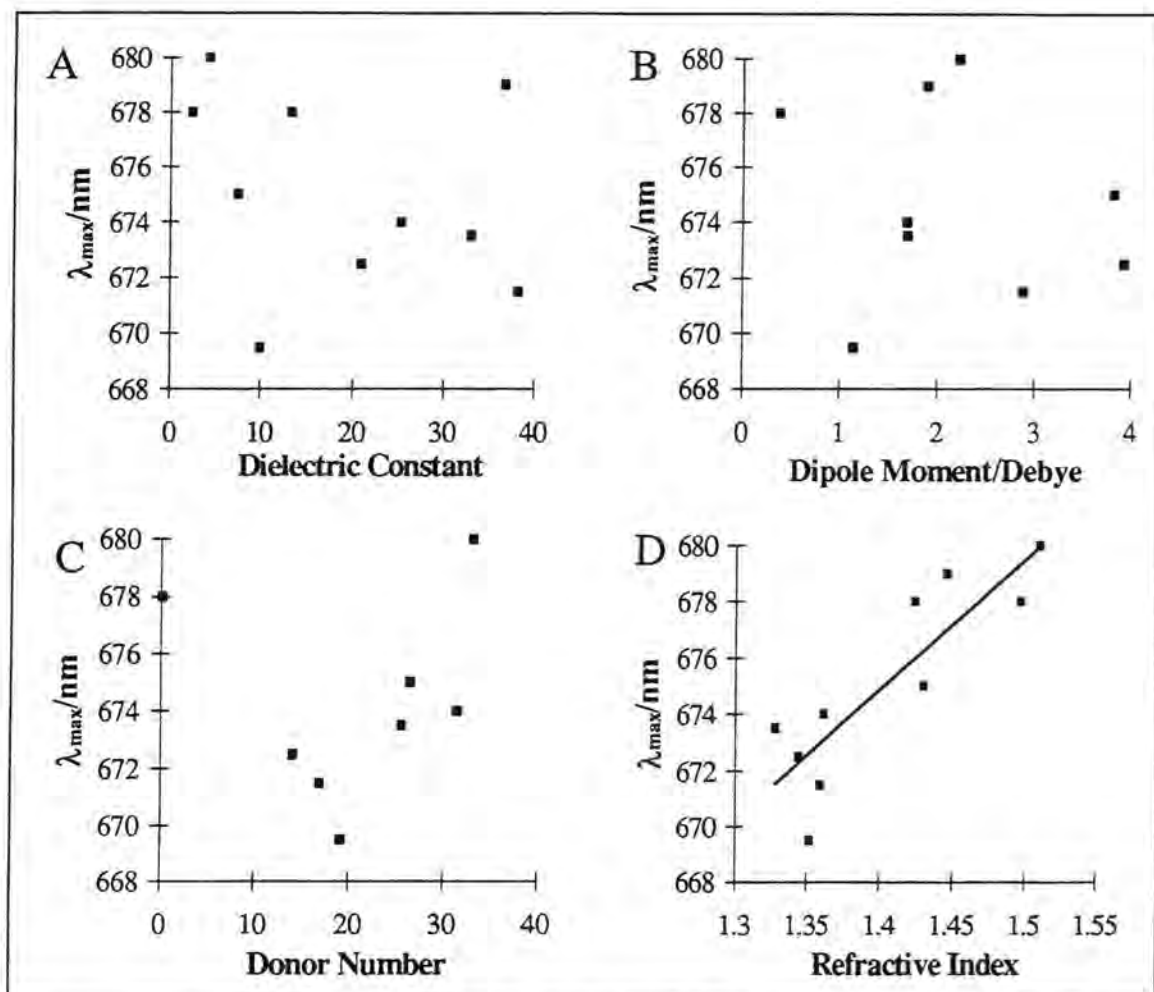
Figure 3.4. Solvent effect on λ_{max} *(UV/Vis.) of* $^tBu_4ZnPc$.

Phthalocyanine	Solvent	λ_{max} /nm	$\Delta\lambda$ /nm
ZnPc	1%pyr/tol	672	-
$^tBu_4ZnPc$	1%pyr/tol	678	9
C10	1%pyr/tol	702	33
ZnPc	MeOH	664[a]	-
$^tBu_4ZnPc$	MeOH	673.5	2.5
$ZnPc(CHMeCO_2H)_4$	MeOH	674	3
$ZnPc(CMe(CO_2Me)_2)_4$	MeOH	671	10
$ZnPcS_2$	MeOH	665.5	4.5

a This wavelength was calculated using Equation 3.3 and λ_{max} in toluene.

Table 3.2. Effect of peripheral substitution on absorption λ_{max} *of ZnPc.*

Peripheral substitution of ZnPc caused the wavelength of maximum absorption to be shifted to lower energy. The extent of the shift ($\Delta\lambda$) varies according to the nature of the substituent (Table 3.2). Tables 3.3A and 3.3B show the radiative emission properties of the excited singlet state of ZnPc and the effect of peripheral substitution. All the phthalocyanines studied have an excitation spectrum which exactly overlays the absorption spectrum, indicating the presence of just one absorbing species. The emission spectra have a Stokes shift of 8 nm ± 1 nm which was constant for all phthalocyanines except C10. Good mirror symmetry of absorption and emission was obtained (Figure 3.5).
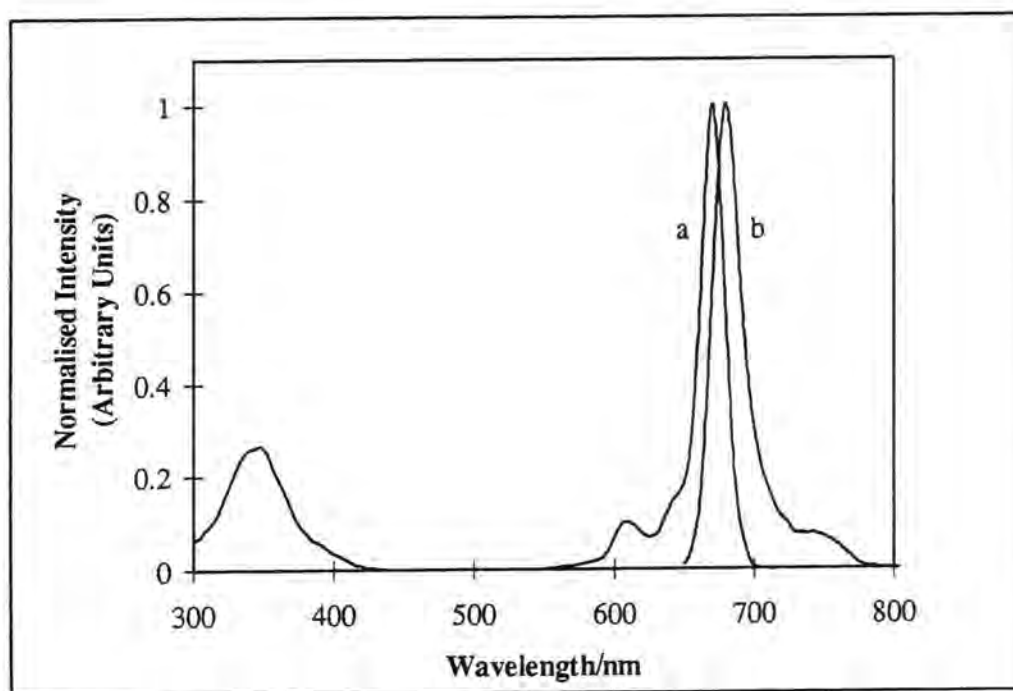
Figure 3.5. a) Absorption and b) Emission (λ_{ex} = 630 nm) spectra of ZnPc(CMe(CO$_2$Me)$_2$)$_4$ in CHCl$_3$. Spectra have been normalised at λ_{max}.

Pc	Solvent	λ_{em} /nm	λ_{ex} /nm	Stokes Shift /nm
ZnPc	1% pyr/tol	680	672	8
$^tBu_4ZnPc$	EtOH	682	674	8
ZnPc(CHMeCO$_2$H)$_4$[a]	MeOH	683	674	9
ZnPc(CMe(CO$_2$Me)$_2$)$_4$	CHCl$_3$	683	676	7
ZnPcS$_2$	EtOH	674.5	667.5	7
C10	1%pyr/tol	717	702	15

a. 0.01 mol dm^{-3} potassium acetate used to prepare monomeric species.

Table 3.3A. Effect of peripheral substitution on emission characteristics of ZnPc.

The quantum yield of radiative emission, Φ_F, was essentially unaffected by peripheral substitution by tertiary butyl, ester or sulfonate groups, however carboxylic acid and decyl substituents caused a reduction in the fluorescence yield.

Pc	Solvent	Φ_F	τ_F /ns
ZnPc	1%pyr/tol	0.3[32]	3.5
tBu$_4$ZnPc	EtOH	0.26 ± 0.03	3.6
ZnPc(CHMeCO$_2$H)$_4$	MeOH	0.17 ± 0.02[a]	-
ZnPc(CHMeCO$_2$H)$_4$	PBS	0.06 ± 0.005[b]	-
ZnPc(CMe(CO$_2$Me)$_2$)$_4$	THF	0.22 ± 0.02	-
ZnPcS$_2$	EtOH	0.35 ± 0.02	-
C10	1%pyr/tol	0.082 ± 0.015	-

a. 0.01 mol dm^{-3} potassium acetate used to prepare monomeric species, b. Measured in PBS using CTAB to monomerise.

Table 3.3B.

Effect of peripheral substitution on fluorescence emission yield of ZnPc.

ZnPc(CHMeCO$_2$H)$_4$ and ZnPc(CMe(CO$_2$Me)$_2$)$_4$ showed typical triplet state characteristics. Measured traces could be described by monoexponential decays and a good linear response of transient height to laser power was achieved at low laser powers (Figure 3.6).
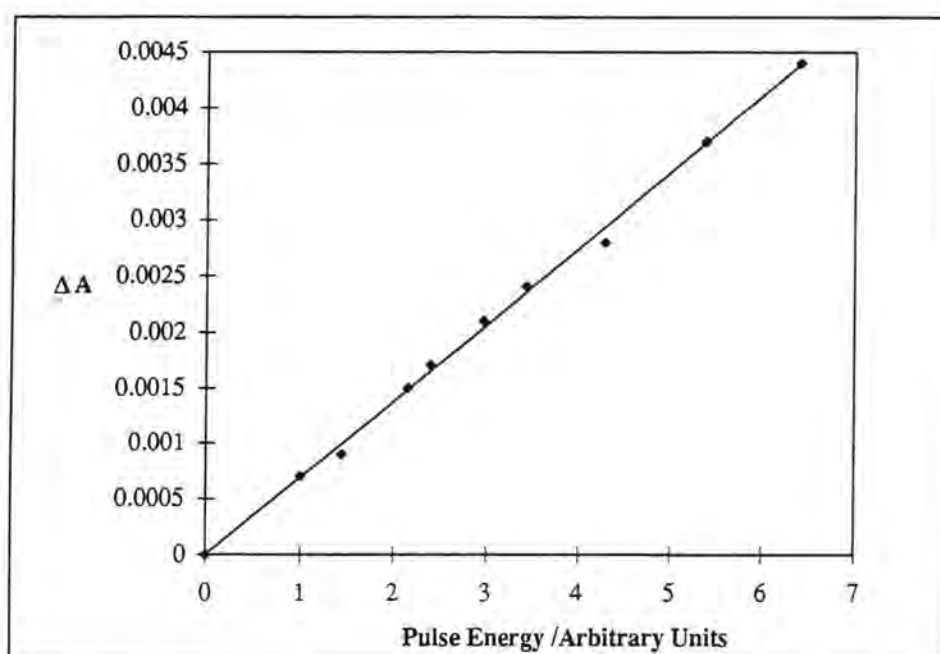
Figure 3.6. Transient absorbance of ZnPc(CMe(CO$_2$Me)$_2$)$_4$ in CHCl$_3$ vs laser pulse energy. (λ_{ex} = 638 nm, λ_{Probe} = 490 nm).

No radical species were generated upon excitation of the phthalocyanines in an oxygen purged solution. This was inferred from the absence of any absorption bands at ~ 600 nm corresponding to radical species and by the transient absorption spectrum which was observed to be unaffected by the time after excitation.

With the exception of C10, the triplet state properties were independent of ring substitution (Table 3.4). C10 showed a shift in the transient absorption spectrum from 490 nm to 520 nm, accompanied by a decrease in triplet state lifetime and increase in the triplet yield. The singlet oxygen yield increased accordingly, with the fraction of triplet species quenched to produce $^1O_2$ constant at ~1.

Pc	Solvent	Φ_T [a]	τ_T /μs	Φ_Δ	S_Δ
ZnPc[17]	1%pyr/tol	0.58 ± 0.08	330 ± 30	0.54	0.93
$^tBu_4ZnPc$	EtOH	0.56 ± 0.05	200 ± 20	0.54 ± 0.05	0.96
C10	1%pyr/tol	0.8 ± 0.1	50 ± 5	0.7 ± 0.06	0.88
$ZnPcS_2$[33]	MeOH	0.46 ± 0.05	270 ± 30	0.52 ± 0.05	1.13
ZnPc-$(CHMeCO_2H)_4$	EtOH[b]	0.52 ± 0.05	290 ± 30	0.57 ± 0.05	1.1
ZnPc-$(CHMeCO_2H)_4$	PBS[c]	0.18 ± 0.02	200 ± 25	-	-
ZnPc-$(CMe(CO_2Me)_2)_4$	$CHCl_3$	0.45 ± 0.05	280 ± 30	0.5 ± 0.05	1.1

a. ε_T was constant for all ZnPcs at 36000 ± 6000. b. 0.01 mol dm^{-3} potassium acetate added to induce monomerisation. c. 0.02 mmol dm^{-3} CTAB used to monomerise.

Table 3.4. Triplet state properties of substituted ZnPc's.

3.3.2.2.3 Low Temperature Measurements

Figure 3.7 shows the effect of variation of temperature on the absorption spectra of each substituted phthalocyanine. Spectra have been corrected for shrinkage of the solvent upon cooling. The ratio of the volume at 77 K (V_{77}) to that at 293 K (V_{293}) is 0.778 for EPA[34] and 0.8 for EtOH[35]. Very different behaviour was observed depending on the nature of the peripheral substituent.
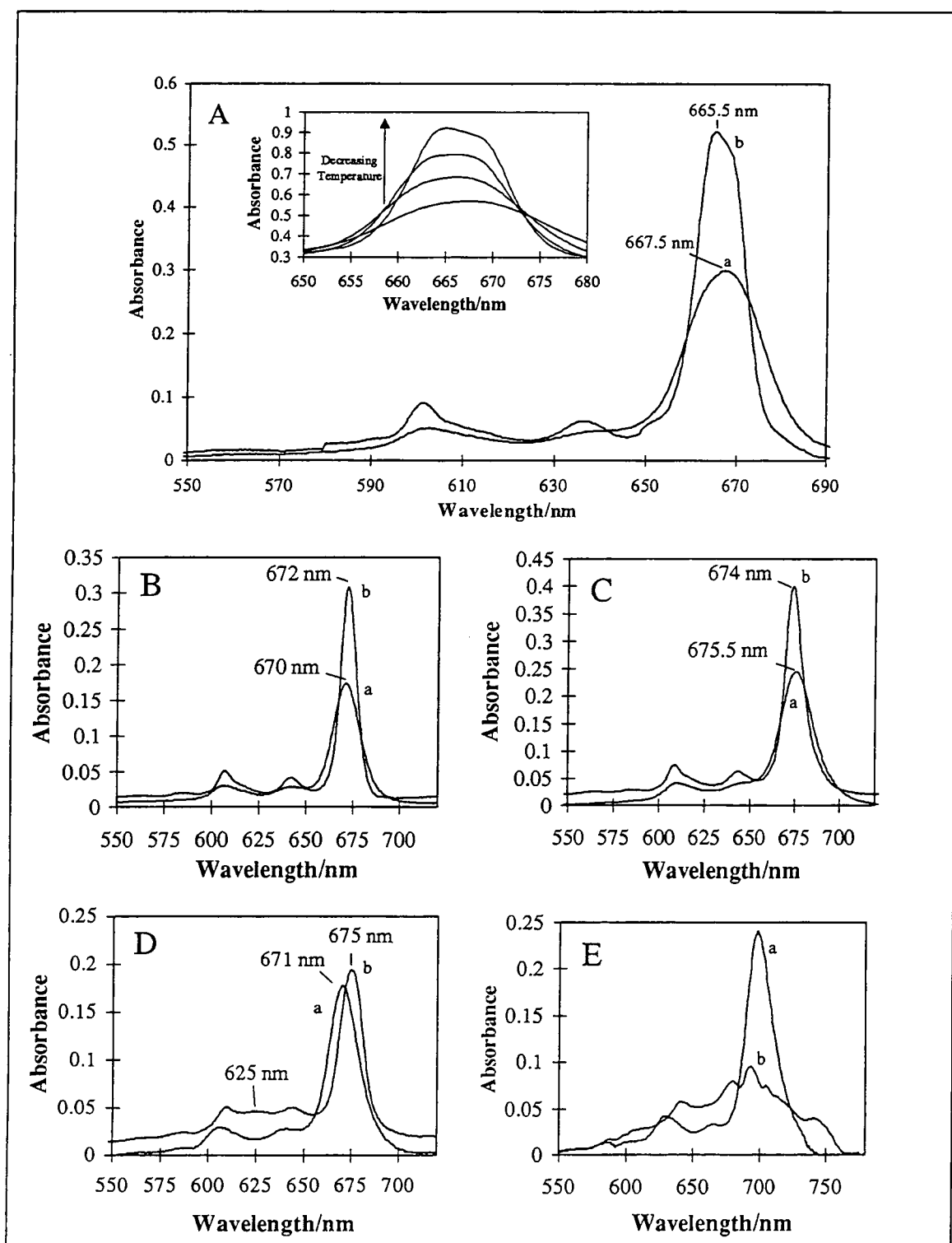
Figure 3.7. Effect of temperature (a. RT, b. 77 K) on the UV/Vis spectra of A. ZnPcS₂ in EtOH (inset: Magnification of Q band peak), B. ᵗBu₄ZnPc in EPA, C. ZnPc(CHMeCO₂H)₄ in EPA, D. ZnPc(CMe(CO₂Me)₂)₄ in EPA, E. C10 in EPA. Concentration of phthalocyanine is 2-3 x 10⁻⁶ mol dm⁻³. Spectra have been corrected for shrinkage of solvent upon cooling.

A. $ZnPcS_2$ in EtOH displayed partial splitting of the Q band accompanied by band narrowing (FWHM (293K) = 21 nm, FWHM (77K) = 12.5 nm). At room temperature, a single peak, λ_{max} = 667.5 nm, was observed for $ZnPcS_2$ in EtOH. At 77 K, this maximum split to give two peaks at 665.5 ± 1 nm and 668 ± 1 nm.

B. $^tBu_4ZnPc$ in EPA showed an apparent increase in the extinction coefficient, narrowing of the full width at half maximum (FWHM) from 17 nm to 10 nm and a red shift from 670 nm to 672 nm at 293 K and 77 K respectively (Figure 3.7 B).

C. The monomeric form of $ZnPc(CHMeCO_2H)_4$ in EPA was induced by adding 0.01 mol dm^{-3} potassium acetate. Similar behaviour to $^tBu_4ZnPc$ was observed except a 1.5 nm blue shift occurred on cooling.

D. The energy of the $S_1 \leftarrow S_0$ transition of $ZnPc(CMe(CO_2Me)_2)_4$ in EPA showed a shift from 671 nm to 675 nm on cooling, in addition to the band narrowing observed for all the phthalocyanines under study. A new absorption peak at 625 nm also appeared.

E. The absorption spectra of C10 in EPA displayed the most striking change on cooling. A highly structured absorption spectrum was observed which bore little resemblance to the monomeric spectrum observed at room temperature. Further discussion of this result, and information regarding fluorescence and triplet state properties of C10 at 77 K may be found in Chapter 4 of this review (pp 111-159).
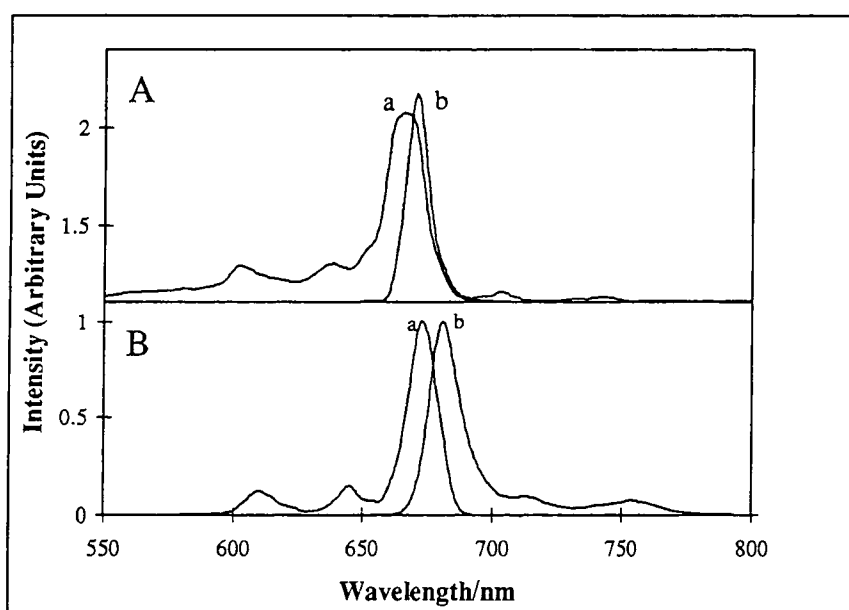
Figure 3.8. a) Excitation (λ_{em} = 750 nm) and b) Emission (λ_{ex} = 630 nm) spectra at 77 K. A. $ZnPcS_2$ in EtOH, B. $ZnPc(CMe(CO_2Me)_2)_4$ in EPA. Spectra are offset for clarity and have been normalised at λ_{max}.

Figure 3.8B displays the excitation and emission spectra obtained at 77 K from ZnPc(CMe(CO$_2$Me)$_2$)$_4$. These spectra are sharpened in an analogous fashion to the absorption spectra. Emission and excitation spectra of ZnPc(CHMeCO$_2$H)$_4$ and ^{t}Bu$_4$ZnPc behaved in an analogous manner. Figure 3.8A shows the spectra obtained for ZnPcS$_2$. The excitation spectrum depicts the same broad Q band as was seen in the absorption spectrum. It should be noted that, despite splitting of the Q band in the excitation spectrum, the emission spectrum consisted of a sharp, single band.

The effect of temperature on the absorption and fluorescence properties of octabutoxy zinc phthalocyanine (ZnPc(BuO)$_8$) were also studied. A dramatic shift was observed upon cooling of this phthalocyanine to 77 K. Red shifts of the absorbance maximum were dependent on the solvent employed and ranged from 13 nm to 40 nm (Table 3.5). Red shifts in the fluorescence emission spectra were also observed, accompanied by a decrease in the Stokes shift of the spectrum.

Solvent	293K			77K			
	λ_{max} /nm	λ_{em} /nm	Stokes Shift /nm	λ_{max} /nm	λ_{em} /nm	Stokes Shift /nm	$\Delta\lambda_a$ (UV)
EPA	734	748	14	774	785	11	40
MeTHF	735	746	11	748	750	2	13
EtOH	740	757	17	778	788	10	38
Et$_2$O:IP	730	741	11	744	747	3	14

a. $\Delta\lambda$ represents the shift in the absorption maximum which occurred at 77 K with respect to the maximum at 293 K.

Table 3.5. Absorption (λ_{max}) and emission (λ_{em}) characteristics of ZnPc(BuO)$_8$ in various organic solvents at 293 K and 77 K.

3.3.2.3 Discussion

3.3.2.3.1 Solution State Properties

Dimerisation constants, K, calculated using Tai's method of analysis (Equation 3.1) are several orders of magnitude smaller than those determined using Fernandez' equation (Equation 3.2). The key to this is the assumption made by Tai that the extinction coefficient of the dimer, ε_D, is negligible at the wavelength of maximum absorption of the monomer. By reference to Figure 3.1c it can be inferred that at a total phthalocyanine concentration of 2 x 10^{-4} mol dm^{-3} in MeOH, ~ 50% of absorption at 670 nm was due to dimeric species. Hence, it is inappropriate to assume ε_D = 0. Under-estimation of ε_D leads to an overestimate in the concentration of monomer species, and

subsequent underestimation of K. For ZnPc(CMe(CO$_2$Me)$_2$)$_4$, therefore, Equation 3.2 provides a more accurate value for K. In the case of CHCl$_3$, K could not be determined since a linear Beer-Lambert plot was obtained over the concentration range studied (up to 1 x 10^{-4} mol dm^{-3}). The dimerisation constant of ZnPc(CMe(CO$_2$Me)$_2$)$_4$ has been shown to vary as the dielectric constant of the solvent system changed. This variation is not a simple linear dependency and it is clear that aggregation is controlled by a number of factors. Dimerisation equilibria are partly controlled by a balance between attractive π π interactions between the hydrophobic phthalocyanine rings and repulsive electronic and steric factors introduced by the substituent[36]. This has been demonstrated by Wohrle[37], who showed that octabutoxy substituted zinc phthalocyanine is easily soluble in organic solvents such as pyridine, toluene and CCl$_4$ whilst the analogous methoxy compound is not. For unsubstituted metallocyanines, monomers are favoured by non-polar solvents, i.e. those with a low dielectric constant. In the work presented here, ester group substituents on the β ring positions (Figure 3.9) of zinc phthalocyanine have been found to promote solubility in chloroform (CHCl$_3$) and dichloromethane (CH$_2$Cl$_2$), as has been mentioned earlier.
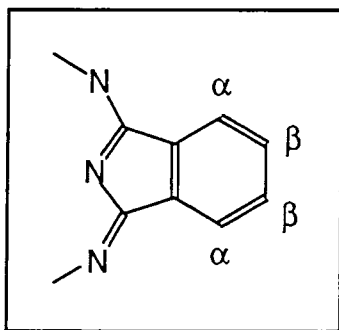
Figure 3.9. α *and* β *positions of zinc phthalocyanine.*

In chloroform, ZnPc(CMe(CO$_2$Me)$_2$)$_4$ was found to be monomeric at concentrations < 1 x 10^{-4} mol dm^{-3}. Similarly an aggregation constant of 3100 dm^3 mol^{-1} was obtained for experimental in CH$_2$Cl$_2$. These values are very low when compared with those reported in the literature. Osburn et al.[7] have postulated an aggregation constant in CHCl$_3$ of K > 1 x 10^8 dm^3 mol^{-1} for a copper phthalocyanine peripherally substituted by ester groups attached directly onto the ring. They suggested that the propensity of phthalocyanines to aggregate is controlled by the electron withdrawing nature of peripheral substituents and demonstrated a correlation between the total substituent constant, σ^*, and K for ester, amide and alkoxy substituents of copper phthalocyanine. This has also been observed by Abraham[38] who rationalised this observation in terms of an increased metal to $\pi\pi^*$ coupling. Comparison between reported K values and σ^* for several substituted zinc phthalocyanines are shown in Table 3.6.

Substituent	σ_I[39]	σ_R	σ^*	K	Solvent	Ref.
$O-CO_2Bz$	0.34	-0.45	-0.11	1300	$CHCl_3$	[7]
$-C_{10}H_{21}$	-0.05	-0.14	-0.19	Monomeric to 1.5×10^{-4} mol dm^{-3}	C_6H_{12}	[21]
$-C-(CH_3)_3$	-0.07	-0.13	-0.2	2.5×10^4	Toluene	[23]
a	0.24	-0.23	0.01	2.04×10^4	Toluene	[23]
$C(CH_3)_2CH_2NH_2$[b]	-0.07	-0.13	-0.2	4×10^5	THF	[23]
Cl	0.47	-0.23	0.24	6×10^3	DMSO	[40]
Br	0.44	-0.19	0.25	4.7×10^4	DMSO	[40]
I	0.39	-0.16	0.23	2.4×10^4	DMSO	[40]
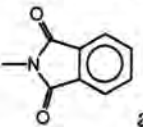
a. Estimated as $NHCOCH_3$, b. Estimated as $C(CH_3)_3$.

Table 3.6. Collation of substituent constant, σ^* and the dimerisation constant, K of substituted ZnPc's.

These results show that many other factors besides σ^*, such as steric hindrance, specific interactions between substituents, and the presence of axial ligands to the metal must be taken into consideration. Amine groups have been shown to increase the aggregation tendencies of ZnPc in THF relative to those of butyl substituted ZnPc in toluene due to intermolecular hydrogen bonding between peripheral substituents[23]. THF has the propensity to act as a ligand to the metal ion of metallophthalocyanines, inhibiting aggregation. Therefore, two competing effects must be considered: *viz.* enhanced aggregation due to hydrogen bonding interactions between substituents, and inhibition of aggregation due to the presence of an axial ligand which introduces steric hindrance to the approach of two molecules. σ^* for these substituents is not expected to be significantly different. Halide substitution[40] inhibited aggregation in the order Cl > I > Br, though their effective substituent constants are approximately equal. Some other influence must, therefore, be responsible for measured differences in K. It is suggested that the low propensity of ZnPc(CMe(CO$_2$Me)$_2$)$_4$ to aggregate is a consequence of the extremely bulky nature of the diester substituents, introducing steric hindrance to the approach of two molecules in a similar fashion to the action of axial ligation. In addition, electronic effects which may promote aggregation due to the electron withdrawing nature of ester groups ($\sigma^* = 0.5$[39]) are reduced since the ester groups are not attached directly to the phthalocyanine but are removed by an alkyl linking unit (-CHMe-). In toluene and methanol, K is greater. This illustrates two different properties. Toluene is a non-polar solvent and ester groups are less soluble in this type of solvent than in $CHCl_3$

or CH_2Cl_2. Thus, unfavourable substituent/solvent interactions promote aggregation in a comparable manner to dimerisation promoted by hydrophobic alkyl chain substituents[41] in aqueous solution. In methanol, unfavourable phthalocyanine ring/solvent interactions become the dominant factor so attractive $\pi\pi$ Van-der-Waals interactions outweigh favourable ester/solvent interactions and steric factors preventing association.

In the case of, $ZnPc(CHMeCO_2H)_4$, the hydrophilic nature of these substituents favours interaction with polar solvents, hence, this phthalocyanine is soluble in organic media with high dielectric constants such as MeOH. Hydrogen bonding between carboxyl groups and solvent molecules is possible, thus aiding solvation. An extreme sensitivity to the ionic strength of the solution was observed. Many reports have been published commenting on increased aggregation of ionic porphyrins[42]/phthalocyanines[11] in aqueous ionic media, however, little has been mentioned regarding the effect of ions in organic systems. Indeed, Pasternack et al.[43] have shown that addition of acetone to a 0.1 mol dm^{-3} ionic strength aqueous solution of nickel tetracarboxyphenylporphyrin counteracts the electrolyte effect and shifts the dimerisation equilibrium towards the monomeric form. Interestingly, the analogous zinc porphyrin was observed to remain monomeric in 0.1 mol dm^{-3} salt solution. This was ascribed to a combination of two effects; the presence of an axial ligand to the metal and non-planarity of the porphyrin ring. Dimerisation is enhanced due to ion pairing between the electrolyte and porphyrin substituents.

A similar effect is likely to be responsible for aggregation of $ZnPc(CHMeCO_2H)_4$ in ethanol by Na^+, K^+, Mg^{2+}, Zn^{2+} or $^tBu_4N^+$ ions, irrespective of the nature of the ions. The concentrations of electrolyte concerned ($\sim 10^{-4}$ mol dm^{-3}) are considerably less than those reported[44],[45] in aqueous solution (0.01 mol dm^{-3} or greater). In fact, with the exception of tetraalkylammonium salts, monomeric $ZnPc(CHMeCO_2H)_4$ species were observed at ionic strengths of this magnitude in ethanol. This behaviour illustrates the complexities of aggregation phenomena. In aqueous solution, substituent groups, in this case carboxylate ions, are hydrated. That is, they are surrounded by a solvation shell of ordered water molecules. This has two conflicting effects. Firstly, hydration reduces the effective negative charge of carboxylate ions, therefore, ionic repulsion effects will be lessened[46]. Secondly, acid groups are protected from ions in the bulk media. Of course, electrolyte ions will also be highly solvated, e.g. the free energy of hydration[47], of Na^+ ions is 375 kJ mol^{-1} and that of Ca^{2+} is 1584 kJ mol^{-1}. Hence large concentrations of ions are necessary for ion pairing to occur. In non-aqueous solution, ion solvation energies are lower[48] with respect to water, for example, the free energy

change, ΔG_{tr}, on transferring a $^tBu_4N^+$ ion from water to ethanol[49] is +18 kJ mol^{-1}. As a consequence of their reduced solvation, ions also have a greater activity in non-aqueous solution - it follows that association with other species will occur far more readily in these systems. Pairing of two entities is an entropically favourable process despite a reduction in the number of free species in solution[50]. This is due to disruption of the solvation shells about both species concerned. The water/solvent molecules forming the solvation shell become more disordered as molecules are released into the bulk solution resulting in an overall increase in the entropy of the system (ΔS). The same effect is achieved by aggregation, in which two faces of monomeric dye molecules, previously in contact with solvent molecules in the solvation shell, are lost. Thus, aggregation of phthalocyanine molecules paired with metal ions is partially driven by energetically favourable entropy terms. An additional driving force for aggregation is the decrease in the diffusion coefficients of dyes which results from an increase in the electrolyte concentration[51].

Disaggregation at concentrations of 0.01 mol dm^{-3} may also be explained using entropic considerations. It has previously[52] been observed that tetramethylammonium salts induce the formation of Acridine Orange dimers in aqueous solution up to an ionic strength of 0.3 mol dm^{-3} due to screening of positive charges on the dye by counter anions. At greater concentrations, the aggregation constant started to decrease. This was ascribed to 'structure breaking' characteristics of the salt. It was thought that methylammonium ions acted to break apart the solvation shell of the dye. In this way favourable entropy terms associated with dimerisation have been removed, ΔG is less negative and aggregation becomes less energetically favourable. It is believed that tetrabutylammonium salts act as structure makers in water[53],[54]. This has been rationalised in terms of the influence of non-polar solutes on cooperative hydrogen bond formation[55]. These solutes serve to protect developing clusters from charge fluctuations which interrupt bonding. Hence solvent order increases.

It is possible to use this argument for the results obtained here. At low concentrations of electrolyte, aggregation was observed due to association of the carboxylic substituents of the phthalocyanine and metal ions. However, at high concentrations ($\sim$ 0.01 mol dm^{-3}), ordering of the ethanol solvent shell around phthalocyanine molecules is disrupted due to the structure breaking properties of Na$^+$, K$^+$ and ClO$_4^-$ ions, the driving force for aggregation is removed, and ZnPc(CHMeCO$_2$H)$_4$ becomes monomeric once more. By contrast, $^tBu_4N^+Cl^-$ and $^tBu_4N^+ClO_4^-$ salts increase ordering, thus disaggregation was not observed. In the latter case, ordering by cations and disruption by anions act competitively. It would appear that the ordering effect of the butylammonium ions is

greater. It should be noted that the effect of ions on the ordering of non-aqueous solvents is generally less than that of water. Two dimensional hydrogen bonding, such as may occur in alcoholic solution, is less influenced by solute than the three dimensional H-bonding that exists in water[56]. This is because non-aqueous solvents are inherently less ordered systems than water (entropy of water = 69.9 J K^{-1} mol^{-1}, entropy of ethanol = 160 J K^{-1} mol^{-1})[57].

The properties of $ZnPc(CHMeCO_2H)_4$ in aqueous solution are very different. The observed insolubility of the carboxylate in distilled water may be explained by reference to the acid dissociation constants. Due to the separation of the carboxylate groups from the phthalocyanine skeleton, phenylacetic acid[58] (pK$_a$ of 4.3 at 293 K in water) may be used as a model for the pK$_a$ of the phthalocyanine carboxylate groups. Accordingly, the acid groups of $ZnPc(CHMeCO_2H)_4$, would be expected to remain largely undissociated in water (pH ~ 4.5-5) and consequently have little effect on the overall solubility of the phthalocyanine - c.f. $ZnPc(CMe(CO_2Me)_2)_4$. $ZnPcS_2$ is soluble in H_2O due to the greater acidity of the sulfonic acid substituents in comparison to the carboxylate groups above (pK$_a$ = 2.5)[59]. PBS renders both $ZnPc(CHMeCO_2H)_4$ and $ZnPcS_2$ soluble. This buffer has a pH of 7.4, a pH at which both sulfonates and carboxylates are fully dissociated. This explanation is corroborated by the effects observed on altering the pH of PBS. Alkaline conditions encouraged dissociation of the acidic groups, thus the state of aggregation was unaffected. At low pH (2) further aggregation occurred due to protonation of carboxylic acid side chains. Phosphate buffer saline (PBS) contains 0.1 mol dm^{-3} NaCl ions. In aqueous solution, $ZnPc(CHMeCO_2H)_4$ is dimeric for the reasons discussed above, i.e. intermolecular ionic repulsions between negatively charged substituents are screened by hydration shells, favourable entropic considerations and solvophobic forces[60]. Any structure breaking capacity of Na$^+$ or Cl$^-$ ions is too weak to have any effect. CTAB, however, effectively induces monomerisation. Ben-Hur et al.[61] have used 1% hexadecyl trimethylammonium bromide (CTAB) solution to monomerise sulfonated metallocyanines however, at this concentration (~0.03 mol dm^{-3}), monomerisation is most likely to be caused by incorporation into micelles. The concentrations used in this study (0.02 mmol dm^{-3}) were well below the cmc of CTAB (0.9 mmol dm^{-3}), therefore, disaggregation is not due to incorporation into micelles. Hence, this effect may be explained in terms of ion pairing. In contrast to the effect of ion pairing discussed above, where pairing in ethanol *induced* dimerisation due to linking of substituent carboxyl groups by metal cations, here dimerisation is prevented due to steric inhibitions introduced by pairing of bulky hexadecyl trimethylammonium groups to the ionic side chains of the phthalocyanine.

3.3.2.3.2 Photophysical Properties

The effect of solvent on λ_{max} is a complex and involved issue. Foley[74] reported a blue shift in the absorption spectrum of $AlPcS_2$ with increasing dielectric constant whilst Harazono[62] *et al.* observed a red shift in the $S_1 \leftarrow S_0$ transition of titanium (IV) oxide phthalocyaninate (TiOPc) as solvent polarity and dipole moment increased. It is generally accepted that the wavelength of $\pi\pi^*$ transitions increases with solvent polarity[63] due to a greater stabilisation of the excited state with respect to the ground state. The results obtained here (Figure 3.4) show a random distribution of absorption maxima with dielectric constant and solvent dipole moment. A possible connection between the electron donating propensity (DN) of the solvent and λ_{max} is suggested whilst a reasonable linear correlation with refractive index was observed. These plots are illustrative of the complexities encountered when trying to apply a simple trend.

In the case of phthalocyanines, it is not possible to consider purely one type of intermolecular interaction. Electrostatic forces between solute and solvent, hydrogen bonding capacity and the potential of the solvent to act as a ligand must all be considered. Harazono attempted to separate these contributions with dubious success[62]. Refractive index is a measure of the polarisability of a solvent. Limantara *et al.*[64] have demonstrated that the dependency of the Q_x and Q_y transitions of bacteriochlorophyll a on the refractive index of polar and non-polar solvents follows Equation 3.3. A red shift of absorption maxima was observed with increasing refractive index.

$$\bar{v} = -d.R(n_D) + e \quad where \quad R(n_D) = \frac{n_D^2 - 1}{n_D^2 + 2} \qquad (3.3)$$

Application of Equation 3.3 where n_D is the refractive index of the solvent to the data obtained for $^tBu_4ZnPc$ yielded a plot (Figure 3.10) with a linear fit of gradient, -1900 cm^{-1} (coefficient d) and intercept, 15300 cm^{-1} (coefficient e). This is in good agreement with Limantara's values of -2333 cm^{-1} and 17680 cm^{-1} (d and e respectively) for bacteriochlorophyll a in polar solvents.
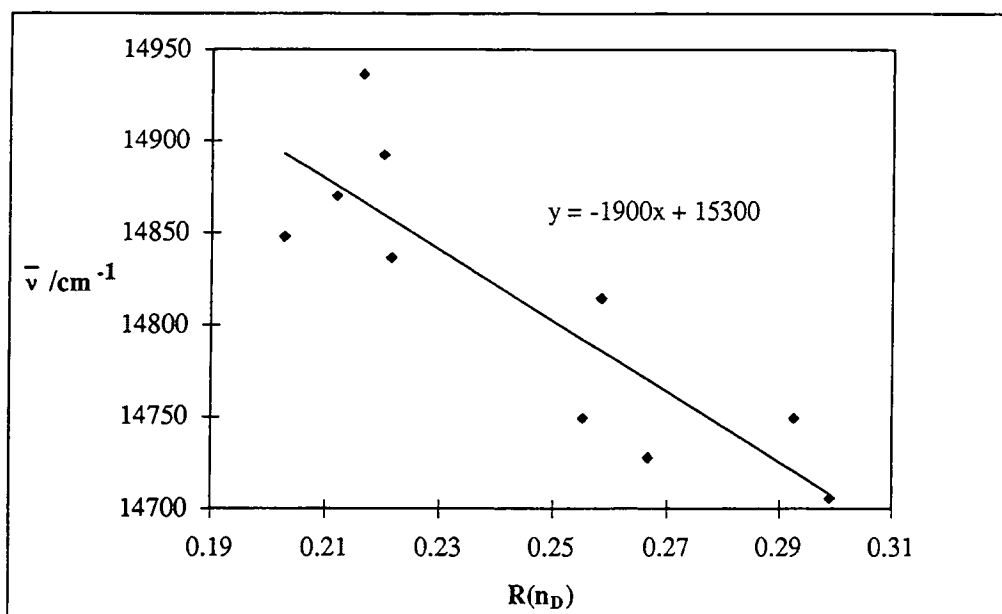
Figure 3.10.

Relationship between solvent refractive index and λ_{max} (UV/Vis.) of $^tBu_4ZnPc$.

The effect of substituents on the position of the Q band absorption may be rationalised in terms of their propensity to donate electrons to the π system of the phthalocyanine ring. It has been shown experimentally that electron donating substituents on the phthalocyanine rings cause red shifts in the absorption spectrum of ZnPc[5]. The magnitude of the shift was reported to depend on the site of peripheral substitution in addition to the strength of the donor. This was corroborated by Ford et al.[16] in 1989 who demonstrated that the absorption spectrum of α substituted octabutoxyzinc phthalocyanine was shifted ~70 nm to longer wavelengths with respect to ZnPc in the same solvent. In contrast, octabutoxy substitution in the β positions had little effect on the position of λ_{max}[37],[65]. Of the compounds investigated in this study, the octadecyl substituents of C10 were observed to have the largest effect, inducing a red shift of 33 nm with respect to the parent phthalocyanine. This is in agreement with a previous study[17] of the basic photophysics of C10. Alkyl chains are known to act as electron donors when attached to a π electron system[66]. A theoretical explanation for these effects has recently been published by Morley et al.[67]. The Q band of phthalocyanine molecules is a $\pi\pi^*$ transition or HOMO to LUMO transition. Substituent donors can stabilise the LUMO by donating electrons to the nitrogen atoms of the ring. α and β substituents both stabilise in this way, however, α substituents are more effective, thus a greater decrease in the transition energy is observed. This explains the smaller shift of $^tBu_4ZnPc$ with respect to C10 since the butyl groups were located in the β positions. Electron withdrawing groups may also be expected to induce a small red shift.

Peripheral substitution had little effect on the propensity of ZnPc's to produce singlet oxygen. This corroborates results by Fernandez et al.[23] who found that substitution by nitrogen containing substituents neither enhanced nor depleted the yield of triplet state and singlet oxygen formation by ZnPc. Similarly, Ben-Hur[12] has reported that sulfonate group substitution of aluminium phthalocyanine had no effect on its photophysical properties. In this study, the fluorescence, triplet and singlet oxygen quantum yields remained approximately constant, with the notable exceptions of $ZnPc(CHMeCO_2H)_4$ in 0.02 mmol dm^{-3} CTAB/PBS and C10. In these cases, a dramatic decrease in Φ_F from 0.25 to 0.06 and 0.082 respectively was observed. For $ZnPc(CHMeCO_2H)_4$ in 0.02 mmol dm^{-3} CTAB/PBS the most reasonable explanation for this and the low value of Φ_T (0.18) is the presence of Br$^-$, a heavy atom which will act to quench the excited state. A comparable value of Φ_F was measured by Valduga[68] for ZnPc in CTAB micelles. C10 displayed a concurrent increase in Φ_T (0.8) with respect to unsubstituted ZnPc, suggesting that k_{isc} has increased[17].

3.3.2.3.3 Low Temperature Measurements

Sharpening of absorption and fluorescence spectra on lowering the temperature may be attributed[69] to a decrease in the thermal motion of surrounding solvent molecules, leading to a reduced inhomogeneous broadening of the transition. Shifts in λ_{max} are more difficult to explain. Cupane et al.[70] observed a red shift upon cooling a solution of Ni(II) octaethyl porphyrin to 100 K. This was ascribed to an equilibrium between planar and non-planar macrocyclic structures, shifting towards the lower energy non-planar conformation at low temperatures. Phthalocyanines are remarkably planar in structure, non-planarity only having been observed in special cases[71], therefore, this scenario is viewed as rather unlikely for this class of compounds. The hypothesis of Hoshino et al.[72] who ascribe a shift of dimeric chlorophyll a from 695 nm to 706 nm on cooling from 160 K to 77 K, to a change in configuration of the dimer is more reasonable. It is feasible that rearrangement of solvent molecules around the phthalocyanine and/or peripheral substituent configuration changes at low temperature may be responsible for the shifts observed here. This has been demonstrated by the effect of temperature on (BuO)$_8$ZnPc (vide infra). Large red shifts in the absorption spectrum upon cooling indicate that the nature of the solvent and potential interactions with peripheral substituents of the phthalocyanine ring are very important. Shifts in EPA and EtOH of ~ 40 nm suggest that stabilisation of the LUMO occurred. The most likely cause of this is formation of hydrogen bonds between solvent molecules and oxygen atoms of the substituent. This is corroborated by behaviour in aprotic solvents, MeTHF and Et$_2$O:IP, in which hydrogen bonding is impossible and far smaller shifts were

obtained ($\Delta\lambda$ = 13 nm and 14 nm respectively). Not surprisingly, low temperatures resulted in a smaller Stokes shift of emission. This stems from reduced rotational deactivation pathways at 77 K due to the rigidity of the solvent glass which inhibits molecular motion. More interesting is the solvent dependency of the magnitude of the change. A significantly larger decrease was observed in aprotic solvents (11 nm → 2 nm) than in protic solvents (14 nm → 11 nm) whilst the absolute value was larger for protic solvents, i.e. those capable of hydrogen bonding. Hydrogen bonding to the chromophore increases the number of vibrational deactivation modes available and hence facilitates energy loss to surrounding molecules. Protic solvents will therefore cause a larger decrease in the energy of emission with respect to absorption. At low temperatures, the number of hydrogen bonds increased whilst vibrational motion is reduced. These conflicting effects mean that the Stokes shift is not reduced as significantly in protic solvents as in aprotic solvents where the only process to be considered is that of reduced vibrational deactivation pathways.

Sheppard et al.[46] suggested that increased polarity of solvent molecules at low temperature was responsible for a red shift in the absorption spectrum of non-ionised merocyanine. It is generally accepted that $\pi\pi^*$ transitions are red shifted with increased solvent polarity, suggesting that this may be a feasible explanation; however, it has already been shown that the $S_1 \leftarrow S_0$ transition energy of zinc phthalocyanines does not exhibit straight forward behaviour with solvent polarity. The effect of temperature on the refractive index of ethanol[73] may be described by Equation 3.4.

$$\frac{dn_D}{dT} = -3.7 \times 10^{-4} \ K^{-1} \qquad\qquad (3.4)$$

where n_D is the refractive index and T is the absolute temperature. dn_D/dT is negative for most solvent media and demonstrates that as the temperature of a solution is lowered, the refractive index increases. Hence, by reference to Figures 3.4 and 3.10 which show a shift in λ_{max} with n_D, a bathochromic shift of λ_{max} may be predicted. The red shifts of $^tBu_4ZnPc$ and $ZnPc(CMe(CO_2Me)_2)_4$ may be explained by this theorem. $ZnPc(CHMeCO_2H)_4$ and $ZnPcS_2$ show an opposite shift suggesting a different interaction which causes destabilisation by solvent molecules at low temperature.

The appearance of an absorption peak at 625 nm in the low temperature spectrum of $ZnPc(CMe(CO_2Me)_2)_4$ (Figure 3.7D) may be ascribed to dimeric phthalocyanine species. Lack of additional emission at 77 K and the absence of this peak in an excitation

spectrum is typical of non-fluorescent dimer species formed by phthalocyanines[74]. It is well known that aggregation of dyes increases at low temperature[75],[76].

As a consequence of sharpening of absorption bands at low temperature, resolution of spectra is improved. This is demonstrated by the spectra of $ZnPcS_2$ in which broad 'flat topped' peaks were observed at 77 K in both UV/Visible and excitation spectra. There are several possible explanations for this. $ZnPcS_2$ used in this study consisted of a mixture of isomers[77] with substituents in both α and β positions of the ring. As has been discussed, α and β substituents have different propensities to affect the position of λ_{max}. It is therefore not unreasonable to assume that a mixture of isomers would result in a broad absorption band consisting of several individual peaks, unresolvable until rotational broadening is quenched. Similar behaviour has been observed for disulfonated aluminium phthalocyanine at room temperature[78]. This was attributed to unsymmetrical polarisation of the molecule in x and y directions in those isomers where sulfonate groups were in asymmetric positions, removing the degeneracy of the S_1 excited state. By considering the emission spectrum recorded for $ZnPcS_2$ at 77 K, in which a single, sharp emission peak was observed (Figure 3.8A), it can be concluded that emission must be from a single molecule. If splitting of the UV/Visible spectrum was due to absorption by more than one phthalocyanine species, e.g., a mixture of α and β substituted isomers, it would be expected that the splitting would also be observed in the emission spectrum. However, in an analogous fashion to that discussed by Bishop, removal of S_1 degeneracy will only result in one emission level due to rapid deactivation of the higher state. It is concluded that the low temperature phenomenon observed here may be ascribed to asymmetric x and y polarisations of the phthalocyanine ring.

3.3.3 Properties in Heterogeneous Solution
3.3.3.1 Micellar Systems

Triton X-100 non ionic surfactant, (Figure 3.11) has been used to investigate the photophysical properties of modified ZnPc's. Triton X-100 (TX) is a polydisperse sample of isooctylphenoxypolyethoxyethanol with an average of 9.5 oxyethylene units per molecule[79].
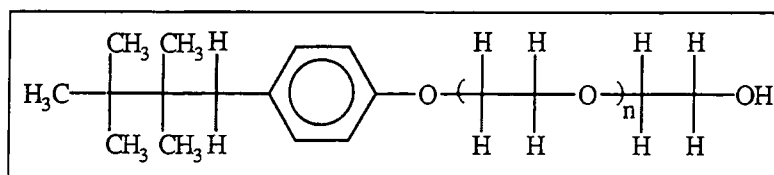
Figure 3.11. Structure of Triton X-100.

This is an amphiphilic molecule, consisting of a hydrophobic head group (alkyl substituted phenyl ring) and long hydrophilic polyoxyethylene tail. At low concentrations free, monomeric surfactant chains exist in solution. When the concentration of surfactant molecules is increased to what is known as the *critical micelle concentration* (cmc), aggregation to form micelles occurs (Figure 3.12). At the cmc (0.26 mmol dm^{-3})[31], the gain in free energy obtained by removing energetically unfavourable water/tail interactions becomes more significant than the loss of entropy associated with the ordered nature of the micelle. The phenyl groups associate to form a hydrophobic core while the oxyethylene chains extend into the aqueous phase. On average, TX micelles are formed from ~140 individual molecules and have a diameter of 110-125 Å and a radius of gyration of 30.9 Å. Triton X-100 reduced, TXR, is a chemically reduced form of Triton X-100, i.e. the phenyl ring is saturated to cyclohexane. This results in removal of absorption bands in the ultraviolet region but the micellar properties of Triton X-100 reduced do not differ significantly from those of Triton X-100[80].
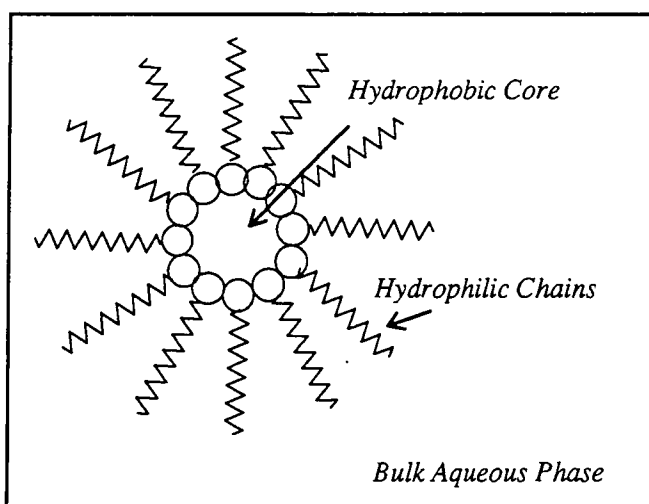
Figure 3.12. Simple diagram of a normal micelle.

3.3.3.2 Photophysical Properties

Incorporation of hydrophobic zinc phthalocyanines into the hydrophobic core of neutral surfactant micelles (Triton X-100) allows aqueous solutions to be prepared. UV/Visible absorption spectra of $^tBu_4ZnPc$, $ZnPcS_2$, $ZnPc(CMe(CO_2Me)_2)_4$ and $ZnPc(CHMeCO_2H)_4$ were characteristic of monomeric species at low concentrations giving linear Beer-Lambert plots below 2×10^{-6} mol dm^{-3}. Above this concentration, $ZnPcS_2$ and $ZnPc(CMe(CO_2Me)_2)_4$ remained monomeric across the concentration range of interest for photophysical measurements ($< 5 \times 10^{-6}$ mol dm^{-3}) while the Beer-

97

Lambert plots of ZnPc(CHMeCO$_2$H)$_4$ and ^{t}Bu$_4$ZnPc showed a small degree of negative curvature (Figure 3.13), indicative of aggregation.
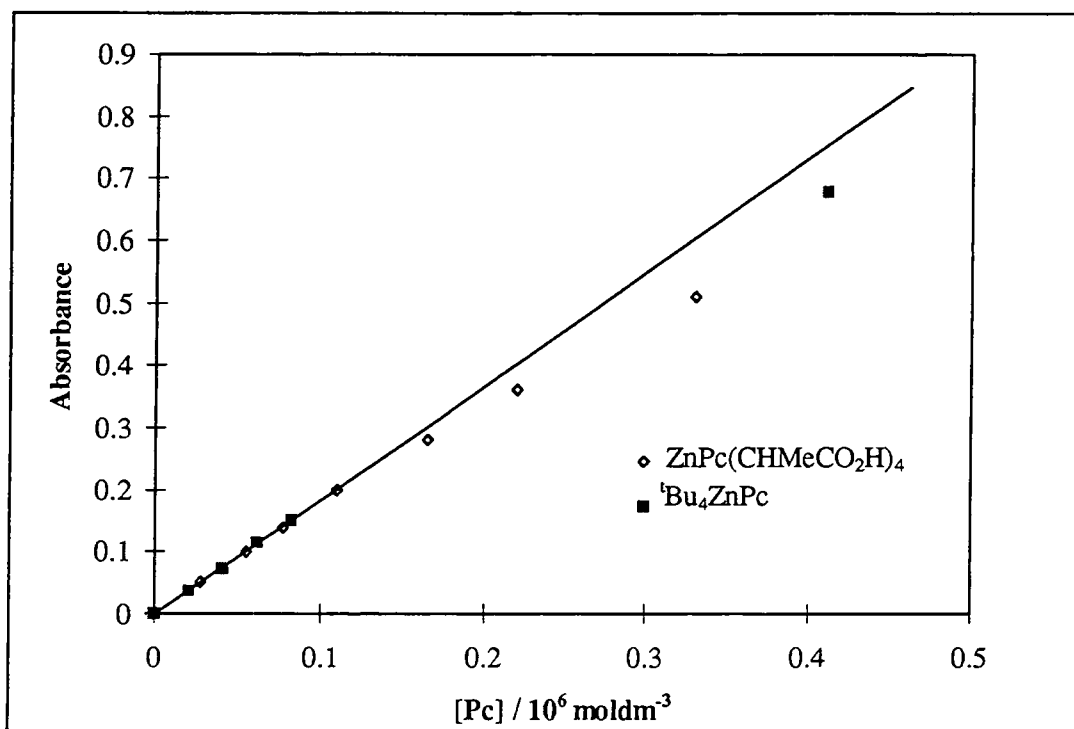
Figure 3.13. Beer-Lambert plots
^{t}Bu$_4$ZnPc and ZnPc(CHMeCO$_2$H)$_4$ in 1% TX/PBS.

The absorption spectra for C10 in 1% TX/PBS and 1% TXR/PBS are shown in Figure 3.14. The spectrum carried out in 1% TX/PBS shows increased absorption between 640 nm and 690 nm which may be due to aggregated species, although linear Beer-Lambert plots were obtained across the concentration range studied. The spectrum of C10 in 1% TXR/PBS is characteristic of monomeric phthalocyanine. Since the micelle properties of this surfactant are not significantly different to those of Triton X-100, these results imply that the saturated nature of Triton X-100 reduced provides a better solvent environment for this phthalocyanine.
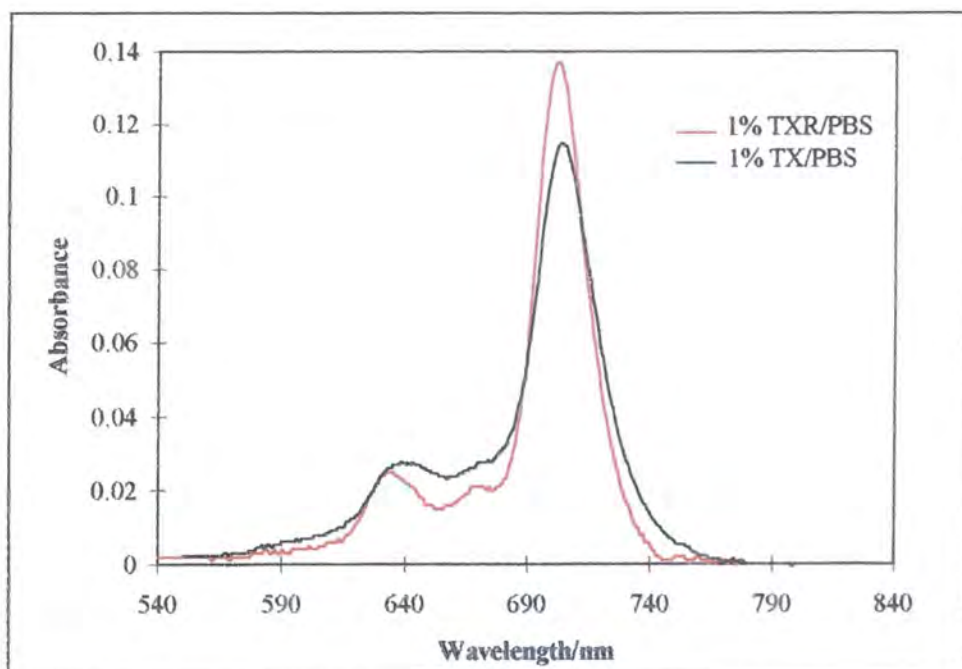
Figure 3.14. Absorption spectra of C10 in 1% TXR/PBS and 1% TX/PBS.

Table 3.7 collates Φ_F, Φ_T, τ_T and Φ_Δ values measured in 1% TX/PBS solution. In the absence of fluorescence lifetime data it is not possible to calculate fluorescence, internal conversion or intersystem crossing rates. It can be seen that for $^tBu_4ZnPc$, $ZnPcS_2$, $ZnPc(CMe(CO_2Me)_2)_4$, and $ZnPc(CHMeCO_2H)_4$, Φ_F is significantly reduced with respect to measurements performed in homogeneous solution (Table 3.3B). It is possible that incorporation into micelles increases the rate of internal conversion by increasing the number of vibrational deactivation pathways available to the fluorophore. Alternatively, aggregation of phthalocyanines may be responsible. This is unlikely, however, since it has been shown that absorption follows the Beer-Lambert law to concentrations far greater than those used to determine fluorescence yields.

Pc	λ_{max} (UV/Vis) /nm	Φ_F	Φ_T	τ_T /µs	Φ_Δ
$ZnPcS_2$	672	0.17 ± 0.02	0.55 ± 0.05	340 ± 40	0.53 ± 0.05
A[a]	684	0.14 ± 0.03	0.5 ± 0.05	210 ± 20	0.55 ± 0.05
E[b]	679	0.16 ± 0.03	0.5 ± 0.05	315 ± 30	0.55 ± 005
C10	704	0.080 ± 0.005	0.57 ± 0.05	110 ± 30	0.5 ± 0.05
$^tBu_4ZnPc$	678.5	0.15 ± 0.02	0.48 ± 0.05	310 ± 25	0.5 ± 0.05
C10[c]	702	0.080 ± 0.005	0.8 ± 0.1	100 ± 20	-

a. A = $ZnPc(CHMeCO_2H)_4$, b. E = $ZnPc(CMe(CO_2Me)_2)_4$, c. In 1% TXR/PBS

Table 3.7. Photophysical properties of substituted ZnPc's in 1% TX/PBS.

99

The quantum yields of triplet state and singlet oxygen formation were comparable with those determined in homogeneous media and are typical of values measured for monomeric phthalocyanines. τ_T displayed an increase with respect to those measured in organic solvents (Table 3.4). C10 behaved differently to the other phthalocyanines. No effect on the fluorescence yield was observed upon incorporation into micelles, however, a significant decrease in the quantum yield of triplet state was observed. Coupled with ground state absorption data, this was ascribed to aggregation of the phthalocyanine. Changes in the fluorescence yield may have been within experimental error and hence undetectable. Incorporation into TXR/PBS micelles increased the measured triplet yield to 0.8 - comparable to that measured in 1% pyr/tol - and confirmed the presence of monomeric species in this system.

3.3.4 Properties in the Solid State

Using the method described in Section 2.2.7.2, it was possible to prepare monomeric samples of $^tBu_4ZnPc$ adsorbed onto silica, cellulose powder, filter paper or protein (BSA). Figure 3.15A shows the remission function calculated for $^tBu_4ZnPc$ on silica. The position of the absorption maximum (λ_{max}) was determined by the nature of the substrate. λ_{max} is a good indicator of the environment of phthalocyanine (See Section 3.3.2.3.2), and shifted progressively from 670 nm to 678 nm to 678.5 nm as the substrate was changed from silica to bovine serum albumin to cellulose respectively. Slight broadening of the spectrum (FWHM = 20 nm, c.f. 19 nm in MeOH) is attributed to the large distribution of environments available on solid substrates. Figure 3.15B shows the remission function of $ZnPc(CHMeCO_2H)_4$ on silica, prepared from a methanolic solution. This phthalocyanine shows evidence of aggregation (denoted by broad, unstructured absorption) superimposed on the spectrum of monomeric phthalocyanine. A large FWHM (43 nm) was obtained as a result of aggregation and the inhomogeneous nature of the environment. The aggregated state of $ZnPc(CHMeCO_2H)_4$ on silica suggests that the dye molecules do not participate in any strong chemical interactions with the substrate.
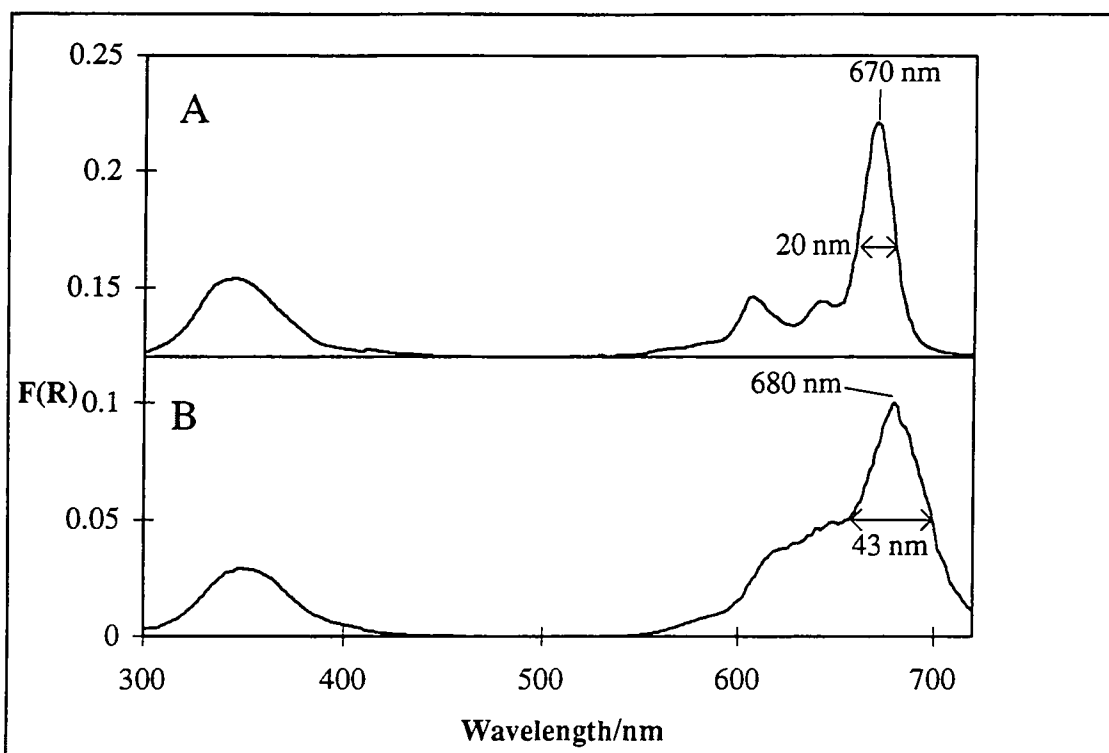
Figure 3.15. Remission functions of phthalocyanines on silica.
A. $^tBu_4ZnPc$. B. $ZnPc(CHMeCO_2H)_4$. Spectra have been offset for clarity.
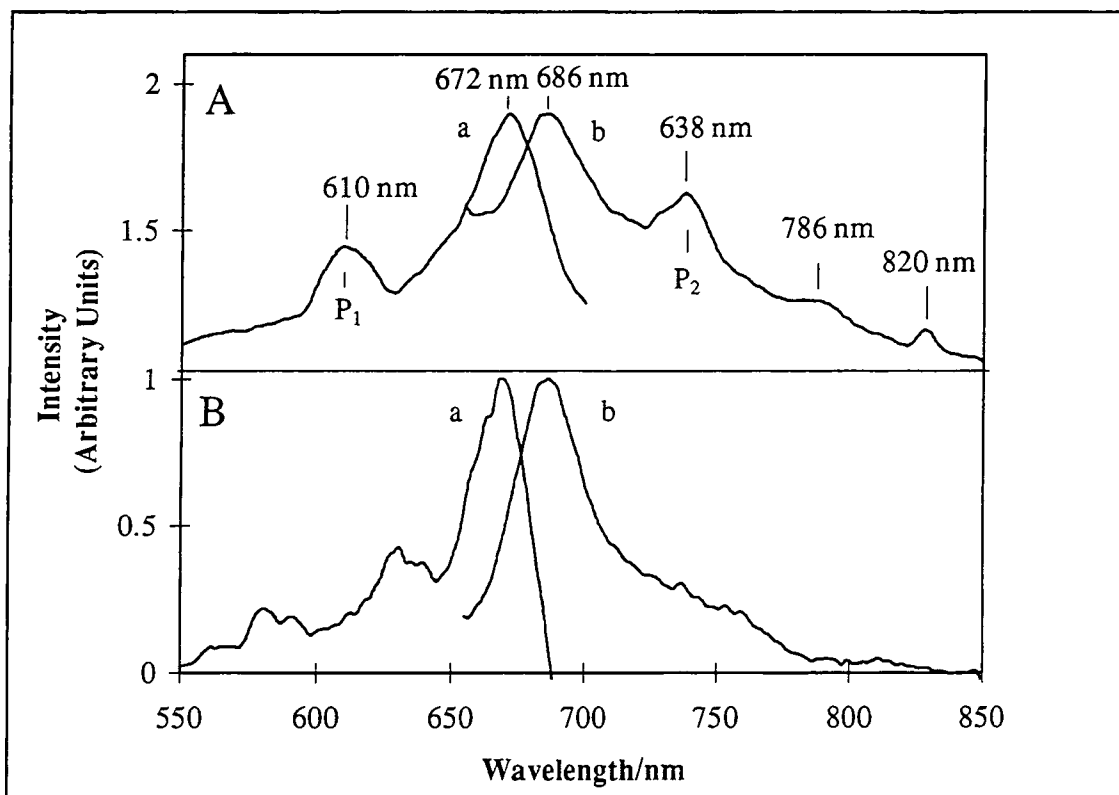
Figure 3.16. A. Excitation (a) and emission (b) spectra of $^tBu_4ZnPc$ on cellulose
($\lambda_{em} = 740$ nm, $\lambda_{ex} = 610$ nm). B. Corrected for artefacts. Spectra have been offset
for clarity.

101

The emission and excitation spectra obtained from a 'dilute' ($\sim$6 μg g^{-1}) sample of ^{t}Bu$_4$ZnPc on cellulose are shown in Figure 3.16. Unexpected peaks were observed at 638 nm, 786 nm and 820 nm in the emission spectrum and 610 nm in the excitation spectrum. The intensity of these peaks relative to phthalocyanine emission was reduced by increasing the concentration of the sample. It was concluded, therefore, that these peaks arose due to an artefact rather than the behaviour of phthalocyanine

The source of these 'emission' bands was investigated. It was found that the positions of the peaks were independent of the substrate used, ruling out fluorescence or absorption artefacts of cellulose. When an empty sample holder was used (with quartz plate) these peaks were still observed, but when the same holder was used without a quartz plate, i.e. when teflon was the only scattering surface, a flat baseline was obtained. It was concluded that 'emission' originated from either the quartz window or an inherent impurity within it. Variation of the excitation wavelength or monitored emission wavelength caused peaks at 610 nm (P$_1$) and 638 nm (P$_2$) to shift (Figure 3.16A). The position of emission peaks at 786 nm and 820 nm remained constant. Clearly, spurious peaks are due to two different phenomena. It is probable that static peaks were caused by fluorescence emission from impurities in the quartz. The same difficulty was encountered whilst making singlet oxygen measurements (Appendix A). The energy difference, ΔE_1, between λ_{max}(P$_1$) and the monitored emission wavelength, λ_{em}, was constant at 2700 $\pm$ 200 cm^{-1}. ΔE_2, the energy difference between λ_{max}(P$_2$) and the wavelength of excitation, λ_{ex}, was 2850 $\pm$ 200 cm^{-1}. $\Delta E_1 = \Delta E_2$. It is tentatively suggested that this phenomenon may be due to a previously unreported Raman band of quartz or of an impurity therein. Spectra were corrected by scanning a 'blank', i.e. substrate only, as a background signal with subsequent subtraction from sample spectra. In this way, excitation and emission spectra resembling solution state, monomeric phthalocyanine were obtained (Figure 3.16B).

Transient absorption decays obtained by diffuse reflectance flash photolysis fitted well to monoexponential decay curves (Figure 3.17), yielding lifetime values of 90 μs $\pm$ 15 μs on silica and 130 μs $\pm$ 20 μs on cellulose. These lifetimes are slightly reduced compared with the lifetime observed in degassed homogeneous solution (170 μs). The decay of ^{t}Bu$_4$ZnPc on a cellulose substrate had a longer lifetime than that of phthalocyanine adsorbed on silica. There have been many reports of extended triplet state lifetimes of molecules adsorbed on cellulose[81],[82]. Cellulose protects samples from oxygen quenching due to the rigidity of the cellulose matrix and poor mobility of oxygen molecules through dry cellulose[83]. This suggests that complete deoxygenation of the sample was not achieved. The transient absorption spectrum was centred at 490 nm,

consistent with triplet species in solution and was independent of delay time (Figure 3.18).
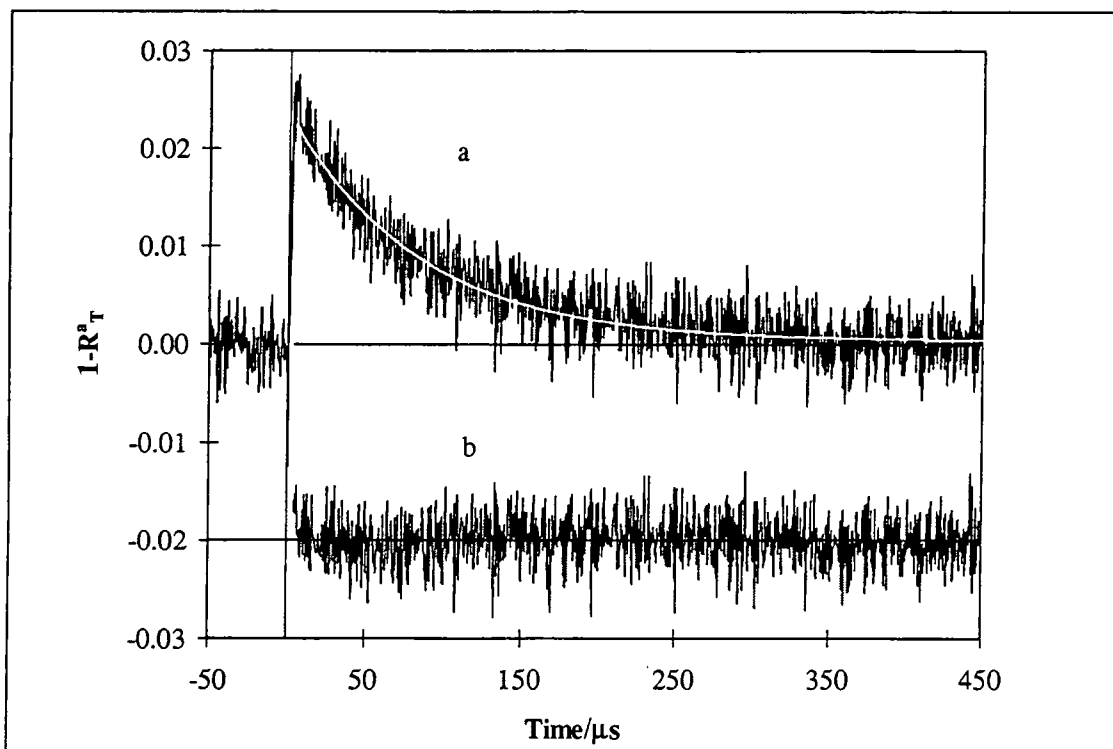
__Figure 3.17.__ a. Typical diffuse reflectance transient decay, $\lambda_{Probe} = 490$ nm, $\lambda_{ex} = 355$ nm. b. Residuals of monoexponential fit (offset for clarity).
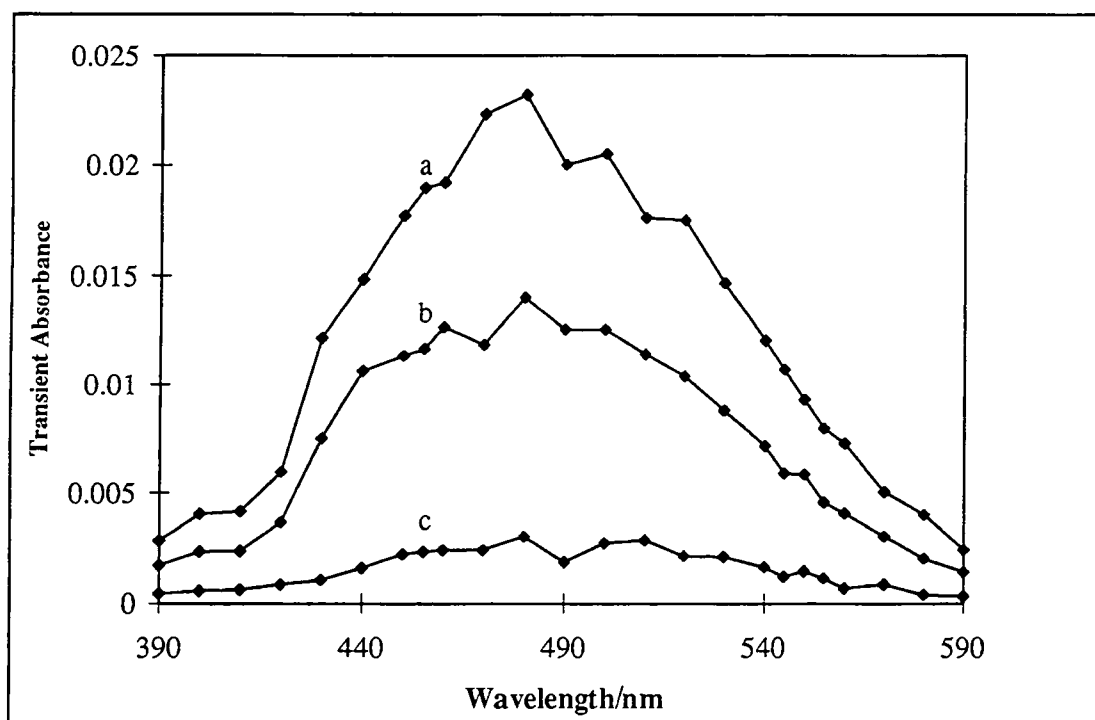
__Figure 3.18.__ Diffuse reflectance transient absorption spectrum of $^tBu_4ZnPc$ on cellulose. a. $\Delta t = 5$ μs, b. $\Delta t = 50$ μs, c. $\Delta t = 200$ μs.

Hence, it is possible to incorporate substituted zinc phthalocyanines onto solid substrates whilst retaining photophysical activity.

3.4 Conclusion

Two novel, substituted zinc phthalocyanines, $ZnPc(CMe(CO_2Me)_2)_4$ and $ZnPc(CMe(CO_2H)_4$, have been synthesised. The photophysical properties, Φ_F, Φ_T, τ_T and Φ_Δ, of $ZnPc(CMe(CO_2H)_4$ and $ZnPc(CMe(CO_2Me)_2)_4$, are typical of substituted zinc phthalocyanines making these ideal candidates as sensitisers for photodynamic therapy. $ZnPc(CMe(CO_2Me)_2)_4$ displays remarkably monomeric character in $CHCl_3$ due to the bulky nature of its peripheral substituents, whilst $ZnPc(CMe(CO_2H)_4$ was soluble in aqueous solution at physiological pH. Such solubility properties are important for intravenous administration in therapeutic applications, however in EtOH solution aggregation of this phthalocyanine displayed an unusual dependence on ionic strength. Aggregation was found to be promoted by ion concentrations between zero and 5×10^{-4} mol dm^{-3}, while disaggregation occurred at concentrations $> 10^{-3}$ mol dm^{-3}. It is likely that ion pairing between acid substituents and cations results in aggregation at low ionic strengths. At higher ionic strengths, 'structure breaking' of solvation shells surrounding phthalocyanine removed energetically favourable entropic factors of aggregation, leading to regeneration of monomeric phthalocyanine species. It has also been shown that disaggregation in PBS can be induced by 0.02 mmol dm^{-3} CTAB due to steric inhibitions introduced by ion pairing. Considerable ion effects such as these may have important consequences *in vivo* where ion transport across cell membranes is a vital biological function[84]. Certain sensitisers are known to locate in the cell membrane[85]. In the case of $ZnPc(CMe(CO_2H)_4$, its aggregation state, and consequently its efficacy as a sensitiser, may be controlled by the ionic strength of the surrounding medium.

The effect of peripheral substitution of ZnPc by various groups (X) has also been considered. The position of the absorption maximum, λ_{max}, was found to be dependent on the position of substitution in the ring (α or β) and the refractive index of the solvent. The photophysical properties of $ZnPcX_n$ were unaffected by the identity of X, differences being observed only in the case of $X = C_{10}H_{21}$. By contrast, effects of low temperature (77 K) on the absorption and fluorescence spectra of $ZnPcX_n$ were found to be highly dependent on the nature of substituents.

It has been shown that, despite their hydrophobicity, these phthalocyanines may be incorporated into aqueous micellar systems or adsorbed onto solid substrates without

loss of photoactivity. This has important consequences with respect to incorporation of phthalocyanines into lipid bilayers or onto tumour tissue *in vivo* where a change in physical (e.g. aggregation) or photophysical (e.g. Φ_Δ, Φ_T) properties would render the dye less efficient.

3.5 References

[1]   Reddi E., Castro G.L., Biolo R. and Jori G., Pharmacokinetic studies with Zn(II) phthalocyanine in tumour bearing mice., *Br. J. Cancer*, **56**, 597-600, 1987.

[2]   Chan W.S., Marshal J.F., Svensen R., Phillips. and Hart I.R., Photosensitising ability of phthalocyanine dyes screened against tissue cell cultures., *Photochem. Photobiol.*, **45**, 757-761, 1987.

[3]   Zhou C., Shunji C., Jinsheng D., Junlin L., Jori G. and Milanesi C., Apoptosis of mouse MS-2, fibrosarcoma cells induced by photodynamic therapy with Zn(II) phthalocyanine., *J. Photochem. Photobiol. B:Biol.*, **33**, 219-223, 1996.

[4]   Van Leengoed H.L.L.M., Cuomo V., Versteeg A.A.C., Van der Veen N., Jori G. and Star W.M., *In vivo* fluorescence and photodynamic therapy with Zn(II) phthalocyanine., *Br. J. Cancer*, **69**, 840-845, 1994.

[5]   Derkacheva V.M. and Luk'yanets E.A., Phthalocyanines and related compounds XVIII. Phenoxy- and (phenylthio)-substituted phthalocyanines., *J. Gen. Chem. USSR*, **50**, 1874, 1980.

[6]   Mikhalenko S.A., Barkanova S.V., Lebelev D.L. and Luk'yanets E.A., Phthalocyanines and related compounds. IX Synthesis and electronic absorption spectra of tetra-4-t-butylphthalocyanine., *J. Gen. Chem. USSR*, **41**, 2770, 1971.

[7]   Osburn E.J., Chau L.K., Chen S.Y., Collins N., O'Brien D.F. and Armstrong N.R., Novel amphiphilic phthalocyanines: Formation of Langmuir-Blodgett and cast thin films., *Langmuir*, **12**, 4784, 1996.

[8]   Koray A.R., Ahsen V. and Bekaroglu O., Preparation of a novel, soluble copper phthalocyanine with crown ether moieties., *J. Chem. Soc. Chem. Comm.*, **932**, 1986.

[9]   Mikhalenko S.A., Derkacheva S.V. and Luk'yanets E.A., Phthalocyanines and related compounds. Tetra and octa aminosubstituted phthalocyanine., *J. Gen. Chem. (USSR)*, **51**, 1405, 1981.

[10]   Rihter B.D., Kenney M.E., Ford W.E. and Rodgers M.A.J., Synthesis and photoproperties of diamagnetic octabutoxyphthalocyanine with deep red optical absorbance., *J. Am. Chem. Soc.*, **112**, 8064, 1990.

[11]   Martin P., Gouterman M., Pepich B.V., Renzoni G.E. and Schindeze D.C., Effects of ligands, solvent and variable sulphonation on dimer formation of aluminium and zinc phthalocyaninesulphonate., *Inorg. Chem.*, **30**, 3305-3309, 1991.

[12]   Ben-Hur E., Hoeben R.C., Ormondt H.V., Dubbelman T.M.A.R. and Steveninck J.V., Photodynamic inactivation of retroviruses by phthalocyanines - the effects of sulfonation, metal ligand and fluoride., *J. Photochem. Photobiol. B:Biol.*, **13**, 145-152, 1992.

[13]   Allen C.M., Weber J.M. and Van Lier J.E., Sulfophthalocyanines for photodynamic inactivation of viruses in blood products - Effect of structural modifications., *Photochem Photobiol.*, **62**, 184-189, 1995.

[14]   Dummin H., Cernay Th., Zimmermann H.W., Selective photosensitisation of mitochondria in HeLa cells by cationic Zn(II) phthalocyanines with lipophilic side chains., *J. Photochem. Photobiol. B:Biol.*, **37**, 219-229, 1997.

[15]   Rosenthal I., Ben-Hur E., Greenberg S., Concepcion-Lam A., Drew D.M. and Leznoff C.C., The effect of substituents on phthalocyanine photocytotoxicity., *Photochem. Photobiol.*, **46**, 959, 1987.

[16]   Ford W.E., Rihter B.D., Kenney M.E. and Rodgers M.A.J., Photoproperties of alkoxy substituted phthalocyanines with deep red optical absorbance., *Photochem. Photobiol.*, **50**, 277-282, 1989.

[17]   Dhami S., Photophysics of phthalocyanines in microheterogeneous systems., p56, *PhD Thesis*, Imperial College, London, 1996.

[18]   Valduga G., Reddi E. and Jori G., Steady state and time resolved spectroscopic studies on zinc(II) phthalocyanine in liposomes., *J. Photochem. Photobiol. B:Biol.*, **16**, 331-340, 1992.

[19]   Polo L., Reddi E., Garbo G.M., Morgan A.R. and Jori G., The distribution of the tumour photosensitiser Zn(II) Phthalocyanine and Sn(IV) etiopurpurin among rabbit plasma proteins., *Cancer Lett.*, **66**, 217-223, 1992.

[20]   Dr. A. Beeby, Unpublished Results.

[21]   Cook M.J., Chambrier I., Cracknell S.J., Mayes D.A. and Russell D.A. Octa alkyl zinc phthalocyanines: Potential photosensitisers for use in the photodynamic therapy of cancer., *Photochem. Photobiol.*, **62**, 542-545, 1995.

[22]   Tai S. and Hayashi N., Strong aggregation properties of novel phthalocyanines., *J. Chem. Soc. Perkin Trans.*, **2**, 1275, 1991.

[23]   Fernandez A., Awruch J. and Dicelio L.E. Photophysical and aggregation studies of [t]Bu$_4$ZnPc's., *Photochem. Photobiol.*, **63**, 784-792, 1996.

[24]   Simpson M.S.C., Beeby A., Bishop S.M., MacRobert A.J., Parker A.W. and Phillips D., Time resolved laser spectroscopy in biochemistry III., *S.P.I.E.*, **1640**, 520, 1992.

[25]   Roze M.P., Berzin'sn E.L. and Neiland O.Y., Synthesis of 3, 4 dicyanophenyl malonic esters and their use in the production of soluble phthalocyanines., *Zh. Org. Khim.*, **28**, 827, 1992.

[26]   Negri R.M., Zalts A., San Roman E.A., Aramendia P.F. and Braslavsky S.E., Carboxylated zinc phthalocyanines: Influence of dimerisation on the spectroscopic properties.   An absorption, emission and thermal lensing study., *Photochem. Photobiol.*, **53**, 317, 1991.

[27]   Kahl S.B. and Li J., Synthesis and characterisation of a boronated metallophthalocyanine for boron neutron capture therapy., *Inorg. Chem.*, **35**, 3878, 1996.

[28]   Poucher C.J., *The Aldrich Library of Infrared Spectra.*, Ed. III, Aldrich Chemical Company, Wisconsin, 1981.

[29]   Kobayashi N. and Lever A.B.P.   Cation or solvent induced supermolecular phthalocyanine formation: Crown ether substituted phthalocyanines., *J. Am. Chem. Soc.*, **109**, 7433-7441, 1987.

[30]   Dhami S., DeMello A.J., Rumbles G., Bishop G., Bishop S.M., Phillips D. and Beeby A., Phthalocyanine fluorescence at high concentration: dimers or reabsorption effect?, *Photochem. Photobiol.*, **61**, 341, 1995.

[31]   Kalyansundarum K., *Photochemistry in Microheterogeneous Systems*, p26, Academic Press, London, 1987.

[32]   Vincett P.S., Voight E.M., Rieckhoff K.E., Phosphorescence and fluorescence of phthalocyanines., *J. Chem. Phys.*, **55**, 4131, 1971.

[33]   Phillips D., The photochemistry of sensitisers for photodynamic therapy., *Pure Appl. Chem.*, **67**, 117, 1995.

[34]   Murov L.S., Carmichael I. and Hug G.L., *Handbook of Photochem.*, p296, Marcel Dekker inc., 2nd Ed., 1993.

[35]   It was assumed that V_{77}/V_{293} for EtOH was equivalent to that reported in Reference 34 for EtOH:MeOH (4:1) solution.

[36]   Abraham R.J., Burbridge P.A., Jackson A.H. and MacDonald D.B., The proton magnetic resonance spectra of porphyrins. Part IV. Coproporphyrin tetramethyl esters., *J. Chem. Soc. B.*, 620, 1966.

[37]   Wohrle D. and Schmidt V., Octabutoxyphthalocyanine, a new electron donor., *J. Chem. Soc. Dalton Trans.*, 549, 1988.

[38]   Abraham R.J., Eivazi F., Pearson H. and Smith K.M., $\pi\pi$ aggregation in metalloporphyrins: Causative factors., *J. Chem. Soc. Chem. Comm.*, 699, 1976.

[39]   All values taken from Reference 34 Page 346 except that of O-CO_2Bz. This value is contained in Reference 7.

[40]   Zhang X.F., Influence of halogenation and aggregation on photosensitising properties of zinc phthalocyanine., *J. Chem. Soc. Faraday Trans.*, **89**, 3347, 1993.

[41]   Wyn-Jones E. and Gormally J., *Aggregation Processes in Solution, Studies in Physical and Theoretical Chemistry*, **26**, 241, Elsevier, New York 1983.

[42]   Fukushima Y., Salt effect on the interaction of 22, 24 diprotonated 5,10,15,20 tetrakis (4-sulphonatophenyl) porphyrin with a β sheet structure of a zwitterionic polypeptide., *Bull. Chem. Soc. Jpn.*, **69**, 1719-1726, 1996.

[43]   Pasternack R.F., Francesconi L., Raff D. and Spiro E., Aggregation of Ni(II), Cu(II) and Zn(II) derivatives of water soluble porphyrins., *Inorg. Chem.*, **12**, 2607, 1973.

[44]   Hofstra U., Koehorst R.B.M., Schaafsma T.J., Excited state properties of water soluble porphyrin dimers., *Chem. Phys. Lett.*, **130**, 555, 1986.

[45]   Munro O.Q. and Marques H.M., Heme-peptide models for hemoproteins 2) N Acetylmicroperoxidase-8. Study of the π–π dimers formed at high ionic strength using a modified version of molecular exciton theory., *Inorg. Chem.*, **35**, 3768, 1996.

[46]   Sheppard S.E. and Geddes A.L., Effect of solvents on the absorption spectra of dyes. IV. Water as solvent: A common pattern., *J. Am. Chem. Soc.*, **66**, 1995, 1944.

[47]   Cox B.G., *Modern Phase Liquid Kinetics*, p46, Oxford Science Publications, New York, 1994.

[48]   Parker A.J., The effects of solvation on the properties of anions in dipolar aprotic solvents., Quarterly Reviews, London: *The Chemical Society*, **XVI**, 163, 1962.

[49]   Isaacs N.S., *Physical Organic Chemistry*, John Wiley and Sons, New York, p178, 1987.

[50]   Nancollas G.H., *Interactions in Electrolyte Solutions*, Elsevier, London, p133, 1966.

[51]   Wyn-Jones E. and Gormally J., *Aggregation Processes in Solution, Studies in Physical and Theoretical Chemistry*, **26**, 250, Elsevier, New York 1983.

[52]   Robinson B.H., Loffler A. and Schwarz G., Thermodynamic behaviour of Acridine Orange in solution., *J. Chem. Soc. Faraday Trans.*, **56**, 1973.

[53]   Coetzee J.F. and Ritchie C.D., *Solute-Solvent Interactions*, **1**, p385, Marcel-Dekker Inc, New York, 1969.

[54]   Marchon J.C., *I.U.P.A.C. Non Aqueous Electrochemistry*, p360, Butterworths, London, 1970.

[55]   Frank H.S. and Wen W.Y., Ion solvent interaction. Structural aspects of ion solvent interaction in aqueous solutions: A suggested picture of water structure., *Disc. Fara. Trans.*, **24**, 133, 1957.

[56]   Popovych O. and Tomkins R.P.T., *Non Aqueous Solution Chemistry*, p18, John Wiley and Sons, USA, 1981.

[57]   Isaacs N.S., *Physical Organic Chemistry*, John Wiley and Sons, New York, p172, 1987.

[58]   Serjeant E.P. and Dempsey B., *Ionisation Constants of Organic Acids in Aqueous Solution*, I.U.P.A.C. Chemical Data Series, p23, Perganon Press, Oxford, 1979.

[59]   Kortum G., Vogel W. and Andrussow K., Dissociation constants of organic acids in aqueous solution., *Pure Appl. Chem.*, **1**, 466, 1961.

[60]   Margalit R. and Rotenberg M., Thermodynamics of porphyrin dimerisation in aqueous solution., *Biochem. J.*, **219**, 445, 1984.

[61]   Ben-Hur E., Dubbelman T.M.A.R. and Steveninck J.V., The effect of fluoride on binding and photodynamic action of phthalocyanines with proteins., *Photochem. Photobiol.*, **54**, 703-707, 1991.

[62]   Harazono T. and Takagishi I., Solvent effects on electronic states of phthalocyanines., *Bull. Chem. Soc. Jpn.*, **66**, 1016, 1993.

[63]   Turro N.J., *Modern Molecular Photochemistry*, p107, University Science Press, California, 1991.

[64]   Limantara L., Sakamoto S., Koyama Y. and Nagae H., Effects of non-polar and polar solvents on the Q_x and Q_y energies of bacteriochlorophyll a and bacteriopheophytin a, *Photochem. Photobiol.*, **65**, 330, 1997.

[65]   Kobayashi N. and Lever A.B.P., Cation or solvent induced supermolecular phthalocyanine formation. Crown ether substituted phthalocyanines., *J. Am. Chem. Soc.*, **109**, 7433, 1987.

[66]   Morrison R.T. and Boyd R.N., *Organic Chemistry*, p165, 3rd Ed., New York University, Allyn and Bacon Inc., 1973.

[67]   Morley J.O. and Charlton M.H., Theoretical investigation of the structure and spectra of zinc phthalocyanines., *J. Phys. Chem.*, **99**, 1928, 1995.

[68]   Valduga G., Reddi E. and Jori G., Spectroscopic studies on Zn(II)Pc in homogeneous and microheterogeneous systems., *J. Inorg. Biochem.*, **29**, 59-65, 1987.

[69]   Sheppard S.E. and Brigham H.R., Some effects of solvents on the absorption spectra of dyes. III Temperature and organic solutions of cyanine dyes., *J. Am. Chem. Soc.*, **66**, 380, 1944.

[70]   Cupane A., Leone M., Cordone L., Gilch H., Dreybrodt W., Unger E. and Schweiter-Stenner R., Conformational properties of Nickel(II) octaethylporphyrin in solution. 2. A low temperature optical absorption spectroscopy study., *J. Phys. Chem.*, **100**, 14192, 1996.

[71]   Friedel M.K., Hoskins B.F., Martin R.L. and Mason S.A., A new metal (II) phthalocyanine structure : X-Ray and Mossbauer studies of the triclinic tin (II) phthalocyanine., *Chem. Comm.*, **400**, 1970.

[72]   Hoshino M., Ikehara K., Imamura M. and Hama Y., Temperature dependence of absorbance spectra of chlorophyll a in hydrocarbons over the temperature range

300K-77K. Enthalpy and entropy changes in the formation of dimeric chlorophyll a., *Bull. Chem. Soc. Jpn.*, **56**, 208, 1983.

[73]   Scaiana J.C., *Handbook of Organic Photochemistry*, **1**, p329, CRC Press, Florida, 1989.

[74]   Foley M.S.C., The photophysics of sulphonated aluminium phthalocyanines as sensitisers for Photodynamic Therapy (PDT)., *PhD Thesis*, Imperial College, London, 1994.

[75]   Ravikant M., Reddy D. and Chandrashekar T.K., Dimerisation effects on spectroscopic properties of water soluble porphyrins in aqueous and micellar media., *J. Chem. Soc. Dalton Trans.*, 2103, 1991.

[76]   Wyn-Jones E. and Gormally J., *Aggregation Processes in Solution, Studies in Physical and Theoretical Chemistry*, **26**, 244, Elsevier, New York 1983.

[77]   Ambroz A., Beeby A., MacRobert A.J., Simpson M.S.C., Svenson R.K. and Phillips D., Preparative, analytical and fluorescence spectroscopic studies of sulphonated aluminium phthalocyanine photosensitisers., *J. Photochem. Photobiol. B:Biol.*, **9**, 87, 1991.

[78]   Bishop S., Preparation and properties of phthalocyanine sensitisers for Photodynamic Therapy., p97, *PhD Thesis*, Imperial College, London, 1993.

[79]   Mittal K.L., *Surfactants in Solution.*, p182, **7**, Plenum Press, New York, 1989.

[80]   Personal Communication. Crooks E., Bristol University.

[81]   Wilkinson F. and Ferreira L.F.V., Diffuse reflectance laser flash photolysis studies of energy transfer at interfaces., *J. Lumin.*, **40**, 704, 1988.

[82]   Levin P.P., Ferreira L.F.V. and Costa S.M.B., Diffuse reflectance laser photolysis studies of geminate recombination kinetics of triplet radical pairs adsorbed on microcrystalline cellulose., *Chem. Phys. Lett.*, **173**, 277, 1990.

[83]   Murtagh J. and Thomas J.K., Effect of humidity and temperature on photoinduced reactions in cellulose., *Chem. Phys. Lett.*, **148**, 445, 1988.

[84]   Smith C.A. and Wood E.J., *Cell Biology*, p107, Chapman and Hall, London, 1992.

[85]   Kessel D., Morgan A. and Garbo S.M., Sites and efficacy of photodamage by tin etiopurpurin in vitro using different delivery systems., *Photochem. Photobiol.*, **54**, 193, 1991.

CHAPTER 4
DIMERISATION OF PHTHALOCYANINES

4.1 Introduction

It has been demonstrated in Chapter 3 that dimerisation and aggregation of zinc phthalocyanines occurs readily and is highly dependent on the nature of peripheral ring substituents and the surrounding medium. In biological media, accumulation of phthalocyanine molecules may lead to high local concentrations (10^{-5} mol dm^{-3} to 10^{-4} mol dm^{-3})[1],[2] and therefore promote aggregation. Accordingly, it is extremely important to determine the efficacies of monomer and dimer components. In this section, the *in vitro* photophysical properties of phthalocyanine dimers are investigated. Luminescence from dimers has been a controversial topic for many years. It is generally accepted that it is the monomeric form of the dye which is responsible for photodynamic action[3] and many reports have been published regarding the lack of fluorescence from aggregated species. It has been shown[4],[5] that the excited states of the well characterised face-to-face stacking dimer of μ-oxo aluminium (III) phthalocyanine are rapidly deactivated by non-radiative routes and Kobayashi and Lever[6] have demonstrated Stern-Volmer quenching of fluorescence from crown ether substituted phthalocyanines as dimerisation was induced by the addition of K$^+$ ions. However, there have also been reports of luminescent phthalocyanine dimers. Yoon *et al.*[7] claimed to have observed emission from aggregated sulfonated aluminium phthalocyanine chloride at high concentrations and Kanezaki and co-workers[8] detected dimer transitions in the fluorescence excitation spectrum of ZnPc at 77 K. The work of Yoon has been questioned by Dhami *et al.*[9] who suggest that reabsorption was responsible for some of the effects observed. The behaviour of porphyrin dyes is markedly different. It is accepted that aggregates such as μ-oxo dimers of scandium octaethylporphyrin ((TPPSc)$_2$O)[10], aluminium tetraphenylporphyrin ((TPPAl)$_2$O)[11] and niobium tetraphenylporphyrin ((TPPNb)$_2$O)[12] - which form face-to-face dimers with non-parallel monomer sub-units - exhibit intense fluorescence from the lowest excited singlet state. This difference in behaviour can be explained using exciton theory[13] which describes the energy levels of an electronically excited dimer molecule based on its ground state geometry.

Aggregation of dye molecules results in the splitting of excited states. The aim of the work described in this chapter was to study the singlet and triplet state properties of

phthalocyanine dimer species. In addition, the use of steady state fluorescence anisotropy as a means of studying excited state energy levels has been investigated. $^tBu_4H_2Pc$ was chosen as a model compound for anisotropy measurements due to the inherent non-degeneracy of its first excited singlet state and its properties compared to those of the metalled compound, $^tBu_4ZnPc$. Results obtained from this study were then applied to the study of phthalocyanine dimer species produced by octaalkyl metallophthalocyanines.

4.2 Theoretical Background
4.2.1 Exciton Theory

Effects of aggregation on the energy levels of phthalocyanine dye molecules may be explained using exciton theory[12],[13],[14],[15] which was developed by Kasha in the 1950's. The theory describes splitting of excited states which may occur in molecular aggregates with strong electronic transitions in the monomer sub-units and negligible electron overlap between those units. If negligible overlap is assumed, molecular units preserve their individuality and wave-functions for the aggregate species may be determined in terms of the wave functions for the electronic states of monomer components. The theory is based on a point-dipole approximation, i.e. it is assumed that transition dipole moments may be considered to be localised at the centre of the molecule. The magnitude of splitting is dependent on the geometry of the constituent monomers. Specifically, the angle between monomer transition moments and the line connecting the monomer centres, θ and the distance separating the sub-unit centres, r, must be considered (Figure 4.1). Three main arrangements will be discussed in this text:

A. Dimers consisting of monomer sub-units with coplanar, parallel transition moments,
B. Dimers with oblique transition moments,
C. Dimers with out-of-plane transition dipole moments.

Figure 4.1 illustrates the effect of θ on the observed splitting of a dimer consisting of two monomers with coplanar, parallel transition moments.
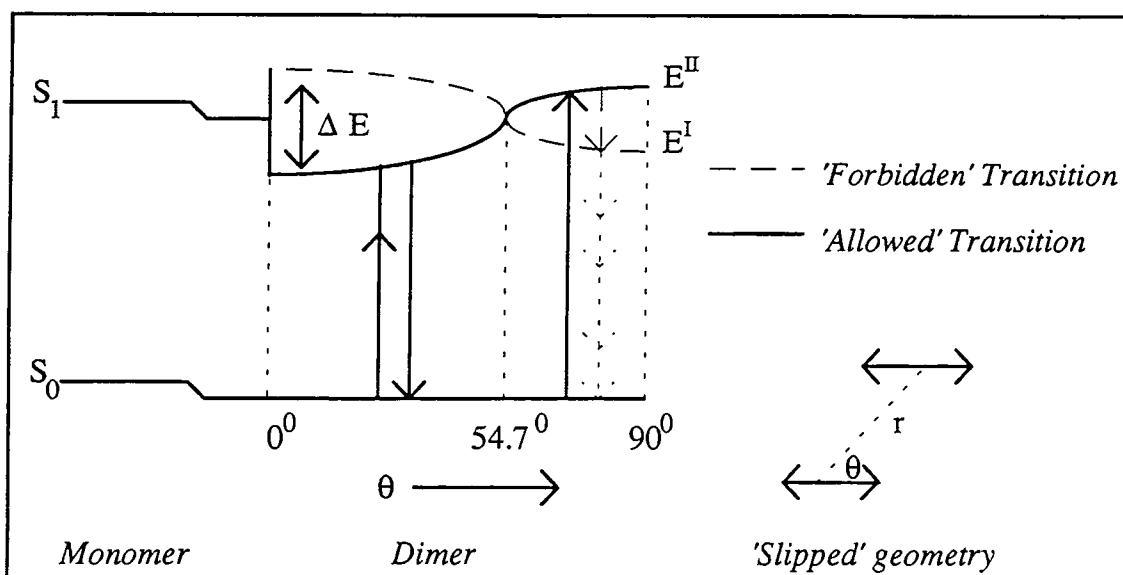
Figure 4.1. Energy level splitting on exciton coupling of a 'slipped' dimer[13].

For this configuration, exciton band splitting, ΔE (E^{II} - E^{I}), may be given by Equation 4.1 where $|M|$ is the transition moment for the singlet-singlet ($S_1 \leftarrow S_0$) transition in the monomer. r and θ have been defined above. $54.7°$ represents the 'magic angle' at which no splitting will occur. Below this value, transitions to the lower level are allowed, whilst at higher values those to the upper level are allowed.

$$\Delta E = \frac{2|M|^2}{r^3}(1 - 3\cos^2 \theta) \qquad (4.1)$$

This may be explained qualitatively by considering the vector sum of constituent transition dipoles. Consider the limiting case of $\theta = 90°$, e.g., when monomer units are cofacially stacked. The higher energy level originates from repulsive forces between dipoles, i.e. when they are aligned, whilst the lower energy level results from opposed dipoles. Vector addition of aligned dipoles leads to a positive dipole moment whilst opposed dipoles cancel each other out and lead to a net dipole of zero. Thus transitions to the lower level are forbidden. At the opposite extreme, $\theta = 0°$ and monomer sub-units lie in the same plane. Aligned dipoles will now give rise to an allowed, lower energy transition whilst opposed dipoles result in a higher energy level to which transitions are forbidden due to a net zero dipole. This results in dimer peaks in the absorption spectrum which are red or blue shifted with respect to the monomer absorption depending on the angle θ. Kasha's rule says that fluorescence usually occurs from the lowest excited state, thus, dimers with lower energy transitions (red shifted) will have allowed radiative deactivation pathways, i.e. they may fluoresce. Those absorbing into upper excited states (blue shifted dimers) will undergo vibrational relaxation to the lower

113

level from which they cannot undergo radiative decay so deactivation will occur via radiationless pathways.

Type B dimers, or those with oblique transition dipoles, give rise to exciton splitting with the energy level diagram shown in Figure 4.2.
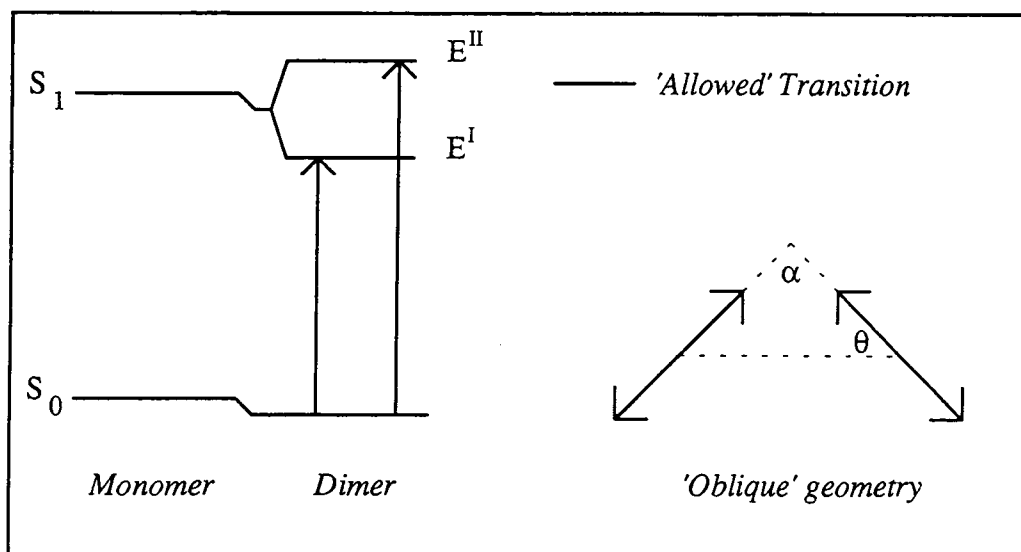
Figure 4.2. Exciton coupling of an 'oblique' dimer[13].

In this case the splitting is given by Equation 4.2.

$$\Delta E = \frac{2|M|^2}{r^3}(\cos\alpha + 3\cos^2\theta)$$

(4.2)

where α is the angle between transition dipole moments shown in Figure 4.2 and other terms are as described previously. In dimers with an oblique geometry, there are finite transition dipoles for in phase and out-of-phase alignments; thus, transitions are allowed to both excited states. This type of dimer will exhibit a symmetric splitting about the monomer Q band in the absorption spectrum and will emit fluorescence from E^I.
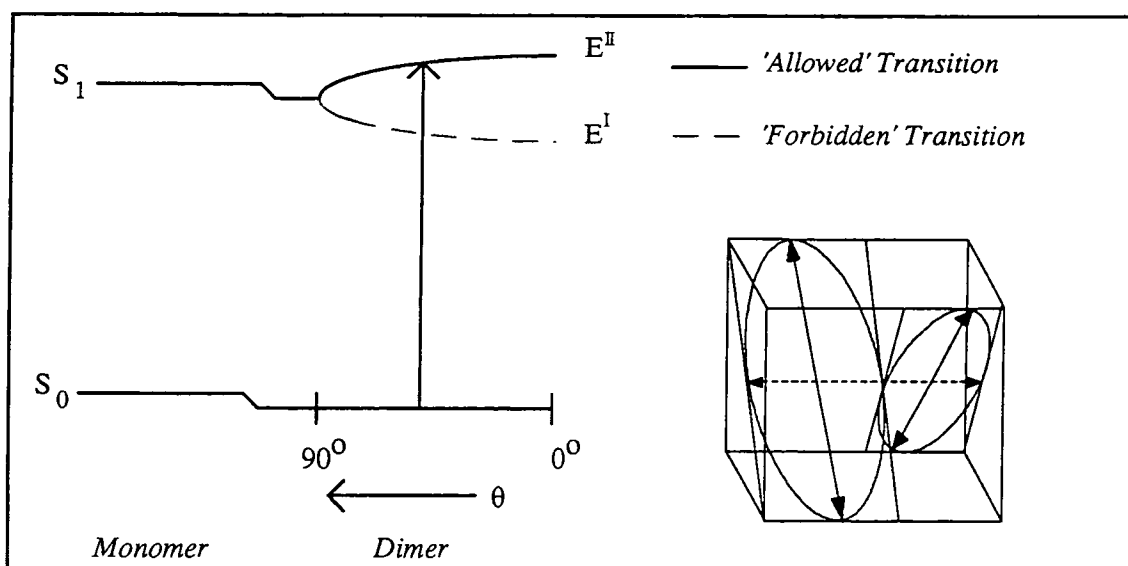
Figure 4.3. Exciton coupling of an 'out-of-plane' dimer[13].

Finally, Type C dimers should be mentioned, i.e. those with non-planar transition dipoles. Figure 4.3 depicts the energy level diagram for a dimer of this type. As α, the angle between monomer molecular planes approaches 90°, E^I becomes progressively more allowed. The exciton splitting is defined by Equation 4.3.

$$\Delta E = \frac{2|M|^2}{r^3}(\cos\alpha - 3\cos^2\theta) \qquad (4.3)$$

Dimers of Types A and B are well represented by published examples of porphyrin[16] and phthalocyanine[4],[6] complexes. Work by Osuka and Maruyama[16] details a range of porphyrin dimers coupled by naphthalene, anthracene or biphenylene bridges at varying substituent positions. 1, 4 naphthalene bound complexes displayed planar, Type A geometry, i.e. $\theta \sim 0°$. As predicted by exciton theory, a red shift of the Q absorption band with respect to that of the constituent monomers was observed and the complex was fluorescent. By contrast, a Type A dimer in which $\theta \sim 90°$ - 1,8 biphenylene bridged zinc diporphyrin - displayed a blue shifted absorption peak and was shown to be virtually non-fluorescent. Various examples of dimers with oblique transition dipoles (Type B) are also discussed. In these complexes, the Soret band was observed to split into two separate transitions and the relative intensities of each absorption were shown to be related to the dihedral angle (θ) between constituent monomers. As expected for Type B dimers, these compounds were fluorescent. μ-oxo porphyrins, $(TPPNb)_2O$[12] and $(OEPSc)_2O$[10] also fall into this category. An example of a Type C dimer has been published by Oba[17], who observed splitting of the absorption spectrum of chlorophyll a' upon dimerisation. A 'T-shape' geometry, in which constituent monomer transition

dipoles are non-planar, was proposed to account for the observed spectroscopic properties.

4.2.2 Fluorescence Anisotropy[18],[19] of Phthalocyanines

The maximum fluorescence anisotropy of any particular molecule is termed the principal anisotropy, r_p, and occurs when excitation of a luminescent molecule leads directly to the first excited state, i.e. the energy level from which the bulk of fluorescence originates. In this situation, the angle between the absorption transition dipole and the emission transition dipole, θ_a, (Figure 4.4) is zero.

δ = Angle formed between planes defined by OZ, A and A, F directions.

θ_a = Angle between absorption, A and emission, F transition dipoles.

Vertically Polarised Incident Radiation
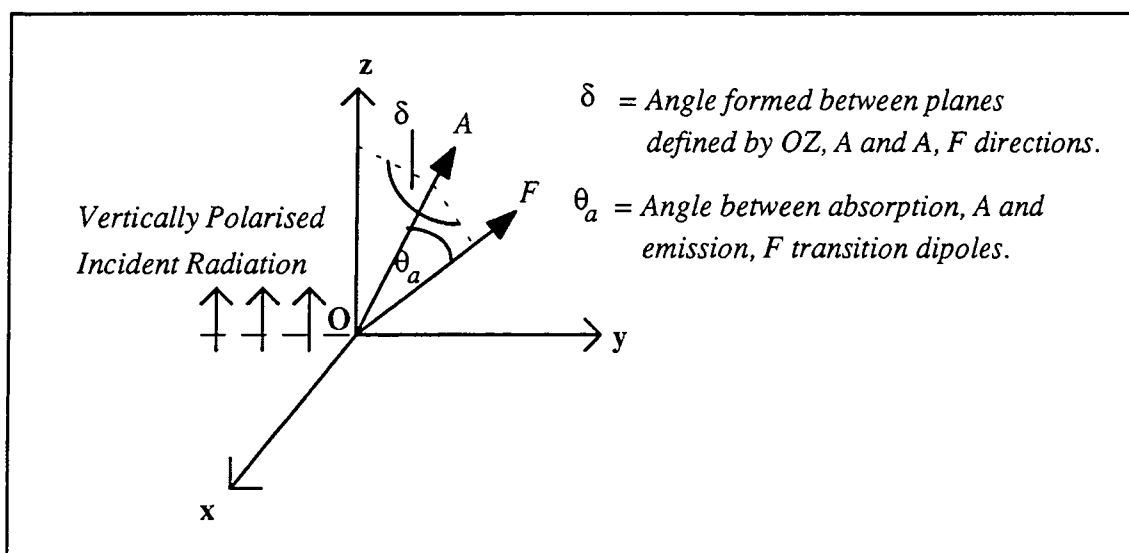
Figure 4.4. Representation of θ_a -
Angle between absorption and emission transition dipoles[18].

When absorption produces a higher excited state, rapid deactivation to the emitting state occurs, which may result in the absorption and emission dipoles being non-coincident, θ_a > 0. In this case, the anisotropy is termed the fundamental anisotropy, r_f. Information regarding the value of θ_a may be obtained using the Perrin Equation (Equation 4.4).

$$r_f = 0.2(3 cos^2 \theta_a - 1) \qquad (4.4)$$

According to this equation, r_f has limiting values of -0.2 and 0.4 when θ_a = 90° and 0° respectively. When θ_a = 0, $r_f = r_p = 0.4$. It should be noted that experimentally determined values are always lower than r_f due to inherent depolarising processes: these include rotational motion, torsional vibrations, excitation energy transfer between molecules and secondary fluorescence. These effects, with the exception of torsional

116

vibrations, may be minimised by optimising experimental conditions. Secondary fluorescence may be eliminated by controlling the intensity of excitation radiation, energy transfer by using low concentrations of fluorophore and rotational motions via highly viscous or rigid solutions. The maximum anisotropy which may be obtained experimentally, having considered these effects is the limiting anisotropy, r_0. However, when molecules such as benzene and deuterobenzene are considered[20], r_0 (0.091 and 0.081 resp.) is vastly different from the theoretical value of r_p (0.4). In order to account for this difference, which is too large to be explained by the depolarising mechanisms mentioned previously, spatial oscillators must be used instead of the linear oscillators assumed so far. In brief, the transition moment is considered to be composed of three dipoles, each oriented along one of the Cartesian coordinate axes, x, y and z. The axes are arranged such that the maximum dipole moment lies along one axis and the minimum along another, thereby determining the direction of the third axis. Using spatial oscillators in this way, r_f may be defined by Equation 4.5.

$$r_f = \frac{3}{5} \sum_1^3 \Gamma_i G_i - \frac{1}{5} \qquad (4.5)$$

where Γ_i represents the absorption intensities along each of the principal axes and $G_i = \Sigma \Gamma_i \cos^2 \theta_a$ where θ_a is the angle between the absorption and emission dipoles. For anisotropic oscillators, $\Gamma_1 = 1$, $\Gamma_2 = \Gamma_3 = 0$ and $G_1 = \cos^2 \theta_a$, which leads to the original Perrin Equation (Equation 4.4). For a symmetric, planar molecule such as benzene, $\Gamma_1 = \Gamma_2 = G_1 = G_2 = 0.5$ and $\Gamma_3 = G_3 = 0$, yielding a principal anisotropy, r_p, of 0.1, thus explaining the low values of r_0 observed. This situation is also applicable to molecules with D_{4h} symmetry such as ZnPc. For an isotropic absorption and emission process no anisotropic fluorescence would be expected.

Thus far, rotational motions of fluorophores have been neglected and, while this assumption is valid in rigid or highly viscous media, rotations due to Brownian motion must also be considered in the solution state. Under these conditions, the anisotropy is time dependent and has been shown to decay exponentially following Equation 4.6

$$r(t) = r_0 e^{-6Dt} \qquad (4.6)$$

where $r(t)$ is the time dependent anisotropy, r_0 is the limiting anisotropy and D is the time dependent diffusion coefficient of rotational motion. It is possible to measure $r(t)$ using time correlated single photon counting techniques. However, $r(t)$ has not been

investigated in this study. Steady state conditions were employed. In this case, the time averaged value, r_{av}, of Equation 4.6 is applicable. This is expressed by the steady state Perrin Equation (Equation 4.7)

$$\frac{r_0}{r_{av}} = 1 + \frac{3\tau_F}{\tau_R} \qquad (4.7)$$

where τ_R is the rotational relaxation time, τ_F is the fluorescence lifetime and r_0 is the limiting anisotropy.

4.3 Materials and Methods

Aluminium phthalocyanine chloride was purchased from Kodak and used as received. 1,4,8,11,15,18,22,25- octadecyl zinc phthalocyanine (C10) was a gift from Prof. M. J. Cook, University of East Anglia, 2,3,9,10,16,17,23,24-octa-hexadecyl phthalocyanine (H_2C_{16}) was a gift from Dr. N. McKeown, University of Manchester and 1,4,8,11,15,18,22,25-octabutoxy phthalocyanine (($BuO)_8H_2Pc$) was purchased from Aldrich. H_2C_{16} and $(BuO)_8H_2Pc$ were converted into the zinc metallated derivatives (ZnC16 and $(BuO)_8ZnPc$ respectively) via the procedure described in Section 2.2.2. Methanol (MeOH), diethyl ether (Et_2O), ethanol (EtOH) and isopentane (IP) were Analar grade or better and were used as received. 2-methyl tetrahydrofuran (MeTHF) was purchased from Aldrich and distilled before use. Triton X-100 (TX-100), tetrabutylammonium fluoride ($^tBu_4NF$) - 98% purity, 1, 4 Diazabicyclo [2,2,2] octane (DABCO) - 99% purity, trans 1,2-dipyridyl ethylene (DiPE) - 97% purity and 4,4'-bipyridine (bipy) - 98% purity were purchased from Sigma-Aldrich. All were used as received.

Anisotropy measurements were performed using the method described in Section 2.1.2.3. Rotational motion of fluorophores was minimised by cooling to 77 K in ether-pentane-alcohol (5:5:2) (EPA) solution or by encapsulating molecules in Triton X-100 micelles. Dimer studies were carried out using the photophysical procedures and apparatus described in Section 2.1. Samples of aluminium phthalocyanine chloride and tetrabutylammonium fluoride ($^tBu_4NF$) were allowed to equilibrate in the dark for twelve hours prior to measurement.

Photophysical techniques are described in Chapter 2 (pp 42-71).

4.4 Results and Discussion

4.4.1 Fluorescence Anisotropy
4.4.1.1-Preparative Studies
4.4.1.1.1 Results

The UV/Vis absorption spectrum of $^tBu_4H_2Pc$ in EPA was investigated over the temperature range between 293 K and 77 K. At liquid nitrogen temperatures (77 K) improved resolution of the spectra was observed, two peaks (630 nm and 642 nm) being observed instead of the single maximum at 640 nm obtained at 293 K (Figure 4.5). A 2 nm red shift in the peaks at 656 nm and 640 nm occurred accompanied by an increase in the intensity. Peaks at 695 nm, 630 nm and 595 nm exhibited only changes in intensity. The relative intensities at 656 nm and 695 nm were reversed at 77 K, the peak at 656/8 nm becoming more intense than that at 695 nm. Aggregation was shown not to be induced via the cooling process.
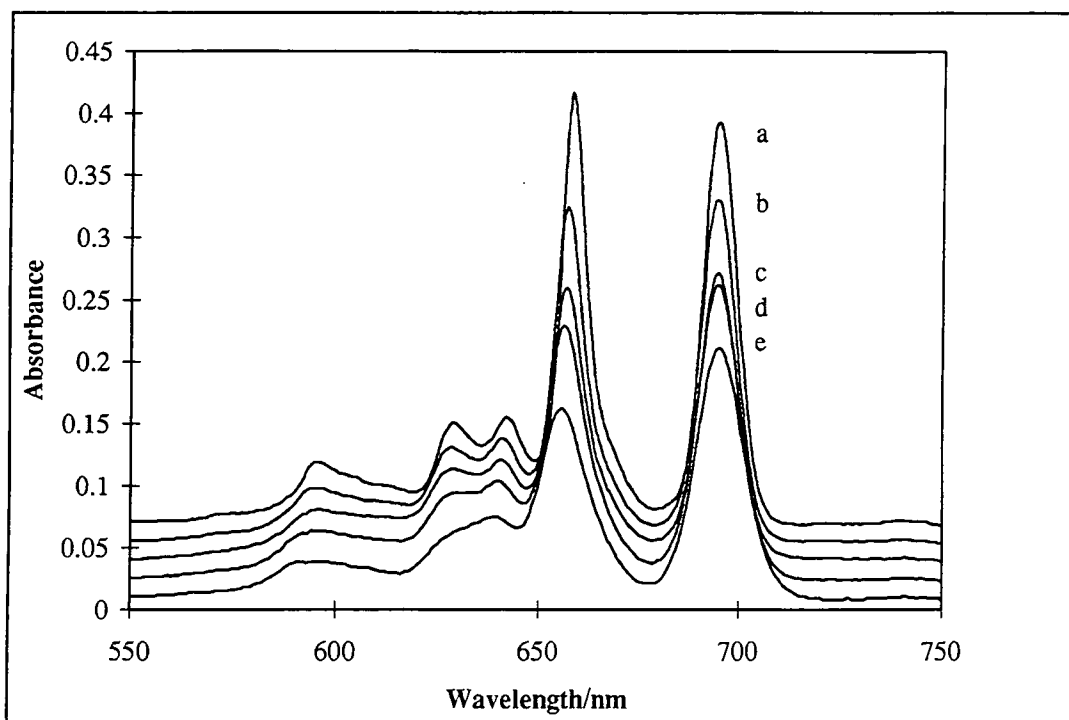
Figure 4.5. Temperature dependence of UV/Visible absorption spectrum of $^tBu_4H_2Pc$ in EPA. a) 77 K, b) 120 K, c) 160 K, d) 210 K, e) 293 K. The baseline absorption of all samples was equal at 750 nm. Spectra have been offset for clarity.

Fluorescence excitation spectra mirrored changes in the absorption spectrum. Emission spectra displayed a main emission peak at 700 nm which became narrower and more intense - as would be expected on cooling (Figure 4.6).
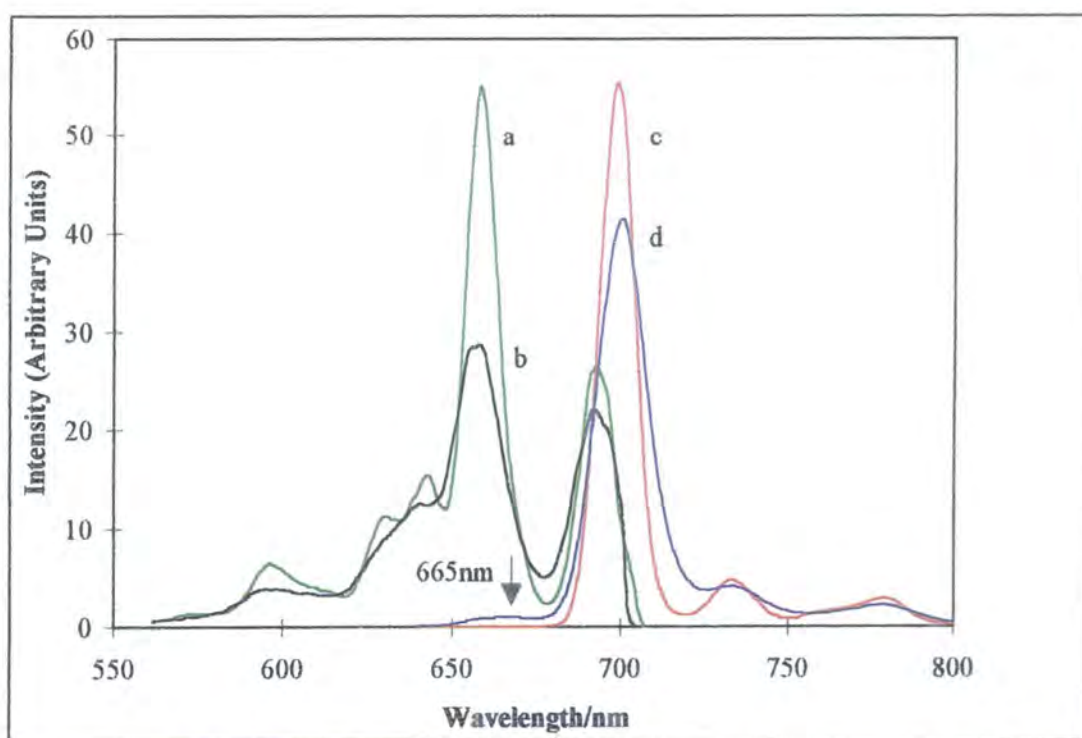
Figure 4.6. Temperature dependence of fluorescence excitation (λ_{em} = 760 nm)
a) 77 K, b) 293 K and emission spectra (λ_{ex} = 630 nm), c) 77 K, d) 293 K, o]
$^tBu_4H_2Pc$ in EPA.

An unexpected peak at 665 nm was observed in the emission spectrum at room temperature which decreased as the sample was cooled to 77 K. The intensity of this emission relative to the main band at 700 nm was investigated using the Boltzmann relation (Equation 4.8).

$$ln\frac{I_{700}}{I_{665}} = -\frac{\Delta E}{kT} \tag{4.8}$$

Figure 4.7 shows a linear dependence of $\ln(I_{700}/I_{665})$ vs $1/T$ and yielded a ΔE value of 1.7×10^{-20} J or 10.7 kJ mol^{-1} which is comparable to the result (9 kJ mol^{-1}) of a crude calculation of ΔE using Equation 4.9.

$$\Delta E = \frac{hc}{\lambda_{665}} - \frac{hc}{\lambda_{700}} \tag{4.9}$$

$^tBu_4ZnPc$ in EPA at 77 K did not show any features beyond a sharpening of the absorption and emission peaks present at 293 K (Section 3.3.2.2.3).
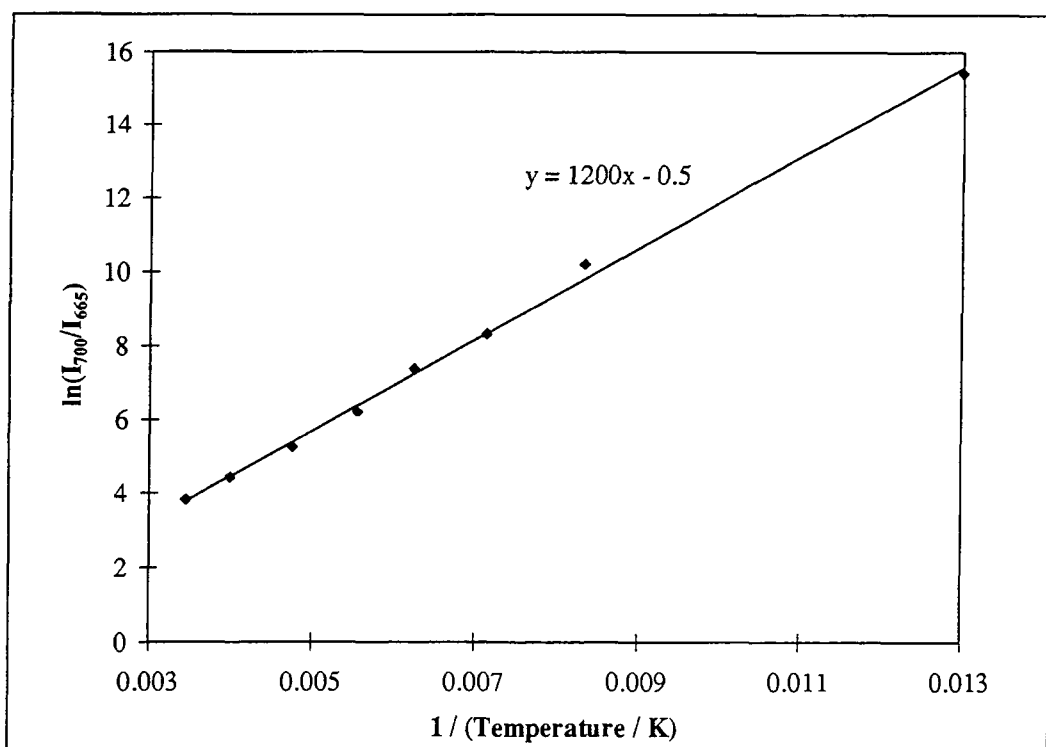
Figure 4.7. Temperature dependence of emission from $^tBu_4H_2Pc$ in EPA at 665 nm.

4.4.1.1.2 Discussion

There have been various reports[21],[22] discussing the energy levels of $^tBu_4H_2Pc$ associated with each band in the absorption spectrum. Peaks at 695 nm and 656 nm can be assigned to the Q_x and Q_y transitions respectively and represent absorption to the first and second energy levels, denoted S_1 and S_2. It is generally accepted that the Q_x and Q_y bands involve transitions perpendicular to each other in the xy plane with Q_x polarised along the H - H axis of the molecule. The degeneracy of Q_x and Q_y has been removed due to the lower symmetry of $^tBu_4H_2Pc$ (D_{2h}) with respect to metallophthalocyanines (D_{4h}). The remaining peaks at 640 nm and 595 nm (at 293 K) may be assigned to vibrational overtones of Q_x and Q_y respectively[23]. Temperature effects on the absorption maxima of Q_x and Q_y may be rationalised in terms of a study by Limantara *et al.*[24] which details the effects of changes in solvent refractive index on the absorption spectrum of bacteriopheophytin a. The report explains the origin of red shifts in the transition wavelengths of Q_x and Q_y which were observed as R increased (R = $(n^2-1)/(n^2+1)$ where n is the solvent refractive index). Q_y displayed a greater shift. This was ascribed to increased solvent interaction which resulted from the large fluctuation of solute dipoles in higher energy levels. It should be noted that Limantara has referred to Q_x as the higher energy transition throughout. For consistency with this work, in which Q_y represents the higher energy transition and Q_x the lower one (polarised along the H - H axis) this nomenclature has been reversed. The results of this study are in agreement

with Limantara's work. Q_y demonstrated a red shift from 656 nm to 658 nm as the refractive index of the solvent increased due to cooling, whilst Q_x remained stationary. The additional peak at 642 nm which became clear at temperatures < 180 K has been observed before but not conclusively assigned[25]. The most likely cause of this transition is absorption to a vibrational mode of Q_x or Q_y. Leznoff and Lever[26] suggest that a small amount of absorption may occur along the 'z' axis. Anisotropy data obtained in this study is in agreement with either of these explanations since absorption into a higher energy level than the emitting state is implied (Section 4.4.1.2).

As expected, the majority of fluorescence occurred from the lowest excited singlet state, S_1, at a wavelength of 700 nm. Calculation of the energy difference between this emission band and the peak observed at 665 nm yielded an energy separation of 10.7 kJ mol^{-1} which is consistent with published data[22] for the energy difference (10.6 kJ mol^{-1}) between the first and second unoccupied molecular orbitals, $6b_{3g}$ and $6b_{2g}$. It is concluded that emission observed at 665 nm was due to fluorescence from the second excited state, S_2. S_2 emission is very uncommon since relaxation to the lowest excited state takes place very rapidly (ps), i.e. before emission has occurred. Soret band emission has previously been reported at 430 nm by Kobayashi[6], however, the authors themselves question its authenticity and suggest the observed emission band may be due to impurities in the sample. In the case of $^tBu_4H_2Pc$, S_1 and S_2 excited states are very close to each other in energy, thus, thermal repopulation of S_2 occurs. Consider a Boltzmann distribution of molecules in S_1 and S_2 excited states (Equation 4.10)

$$\frac{n_2}{n_1} = e^{-\frac{\Delta E}{kT}} \qquad (4.10)$$

where n_2 and n_1 are the populations of S_2 and S_1 respectively, ΔE is the energy gap between states, k is the Boltzmann constant and T is the absolute temperature. ΔE has been shown to be ~ 10.7 kJ mol^{-1}. Hence, when T is 293 K, ~ 1.5 % of excited state molecules will populate the S_2 level, giving rise to detectable emission upon radiative decay. At 77 K the figure becomes negligible (< 10^{-5} %). The excitation spectra resembled the absorption spectra and mimicked any changes that were observed with temperature. It was, therefore, concluded that the anisotropy of $^tBu_4H_2Pc$ and $^tBu_4ZnPc$ could be studied without interference from aggregation effects.

4.4.1.2 Anisotropy Measurements
4.4.1.2.1 Results

The anisotropy, r_{av} of $^tBu_4H_2Pc$ exhibited a strong dependence on both excitation and emission wavelengths. Figure 4.8 shows the correlation between the excitation spectrum of $^tBu_4H_2Pc$ and the anisotropy of emission at 700 nm using excitation wavelengths between 585 nm and 690 nm.
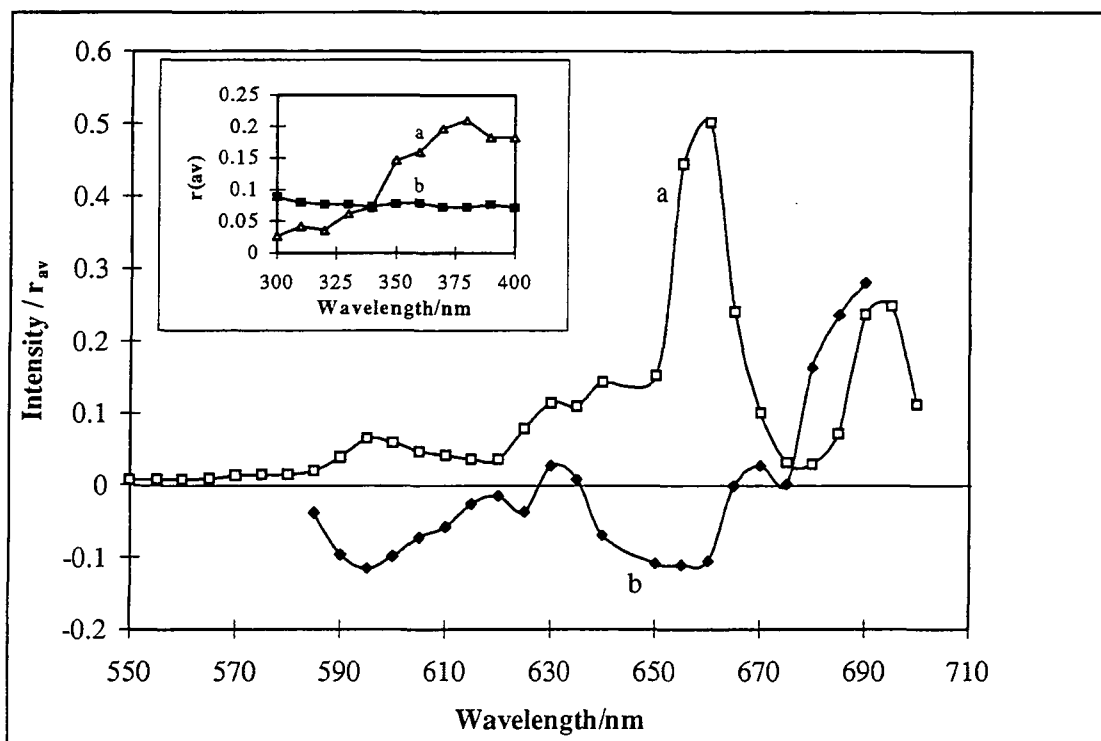
Figure 4.8. **a) Excitation spectrum (λ_{em} = 750 nm) and b) anisotropy (λ_{em} = 700 nm) of $^tBu_4H_2Pc$ in EPA at 77 K. Inset: r_{av} of a) $^tBu_4H_2Pc$ (in EPA at 77 K) and b) $^tBu_4ZnPc$ (in 1% TX/H$_2$O at 293 K) by excitation into the Soret band.**

Excitation into the lowest energy level, S_1, i.e. excitation at wavelengths > 680 nm, gave a large positive value, r_{av} = 0.28 ± 0.005, which rapidly decreased to negative values as the excitation energy increased (-0.1 at 655 nm). It should be noted that 640 nm excitation resulted in a negative anisotropy, r_{av} = -0.07 ± 0.005, whilst 630 nm excitation incurred a positive anisotropy of 0.026 ± 0.005. A steady increase in r_{av} was observed as excitation into higher excited states was induced using 300 nm to 400 nm radiation (Inset of Figure 4.8).
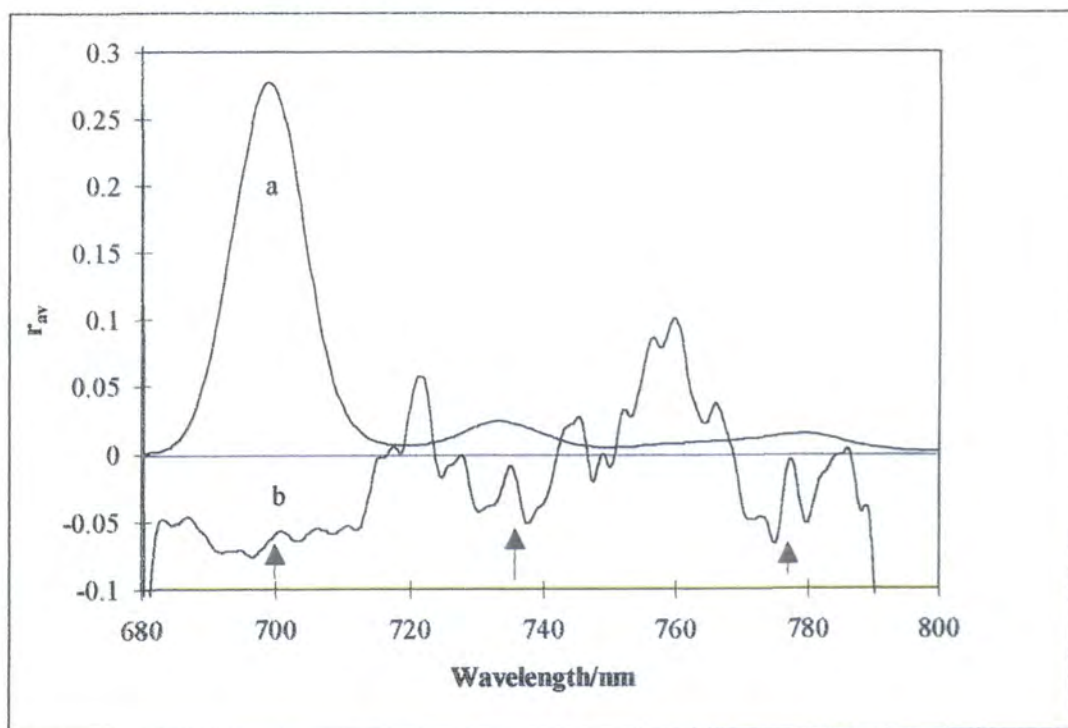
Figure 4.9. a) Emission spectrum of $^tBu_4H_2Pc$ ($\lambda_{ex} = 630$ nm),
b) Anisotropy ($\lambda_{ex} = 610$ nm) in EPA at 77 K.
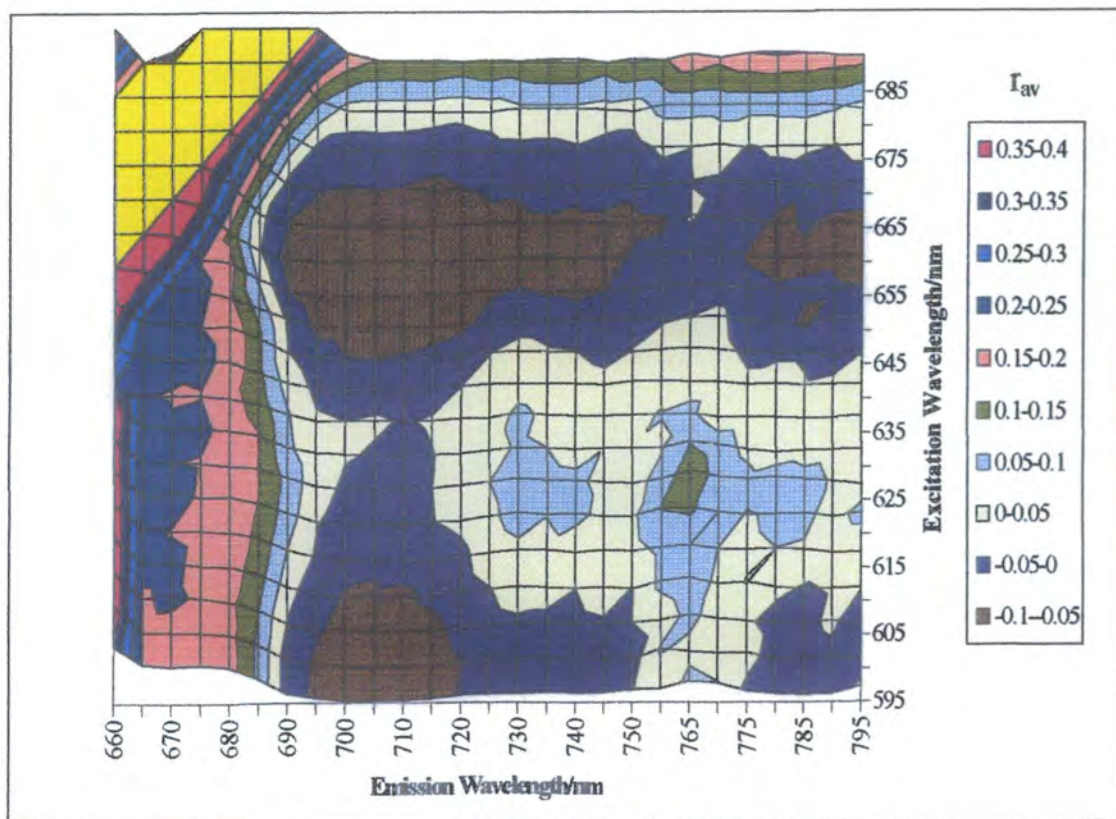
Figure 4.10. Dependence of r_{av} of $^tBu_4H_2Pc$ in 1% TX/H_2O on emission and
excitation wavelength.

The detection wavelength of $^tBu_4H_2Pc$ emission also influenced the magnitude of r_{av} (Figure 4.9). The anisotropy appears to modulate across the spectrum. Three negative regions (arrowed sections of Trace b) can be observed, interspersed with positive sections. The positive regions coincide with minima in the emission spectra. In order to complicate matters further, variations of r_{av} with λ_{em} were dependent on the excitation wavelength used. A 3-dimensional plot was therefore required to visualise the entire picture (Figure 4.10). Large positive anisotropy at emission wavelengths of 665 nm - 685 nm resulted from S_2 emission (λ_{ex} = 595 nm to 635 nm). The yellow plateau obtained with excitation wavelengths greater than 655 nm represents values > 0.4 where scattered incident light dominated the measured radiation.

By contrast with $^tBu_4H_2Pc$, r_{av} values for $^tBu_4ZnPc$ remained constant at 0.075 ± 0.005 as the excitation wavelength was varied between 300 nm and 400 nm (Inset of Figure 4.8). In EPA at 77 K, r_{av} was constant with emission wavelength across the range 665 nm to 695 nm, in 1% TX/H_2O the range from 665 nm to 740 nm was constant. However, variations in the anisotropy as the fluorophore was excited using wavelengths between 605 nm and 665 nm were observed. Figure 4.11 shows how r_{av} depended upon the energy of the incident radiation when measurements were performed in EPA at 77 K (a) and 1% TX/H_2O at 293 K (b). It was observed that modulation in the value of r_{av} was more pronounced when the experiment was carried out at 77 K (r_{max} = 0.1, r_{min} = 0.003) than in 1% TX/H_2O at room temperature. (r_{max} = 0.086, r_{min} = 0.063).
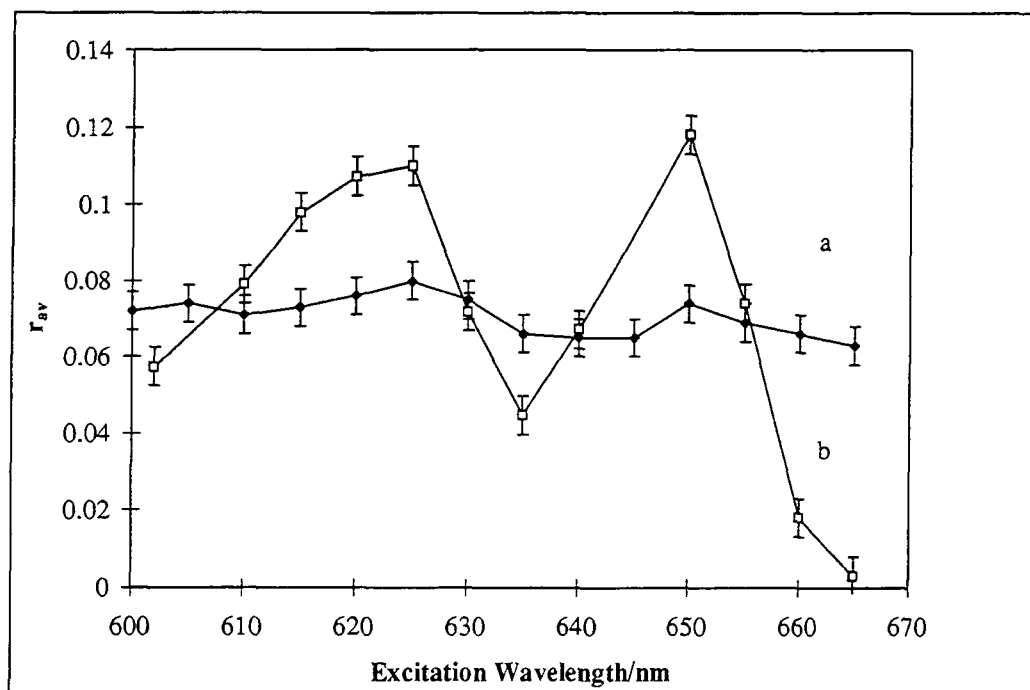
Figure 4.11. Anisotropy of $^tBu_4ZnPc$ as a function of excitation wavelength. a) in 1% TX/H_2O at 293K, b) in EPA at 77K.

Figure 4.12 shows how the average anisotropy of $^tBu_4ZnPc$ in EPA was affected by temperature. Using this information and Equation 4.7, it was possible to calculate the change in the rotational relaxation time, τ_R, of the phthalocyanine molecules.
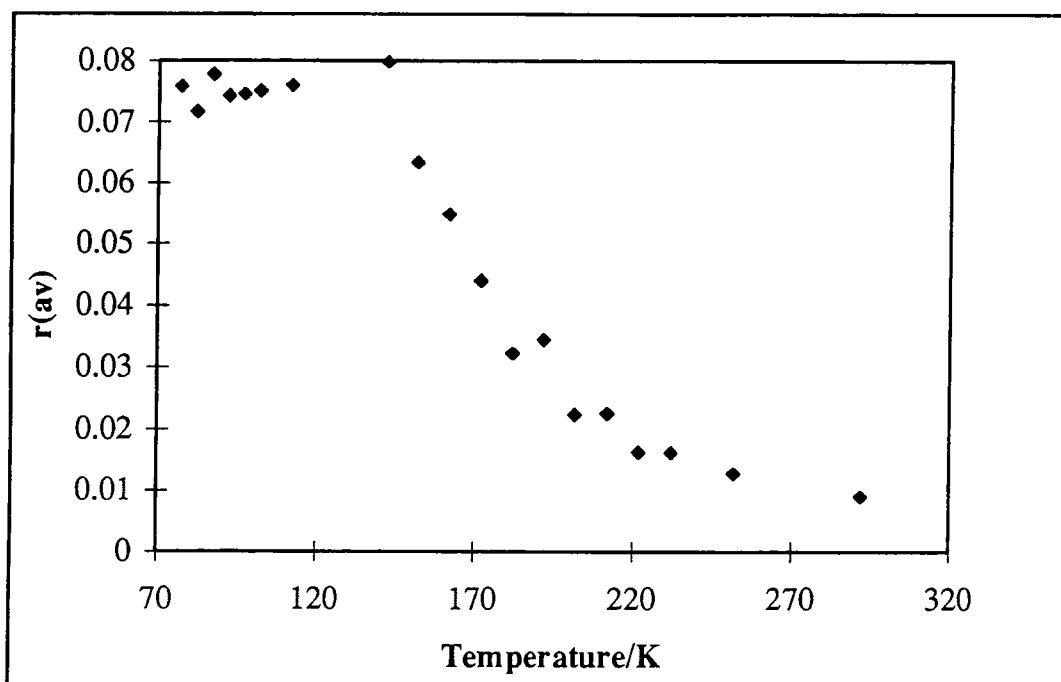
Figure 4.12. Temperature dependence of r_{av} of $^tBu_4ZnPc$ in EPA.
(λ_{ex} = 630 nm, λ_{em} = 665 nm - 685 nm).

r_0, i.e. r_{av} at infinite viscosity, was estimated as 0.075 ± 0.005. The lifetime of fluorescence was assumed to be 3.6 x 10^{-9} s (Chapter 3). Table 4.1 shows rotational relaxation time, τ_R, rotational correlation, τ_c, and depolarisation, φ, data calculated using Equation 4.7 and other simple relations (shown in table)[18].

Temperature /K	r_{av}	τ_R /ns	$\tau_c \; (=\tau_R/3)$ /ns	$\varphi (=1/\tau_c)$ /ns^{-1}
142	0.08	-	-	-
152	0.063	59	19.7	0.051
162	0.055	29	9.8	0.1
172	0.044	15.3	5.1	0.2
182	0.032	8.2	2.7	0.37
202	0.022	4.6	1.5	0.66
212	0.023	4.6	1.5	0.66
222	0.016	3	1	1
232	0.016	3	1	1
252	0.013	2.2	0.7	1.35
292	0.009	1.5	0.5	2

Table 4.1. Decrease in anisotropy of $^t Bu_4 ZnPc$ in EPA with increasing temperature.

4.4.1.2.2 Discussion

$^t Bu_4 H_2 Pc$ belongs to the D_{2h} point group, i.e. the lowest excited state is non-degenerate (Section 4.4.1.2). $^t Bu_4 H_2 Pc$ would, therefore, be expected to act as an anisotropic oscillator. Excitation into the Q_x band leads to emission from the same energy level, θ_a = 0, and theory predicts a limiting anisotropy, r_f, of 0.4. The absorption dipole of the Q_y transition (to the S_2 excited state) lies perpendicular to that of the Q_x transition. Since emission occurs mainly from S_1, the angle between the absorption and emission dipoles is 90°. Therefore, excitation into the Q_y band leads to an r_f of -0.2. Experimentally obtained r_0 values, of 0.3 and -0.1 at excitation wavelengths of 690 nm and 655 nm respectively (λ_{em} = 700 nm), are in good agreement with r_f and it is probable that torsional vibrations are responsible for the small difference between r_f and r_0 (since the medium is rigid, r_0 may be approximated by r_{av}). Vibrations of the luminescent molecule reduce the polarisation of emission and result in a reduced anisotropy. Between these wavelengths, a gradual transition from 0.3 to -0.1 was obtained as mixing of excited states occurred. Such a dependency on the frequency of exciting light was first observed for porphyrins, analogous dye molecules, in 1957 by John Weigl[27] and is described in more detail in a recent report by Maiti et al.[28]. At 630 nm, θ_a increased to zero as irradiation populated a vibrational level of S_1. Excitation at 640 nm resulted in a negative anisotropy. This suggests that the absorbing state had a different dipole moment to the emitting state, i.e. absorption to a higher energy level than Q_x occurred. This may be explained by excitation into a vibrational energy level of Q_y. In addition, the suggestion of Leznoff and Lever[26] that a small amount of absorption occurs along the z-

axis appears reasonable. Considering an angle of 90° between Q_z and Q_x, theory predicts a maximum anisotropy of -0.2 (Equation 4.4). Experimentally, a value of -0.07 was calculated, however, this value is likely to be raised by state mixing of this transition with neighbouring absorption (630 nm) into a vibrational level of S_1.

Differences in anisotropy due to emission wavelength are more difficult to explain and have caused much controversy over the years. Turoverov[29] has demonstrated that the polarisation spectra of protein emission varies with emission wavelength. The magnitude of variation was affected by the wavelength of excitation. This behaviour is directly analogous to that observed in this study for $^tBu_4H_2Pc$ (Figure 4.9). Turoverov concluded that the observed dependence resulted from transitions to different vibrational states. On the other hand, Gurinovich[30] ascribed an emission wavelength dependent polarisation of magnesium phthalocyanine to the presence of several different electronic transitions. The authors expressed the opinion that changes were too large to be accounted for by vibrational motion. In this case, when excitation wavelengths below 680 nm are considered, positive anisotropy at emission wavelengths from 665 nm to 685 nm may be ascribed to emission from S_2. Since excitation at these wavelengths produces the emissive state directly ($\theta_a = 0°$), a large positive anisotropy is not surprising. When $\lambda_{em} > 685$ nm, the emitting state is S_1, thus, $\theta_a = 90°$, and r_{av} becomes negative. Reasons for further variation (i.e. those depicted in Figure 4.9) are less obvious. $^tBu_4ZnPc$ shows no such dependence on emission wavelength. The observed dependence of r_{av} on the excitation wavelength of $^tBu_4ZnPc$ is similarly difficult to account for. r_{av} was determined to have a mean value of 0.071 in both EPA at 77 K and TX-100 at 293 K. This is consistent with a limiting anisotropy of 0.1, expected for a symmetric molecule in which $\Gamma_1 = \Gamma_2 = 0.5$. Metallocyanines possess D_{4h} symmetry in which Q_x and Q_y transitions are degenerate, thus the above condition applies. Bauer et al.[31] have reported a tendency for the anisotropy to decrease as the energy of excitation increases. They suggest that vibrational excess energy increases the torsional vibrations of the molecule and this, accompanied by a possible mixing of states, causes lower values of r_{av}. An increase in the local temperature of the emitting molecule has also been proposed as a possible explanation[32]. Rapid relaxation of vibrational excess energy (VEE) in conjunction with slow dissipation of this energy causes an increase in the temperature of the fluorophore, thereby, increasing vibrations and lowering the anisotropy. Alternatively the energy may be dissipated into the surrounding solvent[33], thus affecting the rotational depolarisation properties of the luminescent molecule. This issue is still under discussion and concrete conclusions as to the origin of the wavelength dependency have yet to be made. It is unlikely that any of these proposals can solely account for the λ_{ex} dependency observed in this study since r_{av} does not decrease

continuously with increasing excitation energy. Two maxima were observed (625 nm and 650 nm) accompanied by a minimum at 635 nm in the wavelength range studied. This trend was observed in both EPA at 77 K and 1% TX/H_2O at 293 K (although the effect is much less pronounced in Triton-X). It is possible that an averaging process occurred in 1% TX/H_2O solution due to greater vibrational/rotational motion under these conditions.

Changes in the anisotropy as the temperature increased reflect increasing rotations and vibrations which depolarise radiative emission. This is exemplified by an increase in the probability of depolarisation by Brownian motion, φ, that was observed on increasing the temperature from 152 K to 292 K (1.76 ns^{-1}) and the corresponding decrease in the rotational correlation time, τ_c, from 20 ns to 0.5 ns. It is possible to predict τ_c in various solvents using Equation 4.11[18].

$$\tau_c = \frac{V\eta}{kT}$$

(4.11)

where V = Volume of rotation of fluorophore, η = viscosity of solvent, k = Boltzmann constant and T = temperature in Kelvin. The volume of rotation was estimated by assuming that rotation about the x or y axis represented the volume of a cylinder, defined using crystallographic dimensions of analogous phthalocyanines[34]. $^tBu_4ZnPc$ was estimated to be a square with 16 Å by 16 Å dimensions[35], i.e. r = 8 x 10^{-10} m and h = 16 x 10^{-10} m. The volume of rotation was therefore calculated to be 3.2 x 10^{-27} m^3 using the standard equation, V = $\pi r^2 h$. For $^tBu_4H_2Pc$, V = 1.3 x 10^{-27} m^3. The viscosity of EPA at room temperature was approximated as the average of the three component solvents, i.e. 0.325 x 10^{-3} Pa s. τ_c in Triton X was calculated using η = 140 x 10^{-3} Pa s[36] and η = 18 x 10^{-3} Pa s[37]. These figures are only approximations. It should be noted that in micellar solution rotational dynamics within the micelle as well as rotation of the micelle itself (τ_c = 72 ns for TX-100[28]) and translational diffusion of the fluorophore across the surface of the micelle must be considered[28]. Table 4.2 lists τ_c calculated for $^tBu_4H_2Pc$ and $^tBu_4ZnPc$ in both EPA and TX.

Fluorophore	Solvent	Temperature /K	τ_c /ns
$^tBu_4ZnPc$	EPA	293	0.26
$^tBu_4H_2Pc$	EPA	293	0.1
$^tBu_4ZnPc$	1% TX/H_2O	293	111[(a)], 14[(b)]
$^tBu_4H_2PC$	1% TX/H_2O	293	47[(a)], 6[(b)]
$^tBu_4ZnPc$	EPA	77	3.6 x 10[13(c)]

a) $\eta = 140 \times 10^{-3}$ Pa s, b) $\eta = 18 \times 10^{-3}$ Pa s, c) $\eta = 1.2 \times 10^{10}$ Pa s[38].

Table 4.2. Estimated rotational correlation times of $^tBu_4ZnPc$ and $^tBu_4H_2Pc$ in EPA and 1% TX/H_2O.

Given the number of approximations which have been made to calculate τ_c in this way, 0.26 ns is in very reasonable agreement with the value determined experimentally in EPA of 0.54 ns. It is evident that in EPA at 293 K, rotational depolarisation factors reduce r_{av} to close to zero. However, in TX, a correlation time of > 6 ns is sufficiently large for polarised emission to be detected.

4.4.1.3 Conclusion

It has been shown that phthalocyanines exhibit fluorescence anisotropy which may be partially explained using standard theory. The anisotropy of fluorescence from $^tBu_4H_2Pc$ displayed an emission and excitation wavelength dependence which may be ascribed to different electronic/vibrational transitions. A new and previously unreported fluctuation in the fluorescence anisotropy from $^tBu_4ZnPc$ was observed as the excitation wavelength varied. This phenomenon was found to be dependent upon the physical conditions of the sample, e.g. the solvent and/or temperature. In order to use anisotropy as a technique to study the environment of a phthalocyanine molecule in solution, careful control of experimental conditions is required. The solvent and temperature as well as the excitation and emission wavelengths must be consistent if a comparison between experiments is to be made.

4.4.2 Dimerisation of Phthalocyanines

4.4.2.1 Aluminium Phthalocyanine Chloride (AlPcCl)

4.4.2.1.1 Results

Addition of small amounts of fluoride (F^-) ions to a methanolic solution of AlPcCl induced changes in the absorption spectrum which are characteristic of phthalocyanine dimer formation[6]. Specifically, formation of a peak at ~ 631 nm was observed, in addition to a shift in λ_{max} of monomer absorption. λ_{max} underwent a continuous blue shift from 673 nm to 662 nm upon increasing [F^-] (Table 4.3). The yield and absorption maximum of dimeric species was dependent on the concentration of fluoride ions (Figure 4.13).
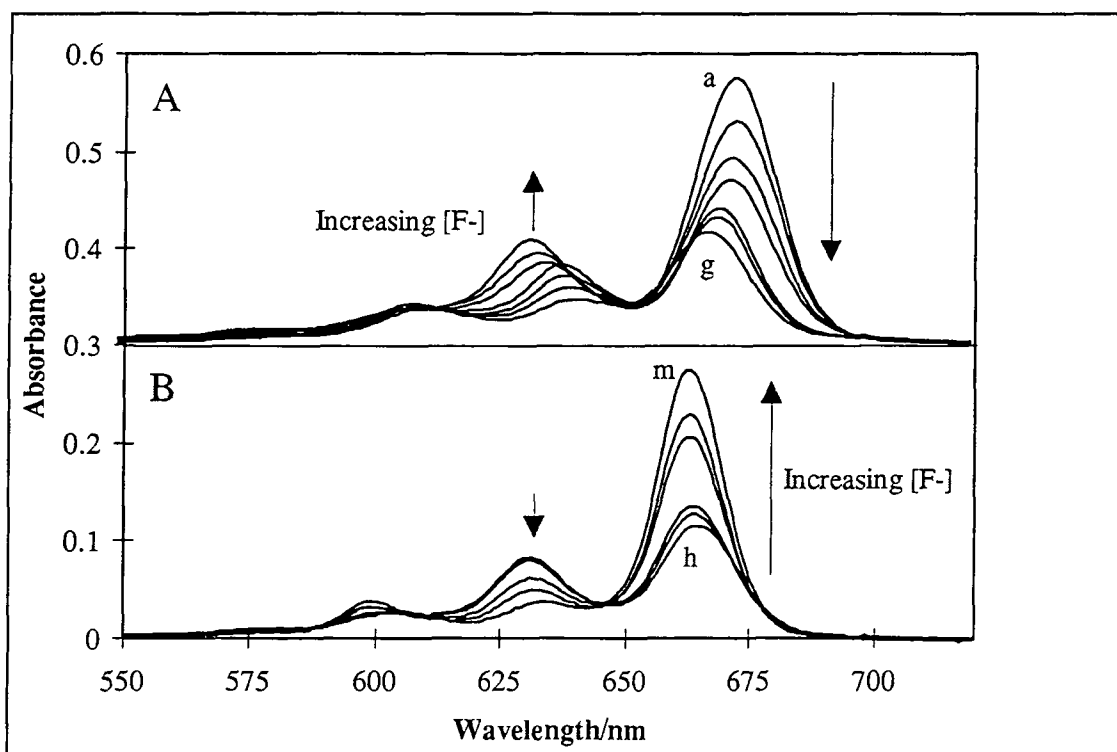
Figure 4.13.

A. Aggregation of 2×10^{-6} mol dm^{-3} AlPcCl + F^- a) 0 mol dm^{-3}, b) 2.5×10^{-7} mol dm^{-3}, c) 5×10^{-7} mol dm^{-3}, d) 1×10^{-6} mol dm^{-3}, e) 5×10^{-6} mol dm^{-3}, f) 1×10^{-5} mol dm^{-3}, g) 2.5×10^{-5} mol dm^{-3}.

B. Disaggregation of 2×10^{-6} mol dm^{-3} AlPcCl + F^-. h) 5×10^{-5} mol dm^{-3}, i) 7.5×10^{-5} mol dm^{-3}, j) 1×10^{-4} mol dm^{-3}, k) 5×10^{-4} mol dm^{-3}, l) 1×10^{-3} mol dm^{-3}, m) 5×10^{-3} mol dm^{-3}.

A and B have been offset for clarity.

131

[F⁻] /mol dm⁻³	λ_max (Monomer) /nm	λ_max (Dimer) /nm
0	673	NA
2.5×10^{-7}	672.5	638
5×10^{-7}	671	636
1×10^{-6}	671	635
5×10^{-6}	669	633
1×10^{-5}	668	631
2.5×10^{-5}	666	631
1×10^{-4}	663	631
1×10^{-3}	662	631

Table 4.3. Absorption maxima of monomer and dimer species of AlPcCl in MeOH.

At low concentrations of F⁻ (5×10^{-7} mol dm⁻³ to 2.5×10^{-5} mol dm⁻³) aggregation was promoted, whilst at high concentrations (5×10^{-5} mol dm⁻³ to 0.01 mol dm⁻³) disaggregation occurred. Effects of dimerisation on the Soret band were more subtle - a 15 ± 3 nm blue shift of λ_{max} was observed but little change in intensity occurred. This is consistent with reported spectral data of crown ether substituted phthalocyanine dimers[6]. Aggregation constants, K, were determined by defining an equilibrium constant, K_{obs}, as depicted in Equation 4.12.

$$K_{obs} = \frac{[Dimer]}{[Monomer]^2} \qquad (4.12)$$

The extinction coefficient of dimer, ε_D was assumed to be zero at the maximum wavelength of monomer absorption, thus [Monomer] was determined using the Beer-Lambert law. Knowing values for [Monomer], $[Pc]_{Total}$ and assuming conservation of mass, i.e. $[Pc]_{Total} = [Monomer] + 2[Dimer]$, allowed the equilibrium concentration of dimeric species to be calculated. Values were corroborated using the method of Tai[39], described in Section 3.2.2. K_{obs} values for various [F⁻] are collated in Table 4.4 and confirm the shift in equilibrium from monomer to dimer and back to monomer as the concentration of fluoride ions increased. Calculated equilibrium constants were consistent for both methods of analysis used. The rate of aggregation, k_{obs}, was determined by monitoring absorbance at λ_{max} of the dimer as a function of time. A large variation was recorded. At fluoride concentrations less than one equivalent ($< 10^{-6}$ mol dm⁻³), equilibrium was achieved rapidly (k_{obs} = 0.0075 s⁻¹), whilst at high fluoride concentrations aggregation could be observed over the course of one hour.
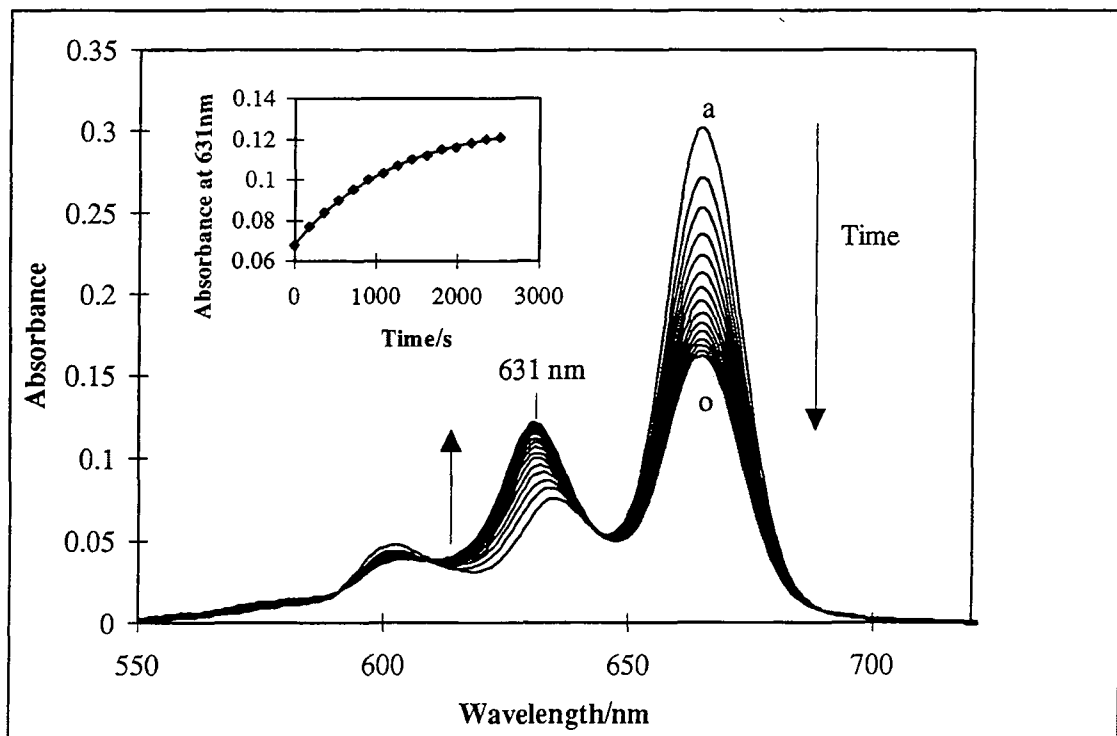
Figure 4.14. Rate of formation of (AlPc)$_2$F$^-$ (2 x 10^{-6} mol dm^{-3} AlPcCl + 2.5 x 10^{-5} mol dm^{-3} F$^-$ in MeOH). a) 'Zero' seconds, o) 2700 seconds (180 s intervals between traces). Dimer is characterised by growth of absorption at 631 nm.
Inset: Fit of first order rate constant.

Figure 4.14 shows formation of dimer, (AlPc)$_2$F$^-$, monitored by measuring the absorption spectrum of a solution containing phthalocyanine (2 x 10^{-6} mol dm^{-3}) and fluoride (2.5 x 10^{-5} mol dm^{-3}) at 3 minute intervals. The recording of the first scan was performed as quickly as possible after mixing and was taken as t=0. The inset shows a fit of first order kinetics to data obtained. k_{obs} and ε_D, measured for a range of fluoride concentrations are also collated in Table 4.4. ε_D was calculated using the Beer-Lambert law (Equation 2.1) having corrected λ_{max} of the dimer for monomer absorption. K_{obs}, k_{obs} and ε_D were not affected by the concentration of phthalocyanine over the range 4 x 10^{-7} mol dm^{-3} to 4 x 10^{-6} mol dm^{-3}.

[F⁻] /mol dm⁻³	K_{obs} /10⁴	ϵ /10⁵ mol dm⁻³ cm⁻¹	k /10⁻⁴ s⁻¹
2.5×10^{-7}	4.1 ± 1.0	1.8	80 ± 5
5×10^{-7}	15 ± 3.0	2.2	75 ± 5
10^{-6}	24 ± 6.0	2.3	-a
5×10^{-6}	46 ± 5.0	1.8	-a
1×10^{-5}	55 ± 5.0	2.0	8.5 ± 0.5
2.5×10^{-5}	80 ± 1.0	2.2	8.1 ± 0.5
1×10^{-4}	34 ± 4.0	2.1	8.2 ± 0.5
1×10^{-3}	3.3 ± 0.4	-	5.2 ± 0.3

a. Too fast to measure by this method.

Table 4.4. Equilibrium constants, rates and extinction coefficients of AlPcCl dimerisation in MeOH upon addition of F⁻.
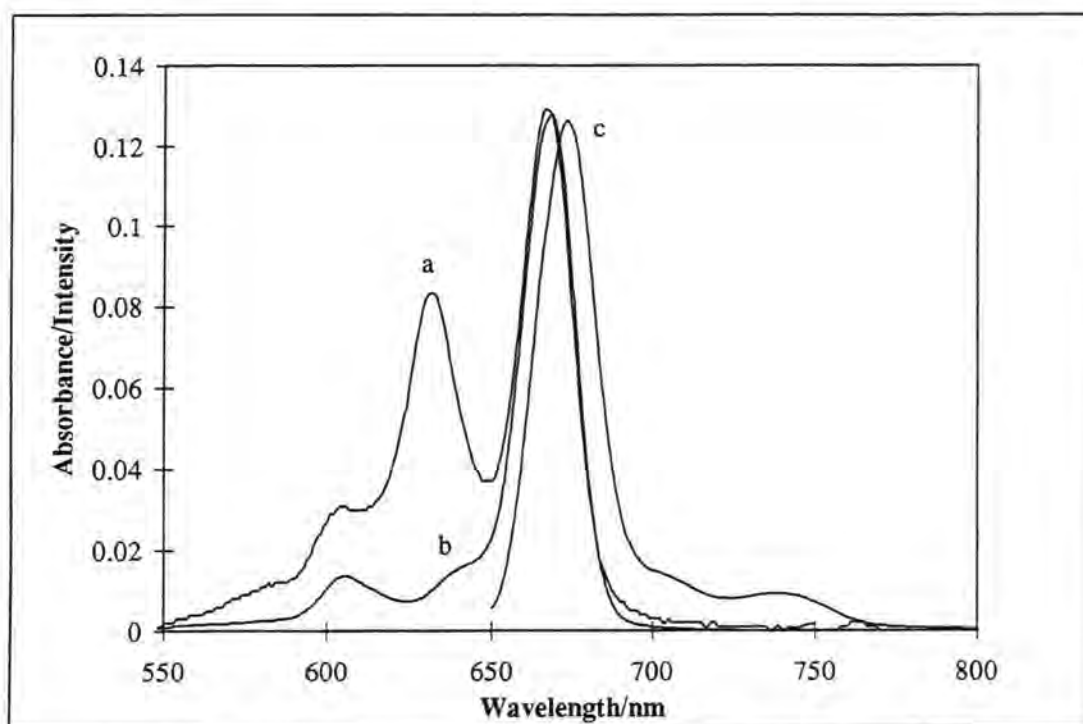
Figure 4.15. a) Absorption, b) Excitation ($\lambda_{em} = 760$ nm) and c) Emission spectra ($\lambda_{ex} = 630$ nm) of (AlPc)$_2$F⁻ (2 x 10⁻⁶ mol dm⁻³ AlPcCl + 2.5 x 10⁻⁵ mol dm⁻³ F⁻) in MeOH.

Dimeric aluminium phthalocyanine, (AlPc)$_2$F⁻, was shown to be non-fluorescent. Figure 4.15 shows the absorption, excitation and emission spectra of an equilibrated sample containing 2.5 x 10⁻⁵ mol dm⁻³ fluoride ions. No emission bands due to fluorescence from aggregated species can be observed and the absence of dimer transitions from the excitation spectrum is clear. Φ_F values of 0.55 ± 0.05, 0.12 ± 0.05 and 0.36 ± 0.04 were

determined for samples of AlPcCl (λ_{ex} = 630 nm), AlPcCl + 2.5 x 10^{-5} mol dm^{-3} F$^-$ (λ_{ex} = 620 nm) and AlPcCl + 5 x 10^{-3} mol dm^{-3} F$^-$ (λ_{ex} = 630 nm) respectively.

Dimer species were also inactive with regard to the production of triplet state molecules. Figures 4.16 a and b show the transient absorption spectra obtained for samples of 2 x 10^{-6} mol dm^{-3} phthalocyanine with zero (Sample A) and 2.5 x 10^{-5} mol dm^{-3} (Sample B) fluoride respectively. A shift of monomer ground state bleaching was observed from 670 ± 2.5 nm to 665 ± 2.5 nm, consistent with the shift induced in the ground state absorption spectrum. Bleaching of dimer absorption (631 nm) did not occur.
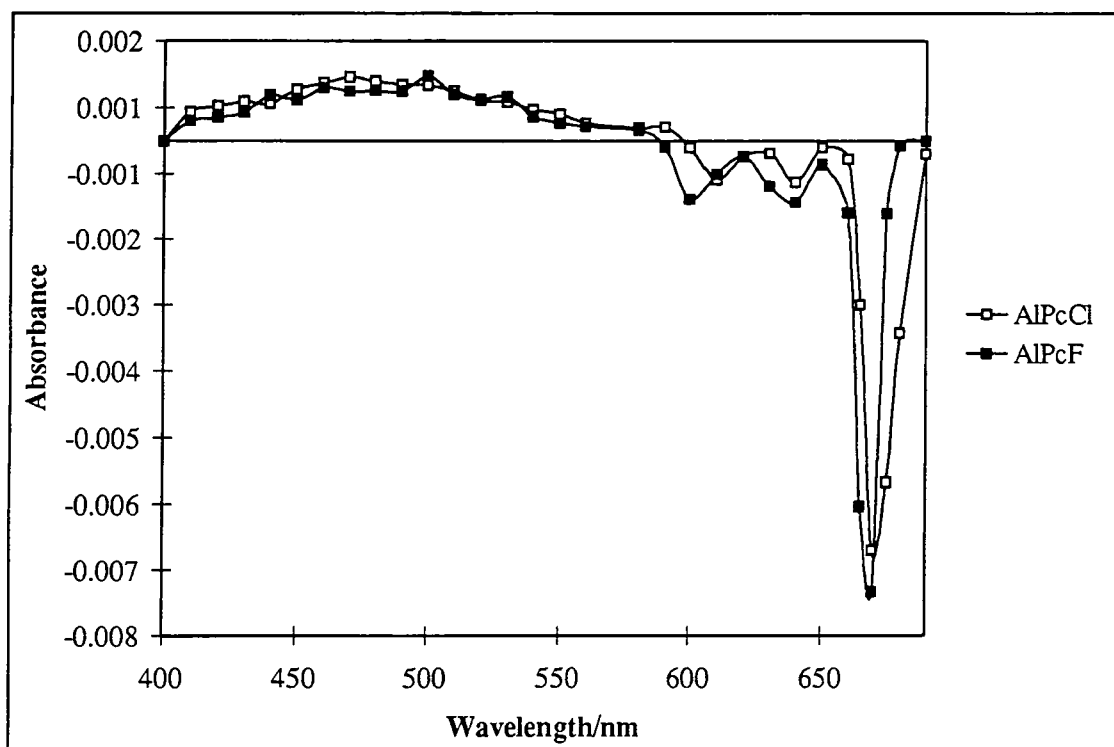
Figure 4.16. Transient absorption spectra of AlPcCl and (AlPc)$_2$F$^-$ (AlPcCl + 2.5 x 10^{-5} mol dm^{-3} F$^-$) in MeOH (λ_{ex} = 638 nm).

This was confirmed by Φ_T measurements. Sample B had a triplet yield of 0.08 ± 0.005 compared with a yield of 0.14 ± 0.03 from the parent phthalocyanine (Sample A) and 0.36 from Sample C (2 x 10^{-6} mol dm^{-3} = [AlPcCl] + 5 x 10^{-3} mol dm^{-3} = [F$^-$]). Triplet lifetimes of 180 ± 15 μs, 285 ± 20 μs and 400 ± 30 μs were measured for samples A, B and C respectively.

Attempts to repeat this work using zinc phthalocyanine and various bidentate bridging ligands were unsuccessful. Dimerisation induced by DABCO, bipy, diPE was investigated using concentrations of each ligand ranging from 1 x 10^{-8} mol dm^{-3} to 0.1 mol dm^{-3} both at room temperature and 77 K. Despite, literature precedent for binding

of porphyrins by bisamines[40],[41] and transition metal, e.g., Fe, Co and Mn, phthalocyanines[42] by ligands such as SCN^-, pyrazine and diisocyanobenzene, no evidence of aggregation was obtained.

4.4.2.1.2 Discussion

The effects of F^- on the absorption spectrum of AlPcCl may be described in terms of the equilibria shown in Figure 4.17.
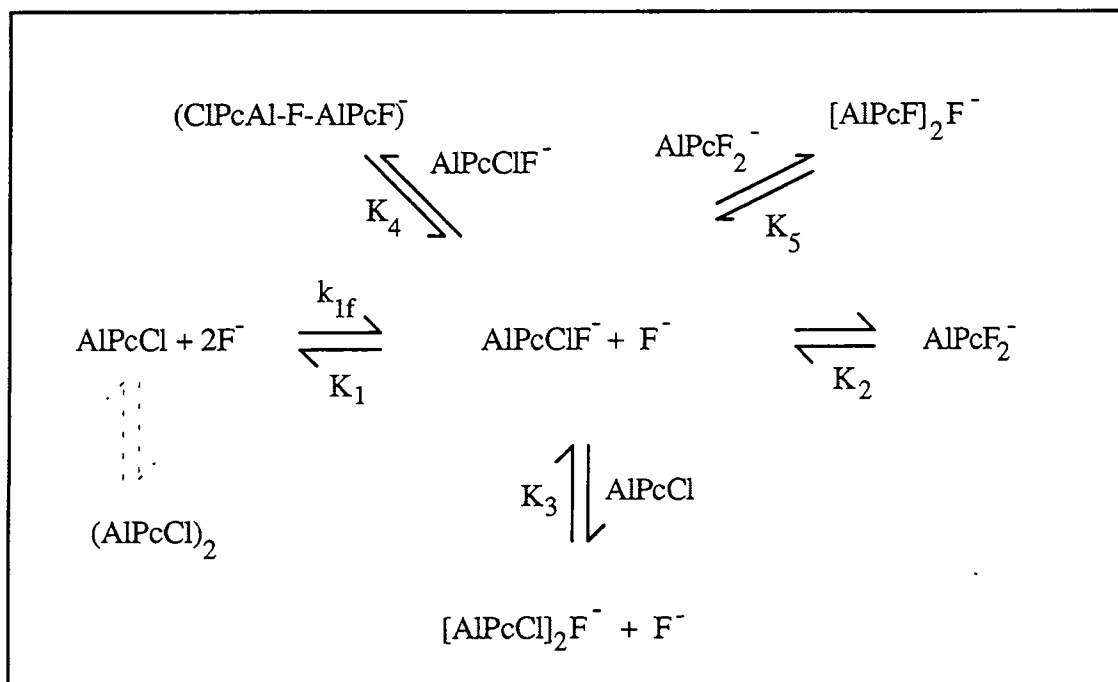
Figure 4.17.

Equilibria involved in dimerisation of AlPcCl in MeOH upon addition of F^-.

AlPcCl solutions were monomeric at the concentration of phthalocyanine used in this study, therefore, aggregation, i.e. AlPcCl $\leftrightarrow$ (AlPcCl)$_2$, at [F^-] = 0 was assumed to be negligible. Addition of low concentrations of F^- ions ($\sim$ 5 x 10^{-7} mol dm^{-3}), induced an immediate shift in the position of λ_{max} (monomer) from 673 nm to 672.5 nm, representative of binding of one fluoride to an axial position of aluminium phthalocyanine. Shifts were observed immediately on adding F^- ions implying that k_{1f} is very fast (i.e. < 1 minute). Following this, an equilibrium between AlPcClF$^-$, AlPcCl and $(F_wCl_xAlPc-F-PcAlCl_yF_z)^-$ where $(F_wCl_xAlPc-F-PcAlCl_yF_z)^-$ represents a mixture of dimeric species and w+x = y+z = 1 was established. The most likely species to be formed at fluoride concentrations of this magnitude is (AlPcCl)$_2$F$^-$. (AlPcCl)$_2$F$^-$ was represented by formation of a new absorption peak at 638 nm and proceeded with an overall rate constant of 0.0080 ± 0.0005 s^{-1}. As the concentration of fluoride increased,

the absorption maxima of monomeric and dimeric species shifted progressively towards lower wavelengths, reaching limiting values of 662 nm and 631 nm respectively. Monomer absorption at this wavelength may be ascribed to difluorinated species, $AlPcF_2^-$. Hypsochromic movement of dimeric phthalocyanine absorption suggests formation of more than one dimer species and indicates a shift of contributing absorption from $(AlPcCl)_2F^-$ to that of more highly fluorinated dimers, $(ClPcAl-F-AlPcF)^-$ and $(AlPcF)_2F^-$. A rate constant of 0.00080 ± 0.00005 s^{-1} was determined over the concentration range 10^{-5} mol dm^{-3} < $[F^-]$ < 10^{-4} mol dm^{-3}. This is comparable to that observed by Martin and co-workers[5] for the aggregation of tetrasulfonated aluminium phthalocyanine hydroxide ($AlPcS_4OH$) in 0.2 mol dm^{-3} NaOH. Dimerisation was ascribed to the formation of a binuclear μ-oxo dimer, $(AlS_4Pc)_2O$ and was observed to occur over four hours.

Experimentally determined equilibrium constants (Table 4.4) may be represented by Equation 4.13 (See Appendix B).

$$K_{obs} = \frac{K_3 K_1 [F^-] + K_4 K_1^2 [F^-]^2 + K_5 K_2 K_1^2 [F^-]^3}{(1 + K_1 [F^-] + K_1 K_2 [F^-]^2)^2} \qquad (4.13)$$

Limiting cases of this equation may be considered. At low $[F^-]$, second and third numerator terms will tend to zero and, if $1 \gg K_1[F^-]$, denominator terms will reduce to 1. Hence, K_{obs} can be represented by Equation 4.14.

$$K_{obs} = K_3 K_1 [F^-] \qquad (4.14)$$

Thus, dimer formation is dominated by K_3. At higher $[F^-]$, $K_4 K_1[F^-]^2$ and $K_5 K_2 K_1^2[F^-]^3$ terms will become progressively more important and dimer formation shifts to production of $(ClPcAl-F-AlPcF)^-$ and finally, $(AlPcF)_2F^-$. At very high fluoride concentrations, i.e. if $K_1[F^-] \gg 1$ then Equation 4.13 reduces to

$$K_{obs} = \frac{K_3 + K_4 K_1 [F^-] + K_5 K_2 K_1 [F^-]^2}{K_1[F^-](1 + K_2 [F^-])^2} \qquad (4.15)$$

Thus, as the concentration of fluoride increases, K_{obs} decreases as inactive, $AlPcF_2^-$ monomeric species are formed (Figure 4.13B). Rate determinations indicate that $(AlPcCl)_2F^-$ formation is very rapid (0.0075 s^{-1}), whilst that of $(AlPcF)_2F^-$ is a factor of

ten slower (0.0008 s⁻¹). It was not possible to measure the formation of (ClPcAl-F-AlPcF)⁻ directly, however, formation of dimer species with intermediate absorption wavelengths (e.g. 634 nm), the most likely position for this dimer, occurred very rapidly and k_{obs} may be estimated to be > 0.01 s⁻¹. All rate data fitted first order kinetics. This is surprising since dimerisation would be expected to be a second order process. However, k_{obs} is a complex function of forward and reverse reactions of all equilibria present in solution[43] and may appear as a 'pseudo' first order reaction.

By reference to exciton theory (Section 4.2.1), fluoride linked phthalocyanines may be classified as Type A dimers in which θ = 90° (Figure 4.18a), i.e. face-to-face dimers with cofacial, parallel transition dipole moments. In phthalocyanine molecules, transition moments are thought to lie in the plane of the molecule along the N-M-N axes, designated the x and y directions[25].

a) Dimer   *b) Difluorinated Monomer*
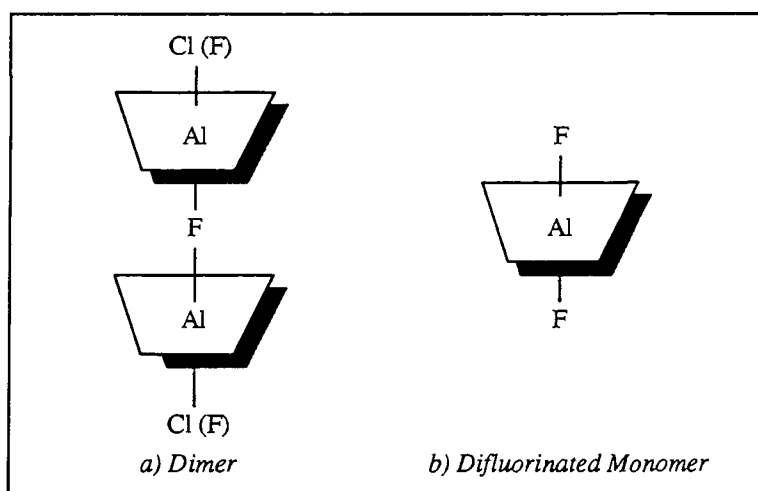
Figure 4.18. Geometry of (AlPc)₂F⁻ dimer (a) and AlPcF₂⁻ monomer (b).

This type of dimer has allowed transitions to the upper energy level but those to the lower level are forbidden. Thus dimer absorption appeared as a single peak, blue shifted with respect to the monomer. Exciton splitting, ΔE, of Type A dimers is represented by equation 4.1. In this case, ΔE was 1710 cm⁻¹. The transition *length*, M_r, was determined using Equation 4.16[6] and converted into the transition *moment*, M using Equation 4.17.

$$M_r^2 = \frac{\varepsilon_{max}}{2513G} \cdot \frac{\Delta\lambda}{\lambda}$$

(4.16)

where G is the degeneracy of the state, Δλ is the half bandwidth, λ is the wavelength of maximum absorption and ε_{max} is the extinction coefficient.

$$M^2 = \frac{e^2 M_r^2}{4\pi hc\varepsilon_0}$$

(4.17)

where e is the charge of an electron, h is Plank's constant, ε_0 is the permittivity of a vacuum and c is the velocity of light. M_r^2 was calculated to be 0.983 Å^2 and M^2 = 1.14 x 10^{-23} m^2. Thus, using Equation 4.1, assuming θ is 90°, r was found to be 4.05 Å. This is in excellent agreement with Martin's value[5] of 4.27 Å for $(AlPcCl)_2O$ and an interplanar distance of 4.11 Å calculated by Kobayashi and Lever[6] for crown ether substituted copper phthalocyanine. A crystal structure study by Wynne[4] showed the phthalocyanine rings of $(AlPcCl)_2O$ to be eclipsed, and separated by a distance of 4.27 Å. These ring-ring distances are all slightly larger than those reported for $(AlPcF^-)_n$ polymer (3.6 Å)[44]. Thus, by comparison with literature precedent, the assignment of the 631 nm absorption to $(AlPcF)_2F$, a cofacial dimer with a ring separation of 4.05 Å and a θ value of 90° would seem reasonable.

Reduced fluorescence and triplet state formation of solutions containing dimeric species may be for one of two reasons: dimer inactivity or the effect of axial ligand replacement. It has already been demonstrated that replacement of sulfonated aluminium phthalocyanine axial hydroxide ligands by fluoride induced a small decrease in Φ_F and a concurrent increase in Φ_T[45]. This is corroborated by values determined using AlPcCl in this study. However, the measured fluorescence yield of $(F_wCl_xAlPc\text{-}F\text{-}PcAlCl_yF_z)^-$ (0.12) is smaller than can be accounted for by fluoride binding (Φ_F of $AlPcF_2^-$ = 0.36). In addition, a decrease in Φ_T was observed (Φ_T = 0.08) which is in contrast to an increase produced by fluoride binding (Φ_T = 0.36). It is, therefore, concluded that reduced photophysical activity is due to the formation of inactive dimer species rather than replacement of axial chloride ligands by fluoride. Lack of fluorescence and triplet state production by this type of dimer is consistent with the predictions of exciton theory and also with observations made by Martin[5] and Kobayashi[6] for other cofacial phthalocyanine dimers. This geometry is prevalent in phthalocyanine dimer formation[46],[4],[6], hence, phthalocyanine aggregates are generally accepted to be non-fluorescent with reduced phototoxicity.

4.4.2.2   1,4,8,11,15,18,22,25-Octadecyl Zinc Phthalocyanine (C10)
4.4.2.2.1 Results

Cooling of a solution of C10 in EPA to 77 K resulted in a significant change in the structure of the UV/Visible absorption spectrum (Figure 4.19). Peaks at 641 nm, 680

nm, 693 nm, 705 nm and 741 nm were apparent compared with a single absorption peak at 698 nm observed at 293 K, characteristic[47] of monomeric C10. The change was a gradual one and thermal cycling experiments showed the temperature dependence to be reversible. The concentration of phthalocyanine was found to affect the changes observed at low temperature. Higher phthalocyanine concentrations resulted in a greater increase in structure on cooling (Figure 4.20). The nature of the peripheral substituents and their interaction with solvent molecules was found to be critical. The effect of temperature on the absorption spectrum of α-substituted $ZnPc(X)_8$ in EPA decreased as the length of the alkyl chain substituent (X) decreased, i.e. $C_{10}H_{21} > C_5H_{11} > CH_3$. The same trend was observed in MeTHF where β-$C_{16}H_{33}$ substituents induced structureless aggregation of ZnPc at 77 K whilst $C_{10}H_{21}$ substituted ZnPc remained monomeric. α-butoxy ligands didn't cause any additional structure in the low temperature spectrum in EPA despite being isoelectronic with the α-C_5H_{11} alkyl substituents.
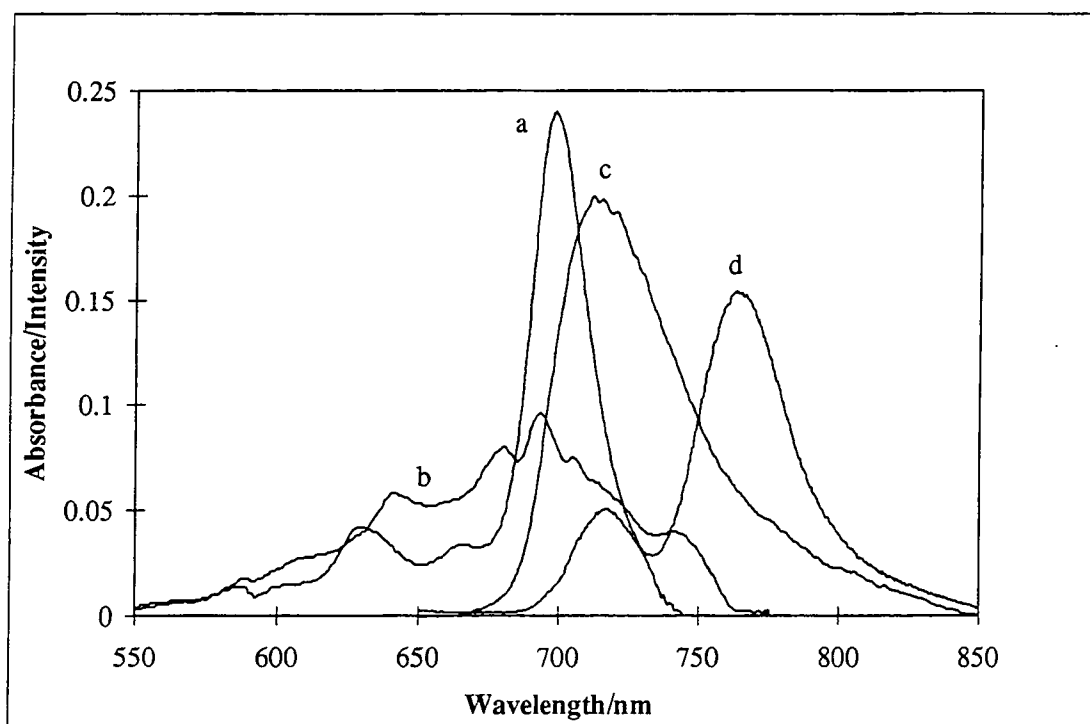
Figure 4.19. Absorption spectra of C10 in EPA at a) 293 K (1.3 x 10^-6 mol dm^-3) and b) 77 K (1.7 x 10^-6 mol dm^-3) and emission spectra of C10 in EPA at c) 293 K and d) 77 K. (λ_{ex} = 630 nm).

Fluorescence emission and excitation spectra exhibited similar behaviour to the absorption spectra. Lowering of the sample temperature from 293 K to 77 K caused emission to change from a single peak at 718 nm to two emission bands centred at 718 nm and 760 nm (Figure 4.19d). The relative yield of emission at 765 nm was observed to increase as the concentration of C10 increased (Figure 4.21).
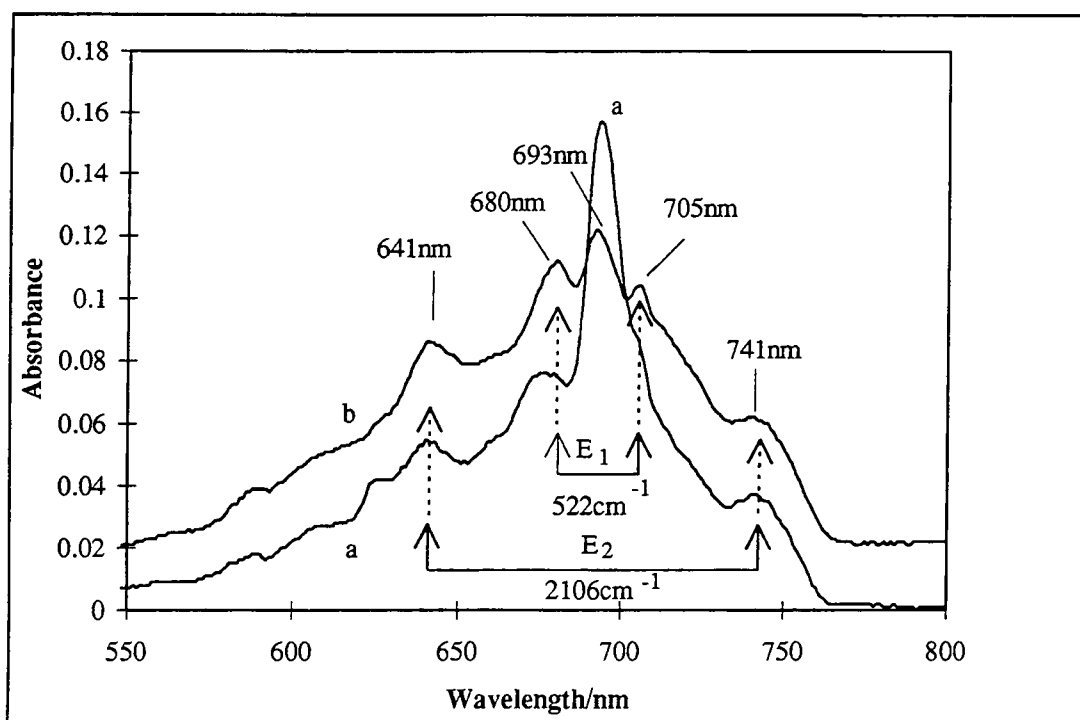
Figure 4.20.

Concentration dependence of absorbance spectra of a) 1.7 x 10⁻⁶ mol dm⁻³ and b) 1.4 x 10⁻³ mol dm⁻³ C10 in EPA at 77 K. Spectra have been offset for clarity.
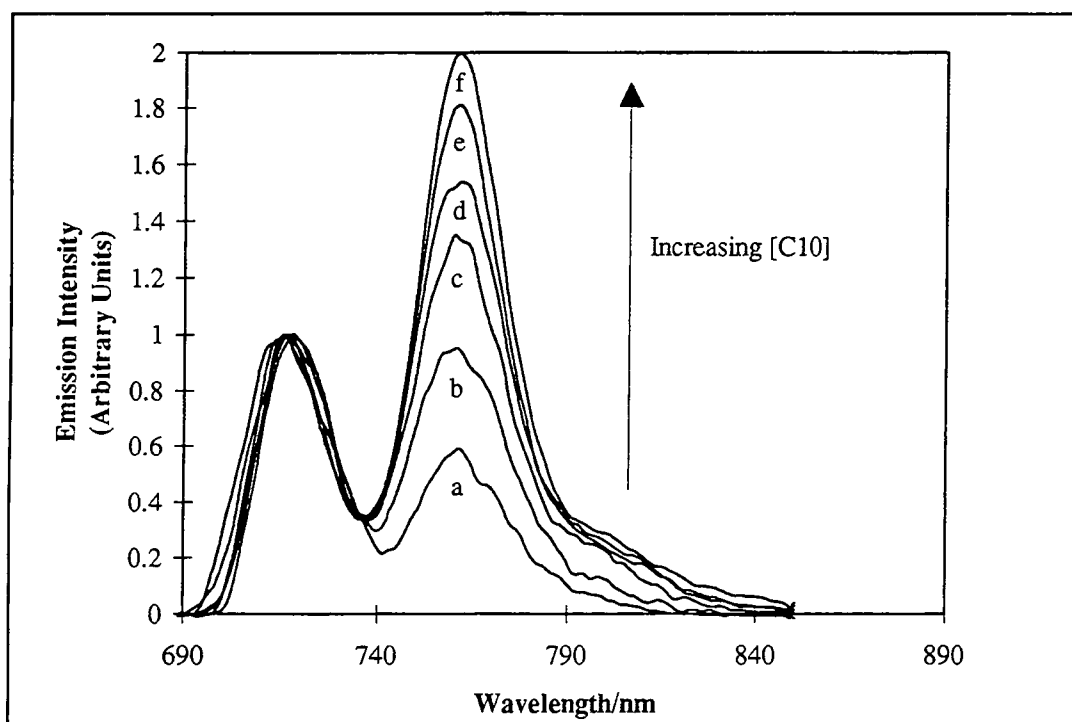
Figure 4.21. Effect of phthalocyanine concentration on the emission spectra of C10 in EPA at 77 K. a) 2.67 x 10⁻⁷ mol dm⁻³, b) 3.72 x 10⁻⁷ mol dm⁻³, c) 7 x 10⁻⁷ mol dm⁻³, d) 1.24 x 10⁻⁶ mol dm⁻³, e) 1.67 x 10⁻⁶ mol dm⁻³, f) 3.04 x 10⁻⁶ mol dm⁻³. Spectra have been normalised at 718 nm.

Excitation spectra obtained by monitoring emission wavelengths (λ_{em}) of 725 nm and 785 nm were very different, indicating the presence of at least two distinct species (Figure 4.22).
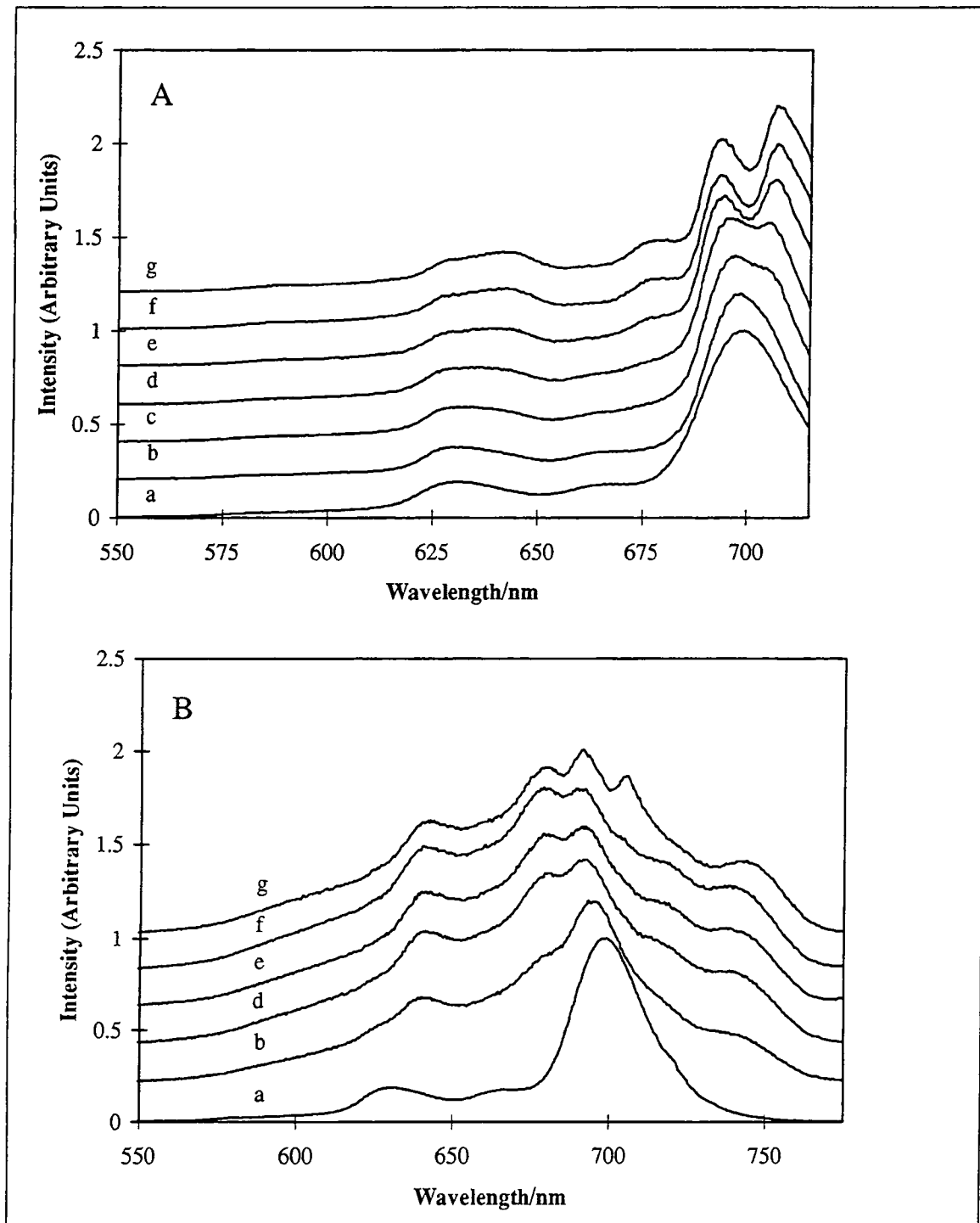
Figure 4.22. Temperature dependence of the excitation spectra of C10 in EPA.
A. λ_{em} = 725 nm, B. λ_{em} = 785 nm. a) 293 K, b) 180 K, c) 170 K, d) 160 K, e) 150 K,
f) 140 K, g) 77 K. Spectra have been offset for clarity.

The fluorescence anisotropy of each emission peak was determined using a range of excitation wavelengths (600 nm - 740 nm). The anisotropy of the first peak was determined by averaging r_{av} values obtained over the emission wavelengths 715 nm - 725 nm and that of the second by averaging over the range 755 nm - 765 nm. Figure 4.23 shows large differences between values of r_{av} calculated for each peak.
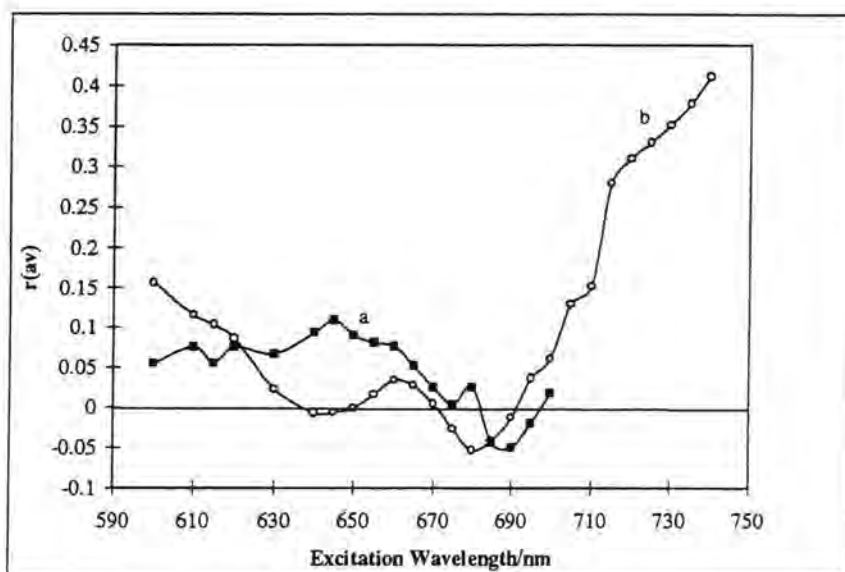
Figure 4.23. Anisotropy of emission from C10 in EPA at 77 K.
a) $\lambda_{em} = 715 - 725$ nm, b) $\lambda_{em} = 755 - 765$ nm.

The fluorescence lifetimes of emitting species were measured using time correlated single photon counting apparatus. Multiexponent decays were observed. Table 4.5 collates lifetimes measured by monitoring emission at 710 nm and 765 nm.

T /K	λ_{em} /nm	τ_1 /ns (Amplitude, Yield)	τ_2 /ns (Amplitude, Yield)	τ_3 /ns (Amplitude, Yield)	χ^2	DW
293	710	2.15 (78.73, 93.47)	0.56 (21.27, 6.53)	-	1.084	1.96
293	765	2.24 (114.06, 102.41)	0.426 (-14.06, -2.41)	-	1.146	1.98
77	710	3.81 (36.1, 88.4)	0.16 (53.9, 5.55)	0.945 (9.79, 6.05)	1.293	2.04
77	765	2.62 (116, 100.63)	0.117 (-16.46, -0.63)	-	1.32	1.89

Table 4.5.

Fluorescence lifetime data of C10 in EPA at 293 K and 77 K, $\lambda_{ex} = 638$ nm.

The error in these measurements can be regarded as ± 10 %. Greater than 88 % of the yield of all decays could be represented by a single decay, τ_1, therefore, contributions of τ_2 and τ_3 to decays are neglected for the purpose of this discussion. The fluorescence lifetime of C10 at room temperature was independent of wavelength of detection and is marginally longer than a literature value of 1.7 ns recorded in 1% pyridine/toluene[48]. Reducing the temperature to 77 K caused an increase in the fluorescence lifetime recorded at 710 nm and 765 nm of ~ 80 % and ~ 20 % respectively.

Triplet state studies also showed a marked temperature dependence. Transient decays (λ_{ex} = 638 nm, λ_{Probe} = 520 nm) displayed an increase in lifetime on cooling, from 50 ± 5 µs at 293 K to 590 ± 60 µs at 77 K. A steady decrease in the rate of deactivation of T_1 was observed until temperatures reached 150 - 160 K which is likely to correspond to the glass transition point of EPA - further cooling had minimal effect (Figure 4.24B). All decays fitted to monoexponential kinetics. Monoexponential decays were also obtained at 77 K when recovery of the ground state (λ_{Probe} = 620 - 750 nm) was monitored. This is a surprising result when the transient absorption spectrum is considered (Figure 4.25Aa). After correction for ground state absorption (Trace b), this spectrum shows absorption due to triplet state species and bleaching due to ground state monomeric phthalocyanine. Given the obvious presence of two separate processes, a monoexponential decay would not be expected. Decays remained monoexponential all temperatures below ~ 150 K. Above this temperature, two component decays were obtained until the concentration of dimer became negligible (> 230 K). At this point, monoexponential decays were once again observed. Figure 4.24A shows an example of a two component decay consisting of a fast, exponential decay (k_{fast} = 9900 s^{-1}) and a slow, second order component (k_{slow} = 0.4 mol dm^{-3} s^{-1}) recorded at an intermediate temperature (200 K) using a probe wavelength of 700 nm. At this temperature, the absorbing transient species shows a definite time dependence. At short time intervals after excitation, e.g. 10 µs, the transient spectrum resembles a difference spectrum, i.e. triplet state absorption and bleaching of the ground state (Figure 4.25Ba). However, at longer time intervals, e.g. 300 µs, the triplet state species have decayed but the spectrum shows the presence of a transient at 700 nm, resembling that of a monomeric phthalocyanine (Figure 4.25Bc). This spectrum has been corrected for ground state absorption by the sample. The yield of transient absorption due to triplet state species was not significantly affected by changes in temperature.

Singlet oxygen studies were not performed due to reduced diffusional rates of oxygen at low temperature which prohibited triplet state quenching.
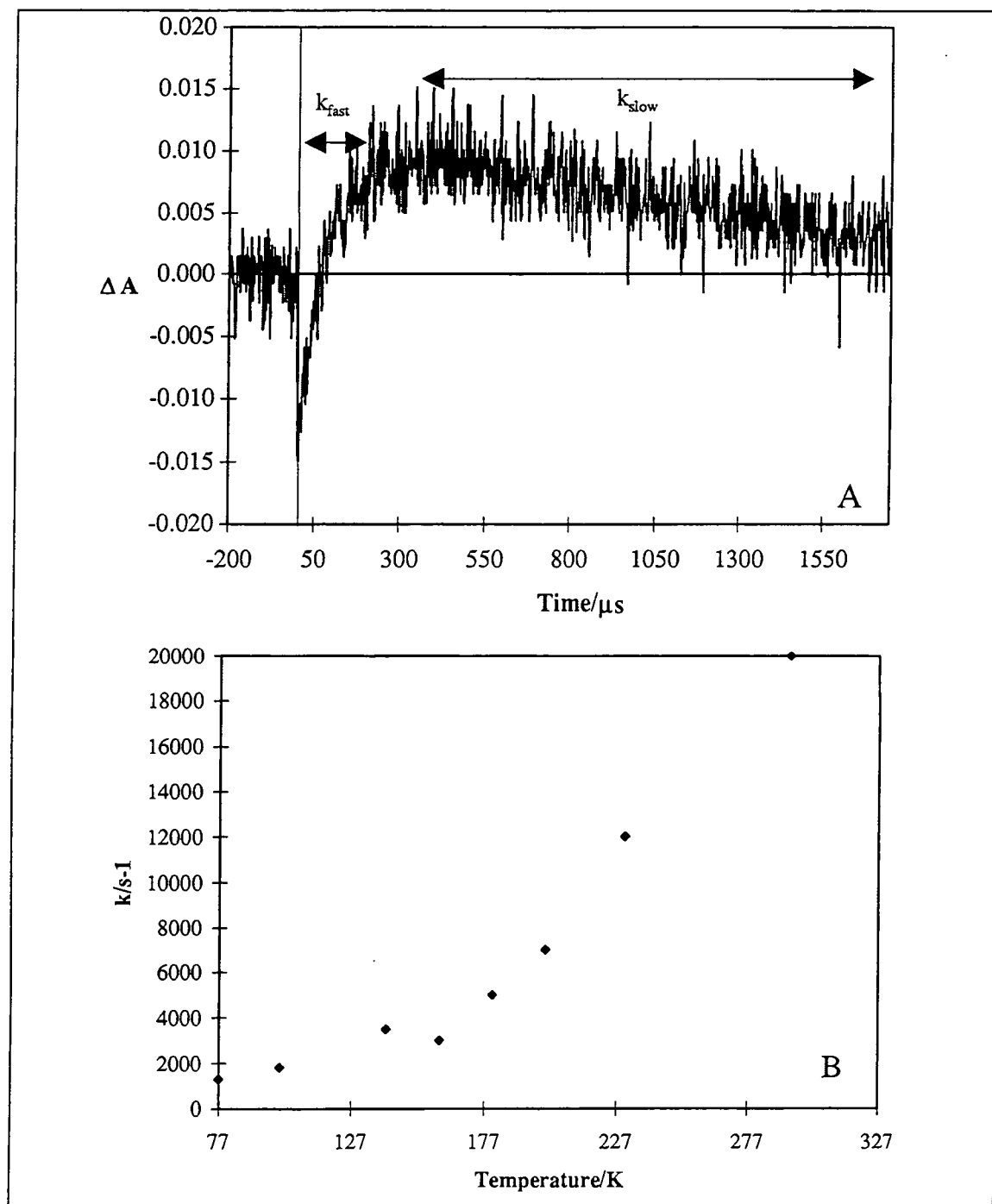
Figure 4.24 A. Transient decay of C10 in EPA at 200 K (λ_{Probe} = 700 nm).
B. Effect of temperature on rate of triplet decay (λ_{Probe} = 520 nm).
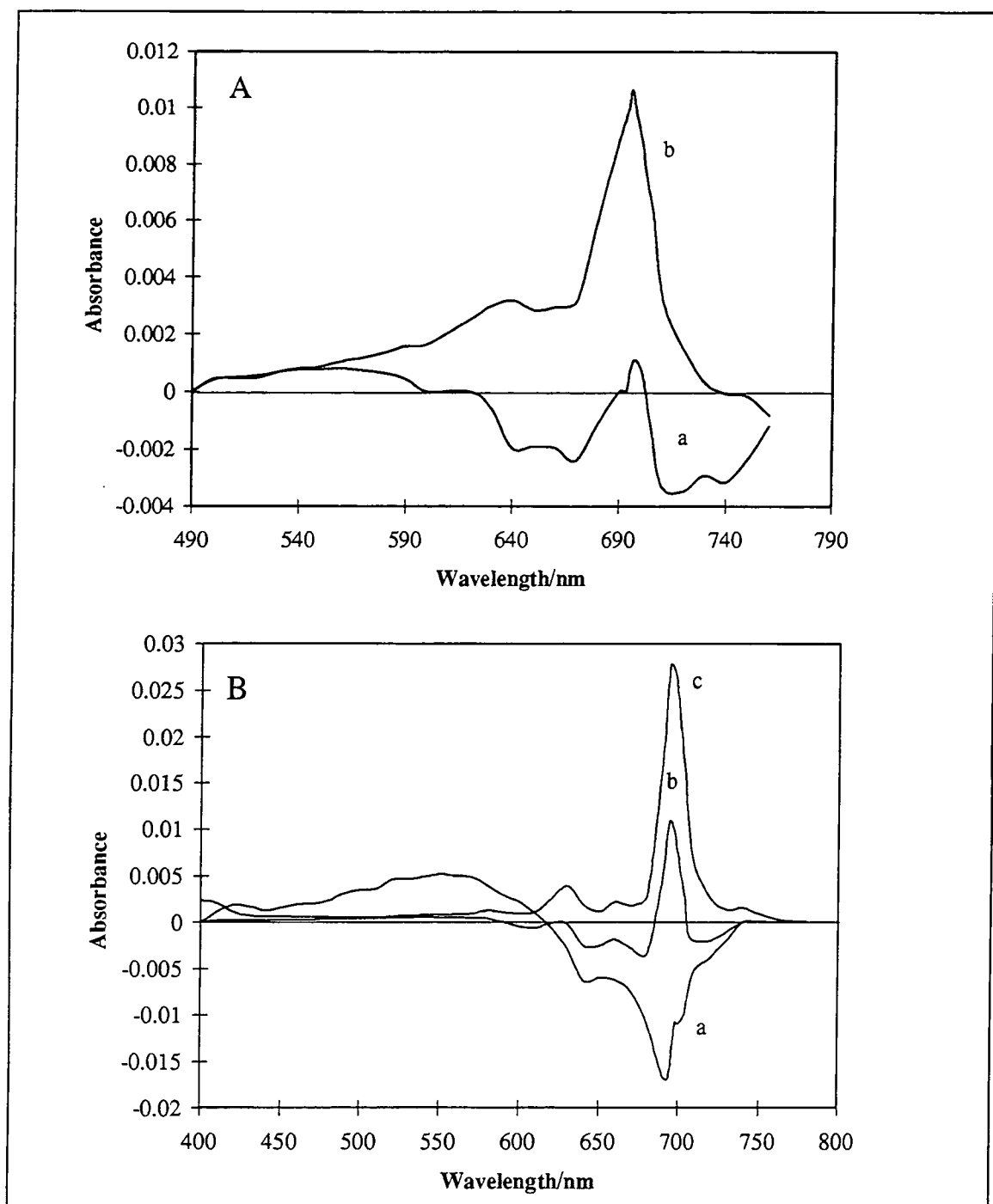
Figure 4.25. Transient absorption spectra of C10 in EPA (λ_{ex} = 638 nm).
A. 77 K, a) 10 μs after excitation, b) Trace a corrected for ground state absorption.
B. 200 K, a) 10 μs after excitation, b) 300 μs after excitation, c) Trace b corrected for
ground state absorption.

4.4.2.2.2 Discussion

The results observed when C10 was cooled to 77 K may be ascribed to dimerisation. Aggregation at low temperatures is not uncommon[49],[50] and it is well established that low temperatures promote dimer formation[51] due to thermodynamic considerations. The extent of aggregation was observed to increase as the concentration of phthalocyanine increased, consistent with the usual behaviour of molecules of this type[9]. Emission at 725 nm is assigned to residual monomer fluorescence. The excitation spectrum of this emission shows a splitting of the Q band at low temperatures, analogous to that observed at 77 K for $ZnPcS_2$ in EtOH (Section 3.3.2.2.3) but more pronounced. A single emission peak results from both transitions, suggesting that degeneracy of the S_1 excited state has been removed. Fluorescence anisotropy measurements (Figure 4.23) indicate this may be feasible since a negative value of r_{av} was obtained at 690 nm (-0.05), i.e. the angle between the emission transition dipole and absorption transition dipole is > 54.7°. At excitation wavelengths below 660 nm, anisotropy was approximately constant at 0.075, consistent with the average value determined for monomeric ${}^tBu_4ZnPc$ (Section 4.4.1.2). A similar trend was observed by Gouterman[10] for the fluorescence polarisation of μ-oxo scandium porphyrin dimers. In these molecules, the polarisation was constant at 0.1 except in a region of excited state splitting where negative polarisation was observed (p_{min} = -0.1[52]). The reason for removal of S_1 degeneracy is not clear. Due to the inherent symmetry of this phthalocyanine it would be expected that x and y polarisation axes would be identical, as indeed they appear to be at room temperature. It would seem that as the temperature is lowered, interactions between the C10 chains render the molecule asymmetric. Explanation of this phenomenon becomes more difficult when the absorption spectrum of a more dilute sample of C10 (1.4 x 10^{-7} mol dm^{-3}) is considered (Figure 4.20a). At this concentration, a significant fraction of monomeric species remain at 77 K and it is clear that splitting of the monomer absorption band did not occur.

Emission at 718 nm was accompanied by the appearance of a new band at 760 nm (Figure 4.19d). The excitation spectrum obtained by monitoring emission at 785 nm (Figure 4.22B(g)) is almost identical to the absorption spectrum and propounds that aggregated phthalocyanine species are responsible for this emission. It can be shown (Figure 4.26) that emission at 718 nm is linearly related to absorption by monomer species, A_m, whilst, that at 760 nm is proportional to dimer absorbance, A_d. A_m and A_d were calculated using Equations 4.18 and 4.19. Equation 4.18 was used to calculate the spectrum of pure dimer species.

$$A_{DTotal}(\lambda) = A_{conc}(\lambda) - Const.\, A_{dil}(\lambda) \qquad (4.18)$$

where A_{DTotal} is the absorbance of pure dimer species, A_{conc} is the absorbance of a concentrated C10 sample, A_{dil} is the absorbance of a dilute C10 sample and Const. is a normalising factor. By subtracting a fraction of A_{DTotal} from C10 samples of interest (Equation 4.19), absorbance due to residual monomer, and hence dimer, species was determined.

$$A(\lambda) - (yA_{DTotal}(\lambda)) = xA_{MTotal}(\lambda)$$

where $\qquad (4.19)$

$$yA_{DTotal}(\lambda) = A_d(\lambda) \quad and \quad xA_{MTotal}(\lambda) = A_m(\lambda)$$
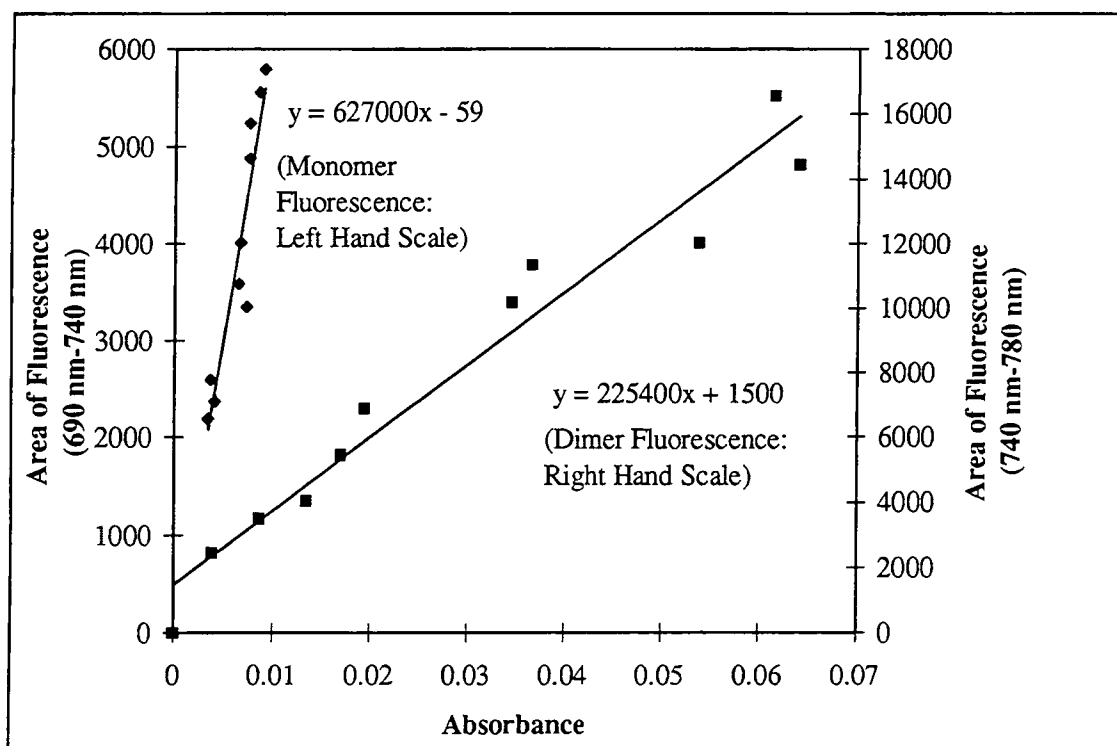
Figure 4.26.

Emission intensity vs absorbance due to monomeric and dimeric C10 in EPA at 77 K.

Such a linear correlation confirms that emission at 760 nm results from dimeric phthalocyanine. From the gradient of each fit it may be calculated that at 77 K Φ_{FD} = $0.35\Phi_{FM}$ where Φ_{FD} and Φ_{FM} are the corrected fluorescence quantum yields of dimer and monomer respectively. This result is very unusual and the first convincing evidence to support the existence of luminescence from phthalocyanine dimers bound solely by

Van der Waals forces. Fluorescence lifetime measurements support the theory of dimer emission at 760 nm. An increase of only 20% was observed on cooling compared with an increase of 80% in the lifetime of emission at 710 nm. This may be attributed to availability of radiationless deactivation pathways in dimeric species. As T is lowered, vibrational and rotational motions are reduced and with them k_{ic}, thus an increase in τ_F was observed. In dimeric phthalocyanine, additional radiationless pathways such as disaggregation/recombination become available, counteracting to some extent the effects of temperature. Hence, a much smaller increase in radiative lifetime was observed in the emission of dimeric species (760 nm).

Dimer absorption was represented by two symmetrically displaced pairs of transitions, E_1 (640 nm & 741 nm) and E_2 (680 nm & 705 nm) (Figure 4.19). At a first glance, these pairs of transitions may be ascribed to the absorption bands of C10 dimers in which exciton splitting of the excited state has occurred and transitions are allowed to both energy levels created. This criterion is met by the geometrical arrangements B or C considered in Section 4.2.1, dimer species with oblique, coplanar transition dipoles or 'clamshell' type geometry, or those with out-of-plane dipoles, i.e. cofacial, staggered phthalocyanine dimers. 'Clamshell' phthalocyanines have been synthesised by Leznoff and co-workers by linking phthalocyanine rings through units such as oxygen[53], hydrocarbon chains[53] or alkoxy units[54]. The extent of coupling between monomer subunits was dependent on the nature of the bridge and existed as a dynamic equilibrium between various geometries. At room temperature, the absorption spectra of these complexes represented a summation of all conformations co-existing in solution and displayed distinct similarities to the monomer absorption spectrum. The fluorescence emission spectrum was also representative of monomer emission, indicating an open 'clamshell' arrangement with little interaction between rings. At 77 K, the absorption spectra displayed a greater degree of coupling, denoted by more intense absorption between 600 nm and 650 nm. A new emission peak at 750 nm accompanying these transitions was ascribed to emission from an exciton coupled excited state. This behaviour is analogous to that observed C10. Emission at 750 nm is of comparable energy to the emission observed from C10 dimers (760 nm). It would, therefore, seem reasonable to assign E_1 and E_2 to the electronic transitions of C10 dimers with clamshell arrangements of differing r and/or θ. This is quantified by Equation 4.2 which demonstrates that small values of r and θ give rise to a greater exciton splitting than when separation between molecules is large or the tilt angle is small. It was not possible to calculate the separation distance, r, since α and θ are unknown quantities.

Further consideration of the low temperature emission spectra in conjunction with the absorption spectrum casts doubt upon this theory. Only one peak due to dimer emission was obtained. If two different dimer configurations were responsible for transitions observed in the absorption spectrum, as discussed above, it is reasonable to expect two emission peaks to be detected. In addition, differences between the excitation spectrum (Figure 4.22B, g) and absorption spectrum (Figure 4.19b) would be expected. Contributions of monomer fluorescence to excitation monitored at 785 nm may be considered to be negligible due to the vast excess of dimer fluorescence detected at this wavelength. It is suggested that a situation similar to that depicted in Figure 4.27 must be responsible for the observed behaviour. Exciton coupling of monomer excited states occurred to give rise to five allowed transitions in the excited state dimer. A shift in the centre of gravity, D, arises due to electrostatic interaction between monomer units. Fast vibrational relaxation from each of these levels to the lowest excited state E' took place, from where emission was observed. Fluorescence anisotropy measurements confirm an energy level arrangement of this type. By analogy to r_{av} measurements for $^tBu_4H_2Pc$ (Section 4.4.1.2), a large positive anisotropy at 740 nm (0.38) may be explained by excitation into the emitting energy level of a molecule with a non-degenerate excited state, in this case E^I. This value is very close to $r_f = 0.4$, the theoretical maximum anisotropy which occurs when $\theta_a = 0°$. Troughs at 640 nm and 680 nm correspond to excitation into E^{IV} and E^V respectively. r_{av} values of -0.007 and -0.054 at these wavelengths correlate to angles of 55.5° and 60.4° (Equation 4.4) between E^{IV} & E^I and E^V & E^I respectively. These values represent minimum limits for θ_a since it is probable that mixing of states artificially raises the measured value. This is demonstrated by transitions to E^{III} and E^{II} in which an increasingly positive anisotropy was observed as the excitation wavelength approached that required for population of E^I.
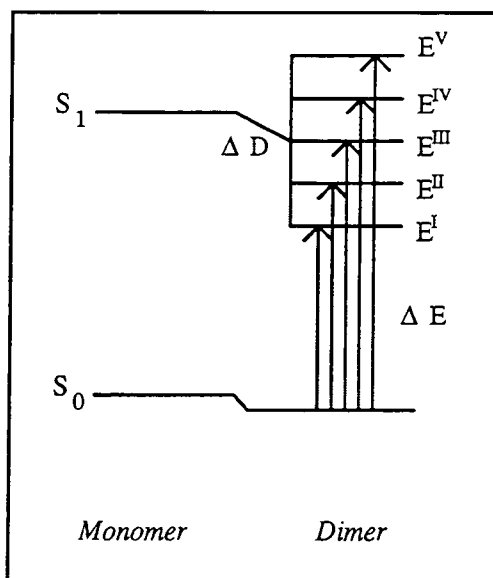
Figure 4.27. Energy level splitting of C10 in EPA at 77 K.

The reasons behind splitting of the monomer excited state into five energy levels are complex and cannot be explained by simple exciton theory. Similar observations have been made by other groups regarding the chemically bonded μ-oxo dimers of silicon phthalocyanine. Ferencz *et al.*[55] report the presence of five absorption peaks in the spectrum of the μ-oxo dimer of tetra(methoxy) tetraoctyloxy substituted silicon phthalocyanine in non aromatic solvents such as dichloromethane and THF. Peaks are similarly distributed with respect to monomer absorption to those observed in this study for C10 aggregation. The oscillator strength of each of these transitions was affected by the nature of the solvent and Schryver suggests that solvent/dye interactions influence excitonic and vibrational coupling between the ring but states that a conclusive physical explanation is not possible based on current knowledge. Oddos-Marcel[56] and co-workers extended this work and suggest that transitions from the HOMO of one monomer to the LUMO of another (ion pair or charge transfer configurations) may be responsible for some of the ground state transitions observed and the changes invoked as a function of environment. These are made possible by strong coupling between monomers. Aggregation of dimers was also suggested as a conceivable explanation, however, a satisfactory interpretation of these effects is still awaited. It is also possible that inequivalent coupling between x and y dipole moments may be responsible. This has been observed for a planar, binuclear zinc phthalocyanine, studied by Kobayashi and co-workers[57]. In planar phthalocyanine dimers, dipoles oriented along the x axis lie along the same line, i.e. $\theta = 0°$, whilst dipoles oriented along the y axis are perpendicular to r, i.e. $\theta = 90°$. This gives rise to two pairs of energy levels. Transitions will be allowed to the lower energy level of the first pair (x dipole coupling) and the higher energy level of the second pair (c.f. rules for Type A dimers), leading to the observation of a doublet in the UV/Visible absorption spectrum. Non-equivalent splitting of x and y dipoles in which transitions to both energy levels were allowed may explain E^I, E^{II}, E^{IV} and E^V energy levels of C10 at 77 K. E^{III} would then have to be ascribed to residual monomer absorption.

A decrease in the non-radiative decay processes of the triplet species of C10 at 77 K is not unexpected. Similar phenomena have been observed for the decay of triplet excited states of pyrazine[58] and propynal[59] at low temperature. Data collected for the decay of pyrazine excited states was shown to display Arrhenius type behaviour, i.e. an activation controlled process was responsible for the decrease in triplet state lifetime observed at high temperature. It was suggested that this was due to vibronic mixing of higher excited triplet states above a threshold energy. Data measured for $^3C10^*$ deactivation did not follow Arrhenius behaviour, i.e. inhibition of more than one process was

responsible for prolonged lifetimes at 77 K. Specifically, a decrease in vibrational deactivation through long hydrocarbon side chains due to changes in Boltzmann population of higher vibrational levels and a reduction in quenching by ground state molecules, C10 (T_1) + C10 (S_0) $\rightarrow$ C10 (S_0) + C10 (S_0), due to an increase in viscosity of the solution. Below the glass transition temperature of EPA ($\sim$ 150 K - 160 K), movement of molecules is severely restricted; further reduction of the temperature having little effect on the triplet state lifetime. More surprising is the apparent independence of triplet yield on temperature since temperature is a direct measure of the aggregation state of C10. It is generally accepted that aggregated phthalocyanines do not produce triplet state species due to the short lived nature of the S_1 states. C10 dimers have unique excited state properties which may be explained in terms of exciton theory. Kasha[60],[13] commented on enhanced triplet state formation in dimers with reduced fluorescence yields. Φ_D has been calculated to be $\sim$ 35 % of Φ_F, thus, it is feasible that some degree of enhancement may be observed in this case. In addition, transient measurements of substituted μ-oxo SiPc dimer by Ferencz[55], showed the position and yield of triplet state species to be very similar to that produced by the monomer. Russegger et al.[59] have shown that in the absence of complicating factors such as aggregation, Φ_{ISC} is unaffected by temperature.

At a temperature of 200 K, probing at wavelengths where ground state absorption occurred, a decay with two clear components was observed (Figure 4.24A). The short lived component of this decay (k_{fast} = 9900 s^{-1}) has a comparable decay rate to triplet state deactivation (k = 8300 s^{-1} at 200 K) and may be ascribed to recovery of ground state equilibrium after bleaching due to triplet formation. The decay fits to monoexponential kinetics despite contributions from two processes, i.e. $^3Pc^* \rightarrow$ Pc and $^3(Pc)_2^* \rightarrow (Pc)_2$. From this it can be inferred that a dynamic equilibrium between $^3Pc^*$ and $^3(Pc)_2^*$, i.e. $^3Pc^*$ + Pc $\rightleftharpoons$ $^3Pc_2^*$, exists within the lifetime of the triplet state. Thus, k_{fast} is an average of the rate of deactivation of both species. The key to the identity of the slow component (k_{slow} = 0.4 dm^3 mol^{-1} s^{-1}) lies in the transient absorption spectrum. A distinct similarity to monomeric C10 was observed implying that monomeric species are being produced on excitation ((Pc)$_2$ $\xrightarrow{h\nu}$ 2Pc). Figure 4.28 summarises the processes occurring upon excitation.

> **Excited State Equilibrium**
>
> $^3Pc^* + Pc$ ⇌ $^3(Pc)_2^*$
>
> $^1Pc^*$ $^1(Pc)_2^*$
>
> $h\nu$ k_{fast} $h\nu$
>
> $Pc + Pc$ ⇌ $(Pc)_2$
>
> **Ground State Equilibrium**
>
> k_{slow} $h\nu$
>
> $Pc + Pc$
>
> **Monomer Formation**
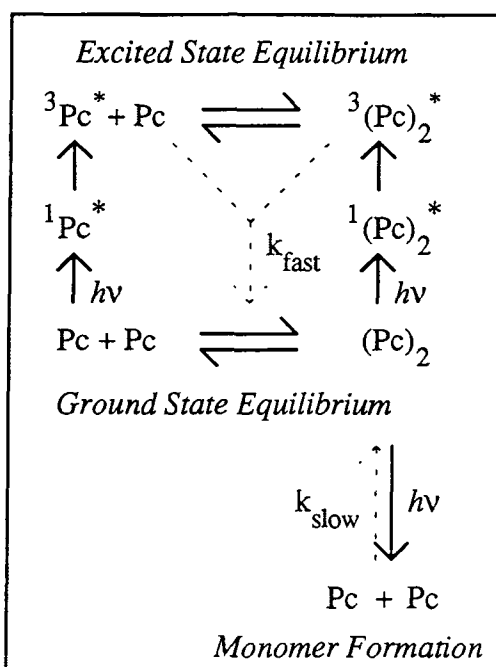
Figure 4.28. Equilibria upon excitation of C10 in EPA at 77 K.

At 200 K, monomers formed upon irradiation may diffuse through the solution to form separated species. k_{slow} obeyed second order kinetics indicating a bimolecular process and may be ascribed to monomer-monomer recombination. Ferraudi and Srisankar[61] have reported a similar reaction when dimeric cobalt and copper phthalocyanines were irradiated with ultraviolet light. Transient species were observed as a result of redox chemistry which produced two radical phthalocyanine species. Recombination to the ground state proceeded via a second order process. At 77 K, monoexponential decays were obtained despite evidence from the transient absorption spectrum of the presence of monomeric phthalocyanine. This may be because at 77 K, triplet decay and monomer-monomer recombination occur at comparable rates; separation of each process being prevented by experimental limitations (signal to noise ratio). Alternatively, it is possible that in a rigid medium, diffusional separation of monomers is impossible so irradiation produced dimeric species with enlarged internuclear separation (such that excitonic coupling did not occur), resulting in an absorption spectrum representative of constituent monomer sub-units. Since separation into two distinct species has not occurred, relaxation would be expected to occur via a first order process. This theory is corroborated by behaviour observed at 160 K and 180 K in which complex decays were obtained. These temperatures are just above the glass transition temperature of EPA, thus, it is possible that both processes contributed to a certain extent.

Attempts to induce aggregation of this type using different peripheral substituents were unsuccessful. Monahan[62],[63],[64] has shown that in organic solvents, aggregation is driven by ring-ring interaction and, hence, must be energetically more favourable than

ring/solvent interactions. Reduced aggregation was observed for β-octapentyl substituents whilst zinc phthalocyanine substituted with β-methyl groups remained monomeric. This suggests that solubilisation of shorter chain alkyl substituents is more favourable in EPA than long chains. This was confirmed by studies of ZnC16 and C10 in MeTHF in which ZnC16 was observed to aggregate to a great extent whilst C10 remained monomeric. This is surprising since peripheral substituents are often added to improve solubility of phthalocyanine molecules in organic and aqueous solvents. Cuellar and Marks[65] have demonstrated an increase in solubility of nickel phthalocyanine in 1-chloronaphthalene upon alkylation, however, in certain cases, e.g. peripheral substitution of magnesium phthalocyanine[66], it has been shown that substitution has hindered rather than assisted solubility. Substitution of a -CH$_2$- unit for an oxygen atom in octabutoxy zinc phthalocyanine also inhibited aggregation. Cook[67] observed a similar difference between alkyl and alkoxy substituted zinc phthalocyanine in crystal packing studies. Exciton coupling was obtained in crystals of octadecyl zinc phthalocyanine whilst no evidence for splitting in the analogous octaalkoxy molecule was seen.

4.4.2.3 Conclusions

The first substantive evidence for a luminescent phthalocyanine dimer species has been reported. C10 has been shown to aggregate in EPA at 77 K. Aggregation was accompanied by the appearance of emission at 760 nm, red shifted with respect to monomer emission, which has been proven to originate from dimeric / aggregated species. The quantum yield of dimer fluorescence was calculated to be ~35% of monomer fluorescence at 77 K. Triplet state studies have also been performed which show the triplet yield of dimeric phthalocyanine at 77 K to be comparable to that of monomeric phthalocyanine. Dimer dissociation to monomeric species was observed upon excitation with either 355 nm or 638 nm radiation. Photophysical properties have been compared with those of a cofacial aluminium phthalocyanine dimer and discussed in terms of exciton theory.

It has been shown that the photophysical properties of dimeric phthalocyanines are controlled by their geometry. With regards to photodynamic therapy, this may have important consequences. It is known that accumulation of high concentrations of sensitiser in cells leads to aggregation and it is generally accepted that aggregates are non-cytotoxic[3]. The results of this study show that production of triplet state species from aggregated phthalocyanines can occur. It is highly probable that under conditions where diffusion of oxygen is possible singlet oxygen would be formed by these dimers.

Hence, the photoactivity of dimers should not be summarily dismissed and may indeed play an important role in the destruction of neoplastic tissue.

4.5 References

[1]   Moan J. and Anholt H., Phthalocyanine fluorescence in tumours during PDT., *Photochem. Photobiol.*, **51**, 379, 1990.

[2]   Ambroz M., MacRobert A.J., Morgan J., Rumbles G., Foley M.S.C. and Phillips D., Time resolved fluorescence spectroscopy and intracellular imaging of disulfonated aluminium phthalocyanine., *J. Photochem. Photobiol. B:Biol.*, **22**, 105, 1994.

[3]   Paardekooper M., Van Gompel A.E.V., De Bont H.J.G.M., Nagelkerke J.F., Stevenick J.V. and Van Den Broek P.J.A., Photodynamic treatment of yeast with chloroaluminum phthalocyanine: Role of the monomeric form of the dye., *Photochem. Photobiol.*, **59**, 161, 1994.

[4]   Wynne K.J., 2 Ligand bridged phthalocyanines - crystal and molecular structure of fluoro(phthalocyaninato) gallium(II), [GaPcF]$_n$ and mu-oxo bis(phthalocyaninato) aluminum(III), (AlPc)$_2$O., *Inorg. Chem.*, **24**, 1339, 1985.

[5]   Martin P.C., Gouterman M., Pepich B.V., Renzoni G.E. and Schindele D.C., Effects of ligand, solvent and variable sulphonation on dimer formation of aluminium and zinc phthalocyanine sulphonates., *Inorg. Chem.*, **30**, 3305, 1991.

[6]   Kobayashi N. and Lever A.B.P., Cation or solvent induced supermolecular phthalocyanine formation: Crown ether substituted phthalocyanines., *J. Am. Chem. Soc.*, **109**, 7433, 1987.

[7]   Yoon M.J., Cheon Y.J. and Kim D.H., Absorption and fluorescence spectroscopic studies on dimerisation of chloroaluminium (III) phthalocyanine tetrasulphonate in aqueous alcoholic solutions., *Photochem. Photobiol.*, **58**, 31, 1993.

[8]   Kanezaki E., Yamanouchi H. and Kanda S., Monomer-Dimer equilibrium of unsubstituted zinc phthalocyanine in N,N-dimethylformamide and detection of dimer transitions in fluorescence excitation spectrum at 77K., *Mol.Cryst. Liq. Cryst.*, **154**, 351-359, 1988.

[9]   Dhami S., DeMello A.J., Rumbles G., Bishop G., Bishop S.M., Phillips D. and Beeby A., Phthalocyanine fluorescence at high concentration: dimers or reabsorption effect?, *Photochem. Photobiol.*, **61**, 341, 1995.

[10]   Gouterman M., Holten D. and Lieberman E., Porphyrins XXXV. Exciton coupling in μ oxo scandium dimers., *Chem. Phys.*, **25**, 139, 1977.

[11]   Kaizu Y., Misu N., Tsiji K., Kaneko Y. and Kobayashi H., Electronic spectra of the aluminium III complexes of 5, 10, 15, 20 tetraphenylporphin and 2, 3, 7, 8, 12, 13, 17, 18 octaethylporphin., *Bull.. Chem. Soc. Jpn.*, **58**, 103-108, 1985.

[12]   Ohno O., Kaizu Y. and Kobayashi H., Luminescence of some metalloporphins including the complexes of the IIIb metal group., *J. Chem. Phys.*, **84**, 1779, 1985.

[13]   Kasha M., Rawls H.R. and El-Byoumi M.A., The exciton model in molecular spectroscopy., *Pure Appl. Chem.*, **11**, 371, 1965.

[14]   Hunter C.A., Sanders J.K.M. and Stone A.J., Exciton coupling in porphyrin dimers., *Chem. Phys.*, **133**, 395-404, 1989.

[15]   Kemnitz K., Tamai N., Yamazaki I., Nakashima N. and Yoshihara K., Fluorescence decays and spectral properties of Rhodamine B in submono-, mono- and multilayer systems., *J. Phys. Chem.*, **90**, 5094-5101, 1986.

[16]   Osuka A. and Maruyama K., Synthesis of naphthalene bridged porphyrin dimers and their orientation dependent exciton coupling., *J. Am. Chem. Soc.*, **110**, 4454, 1988.

[17]   Oba T., Watanabe T., Mimuro M., Kobayashi M. and Yoshida S., Aggregation of chlorophyll a' in aqueous methanol., *Photochem. Photobiol.*, **63**, 639, 1996.

[18]   Kawski A., Fluorescence anisotropy: Theory and applications of rotational depolarisation., *Critical Reviews in Analytical Chemistry*, **23**, 459-529, 1993.

[19]   Lakowitz J.R., *Topics in Fluorescence Spectroscopy*, **2**, Chapter 1, Plenum Press, New York, 1991.

[20]   Russel P.G. and Albrecht A.C., Electronic states of benzene by photoselection. The polarisation of luminescence in benzene, perdeuterobenzene and perchlorobenzene., *J. Chem. Phys.*, **41**, 2536, 1964.

[21]   Gouterman M., Spectra of porphyrins., *J. Molec. Spec.*, **6**, 138-163, 1961.

[22]   Schaffer A.M., Gouterman M. and Davidson E.R., Porphyrins XXV. Extended huckel calculations on location and spectral effects of free base porphyrins., *Theoret. Chim. Acta*, **30**, 9-30, 1973.

[23]   Sevchenko A.N., Solov've K.N., Gradyushko A.T. and Shkirman S.F., Narrow band electronic spectra of metal derivatives of tetrabenzoporphine and phthalocyanine., *Soviet Physics-Doklady*, **11**, 587, 1967.

[24]   Limantara L., Sakamoto S., Koyama Y. and Nagae H., Effects of non-polar and polar solvents on the Q_x and Q_y energies of bacteriochlorophyll a and bacteriopheophytin a., *Photochem. Photobiol.*, **65**, 330, 1997.

[25]   Henriksson A. and Sundbom M., Semiempirical molecular orbital studies of phthalocyanines., *Theoret. Chim. Acta.*, **27**, 213-222, 1972.

[26]   Leznoff C.C. and Lever A.B.P., *Phthalocyanines: Properties and Applications*, p147, VCH Publ. inc., New York, 1989.

[27]   Weigl J.W., The polarisation of the fluorescence of tetraphenylporphyrin., *J. Mol. Spec.*, **1**, 133-138, 1957.

[28] Maiti N.C., Mazumdar S. and Periasamy N., Dynamics of porphyrin molecules in micelles - picosenond time resolved fluorescence anisotropy studies., *J. Phys. Chem.*, **99**, 10708-10715, 1995.

[29] Turoverov K.K. and Kuznetsova I.M., What causes the variation of polarisation degree across the emission spectrum of proteins?, *Biophys. Chem.*, **24**, 327, 1986. And references therein.

[30] Gurinovich G.P., Dependence of the state of polarisation with the fluorescence wavelength., *Izv. Akad. Nauk. Ser. Fiz.*, **22**, 1397-1401, 1958.

[31] Bauer R.K. and Balter A., Thermal rotations and relaxation of vibratonal energy of excited dye molecules in solution., *J. Luminescence*, **20**, 249-259, 1974.

[32] Grudzinski H., Influence of the local temperature of luminescent centres on the emission anisotropy of fluorescence of solutions., *Acta Phys. Pol.*, **A37**, 49, 1970.

[33] Nemkovich N.A., Rubinov A.N. and Tomin V.I., *Optical Spectroscopy in Chemistry and Biology - Progress and Trends*, p31, 1989.

[34] Reynolds P.A., Figgis B.N., Kucharski E.S and Mason S.A., *Acta Cryst. B (Str. Sci.)*, **47**, 899, 1991.

[35] The Cambridge Structural Database was used to obtain a value of r. A value of 16 Å was obtained by estimating the phthalocyanine as a square.

[36] Varnavsky O., Gruno I., Hauser M. and Klein U.K.A., Investigation of the internal mobility of TX-100 micelles by fluorescence anisotropy and excimer probing., *Chem. Phys. Lett.*, **141**, 99, 1987.

[37] Rau H., Greiner G. and Haenmerle H, Temperature dependence of number and size of Triton-X micelles in aqueous solution., *Physik. Chem.*, **88**, 116, 1984.

[38] Murov L.S., Carmichael I. and Hug G.L., *Handbook of Photochemistry*, p296, Marcel Dekker inc., Edn. 2, 1993.

[39] Tai S. and Hayashi N., Strong aggregation properties of novel naphthalocyanines., *J. Chem. Soc. Perkin Trans.*, **2**, 1275, 1991.

[40] Hunter C.A., Meah M.N. and Sanders J.K.M., DABCO - Metalloporphyrin binding: Ternary complexes, host guest chemistry, and the measurement of π–π interactions., *J. Am. Chem. Soc.*, **112**, 5773-5780, 1990.

[41] Anderson H.L., Hunter C.A., Meak M.N. and Sanders J.K.M., Thermodynamics of induced fit binding inside polymacrocyclic porphyrin hosts., *J. Am. Chem. Soc.*, **112**, 5780-5789, 1990.

[42] Hanack M. and Lang M., Conducting stacked metallophthalocyanines and related compounds., *Adv. Mater.*, **6**, 819, 1994.

[43] Steinfeld J.I., Francisco J.S. and Hase W.L., *Chemical Kinetics and Dynamics*, Prentice Hall, New Jersey, 1989.

[44]   Linsky J.P., Paul T.R., Nohr R.S. and Kenney M.E., Studies of a series of haloaluminium, -gallium, and -indium phthalocyanines., *Inorg. Chem.*, **19**, 3131, 1980.

[45]   Bishop S.M., Beeby A., Meunier H., Parker A.W., Foley M.S.C. and Phillips D., The photophysics of disulfonated metallophthalocyanines upon complexation with fluoride., *J. Chem. Soc. Faraday Trans.*, **92**, 2589, 1996.

[46]   Nohr R.S. and Wynne K.J., X-ray crystal structure of a conducting polymer precursor: Bridge stacked gallium fluoride., *J. Chem. Soc. Chem. Comm.*, 1210, 1981.

[47]   Cook M.J., Chambrier I., Cracknell S.J., Mayes D.A. and Russell D.A., Octaalkyl zinc phthalocyanines. Potential photosensitisers for use in the photodynamic therapy of cancer., *Photochem. Photobiol.*, **62**, 542, 1995.

[48]   Dhami S., Photophysics of phthalocyanines in microheterogeneous systems., p59, *PhD Thesis*, Imperial College, London, 1996.

[49]   Sheppard S.E. and Brigham S.E., Some effects of solvent upon the absorption spectra of dyes. III Temperature and organic solutions of cyanine dyes., *J. Am. Chem. Soc.*, **66**, 380, 1944.

[50]   Ravikant M., Reddy D. and Chandrashekar T.K., Dimerisation effects on spectroscopic properties of water soluble porphyrins in aqueous and micellar media., *J. Chem. Soc. Dalton Trans.*, 2103, 1991.

[51]   Kessel D., *Porphyrin Binding and Aggregation in Photodynamic Therapy of Neoplastic Disease*, p210, CRC Press, Boston, 1990.

[52]   Fluorescence polarisation is an old measurement given by, $p = \dfrac{I_{VV} - I_{VH}}{I_{VV} + I_{VH}}$, where p

is the polarisation, I is the intensity of fluorescence and subscripts V and H stand for vertically and horizontally polarised light respectively. Polarisation has largely been replaced by fluorescence anisotropy and may be converted using the equation,

$$r = \frac{2p}{3 - p}.$$

[53]   Dodsworth E.S., Lever A.B.P., Seymour P. and Leznoff C.C., Intramolecular coupling in metal-free binuclear phthalocyanines., *J. Phys. Chem.*, **89**, 5698, 1985.

[54]   Leznoff C.C., Greenberg S., Marcuccio S.M., Minor P.C., Seymour P. and Lever A.B.P., Binuclear clamshell phthalocyanines., *Inorg. Chim. Acta*, **89**, L35-L38, 1984.

[55]   Ferencz A., Neher D., Schulze M., Wegner G., Viaene L. and De Schryver F.C., Synthesis and spectroscopic properties of phthalocyanine dimers in solution., *Chem. Phys. Lett.*, **245**, 23, 1995.

[56] Oddos-Marcel L., Madeore F., Bock A., Neher D., Ferencz A., Rengel H., Wegner G., Kryschi C. and Trommsdorff H.P., Electronic states and relaxation dynamics of silicon phthalocyanine dimers., *J. Phys. Chem.*, **100**, 11850, 1996.

[57] Kobayashi N., Lam H., Nevin W.A., Janoa P., Leznoff C.C., Koyama T., Monden A. and Shirai H. Synthesis, spectroscopy, electrochemistry, spectroelectrochemistry, Langmuir Blodgett film formation and molecular orbital calculations of binuclear phthalocyanines., *J. Am. Chem. Soc.*, **116**, 879-890, 1994.

[58] Terazuma M., Yamauchi S. and Hiroti N., Temperature dependence of the triplet lifetime of pyrazine., *J. Phys. Chem.*, **90**, 4294, 1986.

[59] Russegger P. and Huber J.R., A calculation of the temperature dependent radiationless decay of the propynal triplet state, T_1., *Chem. Phys.*, **61**, 205, 1981.

[60] McRae E.G. and Kasha M., Enhancement of phosphorescence ability upon aggregation of dye molecules., *J. Chem. Phys*, **28**, 721, 1958.

[61] Ferraudi G. and Srisankar E.V., Photochemical redox reactivity of dimeric and monomeric copper(II) and cobalt(II) sulphophthalocyanines., *Inorg. Chem.*, **17**, 3164, 1978.

[62] Monahan A.R., Brado J.A. and DeLuca A.F., The association of copper(II), vanadyl, and zinc(II) 4,4',4",4'''-tetraalkylphthalocyanine dyes in benzene., *J. Phys. Chem.*, **76**, 1994, 1972.

[63] Abkowitz M. and Monahan A.R., ESR and electronic investigation of the self-association of phthalocyanine dyes in solution., *J. Chem. Phys.*, **58**, 2281, 1973.

[64] Monahan A.R., Brado J.A. and DeLuca A.F., The dimerisation of a copper(II) phthalocyanine dye in carbon tetrachloride and benzene., *J. Phys. Chem.*, **76**, 446, 1972.

[65] Cuellar E.A. and Marks T.J., Synthesis and characterisation of metallo and metal free phthalocyanines and uranyl decaalkylsuperphthalocyanines., *Inorg. Chem.*, **20**, 3766, 1981.

[66] Camenzind M.J., Hill C.L., Reactions of dinitriles with manganese powder: First synthesis of manganese(II) octaphenyl porphyrazine and a convenient synthesis of manganese(II) phthalocyanine., *Inorg. Chim. Acta.*, **99**, 63, 1985.

[67] Cook M.J., 1,4,8,11,15,18,22,25-octasubstituted phthalocyanines: the contrasting effects of alkyl and alkoxy substituents on molecular self assembly., *J. Mater. Sc.: Mat. in Elec.*, **5**, 117, 1994.

CHAPTER 5

PROTONATION OF PHTHALOCYANINES

5.1 Introduction

The pH of tumour tissue is often substantially lower (~6.5) than that of normal, healthy tissue (~7.6)[1]. If the structural properties of a sensitiser are modified by a change in pH, this could have a profound effect on the localisation, retention and photoactivity of the dye. Indeed, it has been shown that the degree of ionisation of haematoporphyrin (HP), a porphyrin-type first generation sensitiser, is highly dependent on the pH of its environment[2]. More acidic conditions encourage localisation and improve retention of HP within neoplastic tissue[1],[3]. Cell death has also been reported to increase under conditions of low pH[4].

There have been very few investigations of the photophysical properties of protonated phthalocyanines despite potential effects on the photoactivity of these sensitisers. UV/Visible absorption studies of PcH_n^{n+}, where n = 0 to 4, were published around 1980 by Gaspard[5] and Iodko[6] and in 1993 Lang[7] reported data detailing the effect of monoprotonation on the triplet state properties of sulfonated chloroaluminium phthalocyanine. However, a comprehensive photophysical study of these compounds has not been undertaken to date. Several studies[8],[9] of sulfonated aluminium phthalocyanines in aqueous solution have been carried out at pH's ranging from 12 to 1, but no observations of protonated species have been reported. In concentrated alcoholic solutions of sulfonated aluminium phthalocyanine chloride, Yoon et al.[10] discovered a new species absorbing at 710 nm which was ascribed to the formation of luminescent phthalocyanine dimers. The validity of this hypothesis has already been questioned[11]. Protonation was not considered as a possible cause of spectral changes and in the work presented here evidence pertaining to this explanation is discussed.

The purpose of this study was to provide a complete photophysical evaluation of tetrabutyl zinc phthalocyanine ($^tBu_4ZnPc$) in acidified ethanolic solution. The propensity of disulfonated zinc phthalocyanine ($ZnPcS_2$) and $^tBu_4ZnPc$ to associate with H^+ ions in 1% Triton X-100 /H_2O solution and on solid substrates have also been investigated.

5.2 Materials and Methods

Tetra tertbutyl zinc phthalocyanine ($^tBu_4ZnPc$) and disulfonated zinc phthalocyanine ($ZnPcS_2$) were prepared by Dr. A. Beeby and used as received (unpublished results). Solutions were prepared in absolute alcohol (Haymann Ltd. A.R. quality) and purite water containing 1% Triton-X 100 (Sigmaultra grade) w/v (1% TX/H_2O). The concentration of H^+ ions was assumed to be negligible in freshly prepared solutions and was adjusted using H_2SO_4. For experiments performed in buffered media, a solution was prepared from 0.1 mol dm^{-3} citric acid and 0.2 mol dm^{-3} K_2HPO_4 with subsequent adjustment of pH between 1 and 8 by addition of HCl or NaOH. The pH was measured using a calibrated pH meter (Jenway model 3051). Preparation of solid state samples and experimental details of photophysical techniques employed are described in Chapter 2 (pp 42-71).

5.3 Results and Discussion

5.3.1 $^tBu_4ZnPc$ in Acidified Alcoholic Solution
5.3.1.1 Results
5.3.1.1.1 Singlet State Measurements

Five distinct species were obtained in ethanolic solutions of $^tBu_4ZnPc$ acidified with sulfuric acid (Figure 5.1A). Isosbestic points were observed for each of the conversions (except n = 3 → 4), indicating sequential protonation without the presence of side reactions such as dimerisation or decomposition. By comparison with published results[6] these were assigned to protonated forms of phthalocyanine, PcH_n^{n+}, where n = 0 to 4, and represents the stepwise addition of a hydrogen ion to each azomethine bridge of the pyrrole moieties. Mono, di and tri (n = 1 to 3) protonated species demonstrated a splitting of both Soret and Q bands, whilst the spectrum of tetra protonated phthalocyanine resembled that of the parent phthalocyanine, red shifted to 807 nm (Table 5.1). The integrated area of all the spectra, $\int I_{\bar{v}}.d\bar{v}$, from 300 nm to 850 nm of PcH_n^{n+} remained constant.

n	[H+] /mol dm^{-3}	Soret Band Maxima /nm	Q Band Maxima /nm
0	~0	349	674
1	2.9×10^{-2}	331, 361	686, 712
2	1.76	335, 392	695, 729
3	75% H_2SO_4:EtOH	307, 417	750, 778
4	100% H_2SO_4	443	807

Table 5.1. Absorption maxima of PcH_n^{n+} (n = 0 to 4) in EtOH.
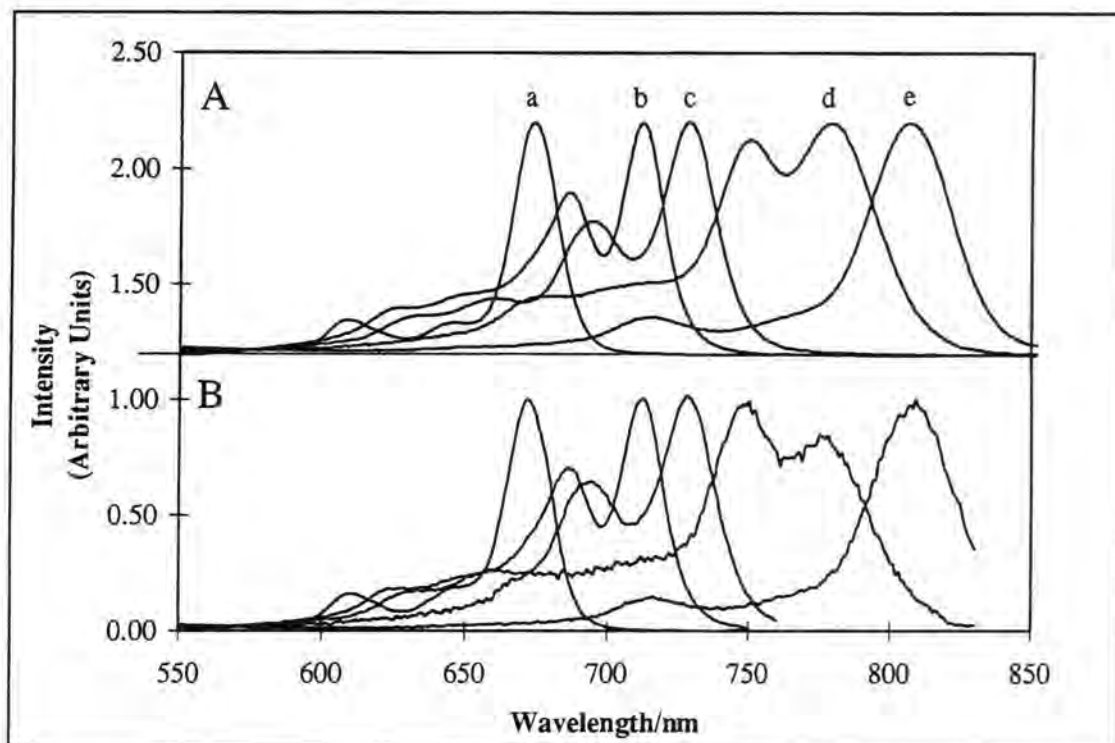
Figure 5.1 Absorption (A) and fluorescence excitation (B) spectra of PcH_n^{n+} in EtOH. a) n = 0 (λ_{em} = 760 nm), b) n = 1 (λ_{em} = 770 nm), c) n = 2 (λ_{em} = 770 nm), d) n = 3 (λ_{em} = 840 nm), e) n = 4 (λ_{em}= 840 nm).

Extinction coefficients, ε_{max}, and pK_a values for each species are shown in Table 5.2. pK_as were calculated using a non-linear fitting procedure to Equation 5.1 (Appendix C).

$$A = (\varepsilon_{Pc} - \varepsilon_{PcH^+})\frac{C_T}{1 + K[H^+]} + \varepsilon_{PcH^+}C_T$$

$$(5.1)$$

where pK_a = -log (1/K), ε_{Pc} and ε_{PcH^+} are the extinction coefficients of $Pc_{n-1}^{(n-1)+}$ and PcH_n^{n+} respectively, C_T is the total concentration of phthalocyanine and H^+ is the concentration of hydrogen ions in mol dm^{-3} (estimated as [H_2SO_4] - Table 5.1). For tri

and tetra protonation (n = 3 & 4) the concentration of acid required (75% and 100% H_2SO_4:EtOH respectively) was too high for this equation to be valid. To analyse the formation of these species, Hammett acidity functions must be considered, however, no values for H_2SO_4 in EtOH have been published to date.

n	λ_{max} /nm (UV/Vis)	pK_a	ε_{max} /dm^3 mol^{-1} cm^{-1}	λ_{max} /nm (Emission)	Φ_F
0	674	-	$1.6 \pm 0.1 \times 10^5$	682	0.26 ± 0.02
1	712	2.9 ± 0.3	$8.7 \pm 0.2 \times 10^4$	717	0.12 ± 0.01
2	729	0.18 ± 0.05	$1.1 \pm 0.1 \times 10^5$	735	0.07 ± 0.01
3	778	-	$6.8 \pm 0.4 \times 10^4$	788	0.03 ± 0.005
4	807	-	$1.8 \pm 0.1 \times 10^5$	820	0.01 ± 0.005

Table 5.2. Absorbance and fluorescence data for PcH_n^{n+} (n = 0 to 4) in EtOH.

Porphyrin (P) molecules display similar behaviour at low pH[12]. Changes in the pH from 9.5, to 4.5, and finally 0.52 induced successive protonation of two inner ring nitrogens, i.e. $PH_2 \leftrightarrow PH_3^+ \leftrightarrow PH_4^{2+}$. A shift to longer wavelengths was observed upon protonation. pK_a values of 5.8 and 2.3 (4.7 and 2.9)[13] were determined for each protonation step of haematoporphyrin IX[14].

Protonation of the phthalocyanine ring resulted in a large decrease in the yield of radiative emission. Successive protonations were accompanied by shifts to longer wavelength of the emission spectrum (Figure 5.2) and large decreases in the fluorescence yield (Table 5.2). Fluorescence excitation spectra mimic the absorption spectra (Figure 5.1B), confirming the existence of a single species. The steady state fluorescence anisotropy was also found to be affected by protonation. Figure 5.3 shows the effect of excitation wavelength on the fluorescence anisotropy of $^tBu_4ZnPc$ ([H$^+$] ~ 0 mol dm^{-3}) and PcH$^+$ ([H$^+$] = 0.022 mol dm^{-3} (0.03 mol dm^{-3} at 77 K)) in EPA at 77 K. Trace a is that of the parent phthalocyanine and fluctuates around r_{av} = 0.075. Trace b was produced by PcH$^+$ and mimics the form of metal-free phthalocyanine (Section 4.4.4.1.2), passing from negative to positive values as the excitation wavelengths were scanned.
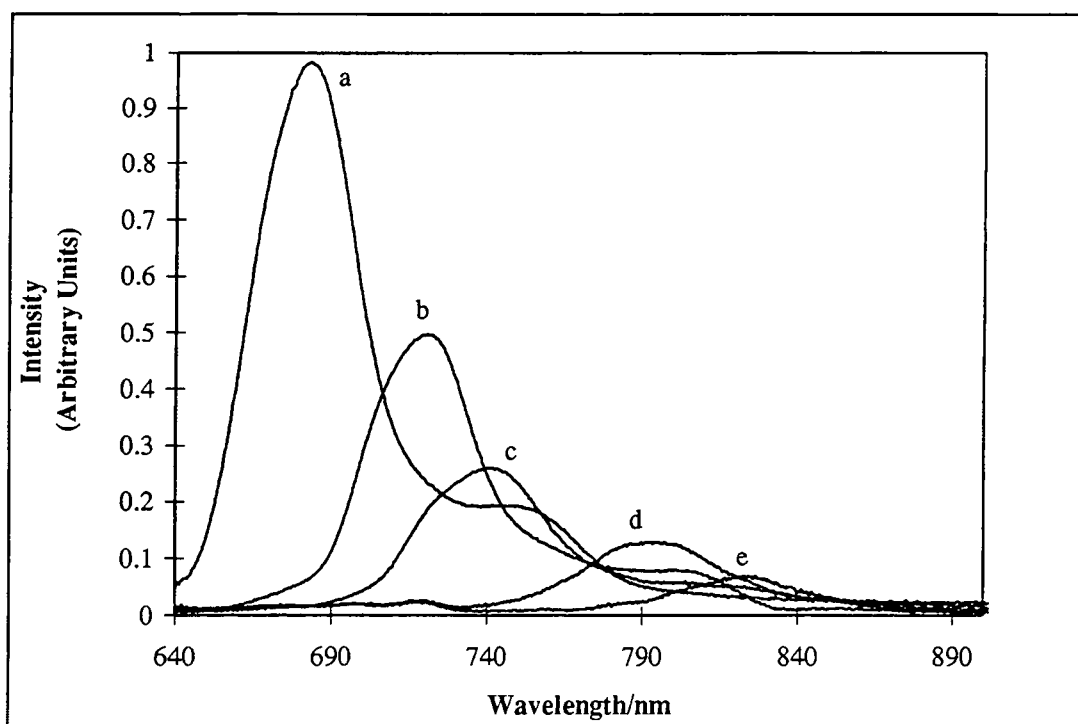
Figure 5.2. Fluorescence emission spectra of PcH$_n$$^{n+}$ in EtOH (λ_{ex} = 632.8 nm). a) n = 0, b) n = 1, c) n = 2, d) n = 3, e) n = 4. Spectra have been corrected for the wavelength dependent response of the detector.

Figure 5.3. Anisotropy of a) $^tBu_4ZnPc$ ([H$^+$] = 0 mol dm^{-3}, λ_{em} = 665 - 685 nm) and b) PcH$^+$ ([H$^+$] = 3 x 10^{-2} mol dm^{-3}, λ_{em} = 700 - 715 nm) in EPA at 77 K.

Fluorescence lifetime data measured for PcH$_n$$^{n+}$ (n = 0 to 4) is collated in Table 5.3. Greater than 90 % of each decay (Figure 5.4) can be represented by a single monoexponential fit. These values represent the measured fluorescence lifetime, τ_F, of
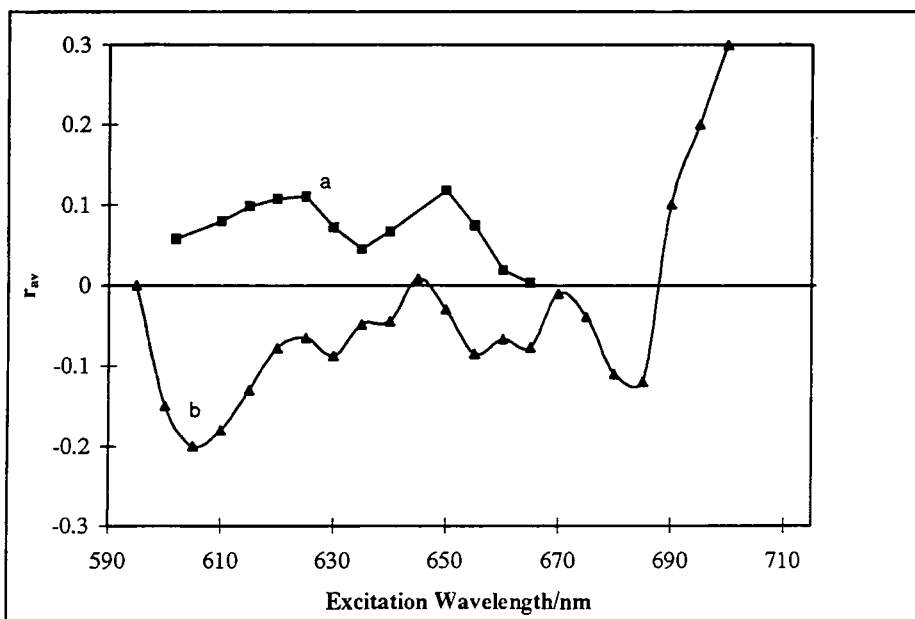
each species and decrease as the phthalocyanine ring is protonated. Small contributions from other decays are also observed and may be explained by the presence of other protonated species. A maximum error of ± 10% may be assumed for these measurements.
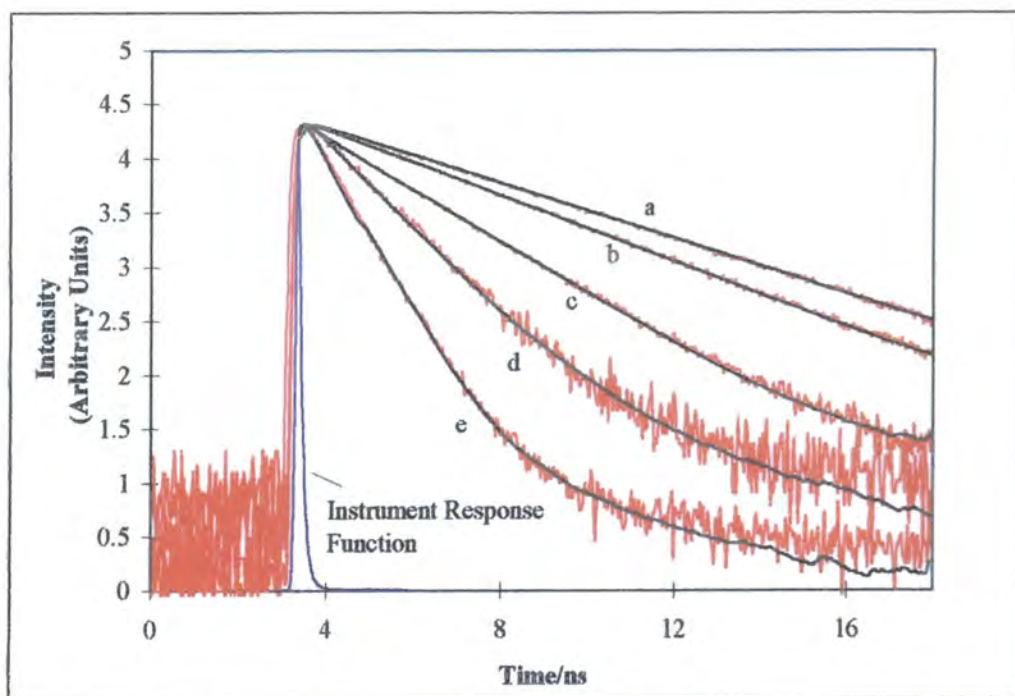
Figure 5.4. Time resolved fluorescence decays of PcH$_n$$^{n+}$ in EtOH, λ_{ex} = 638 nm. a)
n = 0 (λ_{em} = 680 nm), b) n = 1 (λ_{em} = 717 nm), c) n = 2 (λ_{em} = 735 nm), d) n = 3
(λ_{em} = 780 nm), e) n = 4 (λ_{em} = 830 nm). The instrument response function is also
shown.

n	τ_1 /ns (Amplitude, Yield)	τ_2 /ns (Amplitude, Yield)	τ_3 /ns (Amplitude, Yield)	χ^2	DW
0	3.36 (100,100)	-	-	1.36	1.85
1	2.83 (97.12, 98.87)	1.085 (2.88, 1.13)	-	1.16	1.99
2	1.84 (85.9, 92.55)	0.9 (14.1, 7.45)	-	1.36	1.91
3	1.32 (96.99, 94.43)	2.49 (3.01, 5.57)	-	1.34	1.98
4	0.88 (99.26, 96.68)	2.184 (0.49, 1.17)	7.677 (0.25, 2.15)	1.4	1.89

Table 5.3. Fluorescence lifetimes of PcH$_n$$^{n+}$ (n = 0 to 4) in EtOH.

5.3.1.1.2 Triplet State Measurements

Triplet state species were studied by laser flash photolysis. The $^3\pi\pi^*$ excited states of species n = 0 to 2 were populated using 355 nm radiation, tri-protonated species were excited using 680 nm radiation and the tetra-protonated species using 700 nm radiation. Protonation induced a shift in the transient absorption spectrum, a reduction in the triplet quantum yield (Φ_T) and a significant decrease in the excited state lifetime (τ_T). These results (Table 5.4) are consistent with those observed by Lang et al.[7] for sulfonated aluminium phthalocyanine chloride in which a decrease of τ_T from 290 µs to 90 µs was observed upon protonation of one bridging nitrogen.

n	τ_T /µs	λ_{max} /nm	Φ_T	Φ_Δ
0	200 ± 20	490 ± 10	0.58 ± 0.05	0.54 ± 0.03
1	40 ± 4	500 ± 10	0.44 ± 0.04	0.075 ± 0.005
2	35 ± 4	500 ± 10	0.4 ± 0.04	< 0.075
3	31 ± 3	540 ± 20	0.22 ± 0.03	-
4	13 ± 1	560 ± 20	0.18 ± 0.03	-

Table 5.4. Triplet state data for PcH_n^{n+} (n = 0 to 4) in EtOH.

The triplet-triplet extinction coefficient was determined to be 36000 ± 6000 at λ_{max} (500 nm). This value is consistent with that of the parent phthalocyanine at 490 nm and was used in calculations of Φ_T. Conversion of the parent phthalocyanine (n = 0) into PcH^+ induced a 10 nm shift in the transient spectrum. Φ_T decreased from 0.54 to 0.44 and τ_T fell from 200 µs ($[H^+] \sim 0$ mol dm^{-3}) to 40 µs ($[H^+] = 3 \times 10^{-2}$ mol dm^{-3})(Figure 5.5). At intermediate $[H^+]$, when a mixture of Pc and PcH^+ coexisted in solution (assuming Equation 5.2[15]), the observed triplet decay remained monoexponential, depicting an average value of both component lifetimes.

$$^3Pc^* + H^+ \underset{}{\overset{Fast}{\rightleftharpoons}} {}^3PcH^{+*} \tag{5.2}$$
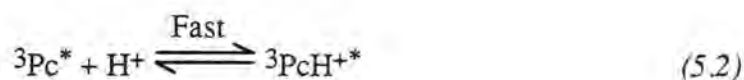
The quantum yields of singlet oxygen formation are given in Table 5.4. PcH^+ and PcH_2^{2+} displayed a large decrease in $^1O_2$ production. In addition, although phosphorescence from the parent phthalocyanine could be observed at 1090 nm[16], triplet state emission from PcH^+ was undetectable over the wavelength range 1000 nm to 1300 nm.
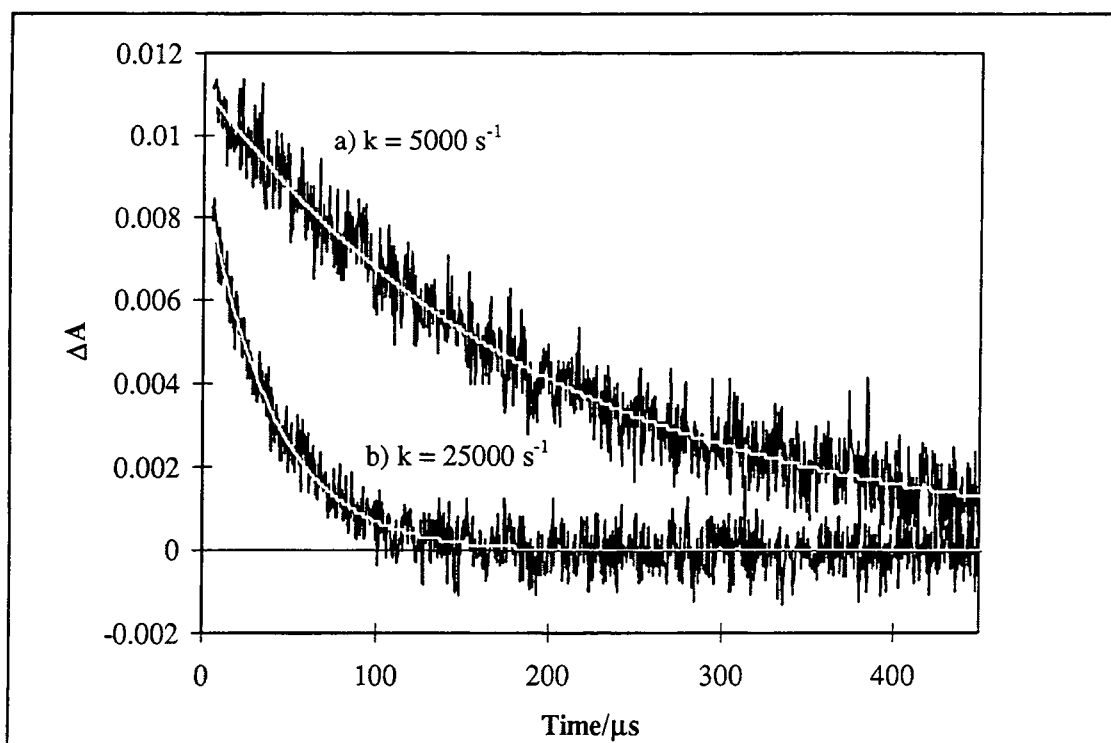
Figure 5.5. Triplet transient decays (λ_{ex} = 355 nm).
a) ${}^tBu_4ZnPc$ (Probe = 490 nm) and b) ${}^tBu_4ZnPcH^+$ (Probe = 500 nm).

5.3.1.2 Discussion

Low pH induced a concomitant shift in absorption and fluorescence spectra, consistent with a series of protonation equilibria[6] (Equation 5.3).

$$Pc \rightleftharpoons^{H^+} PcH^+ \rightleftharpoons^{H^+} PcH_2{}^{2+} \rightleftharpoons^{H^+} PcH_3{}^{3+} \rightleftharpoons^{H^+} PcH_4{}^{4+} \qquad (5.3)$$
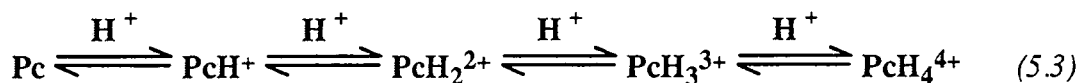
The origin of red shifts in the spectra may be rationalised using the same theoretical framework[17] invoked to explain the effect of peripheral substituents on the wavelength of monomer absorption (Section 3.3.2.3.2). Addition of a hydrogen ion onto peripheral ring nitrogens stabilises the LUMO by withdrawing electrons from α positions of the phenyl ring towards the nitrogen atoms (Figure 5.6). Excitation into the first excited singlet state involves transfer of electron density from inner ring carbon atoms to nitrogen atoms (Figure 1.8). This is facilitated by the electron attracting action of hydrogen substituents, leading to a reduction of the HOMO-LUMO energy gap.
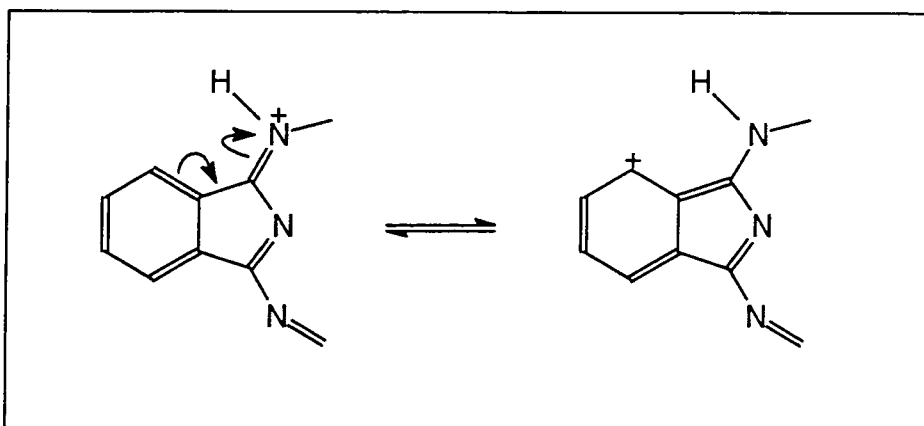
Figure 5.6. Effect of protonation on conjugation of the ring.

Similar shifts have been observed in the absorption spectra of protonated Schiff base metalloporphyrins[18] and attributed to a resonance effect of the withdrawing groups rather than delocalisation of the positive charge onto the ring[19]. This is not surprising since in these molecules, the positive charge is located on an imine moiety of the ring and, hence, is somewhat removed from conjugation of the ring. Large changes in the Soret band were also observed on protonation (Table 5.1). These are analogous to those induced by amino substituents on metallophthalocyanine[20] in which a band was observed at 450 nm due to splitting of the Soret band. The theory of Morley *et al.*[17] predicts very small shifts of the Soret band upon peripheral substitution, thus it would appear that development of this theorum is required to cover all ligand binding cases. Splitting of Soret and Q bands may be attributed to removal of the degeneracy of transitions polarised along x and y directions. Binding of hydrogen to the phthalocyanine ligand lowered the symmetry of the complex from D_{4h} to C_{2v} (Figure 5.7) so that x and y transitions are no longer equivalent. This is corroborated by fluorescence anisotropy measurements. At hydrogen ion concentrations of 3 x 10^{-2} mol dm^{-3} (Figure 5.3), a similar spectrum to that measured for $^{t}Bu_4H_2Pc$ (a D_{2h} complex) was obtained. A negative anisotropy was observed at wavelengths below 690 nm, corresponding to excitation into a higher energy level than the emitting state. Using Equation 4.4, and the measured r_{av} of -0.2, the angle between transition dipole moments of absorbing and emitting states may be calculated to be 90° (λ_{ex} = 605 nm). At wavelengths > 605 nm, state mixing caused the measured value for r_{av} to be higher (less negative) than its true value. An angle of 90° is consistent with removal of x and y degeneracy. At wavelengths above 690 nm a large positive anisotropy was measured (0.3 at 700 nm), i.e. excitation at this wavelength produced the emitting state directly. Effects on the viscosity of the solution due to the addition of acid (0.03 mol dm^{-3}) are negligible. With no added acid, the anisotropy had an average value of 0.075 although fluctuations with λ_{ex} were observed, consistent with observations for a fluorophore of D_{4h} symmetry (Section 4.4.1.2).
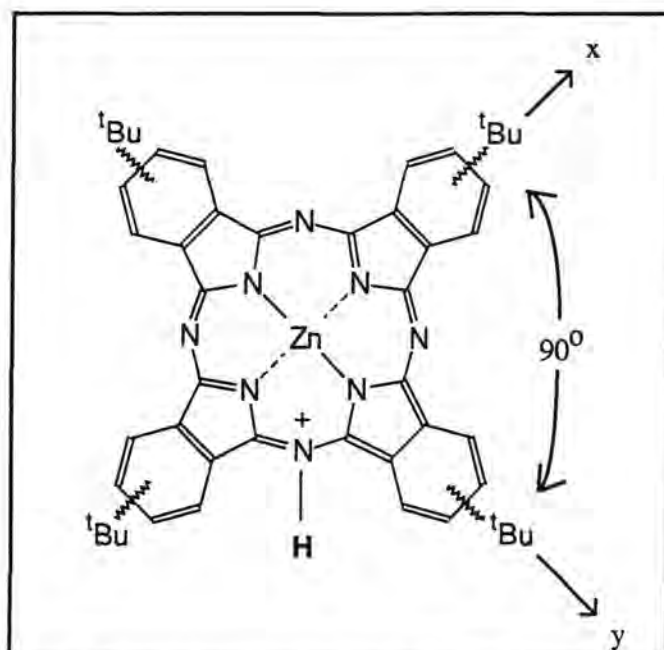
Figure 5.7. Structure of $^tBu_4ZnPcH^+$.

A reduction in photoactivity of $^tBu_4ZnPc$ was observed as the concentration of hydrogen ions increased. Table 5.5 shows radiative and non-radiative rate constants calculated using measured quantum yield and lifetime data. Simple relations used in calculations are shown in the table.

n	k_F^0 / s^{-1} $= \Phi_F / \tau_F$	k_{isc} / s^{-1} $= \Phi_T / \tau_F$	Φ_{ic} $= 1 - (\Phi_F + \Phi_T)$	k_{ic} / s^{-1} $= \Phi_{ic} / \tau_F$
0	$7.2 \pm 0.9 \times 10^7$	$1.6 \pm 0.2 \times 10^8$	0.16 ± 0.05	$4.4 \pm 1.4 \times 10^7$
1	$4.3 \pm 0.6 \times 10^7$	$1.6 \pm 0.2 \times 10^8$	0.44 ± 0.04	$1.6 \pm 0.2 \times 10^8$
2	$3.9 \pm 0.7 \times 10^7$	$2.2 \pm 0.3 \times 10^8$	0.53 ± 0.04	$2.9 \pm 0.4 \times 10^8$
3	$2.3 \pm 0.4 \times 10^7$	$1.7 \pm 0.3 \times 10^8$	0.75 ± 0.03	$5.8 \pm 0.6 \times 10^8$
4	$1.14 \pm 0.6 \times 10^7$	$2.0 \pm 0.4 \times 10^8$	0.81 ± 0.03	$9.2 \pm 1 \times 10^8$

Table 5.5. Rate constants of radiative and non-radiative deactivation pathways of PcH_n^{n+} (n = 0 to 4) in EtOH.

As protonation of the ring increased, the rate of radiative deactivation of S_1, k_F^0, decreased, whilst that of internal conversion, k_{ic}, increased. The rate of intersystem crossing remained constant at $1.8 \pm 0.25 \times 10^8$ s^{-1}. These trends are easily explained in terms of fundamental photophysical behaviour and are directly related to changes in ΔE ($S_1 \leftarrow S_0$ energy gap) upon protonation. The rate of radiative emission[21],[22] is given by Equation 5.4.

$$k_F^0 = A = 8\pi h < \bar{v} >^3 B \qquad (5.4)$$

where A is the Einstein coefficient for spontaneous emission, n is the refractive index of the medium, $\bar{v}$ is the average wavenumber of emission and B is the Einstein transition probability of absorption, given by $\mu^2/6\varepsilon_0(h/2\pi)^2$, where μ is the transition dipole moment and h is Plancks constant. Substitution for B into Equation 5.4 yields Equation 5.5 for the expression of k_F^0.

$$k_F^0 = \frac{8\pi h |\mu|^2}{<\bar{v}>^{-3} 6\varepsilon_0(h/2\pi)^2} \qquad (5.5)$$
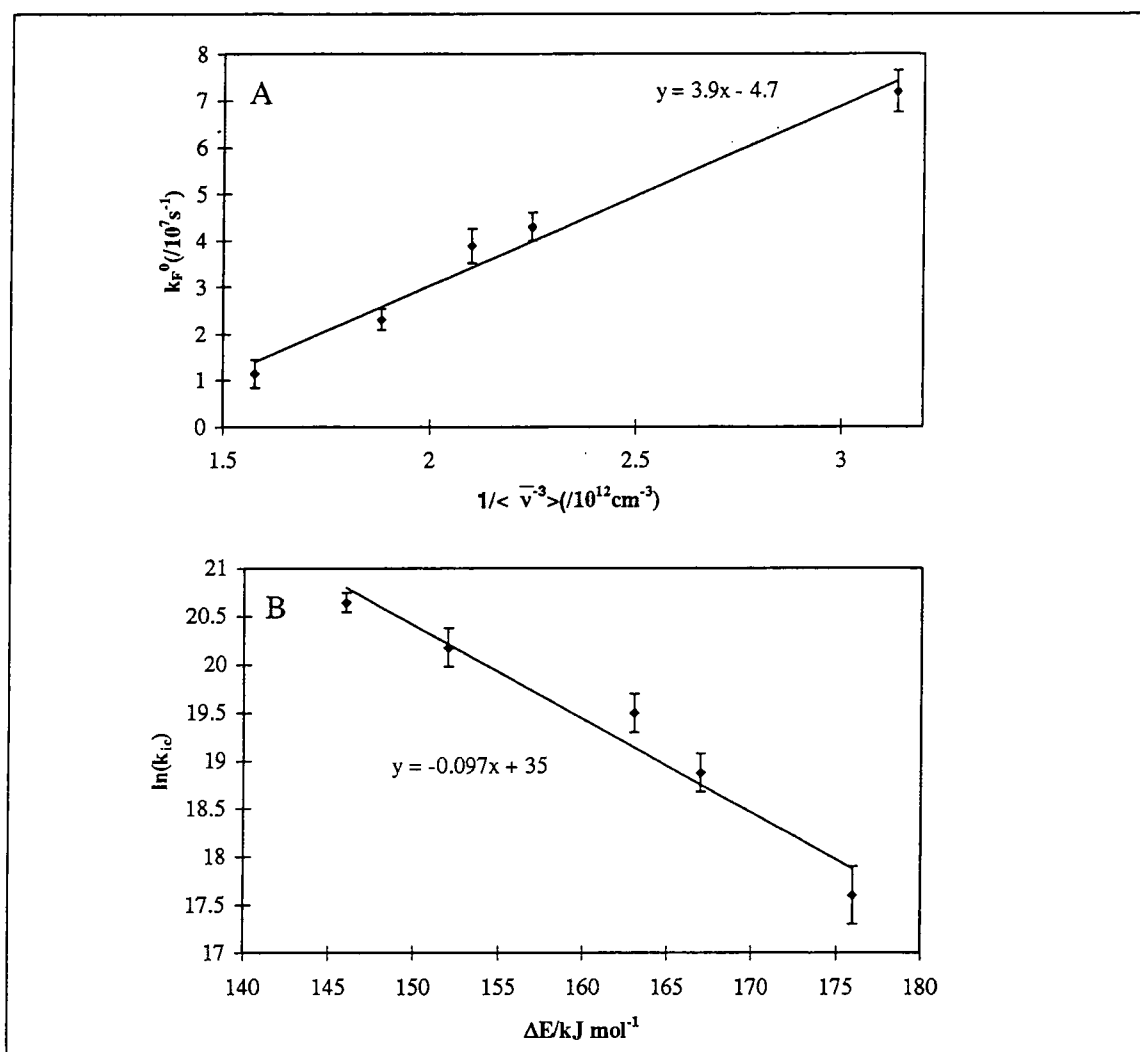
Figure 5.8. Dependence of k_F^0 and k_{ic} on ΔE ($S_1 \leftarrow S_0$) of PcH_n^{n+}.

Figure 5.8A shows a plot of k_F^0 vs $1/<\bar{v}^{-3}>$. A good linear correlation was obtained. This confirms that the absorption intensity (determined by B) remained constant

throughout the series and that the calculated decrease in the intrinsic rate of radiative emission of S_1 (k_F^0) as protonation occurred is consistent with that predicted by theory.

Despite an increase in the intrinsic lifetime, τ_0 ($\tau_0 = 1/k_F^0$), the measured lifetime of fluorescence decreased from 3 ns to 0.88 ns upon complete protonation (Table 5.3). This was due to a concurrent increase in internal conversion pathways. Non-radiative transitions increase as the energy gap between states decreases according to the 'energy gap law'[23] (Equation 5.6).

$$k_{ic} \approx 10^{13} \, exp - \alpha \Delta E \qquad (5.6)$$

where α is a proportionality constant. Figure 5.8B shows a plot of $\ln k_{ic}$ vs ΔE. Least squares analysis of the data yielded an intercept of 35, in reasonable agreement with the value predicted by Equation 5.6 of $\ln(10^{13})$, i.e. 30. k_{ic} values are also in good agreement with previously published data that has been related to the energy of the singlet state[24]. The energy gap law can be qualitatively explained in terms of Frank-Condon factors. As the energy gap between nuclear wavefunctions increases, the extent of overlap decreases and deactivation becomes more unfavourable. If direct spin-orbit coupling to a vibrational level of T_1 occurs, the rate of intersystem crossing may also be expected to depend on the energy difference between S_1 and T_1. k_{isc} was found to remain constant at $1.8 \pm 0.25 \times 10^8$ s^{-1} as pH was lowered. This implies that ΔE between S_1 and T_1 remained approximately constant or that spin-orbit coupling to an upper excited triplet level, T_n occurred.

Equilibria contributing to excited triplet state dynamics are presented in Figure 5.9. k_1 and k_2 represent the triplet decay rate of unprotonated and monoprotonated phthalocyanine species, whilst, k_f, k_b and k_f^*, k_b^* are the rates of H$^+$ binding/dissociation in the ground and excited states respectively.
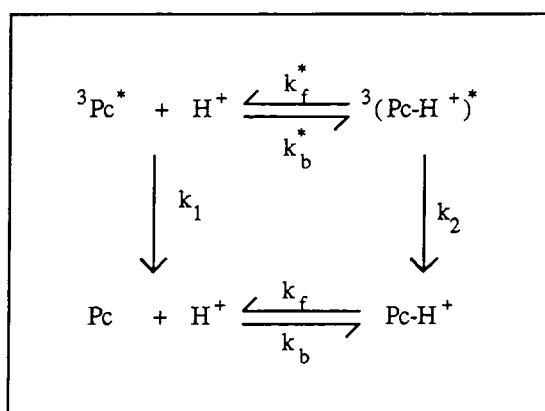
Figure 5.9. Triplet state equilibria of PcH$^+$.

Experimentally, single exponential decays were obtained (Figure 5.5). This suggests that fast exchange between $^3Pc^*$ and $^3PcH^{+*}$ occurred within the lifetime of the excited state such that k_f^* and k_b^* are faster than k_1 and k_2 consistent with theory[15]. The equilibrium constant, K^*, is represented by Equation 5.7.

$$K^* = \frac{k_f^*}{k_b^*} = \frac{[^3PcH^*]}{[^3Pc^*][H^+]}$$

(5.7)

The experimentally observed decay may be represented by the sum of two first order decays, $-d[^3Pc^* + {}^3PcH^{+*}]/dt = k_1[^3Pc^*] + k_2[^3PcH^{+*}]$. Substituting for $[^3PcH^{+*}]$ gives Equation 5.8.

$$-(1 + K^*[H^+])\frac{d[^3Pc^*]}{dt} = (k_1 + k_2K^*[H^+])[^3Pc^*]$$

(5.8)

However, $-d[^3Pc^*]/dt = k_{obs}[^3Pc^*]$, thus the observed rate of decay, k_{obs}, is a first order process that may be expressed by Equation 5.9.

$$k_{obs} = \frac{k_1 + K^*[H^+]k_2}{1 + K^*[H^+]}$$

(5.9)

At high $[H^+]$, $K^*[H^+] \gg 1$ therefore $k_{obs} \sim k_2$ - the rate of decay of $^3PcH^{+*}$ whilst at low $[H^+]$, $1 \gg K^*[H^+]$ hence $k_{obs} \sim k_1$ - the rate of decay of $^3Pc^*$. At intermediate $[H^+]$, an average value was observed which depended on the relative contribution of k_1 and k_2.

A large decrease in the yield of singlet oxygen formation was observed upon protonation. Such a large reduction was inconsistent with the measured decrease in Φ_T and τ_T. This may be explained by lowering of the triplet energy to a value where energy transfer to ground state oxygen is no longer favourable. Lang et al.[7] have reported a substantial reduction in the rate of quenching, k_Q, by O_2 of the triplet state of protonated chloro-aluminium phthalocyanine ($k_Q = 6.6 \times 10^7$ dm^3 mol^{-1} s^{-1}) relative to that of unprotonated phthalocyanine ($k_Q = 1.6 \times 10^9$ dm^3 mol^{-1} s^{-1}). It has been shown[25] that k_Q may be correlated with the energy gap between triplet state species participating in energy transfer. It may be inferred that, since the energy required to promote ground state molecular oxygen to its singlet state will remain constant, the

energy of $^3Pc^*$ must have decreased. It was not possible to corroborate this experimentally since phosphorescence of PcH^+ could not be detected, however, it has been shown that k_{isc}, and therefore ΔE ($S_1 \to T_1$), remained constant upon protonation, thus E_T of PcH^+ may be estimated to be ~ 8400 cm^{-1} (c.f. 9090 cm^{-1} for $^tBu_4ZnPc$), E_Δ = 7882 cm^{-1}.

$$k_Q = \frac{1}{9} k_{diff} / (1 + exp(-\frac{(E_s - E_T - E_\Delta)}{RT}))$$ (5.10)

The Sandros Equation[26] (Equation 5.10), may be used to estimate k_Q based upon singlet and triplet state energies. Using the data above, we can expect a reduction in k_Q by an order of magnitude.

5.3.2 ZnPcS$_2$ in 1% Triton X-100 solution

The UV/Vis absorption spectrum of a concentrated solution of $ZnPcS_2$ in 1% Triton X-100 / H$_2$O solution showed a characteristic monomer spectrum but was observed to produce a new absorbing species at 702 nm over a period of days or weeks (Figure 5.10). This spectrum bears a close resemblance to that reported by Yoon *et al.* in concentrated alcoholic solutions of sulfonated aluminium phthalocyanine chloride[10].
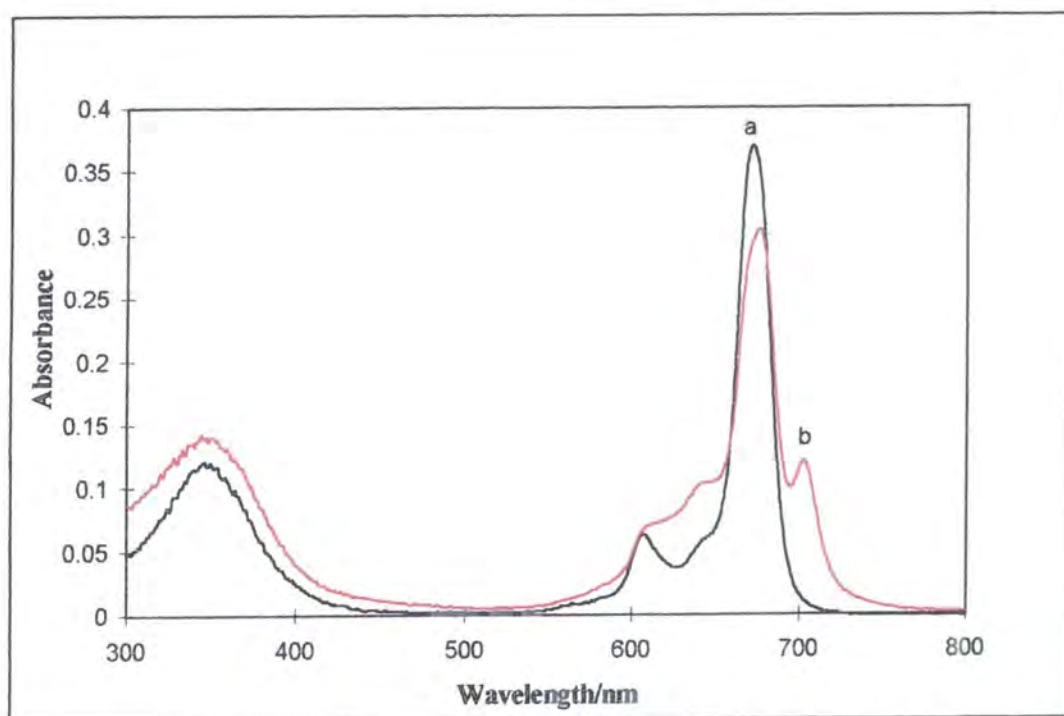
Figure 5.10. UV/Visible absorption spectra of 'Fresh' (a) and 'Old' (days to weeks) (b) Solutions of ZnPcS$_2$ in 1% Triton X-100/H$_2$O solution.

The fluorescence properties of 'old' and 'fresh' solutions were investigated. A 4 mm path length cuvette was used to minimise inner filter effects. An additional emission band at 710 nm from the 'old' solution was revealed (λ_{ex} = 630 nm). Reabsorption effects were not responsible for spectral changes and were ruled out using the method of Dhami *et al*.[11]. In addition, emission at 710 nm was only observed for the 'old' solution although the 'fresh' solution was of equivalent optical density. Figure 5.11 shows the emission and excitation spectra of the new absorbing species. These were calculated by subtraction of a fraction of the 'fresh' solution spectrum from the spectrum of the 'old' solution (Equation 5.11).

$$I_{Old}(\lambda) - xI_{Fresh}(\lambda) = I_{New}(\lambda) \qquad (5.11)$$

where I_{Old}, I_{Fresh} and I_{New} refer to the intensity of the 'Old', Fresh' and 'New' species respectively as a function of wavelength, λ. x is an arbitrary constant. Similarity to the monoprotonated form of $^tBu_4ZnPc$ in EtOH (Figure 2 and 3) is clear. Addition of a small amount of solid CO_2 to the 'fresh' phthalocyanine solution induced emission at 710 nm and an absorption spectrum resembling that of the 'old' solution. Hence, it is concluded that the acidity induced by atmospheric CO_2 dissolved in solution is sufficient to induce protonation, a fact which has not been previously considered.
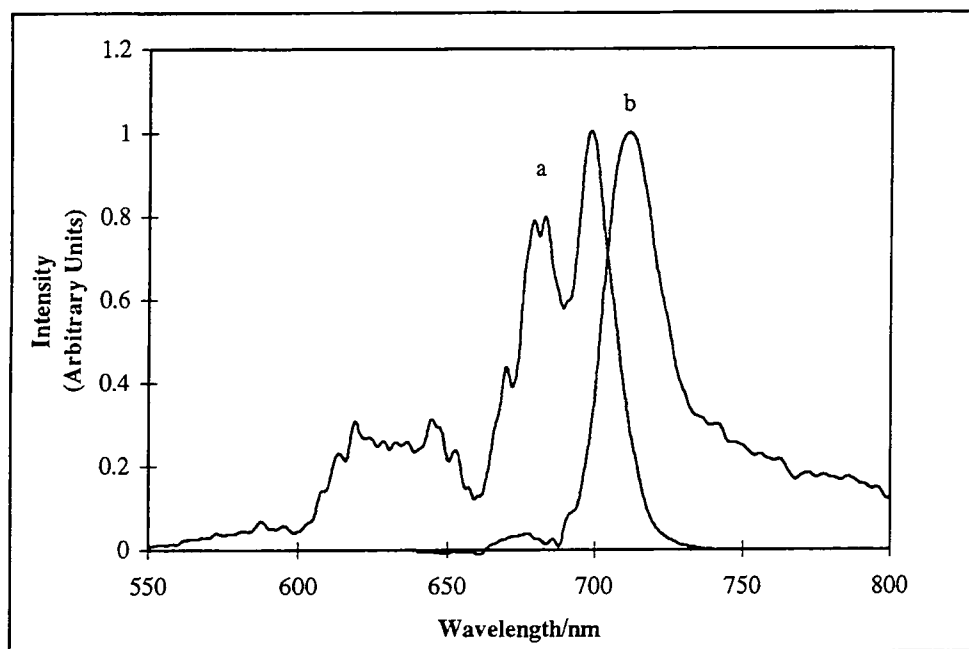
Figure 5.11. Excitation and emission spectra of 'New' species formed in an old solution of ZnPcS$_2$ in 1% TX/H$_2$O (λ_{em} = 760 nm, λ_{ex} = 630 nm).

In buffer solutions with pH's ranging from 7 to 1, ZnPcS$_2$ showed a clear conversion into another species as the pH was lowered (Figure 5.12). By analogy with results

obtained for $^tBu_4ZnPc$ this species was assigned to the PcH^+ ionic form of phthalocyanine. Using Equation 5.1 the pK_a was calculated to be 4.4 ± 0.4.
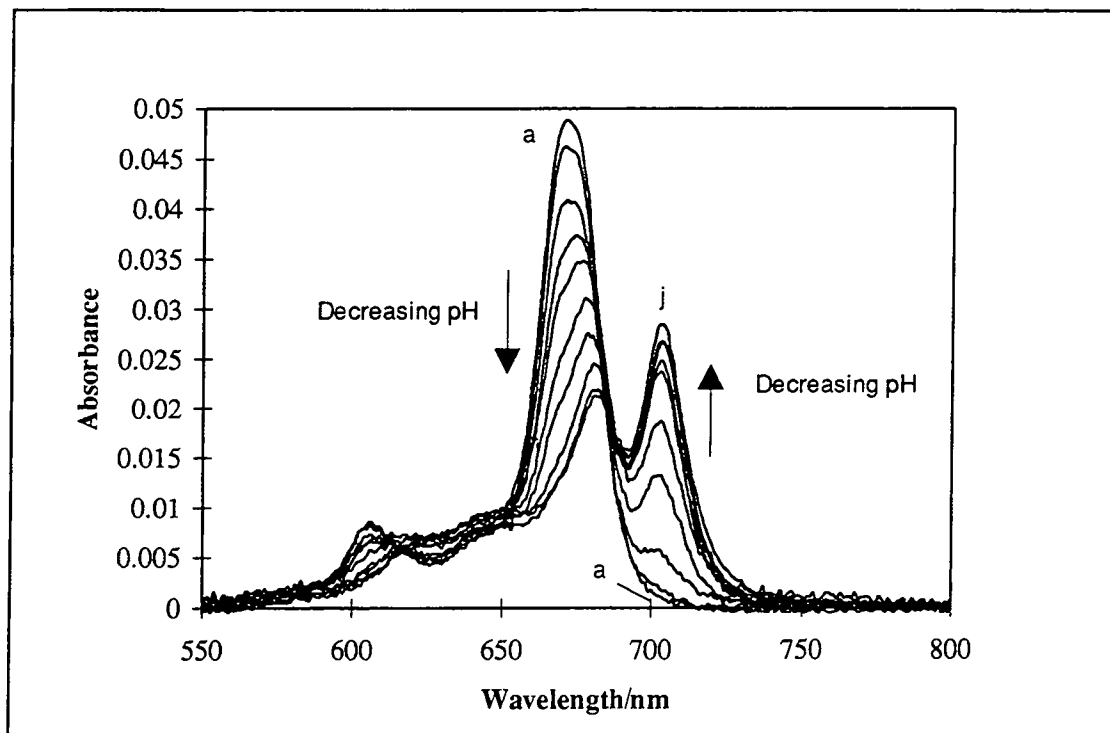
Figure 5.12. Absorbance spectra of $ZnPcS_2$ in buffers ranging from pH 7 to 1.
_pH=a) 7.06 b) 5.8 c) 5.3 d) 4.56 e) 4.17 f) 3.48 g) 3.38 h) 2.5 i) 2.1 j) 1.06._

Figure 5.13 shows the emission spectra of $ZnPcS_2$ in buffers of various pH's. The inset shows the ratio of emission at λ_{max} of $ZnPcS_2$ (679 nm) to that of monoprotonated phthalocyanine emission (707 nm). A typical pH curve was obtained. Using the method of Haugland et al.[27] (Equation 5.12), a pK_a of 4.1 ± 0.5 was determined (Figure 5.14).

$$pH = pK_a + c[log\frac{R - R_{min}}{R_{max} - R}] + log\frac{I_a}{I_b} \qquad (5.12)$$

where R is the ratio of emission of two wavelengths (in this case 679/707 nm) with minimum and maximum limiting values of R_{min} and R_{max} respectively. I_a and I_b are the intensity in acid and base respectively at the wavelength used for the denominator of R (707 nm). Thus, pK_a was calculated from the intercept minus $log(I_a/I_b)$ ($log(I_a/I_b) = 0.6$ for this study).

This value is within experimental error of that calculated using UV/Vis absorption data and is comparable to that reported for protonation of haematoporphyrin[13]. Protonation

of haematoporphyrin at this pH has already been shown to have physiological implications.
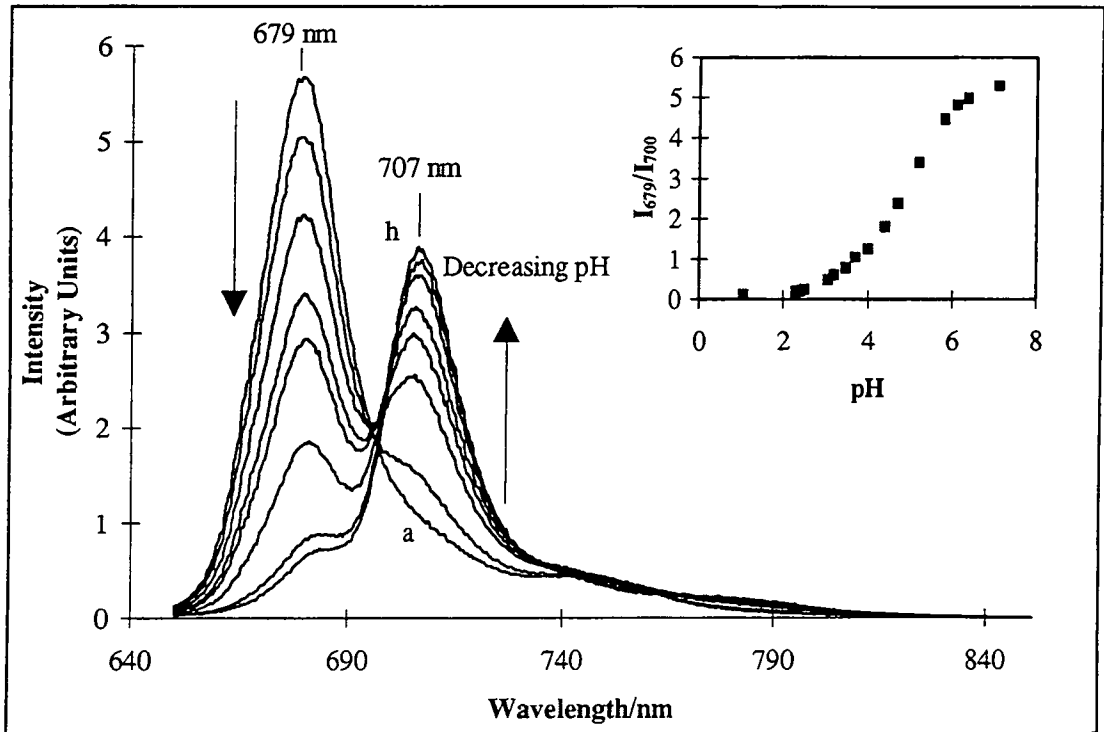
Figure 5.13. Emission spectra of ZnPcS$_2$ in buffers ranging from pH 7 to 1 (λ_{ex}= 630 nm). pH = a) 7 b) 5.3 c) 4.56 d) 4.17 e) 3.92 f) 3.38 g) 2.5
Inset: Ratio of emission from unprotonated and protonated phthalocyanine species (679 / 707 nm).
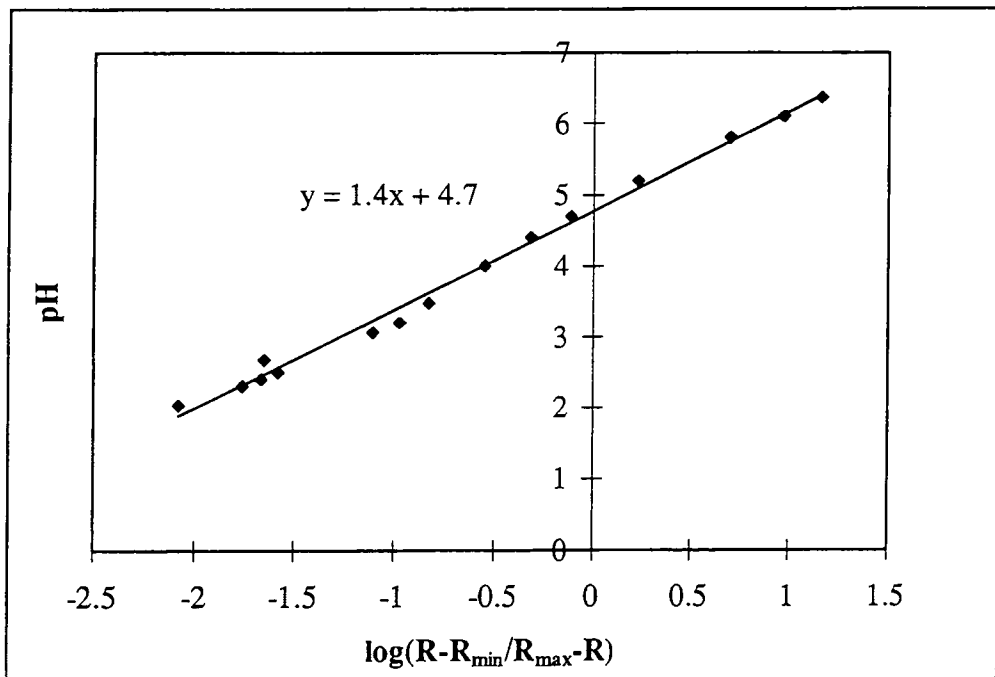
Figure 5.14. Effect of pH on the intensity ratio 679 / 707 nm for ZnPcS$_2$ in buffer.

Table 5.6 compares the photophysical properties of $^tBu_4ZnPc$ (n = 0, 1), $ZnPcS_2$ (n = 0, 1) and $AlPcS_2$ (n = 0, 1) in 1% TX/H_2O solution. Clearly, although the propensity of each phthalocyanine to protonate differs markedly, the resulting decrease in the photophysical properties is similar.

Pc	n	pK_a	Φ_F	Φ_T	τ_T /μs	Φ_Δ
$ZnPcS_2$	0	-	0.16 ± 0.03	0.55 ± 0.05	330 ± 30	0.56 ± 0.05
	1	4.4 ± 0.4	0.1 ± 0.02	0.17 ± 0.02	100 ± 10	< 0.05
$^tBu_4ZnPc$	0	-	0.14 ± 0.03	0.48 ± 0.05	330 ± 30	0.53 ± 0.05
	1	-0.1 ± 0.2	0.085 ± 0.015	0.27 ± 0.03	30 ± 5	0.17 ± 0.2
$AlPcS_2$	0	-	0.48 ± 0.04	0.22 ± 0.02	615 ± 70	0.2 ± 0.02
	1	-0.2 ± 0.2	0.14 ± 0.02	0.06 ± 0.03	72 ± 10	0.09 ± 0.03

Table 5.6. Comparison of photophysical properties of monoprotonated species of
$^tBu_4ZnPc$, $ZnPcS_2$ and $AlPcS_2$ in 1% Triton X-100/H_2O solution.

5.3.3 Solid State Measurements

Figure 5.15 shows the diffuse reflectance spectra of $ZnPcS_2$ and $^tBu_4ZnPc$ adsorbed onto cellulose. An additional peak was observed in the spectrum of $ZnPcS_2$ at 705 nm. Identical spectra were obtained using microcrystalline cellulose or filter paper, however, silica based samples were characterisatic of monomeric phthalocyanine. Exposure of cellulose based samples to ammonia vapour removed the peak at 705 nm such that spectra resembled those recorded when silica was employed. The remission function of $ZnPcS_2$ on 100% cotton fabric was measured (Figure 5.15, Inset). This spectrum is different to those on both cellulose and silica, featuring a broad, structureless band superimposed onto monomeric absorption bands.
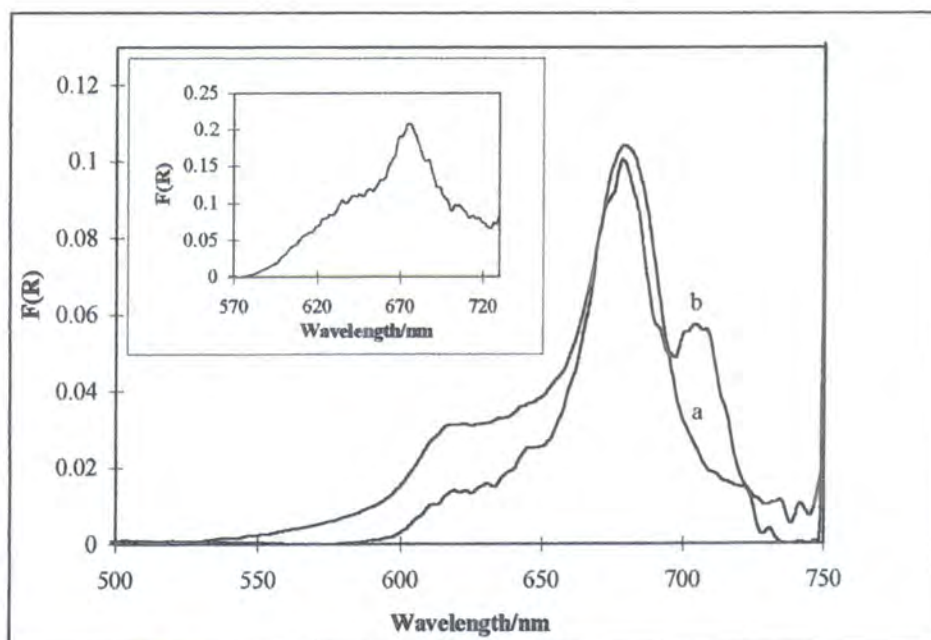
Figure 5.15. Reflectance spectra of a) ${}^{t}Bu_{4}ZnPc$ and b) $ZnPcS_{2}$ on cellulose.
Inset: $ZnPcS_{2}$ on cotton.

Emission and excitation spectra of cellulose based samples of $ZnPcS_{2}$ and ${}^{t}Bu_{4}ZnPc$ are displayed in Figure 5.16. Appearance of a peak at 705 nm in the excitation spectrum of $ZnPcS_{2}$, accompanied by additional emission at 712 nm suggests that a luminescent species has been formed. Emission and excitation of ${}^{t}Bu_{4}ZnPc$ on cellulose and $ZnPcS_{2}$ on cotton were representative of monomeric phthalocyanine emission.
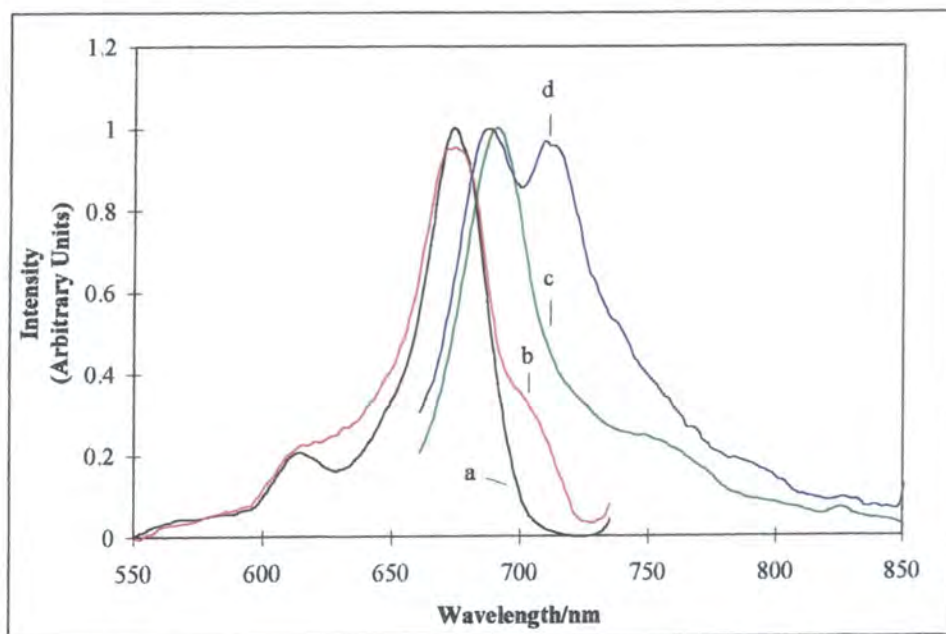
Figure 5.16. Fluorescence excitation spectra of a) ${}^{t}Bu_{4}ZnPc$ and b) $ZnPcS_{2}$ on cellulose (λ_{em} = 740 nm).
Emission spectra c) ${}^{t}Bu_{4}ZnPc$ and d) $ZnPcS_{2}$ on cellulose (λ_{ex} = 630 nm).

Diffuse reflectance flash photolysis experiments revealed that the transient absorption spectrum of $ZnPcS_2$ on cellulose was shifted by ~10 nm from 490 nm to 500 nm with respect to that recorded using silica as the substrate. Decays fitted monoexponential kinetics and yielded lifetimes of 138 ± 15 μs on silica and 216 ± 20 μs on cellulose. Incorporation of $^tBu_4ZnPc$ onto cellulose and silica substrates resulted in identical transient spectra centred at 490 nm.

By analogy to results discussed in Sections 5.3.1 and 5.3.2, the red shifted absorption peak observed by adsorption onto cellulose may be attributed to protonated phthalocyanine species. Singlet state measurements are also consistent with this theory. It has been shown (*vide infra*) that $ZnPcS_2H^+$ in 1% TX/H_2O emits at 707 nm, or 580 cm^{-1} to lower energy than the parent phthalocyanine. Solid state results are in good agreement with this, exhibiting an emission band at 712 nm, red shifted by 511 cm^{-1}. Shifts in the transient absorption spectrum were identical to those observed for monoprotonated phthalocyanine species in ethanol. Triplet state lifetimes of cellulose based samples were longer than those prepared on silica. This is surprising considering lifetimes measured in solution state (330 μs and 100 μs for $ZnPcS_2$ and $ZnPcS_2H^+$ respectively) which indicate that protonated species have a much faster decay rate. In solid state work it is known that diffusion of oxygen across cellulose is hindered (Section 3.3.4), thus it is likely that the measured lifetime has been artificially enhanced, counteracting a decrease induced by molecular changes. As for solution state measurements, $Pc^* + H^+ \rightleftharpoons PcH^{+*}$ equilibria were rapid compared with deactivation processes.

Two possibilities present themselves as the reason behind protonation. Cellulose is a large molecule with numerous sites available which are suitable for hydrogen bonding to adsorbates (Figure 5.17)[28].
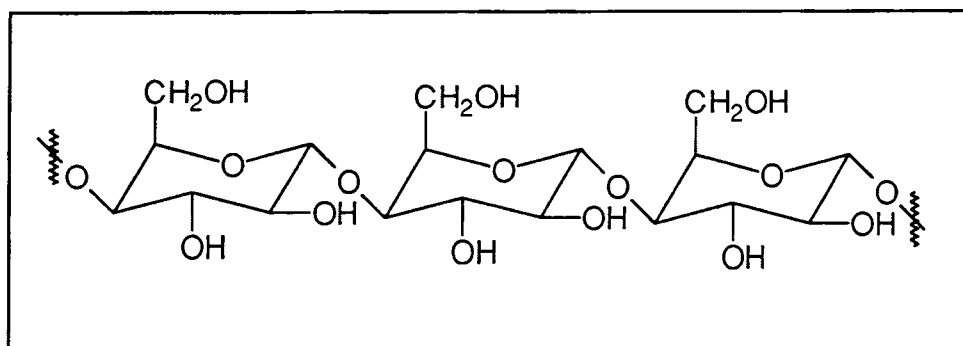
Figure 5.17. Structure of cellulose.

It is plausible that hydrogen bonding to a bridging methine nitrogen of the phthalocyanine ring would induce the results described above. Alternatively, excess free hydrogen ions in cellulose may be responsible for protonation. If hydrogen bonding was responsible, cotton fabric would be expected to produce the same effect as powdered cellulose or filter paper. However, spectra recorded on cotton cloth were comparable to those recorded for $AlPcS_2$ on muslin by Wilkinson[29] and Oldham[30] and are characteristic of a mixture of monomeric and aggregated phthalocyanine species. This implies that excess hydrogen ions which have been removed from the cloth by some process of manufacture, e.g. washing, must be the cause of protonation. Exposure of samples to ammonia vapour removed any traces of protonated phthalocyanine species. The implication of this is that excess hydrogen ions are removed via protonation of ammonia, i.e. $NH_3 + H^+ \rightleftharpoons NH_4^+$. Ammonia is a strong base ($pK_a(NH_4^+) = 9.25$[31]) and binds hydrogen ions more readily than phthalocyanine ($pK_a = 4.3$).

5.4 Biological Relevance

Protonation of sensitisers for use in photodynamic destruction of tumour tissue may have important consequences regarding the efficacy of the dye *in vivo*. As a consequence of large lactic acid concentrations produced as a biproduct of anaerobic glycolysis, the pH of tumour tissue has been demonstrated[32] to vary from 5.85 to 7.68, up to 1.15 units lower than that of healthy tissue (extracellular pH = 7.43, intracellular pH = 7.00). Disulfonated zinc phthalocyanine has been shown to have a pK_a value of 4.3 ± 0.5 in aqueous buffered solution (*vide infra*), thus at pH's of this magnitude a significant proportion of dye molecules would be expected to exist as the protonated form. Meso tetra 4-(sulfonatophenyl) porphyrin (TPPS$_4$) demonstrated this property in RR 1022 epithelial cells which were shown to have a pH low enough to encourage protonation of this phthalocyanine[33]. A dramatic reduction in the propensity of protonated zinc phthalocyanines to produce cytotoxic, singlet oxygen species has been demonstrated. A significant shift in the absorption window to longer wavelength was also observed. This may have a detrimental effect on the yield of excited state molecules produced by the wavelength of the exciting light. Indeed, the *in vivo* absorption spectrum of disulfonated aluminium phthalocyanine has been shown[34] to be red shifted by 15 nm with respect to the spectrum in aqueous solution. A shift of this direction and magnitude was consistent with the therapeutic efficiency of this phthalocyanine causing MS2 fibrosarcoma and L1210 leukaemic cell death. The authors speculated that this phenomenon must be due to a modification of the chemical structure of dye molecules. Protonation of the ring is one possible explanation for these effects. Despite negative effects of protonation, Lin *et al.* observed an increase in the photodynamic efficiency of

Nile Blue derivative at low pH's in the presence of the ionophore, nigericin[4]. A similar effect was observed by a different group when chloroaluminium phthalocyanine was used as sensitiser[35]. It has since been shown that the positive action of nigericin was not due to its ability to lower intracellular pH, nevertheless, in the absence of nigericin, cells were more susceptible to photodynamic therapy at low pH (6.0)[36]. It follows that other mechanisms such as the effect of pH on the localisation and retention of sensitisers must also be considered. The effect of pH on the localisation of porphyrin sensitisers has been studied in detail by Pottier[1] and Brault[3]. Both groups suggest that the ionic distribution of haematoporphyrin will be significantly different at pH = 6.5 (tumour pH) than at pH = 7.6. At the pH of tumour tissue, approximately 44% of porphyrin species will exist as the non-ionic, H_2P form, compared with just 2% at neutral pH. Regarding this simply, retention in interstitial regions may be enhanced due to the lower solubility of non-ionic species and consequent resistance to removal by lymphatic drainage.

If transport across cell membranes is considered, neutral molecules will penetrate into the cell more readily than ionic species due to the net negative charge surrounding plasma membranes. Once inside the cell, a higher environmental pH is experienced by the dye and the ionic distribution alters accordingly effectively trapping the phthalocyanine. This results in intracellular localisation of the dye molecules. A study by Bohmer[37], in which enhanced cellular uptake of haematoporphyrin was observed at low pH corroborates this theory. An alternative explanation was made concerning reduced binding of porphyrin molecules to albumin delivery proteins.

Further experimental studies are required to evaluate the effects of *in vivo* pH on the efficacy of substituted zinc phthalocyanines. It is possible that protonation of phthalocyanine species (leading to cationic molecules) may promote association with cell membranes and a consequent increase in dye retention. This may counteract to some extent the detrimental effects of protonation on the photophysical properties of zinc phthalocyanines, *viz:* reduced Φ_T and Φ_Δ.

5.5 Conclusion

It has been shown that protonation of zinc phthalocyanine molecules at the azomethine bridges causes a significant reduction in photoactivity. As the pH of the solution was lowered using H_2SO_4, a red shift of the absorption and fluorescence spectra accompanied by a concurrent decrease in the fluorescence quantum yield was observed. The quantum yields of triplet production and singlet oxygen sensitisation were also reduced upon protonation. Solutions of $ZnPcS_2$ in 1% TX/H_2O and on solid cellulose substrates were found to protonate under surprisingly mild conditions. It is concluded that bands due to the 'dimer' in the absorption spectrum reported by Yoon et al.[10] were in fact protonated phthalocyanine.

5.6 References

[1]   Barrett A.J., Kennedy J.C., Jones A., Nadeau P and Pottier R.H., The effect of tissue and cellular pH on the selective biodistribution of porphyrin-type photochemotherapeutic agents: A volumetric titration study., *J. Photochem. Photobiol. B:Biol.*, **6**, 309-323, 1990.

[2]   Pottier R., Laplante J.P. and Chow Y.A., Photofrins: A spectral study., *Can. J. Chem.*, **63**, 1463, 1985.

[3]   Brault D., Physical chemistry of porphyrins and their interactions with membranes: The Importance of pH., *J. Photochem. Photobiol., B:Biol.*, **6**, 79-86, 1990.

[4]   Lin C.W. and Shulok J.R., Enhancement of Nile Blue derivative-induced photocytoxicity by nigericin and low cytoplasmic pH., *Photochem. Photobiol.*, **63**, 143-146, 1994.

[5]   Gaspard S., Verdaguer M. and Viovy R., Protonation des phthalocyanines., *J. Chem. Res. (M)*, 3064-3072, 1979.

[6]   Iodko S.S., Kaliya O.L., Kondratenko N.V., Luk'yanets E.A., Popov V.I. and Yapupol'skii L.M., Quantitative characteristics of the stagewise protonation of phthalocyanines., *Zhur. Obshch. Khim.*, **53**, 901-903, 1983.

[7]   Lang K., Wagnerova D.M., Engst P. and Kubat P., Influence of protonation on the reactions of triplet state sulfonated chloro-aluminum (III) phthalocyanine with dioxygen., *J. Chem. Soc. Faraday Trans.*, **88**, 677-680, 1992.

[8]   Savitsky A.P., Lopatin K.V., Golubeva N.A., Poroshina M.Y., Chernyaeva E.B., Stepanova N.V., Solovieva L.I. and Lukyanets E.A., pH dependence of fluorescence and absorbance spectra of free sulfonated aluminum phthalocyanine and its conjugate with monoclonal antibodies., *J. Photochem. Photobiol. B:Biol.*, **13**, 327-333, 1992.

[9] Simpson M.S.C., The photophysics of sulphonated aluminium phthalocyanines as sensitisers for Photodynamic Therapy (PDT)., *PhD Thesis*, Imperial College, London, 1994.

[10] Yoon M.J., Cheon Y.J. and Kim D.H., Absorption and fluorescence spectroscopic studies on dimerization of chloroaluminium (III) phthalocyanine tetrasulphonate in aqueous alcoholic solutions., *J. Photochem. Photobiol. B:Biol.*, **58**, 31-36, 1993.

[11] Dhami S., De Mello A.J., Rumbles G., Bishop S.M., Phillips D. and Beeby A., Phthalocyanine fluorescence at high concentrations: Dimers or reabsorption effect?, *Photochem. Photobiol.*, **61**, 341-346, 1995.

[12] Pottier R., *In vitro* and *in vivo* fluorescence monitoring of photosensitisers., *J. Photochem. Photobiol. B:Biol.*, **6**, 103-109, 1990.

[13] Brault D., Vever-Bizet C. and Le Doan T., Spectrofluorimetric study of porphyrin incorporation into membrane models - evidence for pH effects., *Biochim. Biophys. Acta*, **857**, 238, 1986.

[14] Pottier R.H., Kennedy J.C., Chow Y.F.A. and Cheung F., The pK_a values of haematoporphyrin IX as determined by absorbance and fluorescence spectroscopy., *Can. J. Chem.*, **33**, 57, 1988.

[15] Barltrop J.A. and Coyle J.D., *Principles of Photochemistry*, p49, Wiley and Sons, Bristol, 1978.

[16] Vincett P.S., Voigt E.M. and Rieckhoff K.E., Phosphorescence and fluorescence of phthalocyanines., *J. Chem. Phys.*, **55**, 4131, 1971.

[17] Morley J.O. and Charlton M.H., Theoretical investigation of the structure and spectra of zinc phthalocyanines., *J. Phys. Chem.*, **99**, 1928, 1995.

[18] Ward B., Callahan P.M., Young R., Babcock G.T. and Chang C.K., Red shifts in the optical spectra of porphyrin schiff bases upon protonation., *J. Am. Chem. Soc.*, **105**, 634, 1983.

[19] Ward B., Chang C.K. and Young R., Spectral shifts upon reversible modifications of CHO peripheral substituents in porphyrin, chlorin and bacteriochlorin. A phenomenological explanation for the red shift of protonated schiff base., *J. Am. Chem. Soc.*, **106**, 3943, 1984.

[20] Mikhalenko S.A., Derkacheva V.M. and Luk'yanets E.A., Phthalocyanines and related compounds. XIX Tetra and octa amino substituted phthalocyanines., *J. Gen. Chem.* (USSR), **51**, 1405, 1980.

[21] Kober E.E., Caspar J.V., Lumpkin R.S. and Meyer T.J., Application of the energy gap law to excited state decay of osmium(II)-polypyridine complexes: Calculation of relative nonradiative decay rates from emission spectral profiles., *J. Phys. Chem.*, **90**, 3722, 1986.

[22] Atkins P.W., *Physical Chemistry*, p465, 4th Edn., Oxford University Press, Oxford, 1990.

[23] Turro N.J., *Modern Molecular Photochemistry*, p183, University Science Books, California, 1991.

[24] Barltrop J.A. and Coyle J.D., *Principles of Photochemistry*, p93, Wiley and Sons, Bristol, 1978.

[25] Barltrop J.A. and Coyle J.D., *Principles of Photochemistry*, p126, Wiley and Sons, Bristol, 1978.

[26] Ford W.E., Rihter B.D. and Rodgers M.A.J., Quenching of naphthalocyanine triplets by O_2: Application of the Sandros Equation., *J. Am. Chem. Soc.*, **111**, 2362, 1982.

[27] Whitaker J.E., Haugland R.P. and Prendergast F.G., Spectral and photophysical studies of benzo[c]xanthene dyes: Dual emission pH sensors., *Anal. Biochem.*, **194**, 330, 1991.

[28] Kroschwitz J., *Encyclopaedia of Polymer Science and Engineering*, p123, Wiley and Sons, New York, 1990.

[29] Wilkinson F. and Willsher C., Detection of transient absorption in a dyed cotton fabric and in semicinductor powders by diffuse reflectance laser flash photolysis., *J. Chem. Soc., Chem. Commun.*, 142, 1985.

[30] Oldham T.C., Spectroscopic Investigations of Photodynamic Mechanisms in Cell Cultures., *PhD Thesis*, Imperial College, London, 1996.

[31] Alberty R.A. and Silbey R.J., *Physical Chemistry*, p255, Wiley and Sons, New York, 1996.

[32] Kessel D., *Localisation phenomena: pH effects in Photodynamic Therapy of Neoplastic Disease*, p63, CRC Press, Boston, 1990. - and references therein.

[33] Schneckenburger H., Gschwend M.H., Sailer R., Ruck A. and Strauss W.S.L., Time resolved pH dependent fluorescence of hydrophilic porphyrins in solution and in cultivated cells., *J. Photochem. Photobiol. B:Biol.*, **27**, 251, 1995.

[34] Cubeddu R., Canti G., Musolino M., Pifferi A., Taroni P. and Valentini G., *In vivo* absorption spectrum of disulphonated aluminium phthalocyanine in a murine tumour model., *J. Photochem. Photobiol. B:Biol.*, **34**, 229, 1996.

[35] Varnes M.E., Clay M.E., Freeman K., Antunez A.R. and Oleinick N.L., Enhancement of photodynamic cell killing (with chloroaluminium phthalocyanine) by treatment of V79 cells with the ionophore nigericin., *Cancer Res.*, **50**, 1620, 1990.

[36] Varnes M.E., Bayne M.T. and Bright G.R., Reduction of intracellular pH is not the mechanism for the synergistic interaction between photodynamic therapy and nigericin., *Photochem. Photobiol.*, **64**, 853, 1996.

[37]   Bohmer R.M. and Forstyn G., Uptake of haematoporphyrin derivative by normal and malignant cells: Effect of serum, pH, temperature and cell size., *Cancer Res.*, **45**, 5328, 1985.

CHAPTER 6
LIGAND BINDING AND ELECTRON
TRANSFER PROPERTIES

6.1 Introduction
6.1.1 Ligand Binding

The effect of axial ligands on the photophysics of aluminium and zinc phthalocyanines has not been widely studied and there have been relatively few publications on the subject. It is generally accepted that triplet state sensitiser species are important intermediates in the mechanism of PDT cell destruction (Section 1.2). Thus, any factors which affect photophysical parameters, in particular the quantum yield or lifetime of the triplet state and the rate of intersystem crossing, may have important consequences on the effectiveness of the sensitiser. Work has been carried out to study the effect of axial ligands on the photophysics of disulfonated aluminium phthalocyanine ($AlPcS_2$) by Phillips' group at Imperial College, London[1]. During their studies, it was noticed that addition of fluoride ions to $AlPcS_2$ solution had a significant effect on the absorption spectrum and also on the rate of intersystem crossing, k_{isc}. The wavelength of maximum absorption, λ_{max}, was blue shifted by 4-6 nm (solvent dependent), indicating an increase in the HOMO-LUMO energy gap. Fluorescence and internal conversion rates, k_f and k_{ic} respectively, were unaffected, however k_{isc} increased, resulting in a larger yield of triplet state species. Ben-Hur et al. have reported similar results concerning the effect of F^- on $AlPcS_n$[2]. Clearly, interaction between fluoride ions and aluminium phthalocyanine occurs. It has been suggested that F^- replaces an axial OH^- ligand to form $[AlPcS_2F]$, causing the observed changes in the photophysical properties. Exchange of H_2O/D_2O as axial ligand to $AlPcS_2$ has also been observed to induce photophysical change[3]. The actual process by which axial ligands influence photophysical processes is not fully understood. In studies of ruthenium phthalocyanine by Ferraudi[4] and Doeff[5], the relaxation rates of $^3\pi\pi^*$ and the kinetics of axial ligand exchange are investigated. Ferraudi suggests that perturbations in the electronic structure of the phthalocyanine occur due to the electron withdrawing properties of the ligand. An increase in the lifetime of $^3\pi\pi^*$ states was observed which correlated with the electron withdrawing tendency of the axial ligand (4 t-butylpyridine < pyridine < dimethylformamide < dimethylsulfoxide < CO). This was ascribed to changes in the energy gap between excited and ground states. A similar theory has been proposed by Nappa[6] to explain

the results of his experiments on the complexation of the halogens to zinc tetraphenylporphyrin. A red shift of the absorption spectrum was reported which increased in the order $F^- < Cl^- < Br^-$. The shift increased as the electron donating properties of the ligand increased. It is believed that complexation of these ligands resulted in a greater transfer of charge onto the porphyrin ring.

Ben-Hur et al.[7],[8] have observed that the addition of fluoride ions in vivo inhibited photodynamic action of aluminium, gallium and zinc phthalocyanines. This is surprising considering the beneficial effects of fluoride on phthalocyanine triplet state production. It has been suggested[9] that the fluorocomplex of $AlPcS_2$ has a reduced binding affinity for proteins and biological membranes. Serum albumins and low density lipoproteins are believed to play an important role in the transport of photodynamic sensitisers from the site of injection to receptor sites within malignant cells. Thus, reduced binding to protein may lead to reduced localisation within cells and a consequent decrease in photodynamic efficacy in vivo.

It has been demonstrated that hydrophilic dyes tend to bind to albumins[10] whilst hydrophobic sensitisers show a preference for lipoproteins[11]. In order to be effective, once the drug has reached necrotic tissue, transfer to receptor sites within the tumour must occur. If binding between protein and drug is too strong, transfer will fail and the sensitiser rendered less effective[3]. Albumin is a helical, globular protein, containing several loops and troughs where hydrophobic amino acid residues are situated[12]. These constitute potential binding sites for hydrophobic molecules. Weaker binding by hydrophobic sensitisers to water soluble albumins may therefore prove to be beneficial to the photodynamic process by increasing the concentration of sensitiser transferred to tumour receptor sites.

6.1.2 Electron Transfer Properties
6.1.2.1 Theory

When a molecule absorbs radiation to generate an excited electronic state there is a profound change in the reduction/oxidation potential of the compound, hence this may lead to a change in its redox chemistry which may allow it to enter into electron transfer reactions. Absorption of light leads to the promotion of an electron into a higher energy level, leaving an electron 'hole' in the original molecular energy level. The molecule is a better electron acceptor in its excited state and the redox potential of the couple (E_{ox}/E_{red}) is raised by an amount equal to the energy of the excited state. At the same time, the reduction potential of the excited state is raised as its ability to donate an

electron increases. It is, therefore, possible for phthalocyanines in excited singlet or triplet states to undergo chemical reactions that do not occur in ground state molecules. Electron transfer quenching reactions are a prime example of this and have been widely observed (Section 6.1.2.2). The theory of electron transfer reactions was developed by Marcus[13],[14]. He postulated that transfer occurs within the constraints of the Franck-Condon principle, i.e. nuclei remain motionless for the duration of the transfer process. The atomic configuration of reactant and product encounter pairs may be considered to fluctuate due vibrational motion of the complex and rearrangement of surrounding solvent molecules. Each encounter complex has an analogous potential energy profile, however, due to differences in the electronic configuration of reactants and products bond lengths and solvent orientation differ, thus, each profile occurs in a different region of space (Figure 6.1).
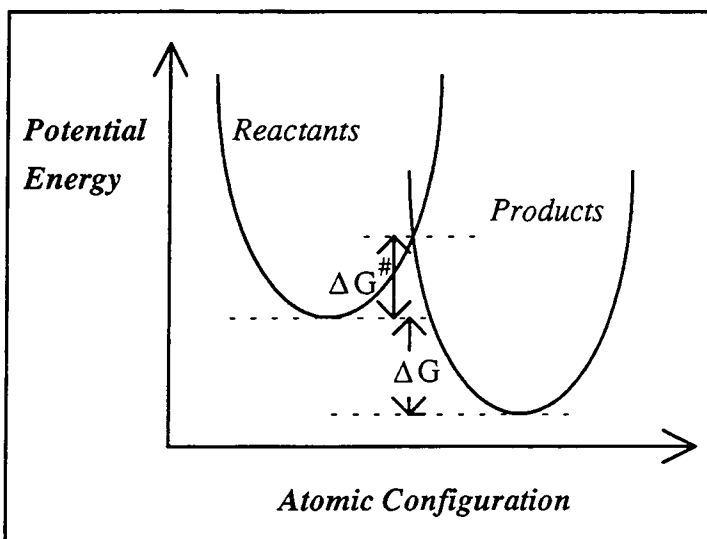
Figure 6.1. Potential energy profile of electron transfer[16].

At the point where the two surfaces intersect, the encounter complexes differ only in the position of an electron and transfer may occur. Marcus related the rate of reaction, k_Q, to the activation energy, $\Delta G^{\#}$, of the transfer via a quadratic equation[15]. Application of this equation using various values of ΔG, the free energy change for reaction, predicts an 'inverted region' in the rate of electron transfer. When ΔG is endothermic (positive) little or no reaction is predicted. As ΔG becomes negative, i.e. exothermic in nature, k_Q is predicted to increase to a maximum value before decreasing in highly exothermic reactions due to overlap between potential energy curves being possible only at high energies.

This hypothesis has been expanded by Rehm and Weller[16] who demonstrated that Marcus theory is a useful guide for slightly positive or negative values of ΔG but found

no evidence for the inverted region. In their experiments, a plateau was obtained where diffusion control is dominant, placing a maximum value on the rate of quenching. Fluorescence quenching via electron transfer may be represented by the scheme depicted in Figure 6.2.

$$^1Sens_0 + {}^1Q \xrightarrow{h\nu} {}^1Sens* + {}^1Q \underset{k_{-d}}{\overset{k_d}{\rightleftharpoons}} {}^1Sens^* ...^1Q \underset{k_{-a}}{\overset{k_a}{\rightleftharpoons}} {}^1(^2Sens^{+.}...^2Q^{+.})$$

$\downarrow 1/\tau_F$ Encounter   Radical Pair
Complex

$\downarrow k_{deac}$

k_d = Rate of Diffusion of Reactants

k_{-d} = Rate of Dissociation of Encounter Complex

k_a = Rate of Electron Transfer (Activation Controlled Rate)

k_{-a} = Rate of Reverse Electron Transfer

k_{deac} = Rate of Deactivation of Radical Ion Pair including Back Electron Transfer to Ground State (k_{rev}) and Radical Dissociation (k_{diss})

Figure 6.2. Processes involved in fluorescence quenching by electron transfer[16].

ΔG, the free energy change for electron transfer, may be calculated using Equation 6.1 and used in Equation 6.2 to calculate the theoretical rate of electron transfer[16].

$$\Delta G = 96.62(E(D^+ / D) - E(A / A^-) - \frac{e_0^2}{4\pi\varepsilon_0\varepsilon\, a}) - \Delta E_{0,0} \qquad (6.1)$$

E is the reduction potential of donor, D and acceptor, A, $E_{0,0}$ is the energy required to produce the excited state, 96.62 is the Faraday Constant, e_0 is the elementary charge, a is the encounter distance, ε is the dielectric constant of the solvent and ε_0 is the relative permittivity of a vacuum. The term, $e_0^2/4\pi\varepsilon_0\varepsilon a$, describes the free enthalpy change upon bringing two radical ions to the encounter distance.

$$k_Q = \frac{k_d}{1 + \frac{k_d}{\Delta V_d k_{deac}}(exp(\frac{\Delta G^\#}{RT}) + exp(\frac{\Delta G}{RT}))} \qquad (6.2)$$

189

where k_d is the rate of diffusion through the solvent medium, $\Delta V_d = k_d/k_{-d}$, k_{deac} is the rate of deactivation of the radical pair, R is the gas constant, T is the temperature and $\Delta G^\#$ is the activation free enthalpy. Rehm and Weller assumed $\Delta G^\#$ to be a monotonous function of ΔG (Equation 6.3).

$$\Delta G^\# = ((\frac{\Delta G}{2})^2 + (\Delta G^\#(0))^2)^{1/2} + \frac{\Delta G}{2} \qquad (6.3)$$

$\Delta G^\#(0)$ is the activation enthalpy when $\Delta G = 0$ and was shown to be 10 kJ mol^{-1} in acetonitrile solution.

6.1.2.2 Electron Transfer Reactions of Phthalocyanines

Excited states of phthalocyanines have been shown to act as both electron donors and electron acceptors, i.e. in a reducing or oxidising capacity. Darwent and co-workers[17] have investigated quenching of singlet and triplet states of AlPcS$_2$ using methyl viologen (MV^{2+}), benzyl viologen (BV^{2+}) and anthraquinone 2,6 disodium sulfonate (AQDS) as electron acceptors. It was found that AQDS, MV^{2+} and BV^{2+} reacted to quench fluorescence originating from the singlet state of AlPcS$_2$. Flash photolysis studies showed the triplet state to be unaffected by the addition of these acceptor species. By comparison, Ohno[18] describes triplet state quenching of ZnPc by 1,4-naphthalocyanine, 1,4-benzoquinone, trinitrofluorenone and organic oxidants at rates which may be correlated to the reduction potentials of each acceptor. Quenching of $^3\pi\pi^*$ states of ruthenium phthalocyanine (RuPc) species by nitroaromatic compounds and viologen salts has also been reported[19].

In addition, phthalocyanines may be reduced by electron donors to form phthalocyanine radical anions[17],[20]. Aramendia[21] has carried out a considerable amount of work concerning quenching of excited states of substituted zinc phthalocyanines by amine donors in micellar solution. Detection of ZnPc$^{-\cdot}$ radical species is reported. Darwent and co-workers[17] investigated electron acceptor properties of aluminium phthalocyanine. When benzohydroquinone (BQH$_2$) was used as an electron donor, products corresponding to both singlet and triplet state reaction were detected. This is unusual since singlet state electron transfer induces a short lived radical pair (Equation 6.4) which has a spin allowed back reaction. Two processes are in competition:

   i) Dissociation from the geminate ion pair to give separate radical ions.
   ii) Back reaction to regenerate the starting materials in the ground state.

Back reaction occurs rapidly and, consequently, electron transfer products from the singlet state are rarely detected. It was suggested that the extended lifetime in this case was due to the influence of two deprotonation steps inherent in encounter complex formation (Equation 6.4).

$$AlPcS_2(S_1) + BQH_2 \rightarrow (AlPcS_2 \cdot^- ... BQ \cdot^-) + 2H^+ \qquad (6.4)$$
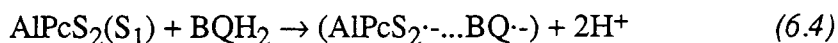
Polar solvents stabilise radical species, thus aiding dissociation[22]. Reaction products resulting from triplet state ($^3\pi\pi^*$) quenching are commonly observed[23],[24],[25]. In this case, back electron transfer is forbidden due to the spin multiplicity of the geminate ion pair. Consequently, free radical formation is favoured.

The mechanism of PDT has not yet been fully established and the extent to which electron transfer reactions contribute to cell destruction is not clear. The importance of singlet oxygen as an intermediate has been stressed by many authors, however, biological studies by Ben-Hur provide conflicting evidence. In a study[26] regarding photosensitisation of Chinese hamster cells by hydrophilic phthalocyanines, lack of reaction enhancement on substitution of H_2O by D_2O introduces doubts concerning the involvement of singlet oxygen in the process. Yet in another study[27], cytotoxic effects of the superoxide radical anion are dismissed. Clearly there is confusion between *in vivo* and *in vitro* studies. Further investigation into electron transfer reactions of sensitisers is required in both homogeneous and heterogeneous media.

6.1.3 Aim

The aim of this study was to research the interaction of substituted zinc phthalocyanines with simple organic and biological molecules in a ligand binding or electron transfer capacity. Changes induced in the photophysical properties of substituted zinc phthalocyanines upon binding of axial ligands have been investigated and used to assess binding of $^tBu_4ZnPc$, $ZnPcS_2$ and C10 to bovine serum albumin. The propensity of ZnPc's to act as electron acceptors has been studied using amine donors such as diazabicyclo[2,2,2]octane (DABCO) and tetramethyl-p-phenylenediamine (TMPD). Following this, electron transfer reactions involving biologically important species, specifically ascorbic acid and selected amino acids, have been investigated with a view to improving understanding of the role of Type I reactions *in vivo*.

6.2 Materials and Methods

6.2.1 Materials

Phthalocyanines. Tetra tertbutyl zinc phthalocyanine (^{t}Bu$_4$ZnPc) and disulfonated zinc phthalocyanine (ZnPcS$_2$) were prepared by Dr. A. Beeby and used as received (unpublished results). 1,4,8,11,15,18,22,25-octadecyl zinc phthalocyanine (C10) was a gift from Prof. M. J. Cook, University of East Anglia[28]. 2,3,9,10,16,17,23,24-Octakis [4',5'-bis(hexylthio)tetrathia-fulvalen-4-ylmethoxymethyl] phthalocyanine (Pc(TTF)$_8$), 2,14,26,38-Tetrakis[4,5-bis(hexylthio)-1,3-dithiol-2-ylidene] 4H,6H,10H,18H,22H,28H,30H,34H,36H,40H,42H,46H,48H-tetrakis([1,3]dithiolo[4,5-c]dioxecino) [7,8-b;7',8'-k;7",8"-t;7'",8'"-c'] phthalocyanine (Pc(TTF)$_4$) and tetrathiafulvalene (TTF) were prepared by Prof. M. R. Bryce's group[29], University of Durham and used as received (Figure 6.3).

Amines. 1, 4-diazabicyclo [2,2,2] octane (Sigma, >99% purity), N, N dimethylaniline (Aldrich, 99% purity), 1, 4 dimethoxybenzene (Aldrich, 99% purity) were used as received. 1,4-N,N,N',N'-tetramethylphenylenediamine (TMPD, Aldrich, 98% purity) was recrystallised from hexane before use.

Amino Acids. N-acetyl L-tryptophanamide, N-acetyl L-tyrosinamide, N-^{t}BOC L-methionine and L-cysteine were purchased from Sigma and used as received.

Others. Tetrabutylammonium cyanide (Aldrich, 96% purity), ascorbic acid (Sigma), ascorbic acid palmitate (Sigma, 96% purity) and bovine serum albumin (Sigma, >99% purity) were used as received.

Solvents. Solvents were Analar grade or better and were used without further purification. Phosphate buffer saline (PBS) was purchased from Sigma and prepared using distilled water. Triton X-100 (TX) was purchased from Sigma.
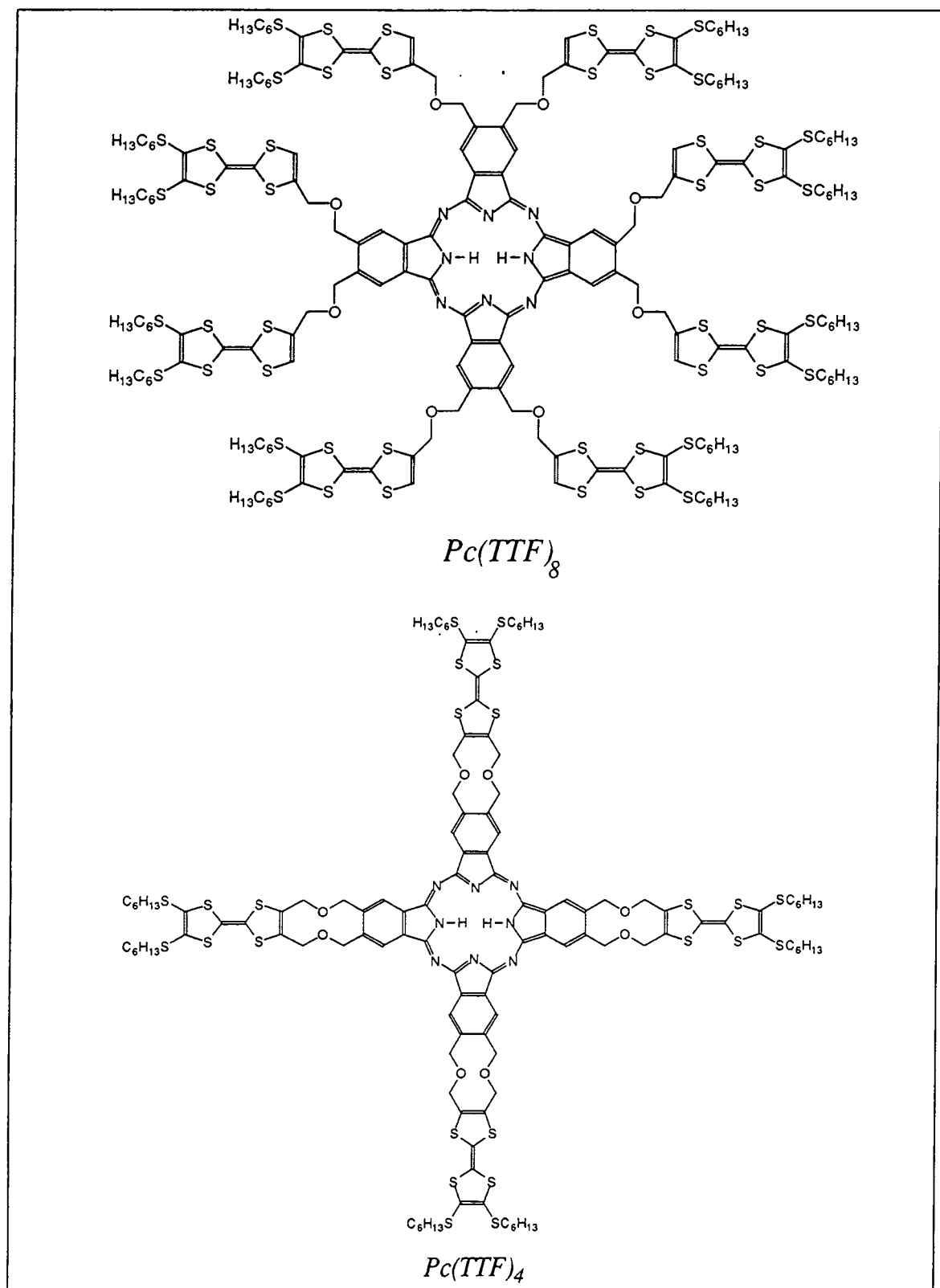
Pc(TTF)$_8$

Pc(TTF)$_4$

***Figure 6.3. Structures of Pc(TTF)*$_8$ *and Pc(TTF)*$_4$.**

6.2.2 Methods

Equilibrium constants for binding, K, were determined using the Hildebrand-Benesi[30] equation (Equation 6.5) and assuming an equilibrium $A + B \rightleftharpoons AB$.

$$\frac{[A]_0 [B]_0}{\Delta A_\lambda} = \frac{1}{K(\varepsilon_{AB} - \varepsilon_A)} + \frac{[B]_0}{(\varepsilon_{AB} - \varepsilon_A)} \qquad (6.5)$$

where $[A]_0$ and $[B]_0$ are the initial concentrations of species A and B respectively, ΔA is the observed change in absorbance and ε_{AB} and ε_A are the extinction coefficients of complex, AB and reactant, A. ΔA was measured for a series of concentrations of B and K obtained by dividing the gradient of a graph of $[A]_0[B]_0/\Delta A$ vs $[B]_0$ by the intercept.

Micellar phthalocyanine solutions were prepared using the methods described in Section 3.2. Except where specified otherwise, protein studies were carried out in 1% Triton X-100 / phosphate buffer saline (1% TX/PBS) solution in order to facilitate contact between hydrophobic and hydrophilic phases. The electron transfer properties of TTF in micellar solution were also investigated in Triton X-100 solution. Due to the relative insolubility of TTF in 1% w/v TX/H_2O solution, the concentration of TX was increased to 10% w/v TX/H_2O. Under these conditions, it was not possible to measure the concentration of TTF directly so the extinction coefficient, ε, was determined in acetonitrile solution (ε_{360} = 1900 dm^3 mol^{-1} cm^{-1}) and used as an estimate for the value of ε_{360} in surfactant solution. Knowing this, and the absorbance of TTF 10% TX/H_2O solution at 360 nm, the concentration of micellar solutions of TTF could be determined.

Irradiation studies were performed using a xenon lamp (Bentham 605) and filter (RG610, Comar Instruments, UK.) combination. Samples were irradiated with stirring for a time interval, t and transferred directly to an absorption spectrometer (ATI Unicam UV2-100) for spectral measurements.

All electrode potentials are quoted vs the normal hydrogen electrode. Literature values have been converted to this scale using E^0 (Ag/AgCl) = 0.222 V vs NHE and E^0, SCE (Standard Calomel Electrode) = 0.24 V vs NHE.

Photophysical measurements were performed using the techniques described and explained in Chapter 2 (pp 42-71).

6.3 Results and Discussion

6.3.1 Ligand Binding

6.3.1.1 Cyanide Ions and Tetrahydrofuran

Figure 6.4A shows the effect of 0.01 mol dm^{-3} CN^- ions on the absorption spectrum of $ZnPcS_2$ in MeOH. A clear shift of the Q band from 666 nm to 672 nm was observed accompanied by splitting of the Soret band. In Figure 6.4B a gradual shift was observed as cyanide concentrations were varied from 0 mol dm^{-3} to 0.01 mol dm^{-3}. At concentrations greater than this no further shift was detected. By analogy to results reported regarding the effect of fluoride on the absorption spectrum of disulfonated aluminium phthalocyanine[1] ($AlPcS_2$) these changes were assigned to binding of CN^- ions to $ZnPcS_2$ as axial ligands (Equation 6.6).

$$\mathbf{ZnPcS_2} + \mathbf{CN^-} \underset{\longleftarrow}{\overset{\mathbf{K}}{\longrightarrow}} \mathbf{ZnPcS_2CN^-}$$

$$(6.6)$$

Hildebrand-Benesi analysis (Figure 6.5) was performed at several wavelengths and yielded a binding constant, $K = 800 \pm 200$ dm^3 mol^{-1}.

$y = 5.50E\text{-}05x + 5.3E\text{-}08$
$\lambda = 400$ nm, $K = 1000 \pm 300$ dm^3 mol^{-1}

$-y = 1.9E\text{-}05x + 2.7E\text{-}08$
$\lambda = 655$ nm,
$K = 700 \pm 150$ dm^3 mol^{-1}

$y = 1.4E\text{-}05x + 1.8E\text{-}08$
$\lambda = 680$ nm, $K = 780 \pm 50$ dm^3 mol^{-1}
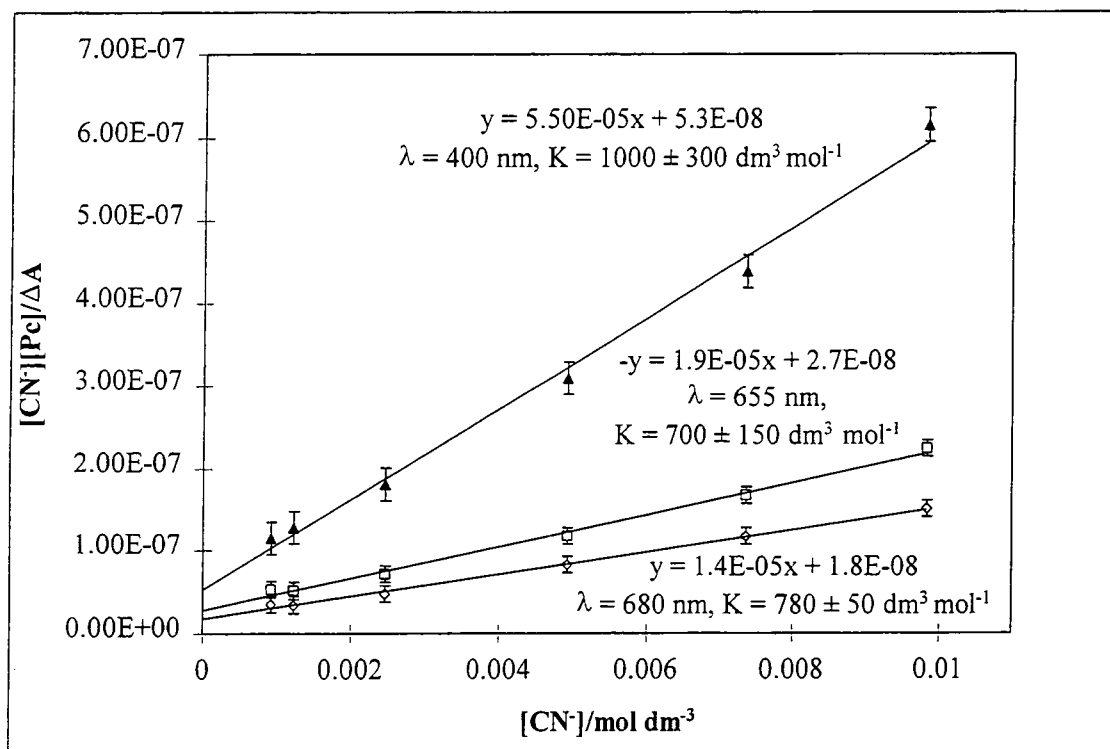
Figure 6.5. Hildebrand-Benesi plots of $ZnPcS_2$ + CN^- in MeOH.
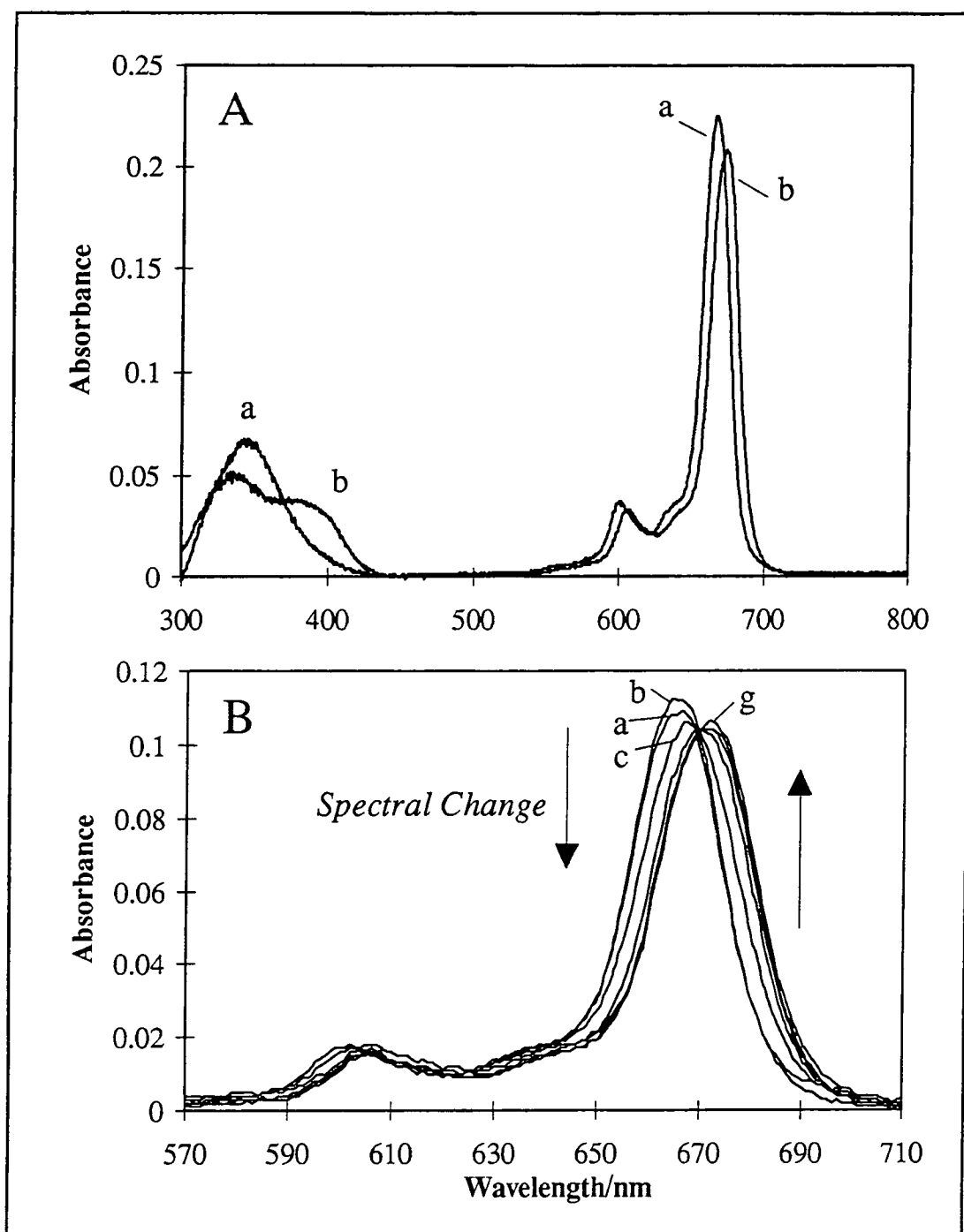
Figure 6.4. UV/Visible absorption spectra of ZnPcS₂ in MeOH + CN⁻ ions

A. a. 0 mol dm⁻³ b. 0.01 mol dm⁻³

B. a. 0 mol dm⁻³ b. 5 x 10⁻⁴ mol dm⁻³ c. 1 x 10⁻³ mol dm⁻³ d. 2.5 x 10⁻³ mol dm⁻³

e. 5 x 10⁻³ mol dm⁻³ f. 7.5 x 10⁻³ mol dm⁻³ g. 0.01 mol dm⁻³.

This value is somewhat lower than that reported by Bishop et al.[1] for fluoride binding to AlPcS$_2$ (4200 dm^3 mol^{-1}) but is comparable to results obtained by Ben-Hur et al.[2] also regarding binding of F$^-$ to AlPcS$_n$ (K = 500 dm^3 mol^{-1}). At the midpoint of conversion to ZnPcS$_2$CN$^-$, [CN-] = 1/K (assuming formation of a 1:1 complex). A calculated

196

cyanide concentration of 1.25×10^{-3} mol dm^{-3} for a K value of 800 dm^3 mol^{-1} is comparable to the experimental value of 1.1×10^{-3} mol dm^{-3}, supporting the result obtained. Cyanide binding to ZnPcS$_2$ corroborates Bishop's theory of complexation between hard/hard and soft/soft ligands and metal ions since CN$^-$ and Zn^{2+} are both considered to be predominantly 'hard' species[31]. It has been demonstrated that triplet state and singlet oxygen yields of ZnPcS$_2$ are unaffected by binding of cyanide ions[32]. Shifts of the absorption spectrum such as this may have important implications with respect to *in vivo* application of photodynamic therapy. The irradiation wavelength selected for treatment is important for maximum efficiency and binding to biological substrates within the patient may lead to a shift of the optimal wavelength. In the case of phthalocyanines, a 5 nm shift of λ_{max} results in a 20% decrease in the absorbance. Gomer *et al.*[33] have observed that the *in vitro* action spectrum for destruction of Chinese hamster ovary (CHO) cells sensitised by haematoporphyrin derivative (HpD) was shifted to higher wavelengths by ~8 nm to 630 nm with respect to the absorption spectrum in cell growth medium. It was shown that the action spectrum was in fact consistent with the absorption spectrum of HpD bound to CHO cells. In whole tumours the situation is different once more and the *in vivo* action spectrum of HpD has been reported to peak at 625 nm[34]. The *in vivo* action spectra of phthalocyanines have also been found to demonstrate a shift with respect to their *in vitro* absorption spectra. Cubeddu[35] has shown that the absorption spectrum of AlPcS$_2$ was shifted by ~15 nm to 685 nm *in vivo* and was consistent with therapeutic efficacy of the dye.

The photophysical properties of a phthalocyanine may be affected by axial ligand binding. For example, the fluorescence yield, Φ_F, triplet yield, Φ_T and triplet lifetime, τ_T of ZnPc(CMe(CO$_2$Me)$_2$)$_4$ were determined to be significantly different in a coordinating solvent than in a non-coordinating medium. Table 6.1 depicts values measured in THF and CHCl$_3$.

Solvent	λ_{max} (UV/Vis) /nm	Φ_F	Φ_T	τ_T	Φ_{IC}
CHCl$_3$	676.5	0.22 ± 0.02	0.45 ± 0.05	280 ± 30	0.33 ± 0.05
THF	671	0.24 ± 0.02	0.65 ± 0.06	420 ± 40	0.11 ± 0.06

Table 6.1. Effect of THF on the photophysical properties of ZnPc(CMe(CO$_2$Me)$_2$)$_4$.

It is likely that these changes were caused by binding of THF to ZnPc(CMe(CO$_2$Me)$_2$)$_4$ as an axial ligand. The precise mechanism by which axial metal ligands induce photophysical change is not generally understood. The results described above indicate that contributions from two separate processes may be responsible - a decrease in

internal conversion pathways, k_{ic}, and an increase in the rate of intersystem crossing, k_{isc}. In the absence of time resolved data to characterise fluorescence lifetimes it is not possible to calculate the rate of each process. Studies performed by Phillips' group at Imperial College, London have demonstrated that the nature of the axial ligand is important. Exchange of the axial H_2O ligands on $AlPcS_2$ in aqueous solution for D_2O was observed to produce an increase in the triplet yields solely as a result of a decrease in k_{ic}. This was ascribed to a decrease in Franck-Condon factors[3]. By contrast, F^- ions induced a decrease in Φ_F of $AlPcS_2$ and an increase in Φ_T and τ_T simply through an increase in the rate of intersystem crossing, k_{isc}: k_{ic} was not affected. The reasons behind this behaviour are unclear although it is proposed that changes in the $S_1 \rightarrow T_1$ energy gap may play some role.

6.3.1.2 Bovine Serum Albumin

The binding of bovine serum albumin (BSA) to substituted zinc phthalocyanines was investigated using changes in photophysical properties as indicators of complexation. Figure 6.6 shows monomerisation of $ZnPcS_2$ in PBS upon addition of BSA. In 1% TX/PBS solution, $^tBu_4ZnPc$ and $ZnPcS_2$ were monomeric, whilst C10 was slightly aggregated (Chapter 3). BSA (5×10^{-4} mol dm^{-3}) induced a 1 nm red shift in the absorption maximum (λ_{max}) of $ZnPcS_2$ from 672 nm to 673 nm. Addition of BSA had no effect on the ground state absorption spectra of C10 or $^tBu_4ZnPc$ in 1% TX/PBS. These results are comparable to those obtained by Davila[36] relating to aqueous solutions of trisulfonated aluminium phthalocyanine chloride ($AlPcS_3$) and tetrakis 4-sulfonatophenyl dichloro tin porphyrin (SnTsPP). $AlPcS_3$ showed a 2 nm red shift upon addition of protein whilst the only indication of binding in the case of SnTsPP was a subtle broadening of the Soret band. Small changes in the electronic structure such as these indicate very weak binding between these phthalocyanines and water soluble BSA protein. Results obtained in this study indicate a similar weak binding between $ZnPcS_2$ and BSA but are inconclusive for $^tBu_4ZnPc$ and C10.
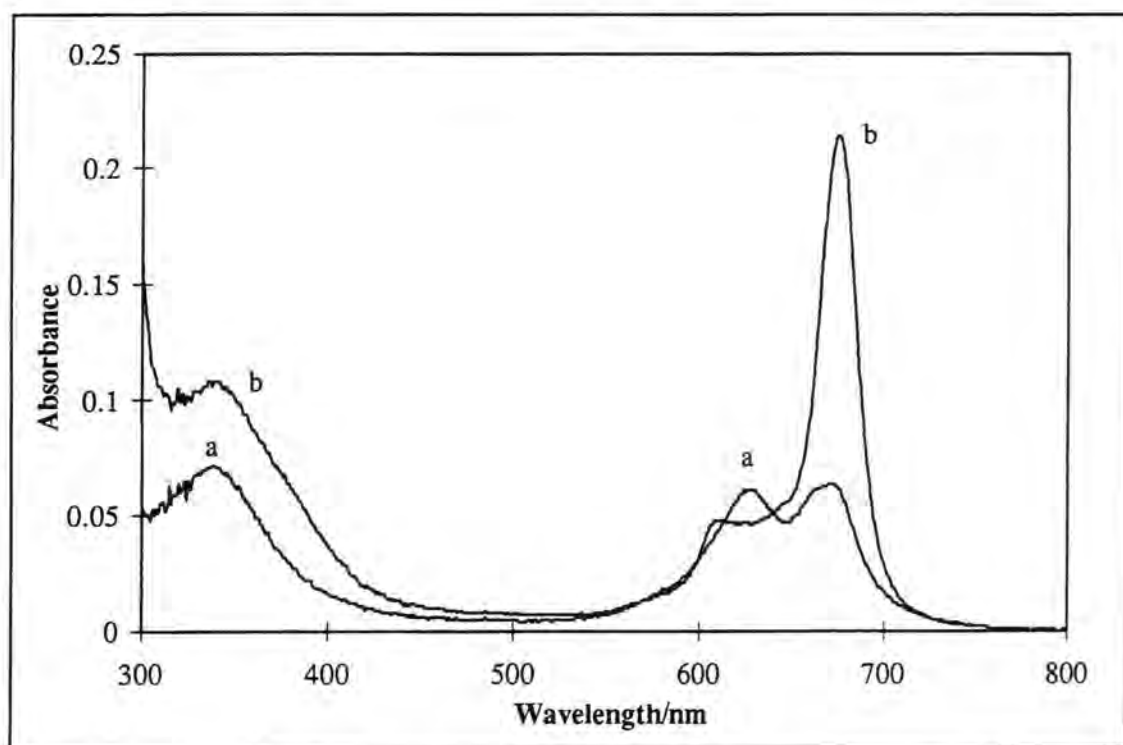
Figure 6.6. Disaggregation of ZnPcS₂ in PBS upon addition of BSA
a. ZnPcS₂ in PBS b. ZnPcS₂ in PBS + 5 x 10⁻⁴ mol dm⁻³ BSA.

Sample	Φ_F	Φ_T	Φ_{iC}	τ_T /μs	Φ_Δ
ZnPcS$_2$	0.17 ± 0.02	0.55 ± 0.05	0.28 ± 0.05	340 ± 40	0.53 ± 0.05
+BSA	0.17 ± 0.02	0.52 ± 0.05	0.31 ± 0.05	350 ± 40	0.48 ± 0.05
tBu$_4$ZnPc	0.15 ± 0.02	0.48 ± 0.05	0.37 ± 0.05	310 ± 25	0.5 ± 0.05
+BSA	0.15 ± 0.02	0.48 ± 0.05	0.37 ± 0.05	340 ± 40	0.5 ± 0.05
C10	0.080 ± 0.005	0.57 ± 0.05	0.35 ± 0.05	110 ± 30	0.5 ± 0.05
+BSA	0.080 ± 0.005	0.52 ± 0.05	0.4 ± 0.05	125 ± 30	0.47 ± 0.05

Table 6.2. Effect of bovine serum albumin on the photophysical properties of
substituted zinc phthalocyanines in 1% TX/PBS.

Table 6.2 collates the fluorescence yield, Φ_F, triplet state yield, Φ_T, triplet state lifetime, τ_T and yield of singlet oxygen formation, Φ_Δ, measured for each phthalocyanine in the absence and in the presence of BSA. Clearly, BSA had no effect on the photophysical efficiency of zinc phthalocyanines. These results differ from those obtained in a study by Davila[36] in which triplet state and singlet oxygen formation by ZnPcS$_3$ were reported to increase upon binding to protein. This was ascribed to disaggregation of ZnPcS$_3$ in PBS upon addition of protein. Since ZnPcS$_2$ was shown to be monomeric under the conditions used in our study, phenomena due to disaggregation may be discounted.

Foley *et al.*[37] have recently reported a decrease in the yield of fluorescence due to binding of AlPcS$_2$ to human serum albumin (HSA), however, no such decrease was observed for any of the zinc phthalocyanines used in this investigation. Studies performed regarding the quantum yield of singlet oxygen formation sensitised by haematoporphyrin in which the yield was shown to be unaffected by binding to HSA are corroborated[38].

Table 6.3 shows the effect of BSA on the fluorescence anisotropy of these phthalocyanines in comparison with $^tBu_4H_2Pc$.

Phthalocyanine	λ_{em} /nm	Anisotropy
$^tBu_4ZnPc$	685 - 760	0.078 ± 0.005
$^tBu_4ZnPc$ + BSA	685 - 760	0.102 ± 0.005
$ZnPcS_2$	685 - 760	0.054 ± 0.005
$ZnPcS_2$ + BSA	765 - 760	0.092 ± 0.005
C10	710 - 790	0.102 ± 0.005
C10 + BSA	710 - 790	0.130 ± 0.005
$^tBu_4H_2Pc$	700	-0.074 ± 0.005
$^tBu_4H_2Pc$ + BSA	700	-0.066 ± 0.005

Table 6.3. BSA (5×10^{-4} mol dm^{-3}) increases the fluorescence anisotropy, r_{av} of metallophthalocyanines ($\lambda_{ex} = 600$ nm).

An increase in the anisotropy, r_{av}, of metallophthalocyanines was obtained upon the addition of protein. Assuming that the fluorescence lifetime does not increase, this indicates an increase in the rotation relaxation time of the fluorophore (Equation 4.7), i.e. an increase in its size or an increase in the viscosity of the medium. The only feasible explanation for the effective size of phthalocyanine changing upon addition of BSA is that binding occurred. It may be argued that interactions between micelles and albumin were responsible and not direct phthalocyanine:BSA binding. Results obtained using metal free phthalocyanine suggest that surfactant binding is not responsible since, in this case, no increase in r_{av} was observed. Experimental conditions differed only in the identity of the fluorophore employed. Similarly, changes incurred as a result of a viscosity increase should manifest themselves in the anisotropy of $^tBu_4H_2Pc$. These results are consistent with those of Ambroz *et al.*[39] in which an increase in r_{av} to 0.06 was observed upon binding of AlPcS$_2$ to HSA. From these results, it can be inferred that $^tBu_4ZnPc$, $ZnPcS_2$ and C10 bind to BSA.

It has been reported that quenching of phthalocyanine triplet state species by molecular oxygen is inhibited upon binding to protein[40],[41]. Davila and Harriman[36] have shown
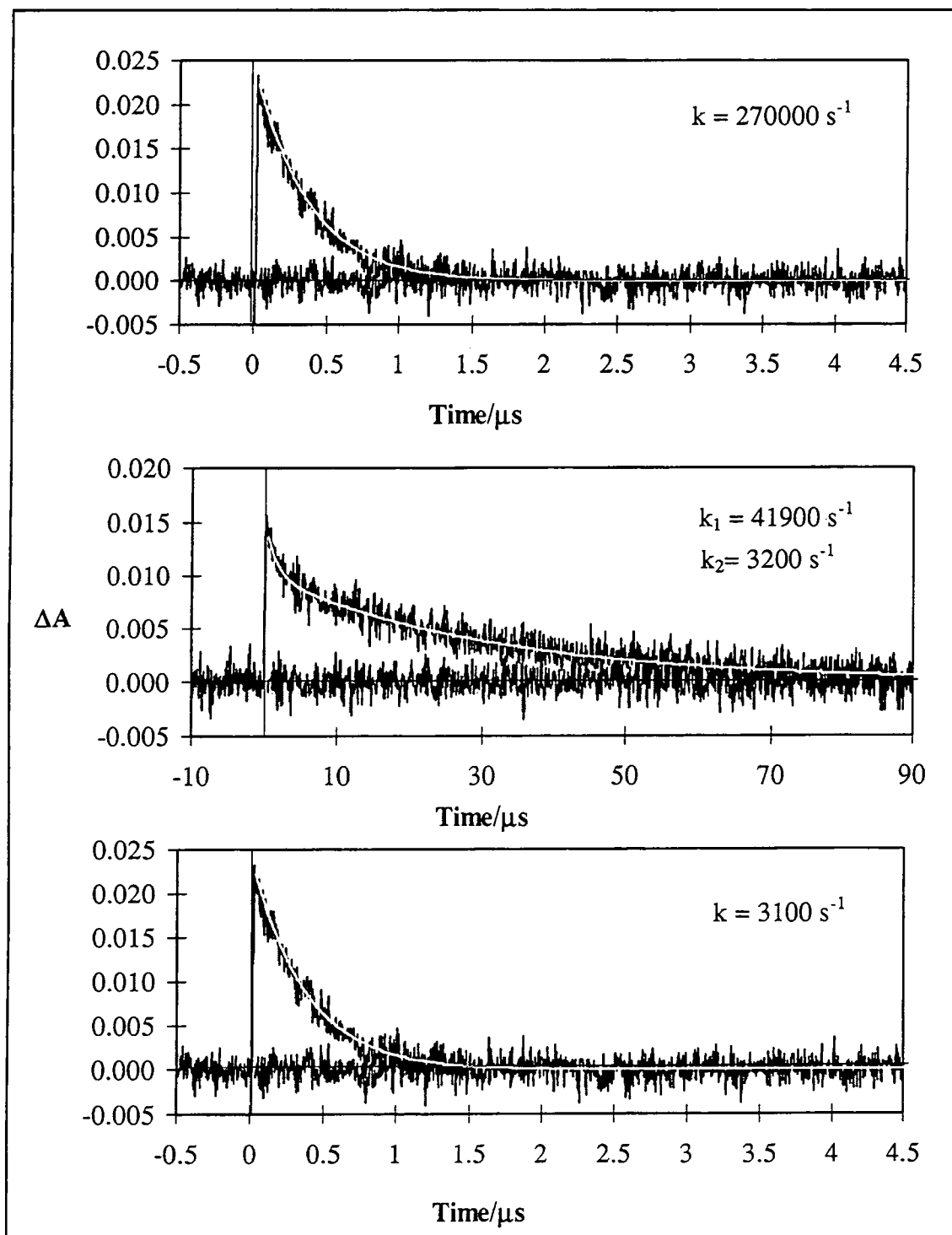
Figure 6.7. Triplet transient decay of $^{t}Bu_{4}ZnPc$ in 1% TX/PBS + 4 x 10^{-4} mol dm^{-3} BSA. Irradiation by A. 4 laser shots B. 30 laser shots C. 44 laser shots $(\lambda_{ex} = 638$ nm, ~ 0.2 mJ/pulse). Exponential fits and residuals are shown.

that the triplet state lifetime of various phthalocyanines was affected by binding to human serum albumin. Biexponential decays were obtained which were assigned to binding of sensitisers to different sites available within the protein which protect the dye from oxygen by varying amounts. It was proposed that extended lifetimes were due to binding to an inner site, which protected excited states from quenching by oxygen. For bulky phthalocyanines with axial ligands, such as AlPc, no evidence of an extended lifetime was observed, suggesting that binding occurred exclusively to exposed sites on the surface of the protein. In an attempt to corroborate binding of hydrophobic zinc phthalocyanines to BSA, reaction of $^3\pi\pi^*$ states of $ZnPcS_2$, $^tBu_4ZnPc$ and C10 with O_2 in the presence of BSA was studied. The lifetime, τ_T, was found to be dependent on the number of laser pulses used to excite the sample. Figure 6.7 shows the triplet transient decay recorded after 4, 30 and 44 laser pulses of ~ 0.2 mJ/pulse. After four shots (Sample B), a lifetime of 4 ± 2 μs was recorded for an oxygen concentration of 2.6×10^{-4} mol dm^{-3} (aerated sample). This increased to 325 ± 25 μs after 44 shots (Sample C) and is comparable to that measured in the absence of oxygen (310 μs - Table 6.2). At an intermediate number of pulses a biexponential decay was obtained (Sample B), indicative of decay from two distinct types of triplet species. Agitation of Samples B and C regenerated the short lived transient of Sample A.

The absorption spectra of the solutions were recorded before and after irradiation. Evidence of increased absorption between 310 and 330 nm was observed. This is representative of photooxidation of the tryptophan residue of BSA to N-formylkynurenine (NFK)[42],[43] - a well known product of singlet oxygen reaction with tryptophan. To investigate this further, a controlled study of photooxidation of BSA sensitised by $^tBu_4ZnPc$ was performed. Formation of NFK was recorded by monitoring the absorbance of the solution at 322 nm. As Figure 6.8 shows, a steady increase in 322 nm absorption was observed followed by a plateau region. Photooxidation sensitised by C10 and $ZnPcS_2$ gave similar results. Concurrent photodegradation of the phthalocyanines was observed. This explains the reason behind the plateau region of Figure 6.8 where production of NFK reaches a maximum. Specifically, photodegradation of phthalocyanine resulted in the production of ever-decreasing amounts of singlet oxygen - the active species involved in oxidation of BSA - thus, the rate of production of NFK decreased until the concentration of singlet oxygen was insufficient to induce further oxidation of tryptophan within the BSA.
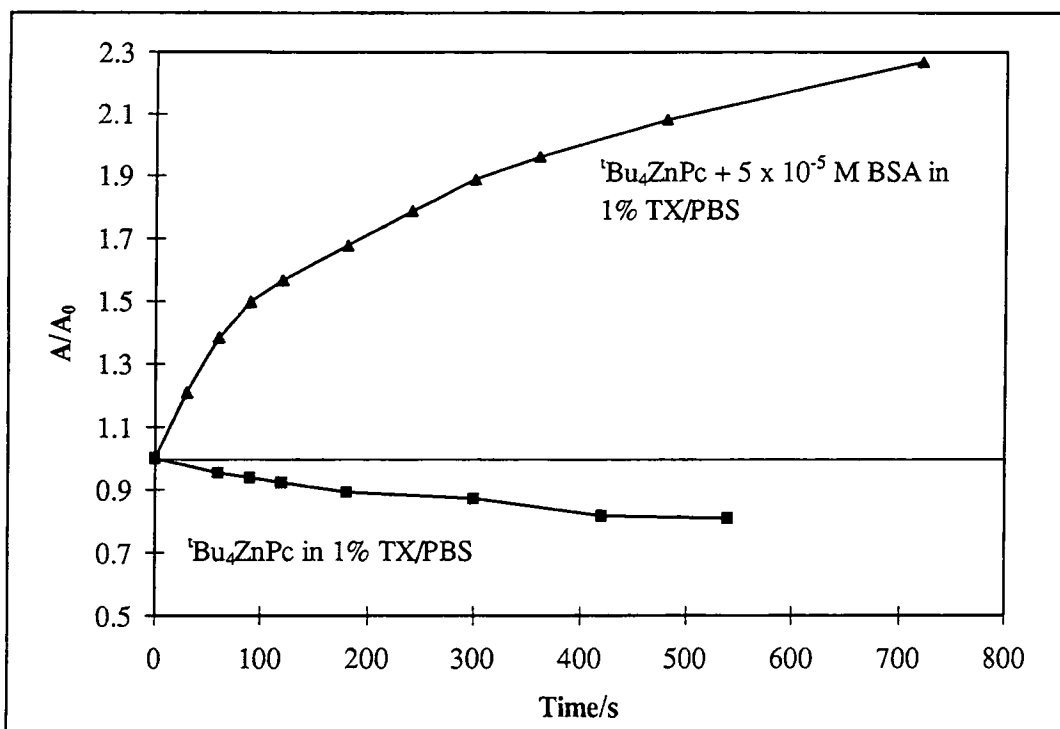
Figure 6.8. Increase in absorbance at 322 nm for $^tBu_4ZnPc + 5 \times 10^{-5} mol\ dm^{-3}$ BSA upon irradiation by red light ($\lambda > 610$ nm). Effect of irradiation on a phthalocyanine only solution is also shown.

Figure 6.8 also shows the change in absorbance at 322 nm of a phthalocyanine only solution. A decrease was observed which confirms that growth of absorption at 322 nm in the presence of BSA was not due to formation of photodegradation products of the phthalocyanine. Photooxidation of tryptophan is not a new or uncommon phenomenon and has been studied in detail by several groups[44],[45],[46].

In order to study the effect of BSA on phthalocyanine triplet state properties in the absence of photooxidation, 0.01 mol dm^{-3} NaN$_3$ was added to quench singlet oxygen species as they were produced ($k_Q = 3.8 \times 10^8$ dm^3 mol^{-1} s^{-1})[47], i.e. $\tau_\Delta = 0.25$ μs. Figure 6.9 shows an example of triplet state quenching by ground state oxygen under these conditions. In contrast to the results described above, monoexponential decays were recorded at all concentrations of oxygen and were independent of irradiation frequency.
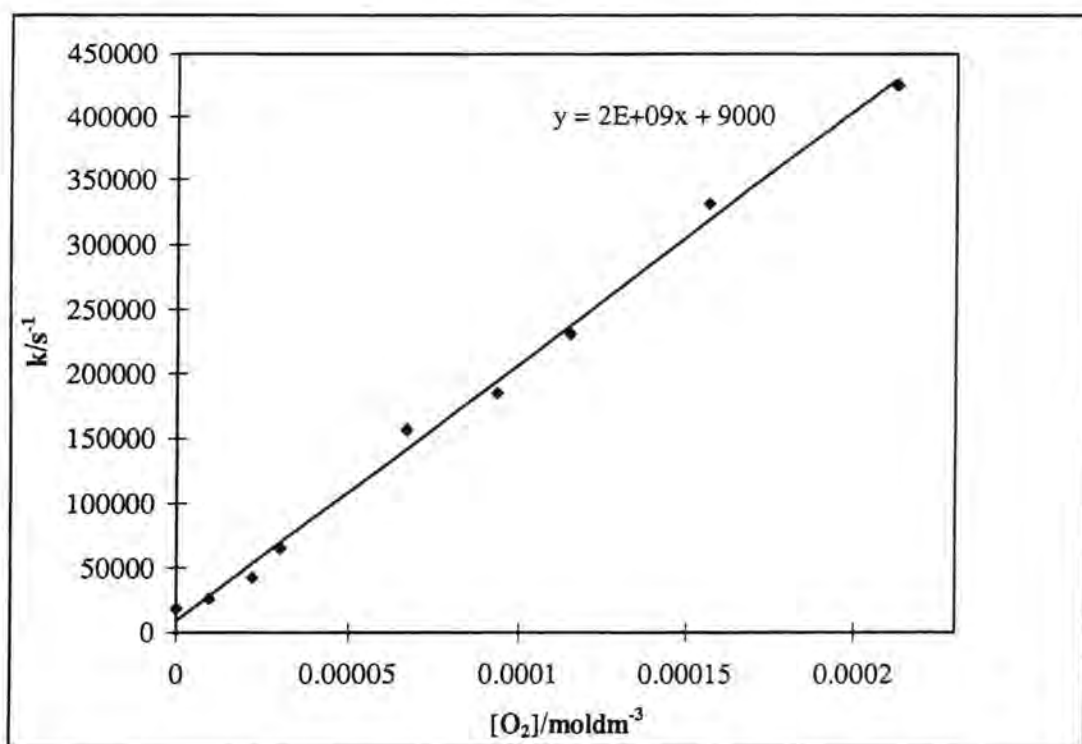
Figure 6.9. C10 triplet state quenching by O_2 in 1% TX/PBS.
($\lambda_{ex} = 638$ nm, ~ 0.2 mJ/pulse)

Table 6.4 collates quenching rate constants determined for each phthalocyanine and the effect of BSA.

Phthalocyanine	$k_Q /10^9$ dm^3 mol^{-1} s^{-1}
$^tBu_4ZnPc$	1.9 ± 0.2
$^tBu_4ZnPc$+BSA	1.4 ± 0.1
$ZnPcS_2$	1.2 ± 0.2
$ZnPcS_2$+BSA	1.0 ± 0.1
C10	1.4 ± 0.2
C10+BSA	1.9 ± 0.3

Table 6.4. Rate constants of triplet state quenching by oxygen in the presence of
5×10^{-4} mol dm^{-3} BSA.

Since k_Q was unaffected by the presence of BSA, it is apparent that BSA has no significant protective effect on the quenching of zinc phthalocyanine triplet state species by oxygen. It may be concluded, therefore, that the protective effects described above (Figure 6.7) were not a consequence of Pc:BSA binding and may be due to interaction with oxidised protein species. Several explanations present themselves. Firstly, it is

possible that whilst binding to parent BSA is very weak (if it is present at all), oxidation of tryptophan residues to NFK may promote binding either directly or through conformational changes of the protein. However, shifts in sensitiser ground state absorption spectra were not observed, thus, this explanation is unlikely. Secondly, and much more simply, it is possible that oxidation of protein molecules in the illuminated volume depleted the available supply of oxygen, hence reducing quenching ($k = 3100$ s^{-1}). Agitation of the sample regenerated the oxygen concentration and the triplet state species was quenched once more ($k = 270000$ s^{-1}). Alternatively, it is possible that photoinduced cross-linking of BSA occurred to create a protective network surrounding phthalocyanine, thus shielding excited states from deactivation. It is known that cross-linking of proteins occurs following amino-acid oxidation[48],[49], thus this may be a viable explanation, however, further work is required to confirm the reason for these results.

From the experimental observations described above, it is not possible to confirm Pc:BSA binding of ^{t}Bu$_4$ZnPc or C10. Fluorescence anisotropy measurements suggest an interaction, however, this has not been corroborated by any of the photophysical measurements performed. No effect on the absorption, fluorescence or triplet state properties was observed and triplet state quenching by oxygen was unaffected by the presence of BSA.

6.3.2 Electron Transfer Reactions
6.3.2.1 Simple Organic Quenchers
6.3.2.1.1 Results

Electron transfer reactions of excited state phthalocyanines with several simple amine and sulfur based quenchers have been investigated (Figure 6.10).
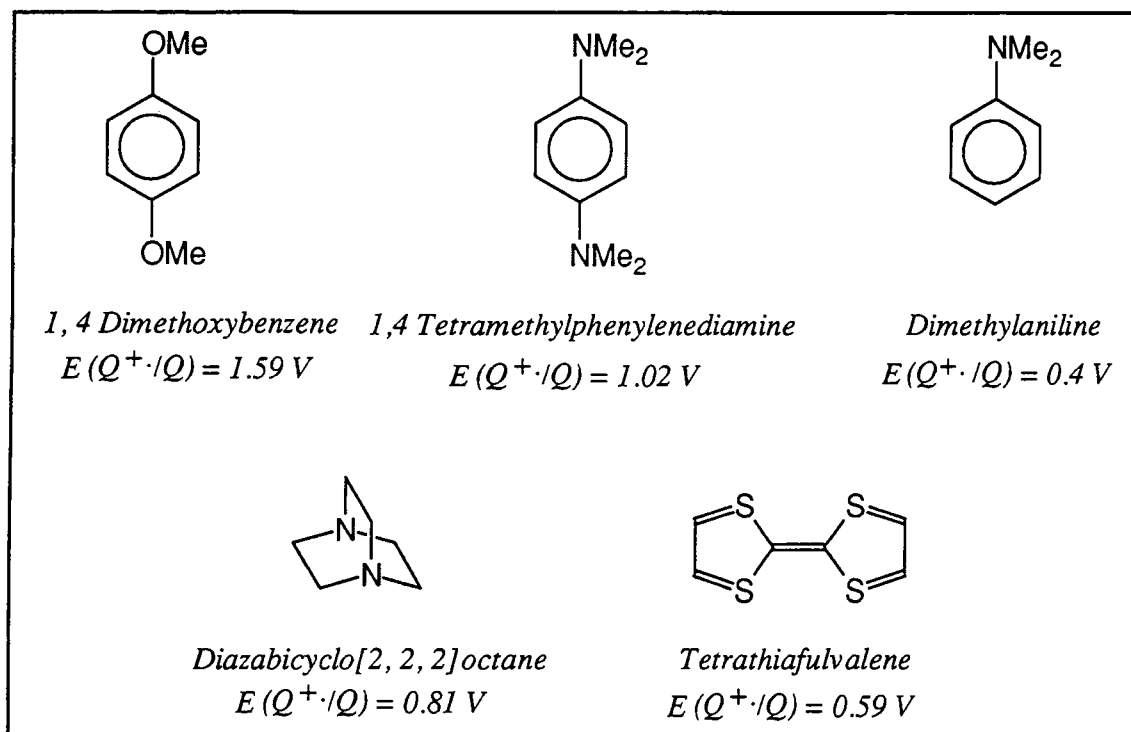
Figure 6.10. Structure of simple organic quenchers.

a) Diazabicyclo[2,2,2]octane (DABCO)

The fluorescence yield of ZnPc in 1% pyr/tol solution was unaffected by DABCO at concentrations below 0.01 mol dm^{-3}, however, a blue shift of the emission maximum, λ_{max}, from 680 nm to 679 nm was observed. A 1 nm hypsochromic shift of the ground state absorption spectrum was also observed (672 nm → 671 nm). Addition of further DABCO resulted in a steady decrease in the yield of fluorescence emission. λ_{max} remained constant at 679 nm and no further shift in the energy of the $S_1 \leftarrow S_0$ transition was detected. A Stern-Volmer analysis[50] (Equation 6.7) was performed to determine a rate constant, k_Q, for the quenching process.

$$\frac{\Phi_0}{\Phi} = 1 + k_Q \tau_F [Q] \qquad (6.7)$$

where Φ_0 is the yield of emission at $[Q] = 0$ mol dm^{-3}, Φ is the yield at a quencher concentration, Q, k_Q is the rate constant for quenching and τ_F is the fluorescence lifetime at $[Q] = 0$ mol dm^{-3}. Figure 6.11 shows the linear plot obtained.
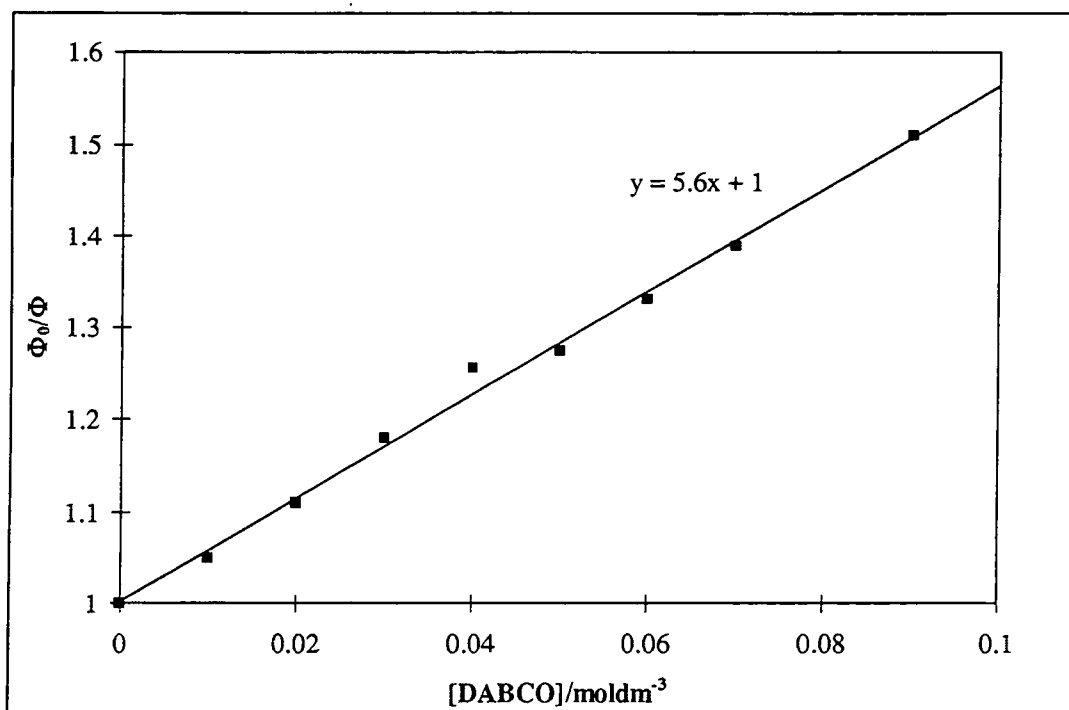
Figure 6.11.

Stern-Volmer plot showing quenching of ZnPc emission by DABCO in 1% pyr/tol.
$\tau_F = 3.5$ ns, $\lambda_{ex} = 630$ nm.

k_Q was calculated to be $1.6 \pm 0.1 \times 10^9$ dm^3 mol^{-1} s^{-1}. A fluorescence lifetime study of the quenching by DABCO was carried out, and a value of $k_Q = 1.2 \pm 0.1 \times 10^9$ dm^3 mol^{-1} s^{-1} determined. This value is an order of magnitude lower than the diffusion limited rate in toluene (1.1×10^{10} dm^3 mol^{-1} s^{-1}). τ_F was unaffected by 0.01 mol dm^{-3} DABCO.

It is unlikely that quenching was due to an energy transfer process since the singlet energy of DABCO is much greater than that of the phthalocyanine. The results described above may be explained by the reaction scheme depicted in Figure 6.12. K_b represents the equilibrium constant for complex formation and all other terms are defined in Section 6.1.2.1.

ZnPc $\underset{K_b}{\overset{DABCO}{\rightleftharpoons}}$ ZnPc.DABCO $\xrightarrow{h\nu}$ ^{1}ZnPc.DABCO* $\underset{DABCO}{\overset{k_d}{\rightleftharpoons}}$ ^{1}(DABCO...ZnPc.DABCO)*

Encounter Complex

k_{rev} - DABCO

k_a

k_{-a}

$^1(\,^2DABCO^{+\cdot} ... \,^2DABCO.ZnPc^{-\cdot}\,)^*$
Ion Pair

k_{diss}

DABCO$^{+\cdot}$ + DABCO.ZnPc$^{-\cdot}$
Solvated Ions
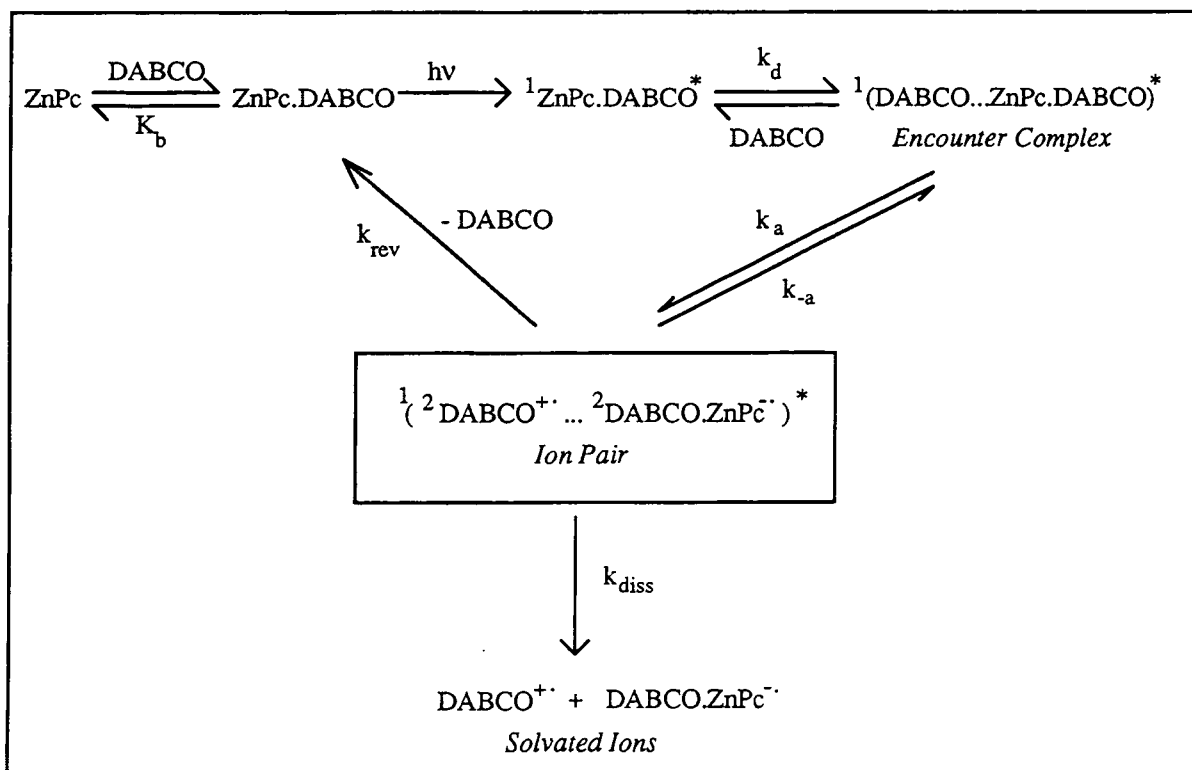
Figure 6.12. Formation of DABCO...ZnPc.DABCO ion pair upon irradiation of ZnPc in 1% pyr/tol in the presence of > 0.01 mol dm^{-3} DABCO.

Addition of small amounts of DABCO lead to the formation of a ground state complex - DABCO.ZnPc - in which a molecule of DABCO has replaced the pyridine as the axial ligand on the phthalocyanine . Evidence for this comes from the shift in the absorption spectrum. The fluorescence lifetime was unaffected by ligand exchange (0.01 mol dm^{-3} DABCO). It is possible that at concentrations of 0.01 mol dm^{-3} two opposing effects must be considered - a longer lifetime due to complex formation and reduction of this lifetime due to quenching - leading to a net zero change. Alternatively, the electrode potential of ZnPc may be changed by DABCO binding such that ZnPc.DABCO is less susceptible to reduction than ZnPc.py. Upon addition of further quantities of DABCO, photo-induced electron transfer from free DABCO molecules to ZnPc.DABCO was observed. This may be assumed to follow the reaction profile of Rehm and Weller[16]. Phthalocyanine radical anions could not be observed by nanosecond flash photolysis. This was for two reasons. Firstly, toluene is a non-polar solvent, hence solvation of radical products is poor and energetically unfavourable, i.e. k$_{diss}$ is small. Secondly, the ion pair resulting from singlet state quenching has a spin allowed back reaction. Consequently, k$_{rev}$ is large and observation of radicals produced by singlet state quenching is rare. Triplet state quenching by DABCO was not observed.

b) N, N-Dimethylaniline (DMA)

Quenching of phthalocyanine fluorescence by DMA followed a simple Stern-Volmer relation (Figure 6.13) with a quenching rate constant of $7.1 \pm 0.6 \times 10^8$ dm^3 mol^{-1} s^{-1} in 1% pyr/tol. No effect on the absorption spectrum was observed over the concentration range employed.
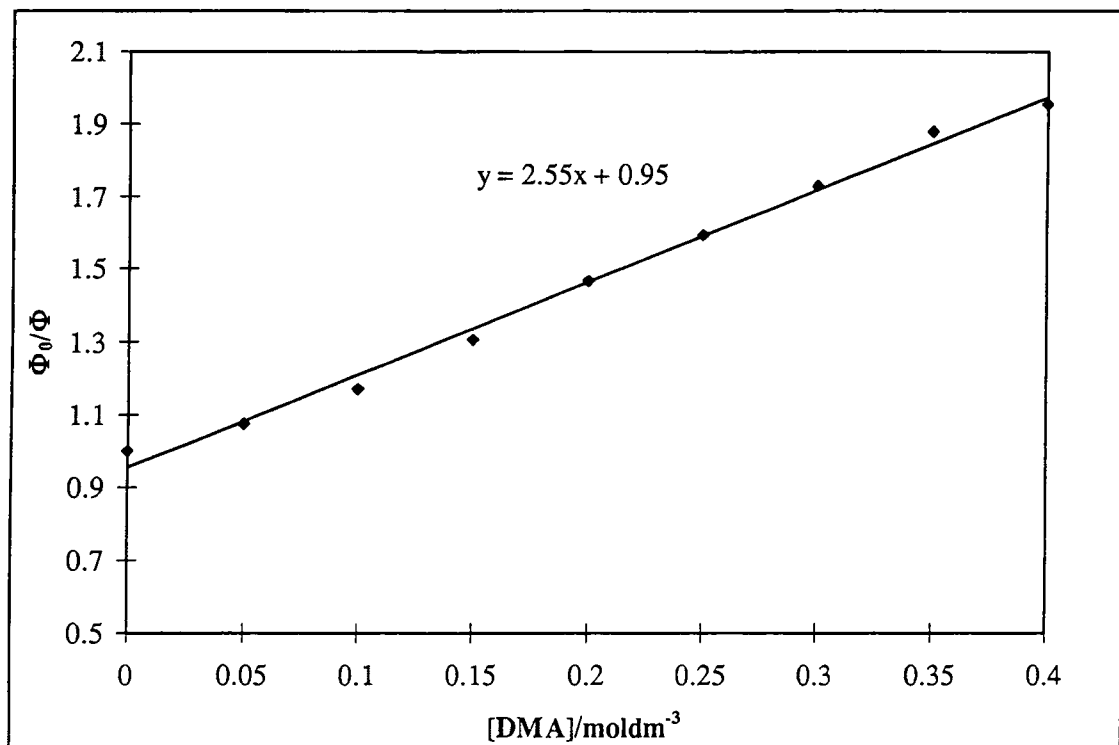
Figure 6.13. Stern-Volmer plot of ZnPc singlet state quenching by dimethylaniline in 1% pyr/tol, $\tau_F = 3.6$ ns, $\lambda_{ex} = 630$ nm.

No evidence of $^3\pi\pi^*$ state quenching was obtained, $k_Q < 10^5$ dm^3 mol^{-1} s^{-1}.

c) N, N, N', N'- Tetramethylphenylenediamine (TMPD)

Tetramethylphenylenediamine (TMPD) had no effect of the absorption properties of ZnPc, but acted as an efficient quencher of the first excited singlet state. A plot of Φ_0/Φ vs [TMPD] yielded a graph of positive curvature (Figure 6.14), and modification of the Stern-Volmer equation was necessary to account for this behaviour.
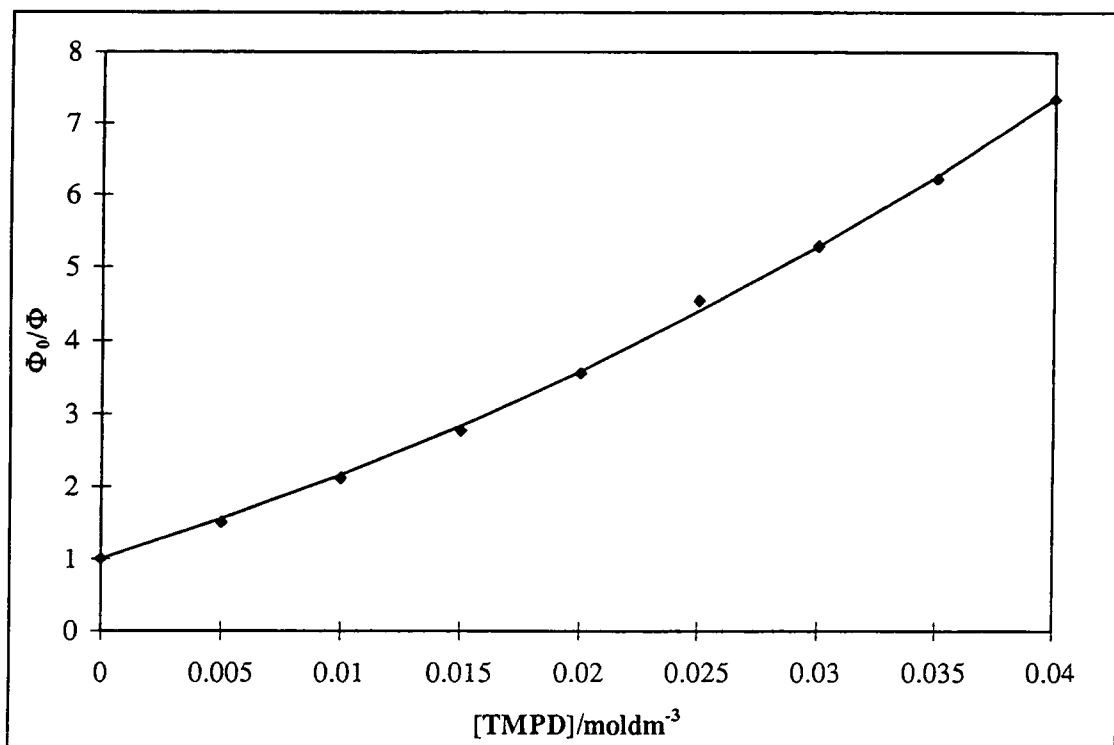
Figure 6.14. Stern-Volmer plot of ZnPc fluorescence quenching by TMPD in 1%
pyr/tol, $\tau_F = 3.5$ ns, $\lambda_{ex} = 630$ nm. Fit of static quenching model.

Curved Stern-Volmer plots can usually be accounted for using one of three explanations:

    i) Ground state complex formation

    ii) Static quenching

    iii) Finite sink approximation

Ground state complex formation can result in an increase in rate constant, k_Q, if the complex formed between fluorophore and quencher is non-fluorescent. Complex formation is usually indicated by a shift in the UV/Vis spectrum, therefore, in this case can be dismissed.

Static quenching[51],[52] occurs at high concentrations, when the fluorophore and quenching molecule are already within the interaction sphere of volume, V, on excitation. Under these conditions, diffusion is not required and quenching occurs almost instantaneously. The probability of this situation arising depends on the volume of interaction, V and the concentration of quencher molecules, [Q]. If the quencher is randomly distributed, then the probability of static quenching is given by the Poisson distribution, $e^{V[Q]}$. Thus, the Stern-Volmer equation may be modified[51] to give:

$$\frac{\Phi_0}{\Phi} = 1 + K_{SV} \ [Q] e^{V[Q]} \qquad\qquad (6.8)$$

where K_{SV} is the Stern-Volmer constant, $k_Q \tau_F$. Application of this equation to the experimental data gave a good fit (Figure 6.14). A quenching constant of $1.5 \pm 0.1 \times 10^{10} \ dm^3 \ mol^{-1} \ s^{-1}$ and a volume of interaction, V of $5.5 \ dm^3 \ mol^{-1}$ were determined. V represents the volume surrounding a fluorophore in which quenching may occur without the need for diffusion controlled collision of both reactants. The value determined in this study ($5.5 \ dm^3 \ mol^{-1}$) is comparable to that reported by Zeng[51] for static quenching of hydroxyl dimethyl carbazole by α-tocopherol ($3.7 \ dm^3 \ mol^{-1}$).

The finite sink approximation[53],[54],[55] is a modification of the Smoluchowski, Collins and Kimball (SCK) expression for the rate constant of a dynamic quenching system. This is based on a solution of the time independent flux equation[54] within the limits $[Q](\infty)$ at $r(\infty)$ and $[Q](R)$ at R, where R is the reactant encounter distance. This leads to Equation 6.9 (the reader is referred to References 53 and 54 for derivation of this equation).

$$k_Q = \frac{4\pi NDR k_a}{4\pi NDR + k_a} \qquad\qquad (6.9)$$

where N is Avogadro's constant, D is the sum of the diffusion coefficients of the reactants, and k_a is the activation energy controlled rate constant describing quenching at a distance R. In the case of efficient quenching, Equation 6.9 fails to account for a dependence of k_Q on the quencher concentration. An increase of k_Q with $[Q]$ may be due to static effects described earlier or to effects introduced by an initial time dependence of the concentration gradient. These can be eliminated by assuming that only the first encounter between fluorophore and quencher molecule is of importance, thereby defining an initial average separation, r_0 (sink radius). The diffusive region of interest will therefore lie within the limits $R < r < r_0$ and the flux equation can be integrated using the boundaries $[Q](r_0)$ at r_0 and $[Q](R)$ at R to give Equation 6.10.

$$k_Q = \frac{4\pi NDR k_a}{4\pi NDR + k_a \ (1 - R/r^0)} \qquad\qquad (6.10)$$

The sink radius, r_0 has been defined as the most probable nearest neighbour separation. Substitution of the appropriate distribution for r_0 ($r_0 = (2\pi N[Q])^{-1/3}$) into the inverse of

Equation 6.10 and division by the fluorescence lifetime in the absence of quencher, τ_f, yields the alternative Stern-Volmer relationship:

$$K_{SV}^{-1} = K_{SV}^{0}{}^{-1} - \frac{(2\pi N)^{\frac{1}{3}}}{4\pi ND\tau_F}[Q]^{\frac{1}{3}} \qquad (6.11)$$

where

$$K_{SV}^{0} = \frac{4\pi NDR\tau_F k_a}{4\pi NDR + k_a} = k_Q\tau_F \qquad (6.12)$$

Thus, the quenching coefficient, k_Q was obtained from the intercept of a plot of K_{SV}^{-1} vs $[Q]^{1/3}$ (Figure 6.15). k_Q using this approximation was calculated to be $1.2 \pm 0.1 \times 10^{10}$ dm^3 mol^{-1} s^{-1}.
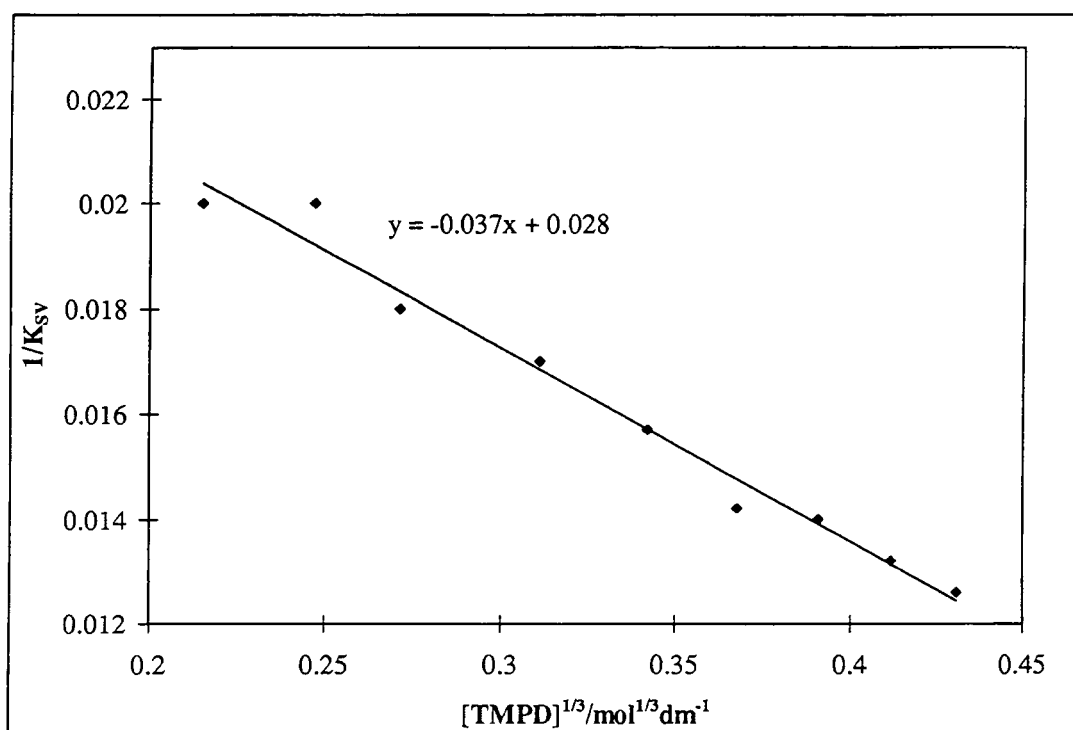
Figure 6.15. Application of finite sink approximation to TMPD quenching data.

For comparison, the rate obtained by fitting a straight line to the data acquired at low concentrations of TMPD was determined. In this case, $k_Q = 1.5 \pm 0.1 \times 10^{10}$ dm^3 mol^{-1} s^{-1}.

Flash photolysis investigations of $^3\pi\pi^*$ states of ZnPc in 1% pyr/tol solution revealed efficient quenching of the triplet state by TMPD (Figure 6.16). A quenching rate of 3.7

$\pm\ 0.3 \times 10^8$ dm^3 mol^{-1} s^{-1} was obtained from the gradient of a plot of k (rate of triplet state deactivation) vs [TMPD].
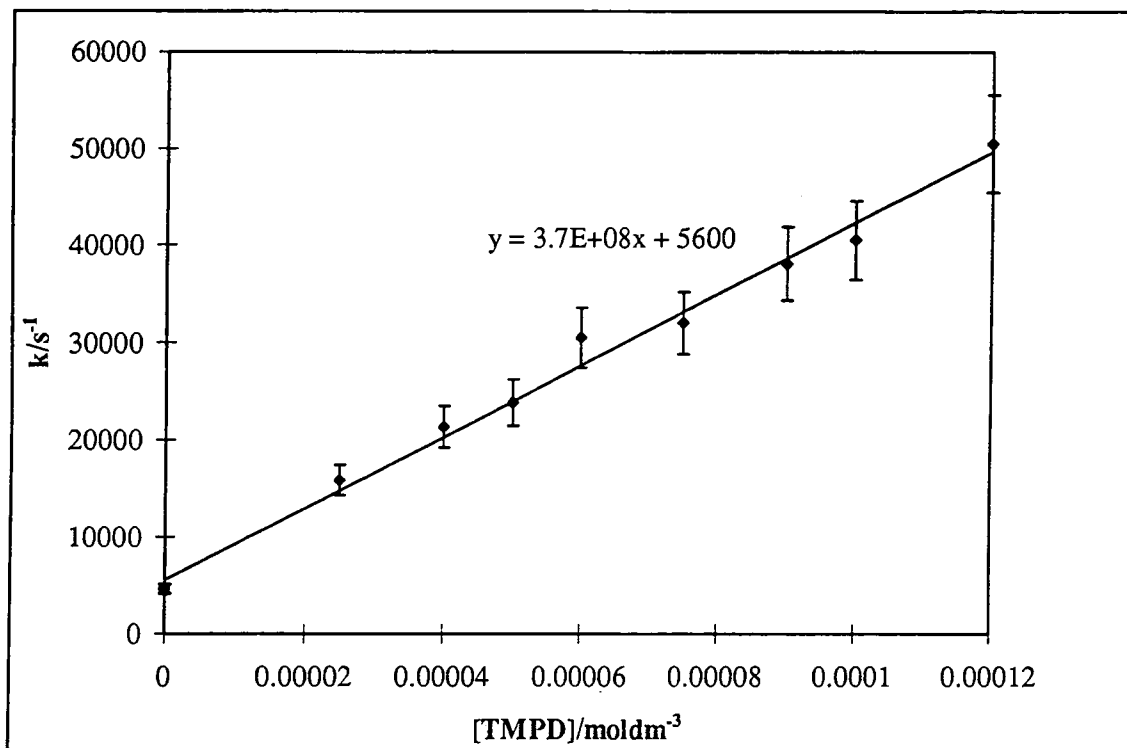
Figure 6.16. $^3ZnPc^*$ _Triplet state quenching by TMPD in 1% pyr/tol._

Triplet state quenching may be assumed to follow a mechanism analogous to that proposed for singlet state quenching (Figure 6.2). Due to the spin forbidden nature of back electron transfer by ion pairs formed though triplet state electron transfer, k_{rev} is slow and the rate of dissociation, k_{diss} may be expected to dominate. However, the non-polar nature of toluene inhibited ion pair separation and recombination occurred; thus no evidence of phthalocyanine radical anions was observed.

d) 1, 4 Dimethoxybenzene (DMB)

The absorption, fluorescence and triplet state characteristics of ZnPc in 1% pyr/tol were unaffected by DMB. It was concluded that complex formation between ground or excited states of phthalocyanine and dimethoxybenzene and electron transfer quenching of singlet or triplet state species by DMB did not occur.

e) Tetrathiafulvalene (TTF)

<u>i) Homogeneous Solution</u>

Tetrathiafulvalene (TTF) was found to efficiently quench the first excited singlet state of $^{t}Bu_4ZnPc$ in 1% pyr/tol, $k_Q = 1.1 \pm 0.1 \times 10^{10}$ dm^3 mol^{-1} s^{-1}, c.f. $k_{diff} = 1.1 \times 10^{10}$ dm^3 mol^{-1} s^{-1} in toluene. By contrast, when octadecylzinc phthalocyanine was used as the electron acceptor, no evidence of fluorescence quenching was observed. Electron transfer quenching of fluorescence emission from $^{t}Bu_4H_2Pc$ also yielded a diffusion limited quenching rate constant of $1.1 \pm 0.1 \times 10^{10}$ dm^3 mol^{-1} s^{-1} in toluene ($\tau_F = 5.6$ ns[56]). TTF had no effect on the lifetime of triplet state species. The fluorescence yields of coupled TTF-Pc complexes, Pc(TTF)$_8$ and Pc(TTF)$_4$ (Figure 6.3) were measured. Values of $< 10^{-4}$ and $1.7 \pm 0.3 \times 10^{-3}$ were obtained for Pc(TTF)$_8$ and Pc(TTF)$_4$, respectively. These yields are negligible when compared with that determined for the parent phthalocyanine, $^{t}Bu_4H_2Pc$ ($\Phi_F = 0.5$). We propose[29], that in compounds Pc(TTF)$_8$ and Pc(TTF)$_4$, rapid intramolecular electron transfer occurred between the covalently linked TTF moieties to generate a charge transfer state, which rapidly returned to the ground state, resulting in reduced fluorescence yields of these compounds.

<u>ii) Heterogeneous Solution</u>

Having established that TTF will undergo redox reactions with excited singlet state phthalocyanine in homogeneous solution, quenching kinetics in micellar solution (10% TX/H$_2$O) were investigated. Stern-Volmer plots obtained when singlet states of $^{t}Bu_4ZnPc$ and C10 in 1% TX/PBS were quenched by TTF in 10% TX/H$_2$O are displayed in Figure 6.17. The rate constants of electron transfer were estimated using the gradient at low concentrations of quencher molecules. Under these conditions it may be assumed that the concentration of surfactant (TX) was constant and that $[Q]_T = [Q]_L$, i.e. the total concentration of added quencher equals the concentration in the lipid phase. The value obtained for $^{t}Bu_4ZnPc$ ($k_Q = 1.8 \pm 0.1 \times 10^{11}$ dm^3 mol^{-1} s^{-1}) is an order of magnitude greater than that obtained in homogeneous media

In this system, it was possible to measure a decrease in the yield of fluorescence of C10 upon adding TTF ($k_Q = 5.4 \pm 1 \times 10^{10}$ dm^3 mol^{-1} s^{-1}). This value was unattainable in 1% pyr/tol solution. The large increase in k_Q in micellar solution may be explained by the location of fluorophore and quencher. Due to their hydrophobic nature, phthalocyanines and TTF are both expected to be located within the micellar core, allowing enhanced contact between the phthalocyanine and TTF, i.e. a much greater

proportion of static quenching. It can be deduced from the negative curvature of these graphs that the quenching rate constant decreased at high concentrations of donor molecules.
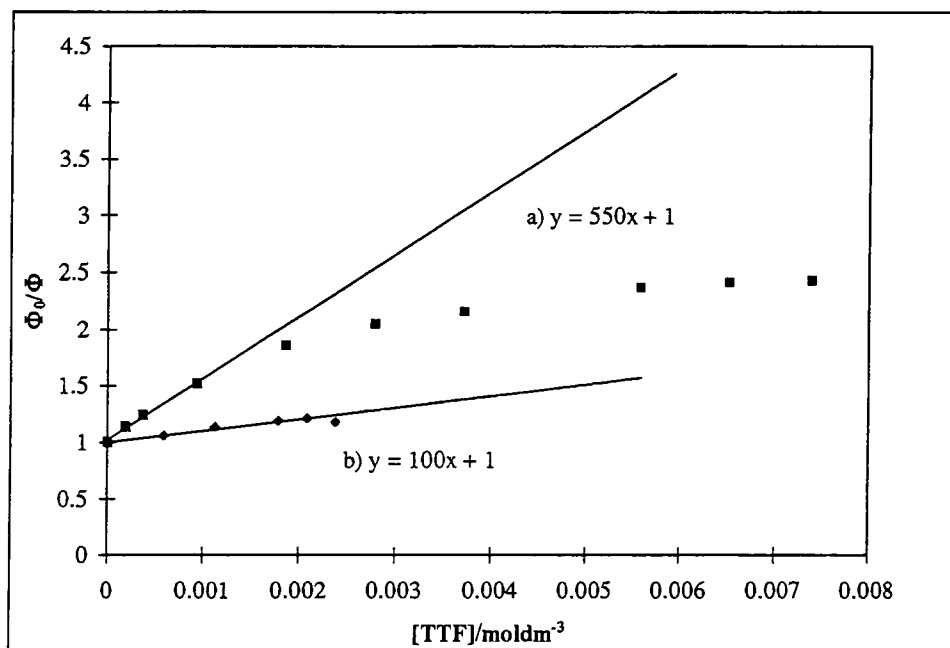
Figure 6.17.

Stern-Volmer plots for quenching of a) $^{t}Bu_{4}ZnPc$ in 1% $TX/H_{2}O$, $\tau_{F} = 3.6$ ns and b)
C10 in 1% $TX/H_{2}O$,$\tau_{F} = 2.2$ ns, by TTF in 10% $TX/H_{2}O$ ($\lambda_{ex} = 630$ nm).

This is unusual for micellar quenching studies since static quenching is known to lead to positive curvature in the Stern-Volmer plots (Section 6.3.2.1.1.c), indeed plots such as these have been routinely observed in micellar quenching studies[20],[57]. It is probable that negative curvature observed in this study was due to a concurrent increase in [micelle] with [quencher]. The mean number of quencher molecules associated with each micelle may be given[58] by Equation 6.13.

$$< n >= \frac{[Q]}{[Surfac\,tan\,t] - cmc\,/\,\overline{N}} \qquad (6.13)$$

where <n> is the mean number of quencher molecules per micelle, [Q] is the total quencher concentration, [surfactant] is the concentration of surfactant (Triton X), cmc is the critical micelle concentration of Triton X (0.24 mmol dm^{-3}) and $\overline{N}$ is the aggregation number of each micelle (143)[59]. Thus, an increase in [surfactant] at any particular [Q] leads to a decrease in <n>, i.e. the number of quenchers available per fluorophore (assuming a maximum of one fluorophore per micelle). Alternatively, a dependence of

k_Q on [Q] may be due to partitioning properties of Q (TTF) between the aqueous and lipid phases. If the concentration of TTF in the lipid phase does not increase linearly as the total concentration increases, the increase in accessible quencher molecules would become progressively smaller leading to a reduced quenching rate. The rate constant, k_Q, determined in this study is a complex mix of many parameters including the micellar concentration, the quenching rate constant in the lipid phase, k_Q', the volume of activation for static quenching, V and the partitioning coefficient, K_p or binding coefficient[60], K_b. It is not possible to determine these parameters without further work regarding the effect of micellar concentration on the quenching rate.

Quenching of phthalocyanine triplet states by TTF was investigated, however, no reduction in lifetime or formation of radical species was observed in either polar (MeCN) or non-polar solvents (pyr/tol).

6.3.2.1.2 Discussion

Table 6.5 summarises the quenching rate constants determined in this study.

Phthalocyanine	Quencher	Solvent	$k_Q(S_1)$ /dm^3 mol^{-1} s^{-1}	$k_Q(T_1)$ /dm^3 mol^{-1} s^{-1}
ZnPc	DABCO	1% pyr/tol	$1.4 \pm 0.2 \times 10^9$	$< 10^5$
ZnPc	DMA	1% pyr/tol	$7.1 \pm 0.6 \times 10^8$	$< 10^5$
ZnPc	TMPD	1% pyr/tol	$1.5 \pm 0.1 \times 10^{10}$a $1.5 \pm 0.1 \times 10^{10}$b $1.2 \pm 0.1 \times 10^{10}$c	$3.7 \pm 0.4 \times 10^8$
ZnPc	DMB	1% pyr/tol	$< 2.5 \times 10^8$	-
^{t}Bu$_4$ZnPc	TTF	1% pyr/tol	$1.1 \pm 0.1 \times 10^{10}$	$< 1.5 \times 10^6$
C10		1% pyr/tol	-	-
^{t}Bu$_4$ZnPc		10% TX/H$_2$O	$1.8 \pm 0.1 \times 10^{11}$	-
C10		10%TX/H$_2$O	$5.4 \pm 1 \times 10^{10}$	-
^{t}Bu$_4$H$_2$Pc		1% pyr/tol	$1.1 \pm 0.1 \times 10^{10}$	-

a. Static Quenching Model, b. Approximation using linear fit at low concentrations of quencher, c. Finite Sink Model.

Table 6.5. Summary of electron transfer rates.

Experimentally determined values of k_Q may be compared to those predicted by Rehm Weller theory. Equations 6.1 and 6.3 were used to calculate the free energy of activation, $\Delta G^\#$ and the overall free energy change for the electron transfer process, ΔG.

Substituting these parameters into Equation 6.2 allowed the predicted value of k_Q to be calculated. k_d was estimated[61] using Equation 6.14.

$$k_d = \frac{8RT}{3\eta} \qquad\qquad (6.14)$$

where R is the gas constant (8.314 J K^{-1} mol^{-1}), T is the temperature (298 K) and η is the viscosity of the solvent. The term $k_d/\Delta V_d k_{deac}$ was estimated as 0.25 and $\Delta G^{\#}(0)$ as 10 kJ mol^{-1} (the values determined by Weller for acetonitrile solution). Although, strictly speaking, this value will vary with solvent, the magnitude of the change is not expected to have a significant effect on the calculated value of k_Q, thus, this approximation is deemed reasonable. The reaction encounter distance, a was estimated as 1 nm. A further approximation that should be noted is that reported reduction potentials have been used which were not measured in the same solvents as those employed in this study. Table 6.6 collates calculated values for quenching of $^1Pc^*$ species of ZnPc or $^tBu_4ZnPc$. The ground state redox potential of these phthalocyanines has been taken as E (ZnPc / ZnPc$^-$) = -0.6 V[62] and the singlet state energy, $\Delta E_{0,0}$, as 1.83 eV[20].

Quencher	E (Q^{+}/Q) V vs NHE	ΔG /kJ mol^{-1}	$\Delta G^{\#}$ /kJ mol^{-1}	k_Q (calc) /dm^3 mol^{-1} s^{-1}	k_Q (obs) /dm^3 mol^{-1} s^{-1}
TMPD	0.4[16]	-138	0.72	8.3 x 10^9	1.5 x 10^{10}a
TTF	0.59[63]	-120	0.83	8.1 x 10^9	1.1 x 10^{10}b
DABCO	0.81[64]	-99	1	8 x 10^9	1.4 x 10^9
DMA	1.02[16]	-78.3	1.24	7.8 x 10^9	7.1 x 10^8
DMB	1.59[16]	-23.2	3.71	5 x 10^9	< 2.5 x 10^8

a. Calculated using static quenching model, b. Phthalocyanine = $^tBu_4ZnPc$.

Table 6.6. Calculated quenching rates of $^1ZnPc^*$ by simple organic electron donors in 1% pyridine / toluene.

Comparison of these values with those obtained experimentally (Table 6.5) shows that some discrepancy exists between theoretically predicted values and data obtained. Weller suggested that a reaction proceeding within a factor of two of the theoretical rate constant may be assumed to follow an outer sphere electron transfer mechanism. TMPD and TTF fit this criterion well. The observed rates of quenching by DABCO, DMA and DMB are somewhat slower than predicted. Since it has been shown that DABCO forms a complex with ZnPc before quenching occurs, it is not surprising that in this case, k_Q was slower than that expected for pure electron transfer. In addition, calculated k_Q

values are critically dependent on the electrode potentials chosen for quencher compounds and reduction of the ground state of phthalocyanine. Some variation exists in published values for electrode potentials; for example, values of -0.6 V[62] and -0.72 V[65] are reported for E (ZnPc / ZnPc$^-$·) and values for E (DABCO$^+$· / DABCO) range from 0.81 V[63] to 1.14 V[66]. Thus, inaccuracy in predicted values of k_Q is not surprising. Perhaps most significantly, use of toluene as solvent may have a large effect on E for all species involved. In the main, literature values reported were determined in acetonitrile, a highly polar solvent, in which electron transfer properties are expected to be different to those in a non-polar solvent such as toluene. Poor solubility of ZnPc in MeCN prevented experiments being performed in this solvent system.

Quenching of $^3Pc^*$ by DABCO, DMA and TTF was not observed. Quenching by TMPD was a factor of thirty slower (3.7 x 10^8 dm^3 mol^{-1} s^{-1}) than the calculated diffusion controlled rate in toluene (1.1 x 10^{10} dm^3 mol^{-1} s^{-1}). The concentration of quencher molecules is in large excess over the concentration of excited phthalocyanine species, thus, changes in the concentration via reaction with singlet state species will be minimal. In addition, it may be shown using Equation 6.7 and the calculated rate constant for singlet state quenching (1.4 x 10^{10} dm^3 mol^{-1} s^{-1}) that at the concentrations of TMPD used for triplet state quenching ($< 10^{-4}$ mol dm^{-3}) $< 1\%$ of singlet state species have been quenched, hence, this is unlikely to account for such a large difference. A more plausible explanation is that triplet state quenching is activation controlled as opposed to singlet state quenching which is diffusion controlled.

Studies comparing quenching of ZnPc with peripheral tertiary butyl and decyl ligands by TTF, have clearly demonstrated that $^tBu_4ZnPc$ is a better electron acceptor than C10. This may be for a number of reasons. Firstly, the energy required to produce the singlet state of C10 is lower than that of $^tBu_4ZnPc$, leading to a lower excited state reduction potential. The reduction potential of $^1(^tBu_4ZnPc)^*$ was calculated[67] to be 1.23 V whilst that of $^1(C10)^*$ was only 1.17 V (assuming the ground state reduction potential to be the same as ZnPc (-0.6 V)). However, substitution of these values into Equations 6.1 to 6.3 leads to k_Q (calc) in H$_2$O = 4.5 x 10^9 dm^3 mol^{-1} s^{-1} for $^tBu_4ZnPc$ vs 4.4 x 10^9 dm^3 mol^{-1} s^{-1} for C10. Thus, quenching rates would not be expected to be significantly different. Alternatively, it is possible that during studies performed in micellar solution, each phthalocyanine may be located in a different region of the micelle, leading to varying accessibility to quencher molecules. Zhang et al.[68] have shown that the electron transfer rate from tyrosine to tetra sulfonated gallium phthalocyanine (GaPcS$_4$) was greatly increased upon incorporation into micelles of cetyltrimethylammonium chloride (CTAC). By contrast, that of disulfonated zinc phthalocyanine (ZnPcS$_2$) was unaffected.

This difference in behaviour was ascribed to location of GaPcS$_4$ on the surface of the micelle and ZnPcS$_2$ in the inner hydrophobic core. However, in this study, a similar trend was observed in homogeneous solution, i.e. quenching of fluorescence originating from ^{t}Bu$_4$ZnPc was observed whilst that of C10 was unaffected. It is unlikely, therefore, that the observed differences were caused solely by the position of the sensitiser within the micelle. A final consideration concerns the value of ground state reduction. It has been assumed that E (C10/C10$^-$) and E (ZnPc/ZnPc$^-$) are equivalent. The observed differences in k$_Q$ may be explained if this is not the case and C10 is inherently less likely to participate in electron transfer processes. This appears reasonable when published data is considered since peripheral CN substituents have been shown to have a large effect on the reduction potential of ZnPc (E (ZnPc(CN)$_8$) / (ZnPc(CN)$_8$)$^-$ = 1.0 V)[62].

6.3.2.2 Biological Molecules
6.3.2.2.1 Amino Acids

Having shown that amines will react with the excited states of phthalocyanines, photodynamic interaction with amino acids and their derivatives was investigated. Electron transfer reactions of N-acetyl tryptophanamide, ^{t}BOC methionine, cysteine and N-acetyl tyrosinamide (Figure 6.18) were studied.

tBOC Methionine

Cysteine

N-Acetyl Tryptophanamide

N-Acetyl Tyrosinamide
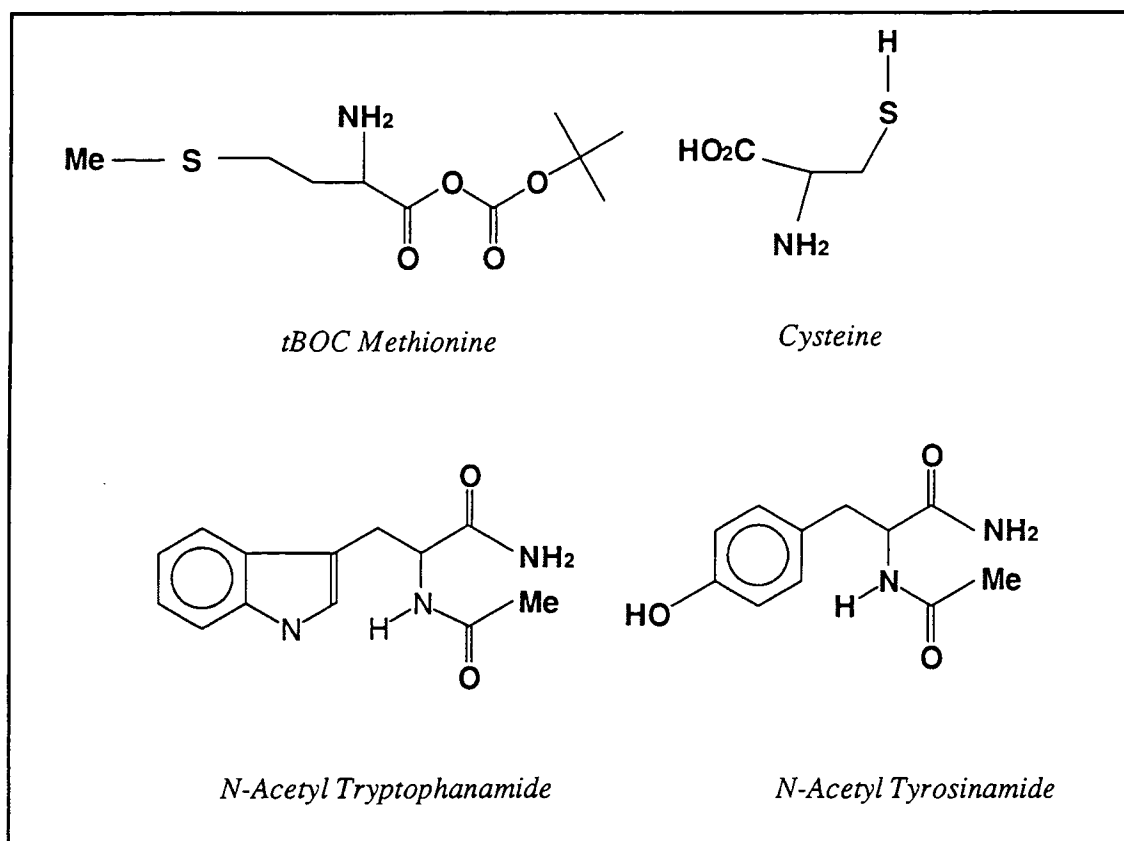
Figure 6.18. Structures of amino acids.

No evidence of quenching of $^tBu_4ZnPc$ singlet state species was detected for any of the aminoacids under study in either methanol or 1% TX/H_2O solution ($k_Q < 1.4 \times 10^9$ dm^3 mol^{-1} s^{-1}).

Studies of $^tBu_4ZnPc$ triplet state quenching by ^tBOC methionine in methanol revealed a non-linear reduction in the lifetime of $^3\pi\pi^*$ species with increasing ^tBOC methionine concentrations (Figure 6.19). No effect on the wavelength of maximum ground state absorption was observed at ^tBOC methionine concentrations of 0.01 mol dm^{-3} so it was assumed that ground state complex formation did not occur. No evidence for the formation of radical species was obtained. The wavelength of maximum absorption of triplet species, $\lambda_{max} = 490 \pm 10$ nm, was unaffected by the addition of 0.01 mol dm^{-3} ^tBOC methionine.
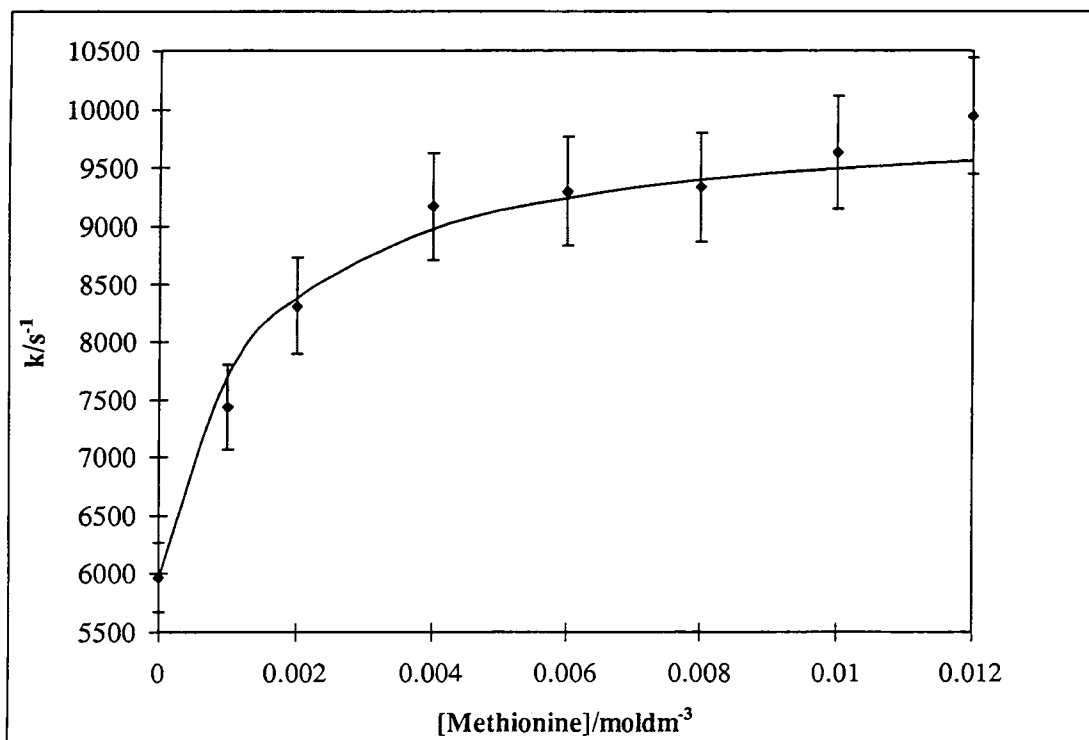
Figure 6.19. Increase in rate of decay of $^3\pi\pi^*$ states of $^tBu_4ZnPc$ in MeOH upon addition of ^tBOC methionine. The fit of Equation 5.9 (substituting [Met] for [H^+]) to the data is also shown.

Methionine has been shown to have a reduction potential of 1.34 V vs NHE, thus Equation 6.1 predicts an endothermic electron transfer reaction with phthalocyanine. In addition, no evidence of radical species was obtained, therefore, quenching of τ_T by this mechanism is unlikely. It is probable that methionine (Met) formed an excited state complex (exciplex) with triplet state zinc phthalocyanine ($^3Pc^*$) which existed in

equilibrium with unbound species (Figure 6.20). As the concentration of ^{t}BOC methionine increased, the equilibrium shifted to the right, forming a complex with decay rate, k_2. At zero concentration, the measured rate of decay was representative of that of the parent phthalocyanine, k_1. Experimentally, two limiting cases, k_1 and k_2, were measured to be 6000 ± 300 s^{-1} and 9500 ± 500 s^{-1} respectively. These correspond to a lifetime of 100 μs for bound Pc.Met species (0.01 mol dm^{-3} ^{t}BOC methionine) and 170 μs for ^{t}Bu$_4$ZnPc (0 mol dm^{-3} ^{t}BOC methionine). At intermediate concentrations of ^{t}BOC methionine, the measured decay was representative of the average lifetime of bound and unbound phthalocyanine species. Monoexponential character was retained, indicating a fast binding equilibrium relative to the rate of triplet state deactivation (Section 5.3.1.2). Figure 6.19 shows the fit of Equation 5.9 (substituting [Met] for [H$^+$]) to the measured data. A value of 770 dm^3 mol^{-1} was calculated for K*.
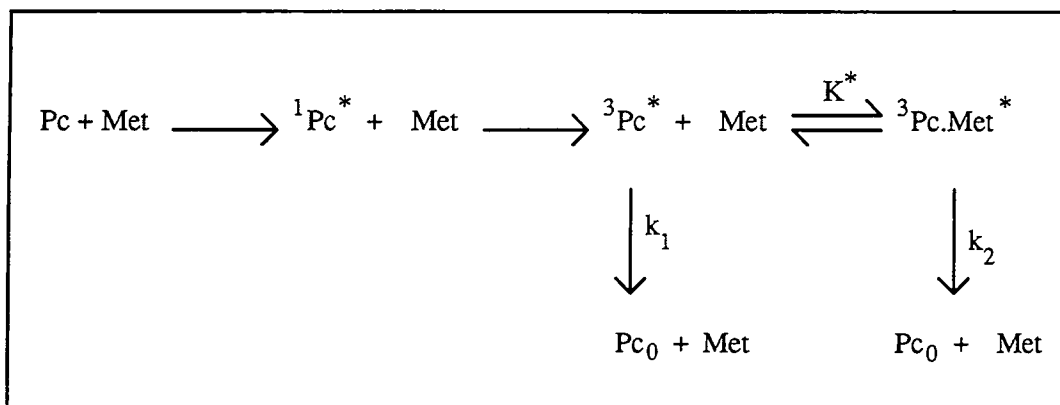
Figure 6.20. Formation and decay of ^{3}Pc.Met Complex.*

Exciplex formation is encouraged by net stabilisation of the electrons which occupy the HOMO of both species. Consider complex formation in terms of molecular orbital theory[69]. Upon binding of two species, HOMO's and LUMO's interact to produce two new molecular orbitals, one destablised with respect to the originals and one stabilised (Figure 6.21). In ground state complexes, a net stabilisation of zero is obtained since two electrons are stabilised and two are destabilised. However, in excited state complexes, three electrons are stabilised and only one is destabilised, leading to net stabilisation upon complex formation.
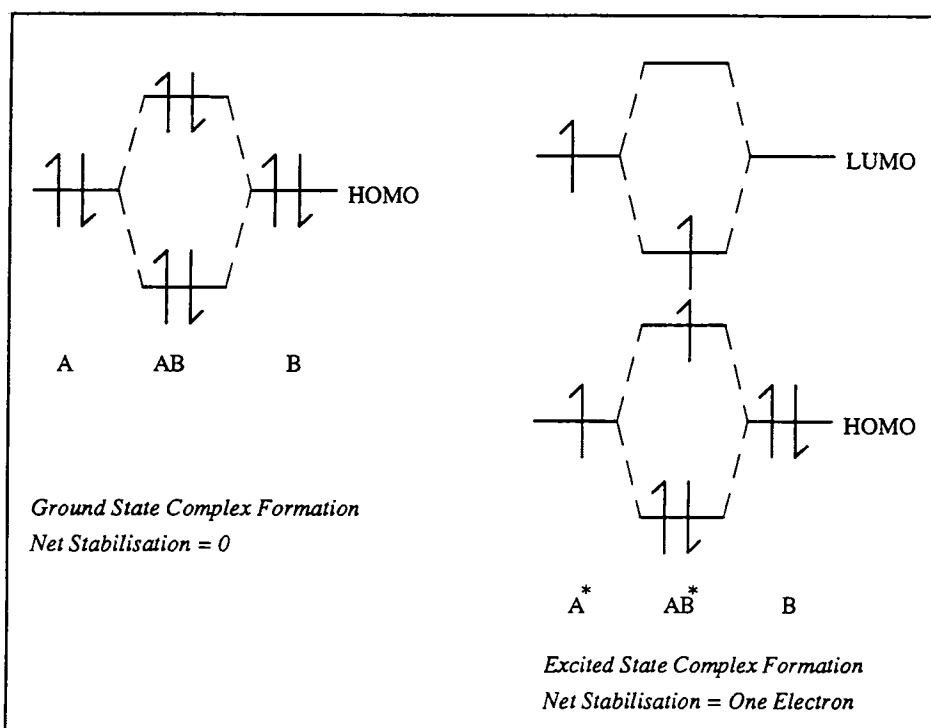
Figure 6.21. Molecular orbital description of exciplex formation.

Flash photolysis studies of tryptophan, tyrosine and cysteine derivatives in MeOH or 1% TX/H_2O solution showed the lifetime of $^3Pc^*$ to be unaffected by concentrations up to 0.01 mol dm^{-3} tryptophan and tyrosine and 0.5 mol dm^{-3} cysteine. This places maximum limits on the quenching rate of 1×10^5 dm^3 mol^{-1} s^{-1} and 1×10^3 dm^3 mol^{-1} s^{-1} respectively.

Using Weller's equations (Section 6.1.2.1), theoretical quenching rate constants may be calculated (Table 6.8). Due to the polar nature of MeOH the electrostatic term of Equation 6.1 is very small (~ 0.04 eV) and was neglected in calculations. Considering these values, it is surprising that electron transfer from tryptophan, tyrosine and cysteine derivatives to singlet state phthalocyanine species was not observed. It might also be expected that cysteine would undergo reaction with triplet state phthalocyanine. Triplet state quenching by tryptophan and tyrosine species, however, is highly energetically unfavourable and consequently it is not surprising that evidence of reaction was not obtained.

Amino Acid	$E (Q/Q^{+})$ /V	k_Q (Singlet) /dm^3 mol^{-1} s^{-1}	k_Q (Triplet) /dm^3 mol^{-1} s^{-1}
Cysteine[3]	0.63	7.4×10^9	1.7×10^7
Tyrosine[3]	0.93	5.9×10^9	5.4×10^2
Tryptophan[3]	1.01	4.9×10^9	90
Methionine[70]	1.34	4.9×10^7	-

Table 6.8. Calculated quenching rates of $^tBu_4ZnPc^*$ by amino acids in MeOH.

Despite apparent contradiction with theory, these results are consistent with experimental observation of other groups. Studies on the binding of AlPcS$_2$ to human serum albumin by Foley et al.[37] have shown that the lifetime of the singlet state is affected by complexation. Evidence of a component with a reduced fluorescence lifetime suggests that the emission must be quenched in some way, possibly by amino acid residues on the protein. However, quenching studies, showed no evidence of phthalocyanine singlet or triplet state quenching by tryptophan, tyrosine, methionine, glutathione or histidine. A rate constant of 7×10^5 dm^3 mol^{-1} s^{-1} was measured for cysteine quenching of the triplet state[3]. No such quenching of excited states of zinc phthalocyanine by bovine serum albumin has been recorded (Section 6.3.1.2). The photooxidation of tyrosine and tryptophan by aluminium phthalocyanine (AlPc) and gallium phthalocyanine (GaPc) and the mechanism of oxidation of tyrosine by GaPc and ZnPc have been investigated by Ferraudi[71] and Zhang[68] respectively. They have shown that the propensity of phthalocyanine to undergo Type I reactions was largely dependent on the identity of the central metal ion. ZnPc was the least reactive of these ($k < 10^5$ dm^3 mol^{-1} s^{-1}) and in flash photolysis studies there was no evidence of radical species being produced. The rate of photooxidation was also found to be highly dependent on the pH of the solution. Maximum rates were obtained at pH's of 10 or 11 indicating that the phenoxide form of tyrosine and the deprotonated form of tryptophan are more efficient electron donors. At pH 7, the conditions employed in this study, the yield of radical ions was negligible.

6.3.2.2.2 Ascorbic Acid

Ascorbic acid, commonly known as Vitamin C, is an essential component in most biological tissue (0.4 nmol dm^{-3})[72]. The possible role of ascorbic acid in photoinduced Type I reactions was investigated by studying its effect on the excited states of $^tBu_4ZnPc$. Ascorbic acid palmitate, in which the 6-hydroxy group of ascorbic acid is esterified by a fatty acid (Figure 6.22), was used to promote solubility in organic solvents. The functional groups which influence electron transfer reactions of this material are retained.

Ascorbic Acid   *Ascorbic Acid Palmitate*
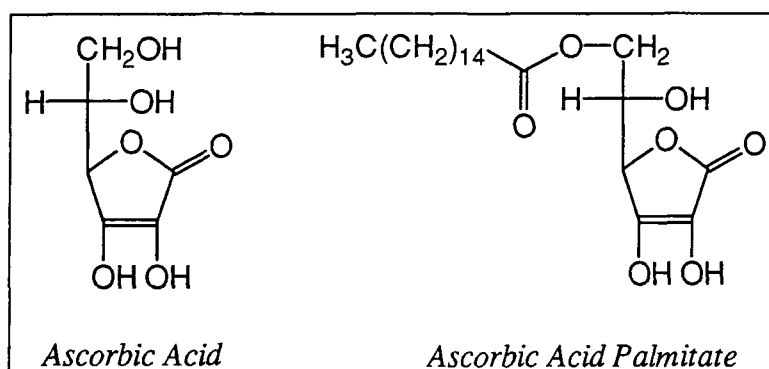
Figure 6.22. Structures of ascorbic acid (AA) and ascorbic acid palmitate (AAP).

Homogeneous Solution

Quenching of excited singlet states of ZnPc in 1% pyr/tol by ascorbic acid palmitate (AAP) was prohibited due to solubility factors. A maximum concentration of 2×10^{-3} mol dm^{-3} AAP was achieved. At this concentration, no effects on the ground state absorption spectrum or fluorescence emission properties of phthalocyanine were observed. In methanolic solution a concentration of 0.02 mol dm^{-3} was attained - again fluorescence quenching was not observed ($k_Q < 7.1 \times 10^8$ dm^3 mol^{-1} s^{-1}).

AA and AAP in methanolic solution quenched the lifetime of $^3\pi\pi^*$ states of $^tBu_4ZnPc$. Figure 6.23 shows the increase in the rate of deactivation of T_1 measured with increasing concentration of AA and AAP. The presence of a new absorbing species at 570 nm and 600 nm with a lifetime of ~2500 μs (Figure 6.24) was used to infer an electron transfer process. The measured transient shows rapid decay of triplet state followed by absorption and gradual deactivation to the ground state of a long lived species. Figure 6.25 depicts the transient absorption spectrum of this species.
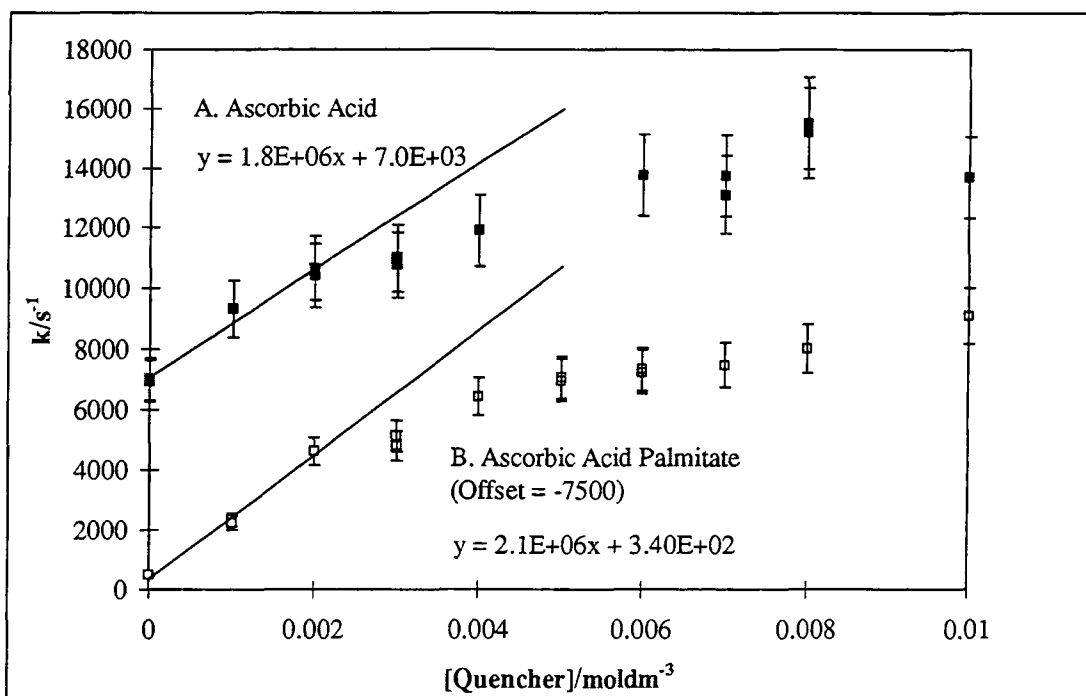
Figure 6.23. Quenching of the triplet state of $^tBu_4ZnPc$ by ascorbic acid and ascorbic acid palmitate in MeOH. Points measured for each quencher have been offset for clarity.
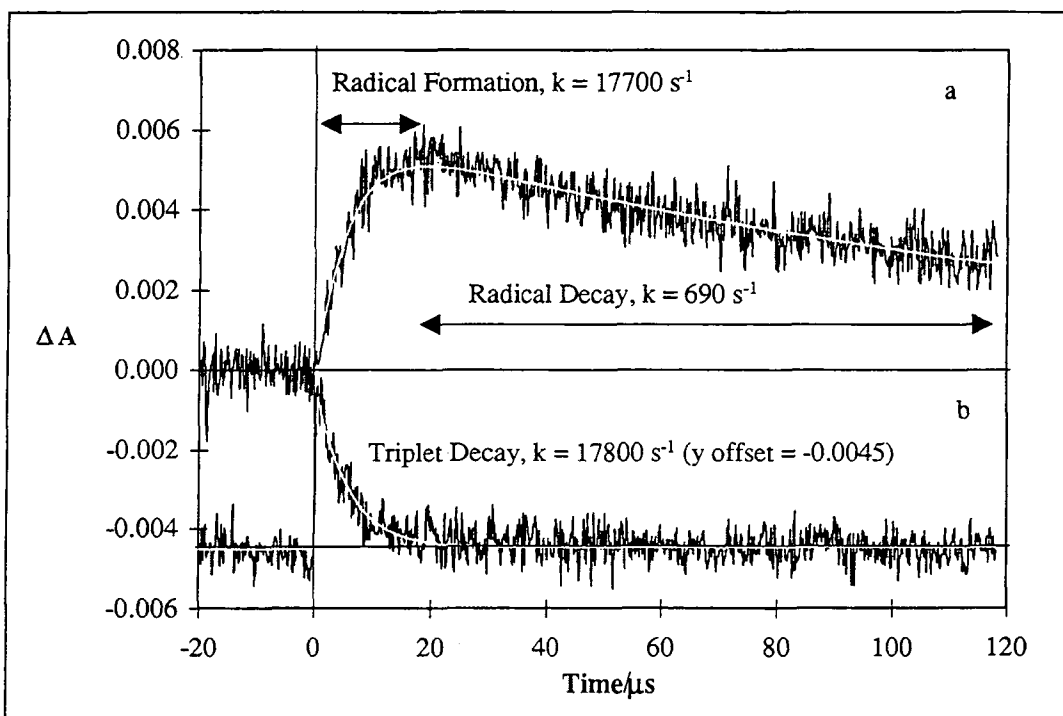
Figure 6.24. Transient study of $^tBu_4ZnPc$ in MeOH + 0.01 mol dm^{-3} ascorbic acid palmitate, $\lambda_{ex} = 638$ nm. Deactivation of triplet species (b) (probe wavelength = 490 nm) and formation and decay of Pc$^-$ radical (a) (probe wavelength = 600 nm). Decays have been offset for clarity.

225
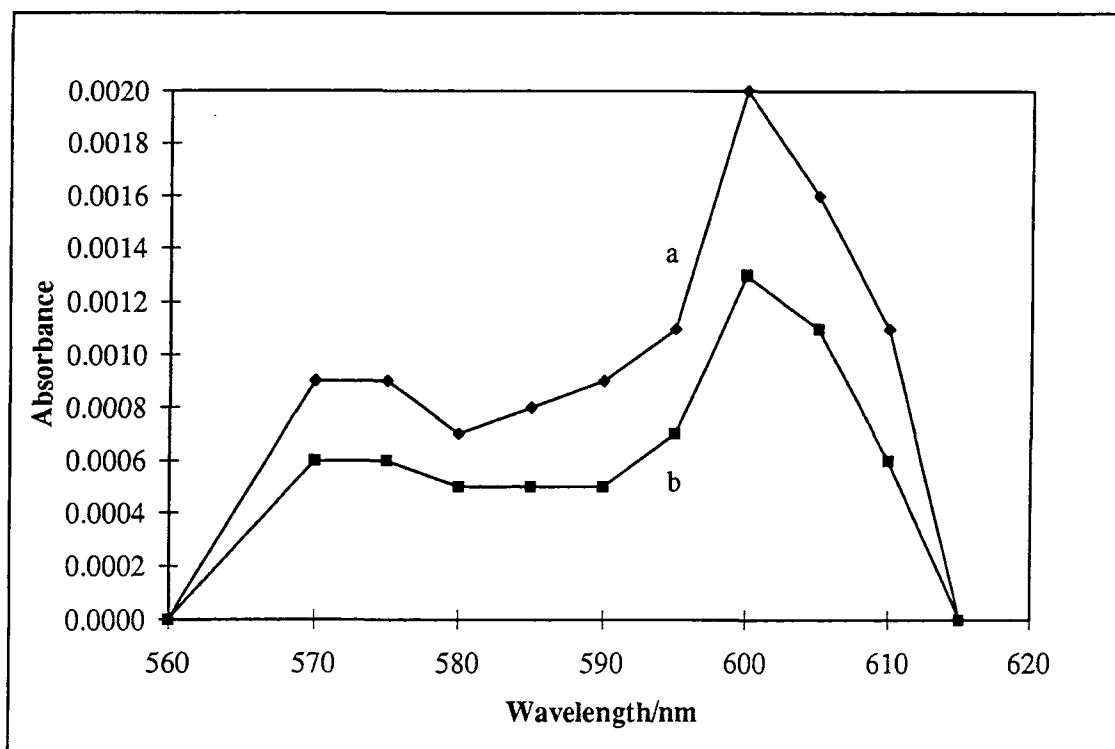
Figure 6.25. Transient absorption spectrum of $^tBu_4ZnPc^-$ radical in MeOH.
a) $\Delta t = 300$ μs, b) $\Delta t = 1$ ms ($\lambda_{ex} = 638$ nm).

Peaks at 575 nm and 600 nm were observed and by analogy to previously reported transient spectra assignment to ZnPc$^-$ radical species was made. Aramendia[20] investigated photochemically induced electron transfer from amines to ZnPc - $\lambda_{max} = 580$ nm, Mack[65] observed electron transfer from hydrazine to ZnPc upon irradiation - λ_{max} at 319 nm, 432 nm, 570 nm, 635 nm and 956 nm and Clack[73],[74] generated the radical anion of ZnPc electrochemically - λ_{max} at 323 nm, 560 nm and 635 nm. The observed rate of quenching, k_Q, was estimated from the gradient at low concentrations of quencher. Rates of $1.8 \pm 0.2 \times 10^6$ dm^3 mol^{-1} s^{-1} and $2.1 \pm 0.2 \times 10^6$ dm^3 mol^{-1} s^{-1} were determined for AA and AAP respectively. As expected in a homogeneous medium, these values are within experimental error of one another.

AA/AAP have several ionic forms[75] which are dependent on the pH of the medium (Figure 6.26). In this study, the pH can be assumed to be ~7, thus the redox couple of interest is that of HA·/HA$^-$. This has a reduction potential, E, of 0.74 V vs NHE[76].
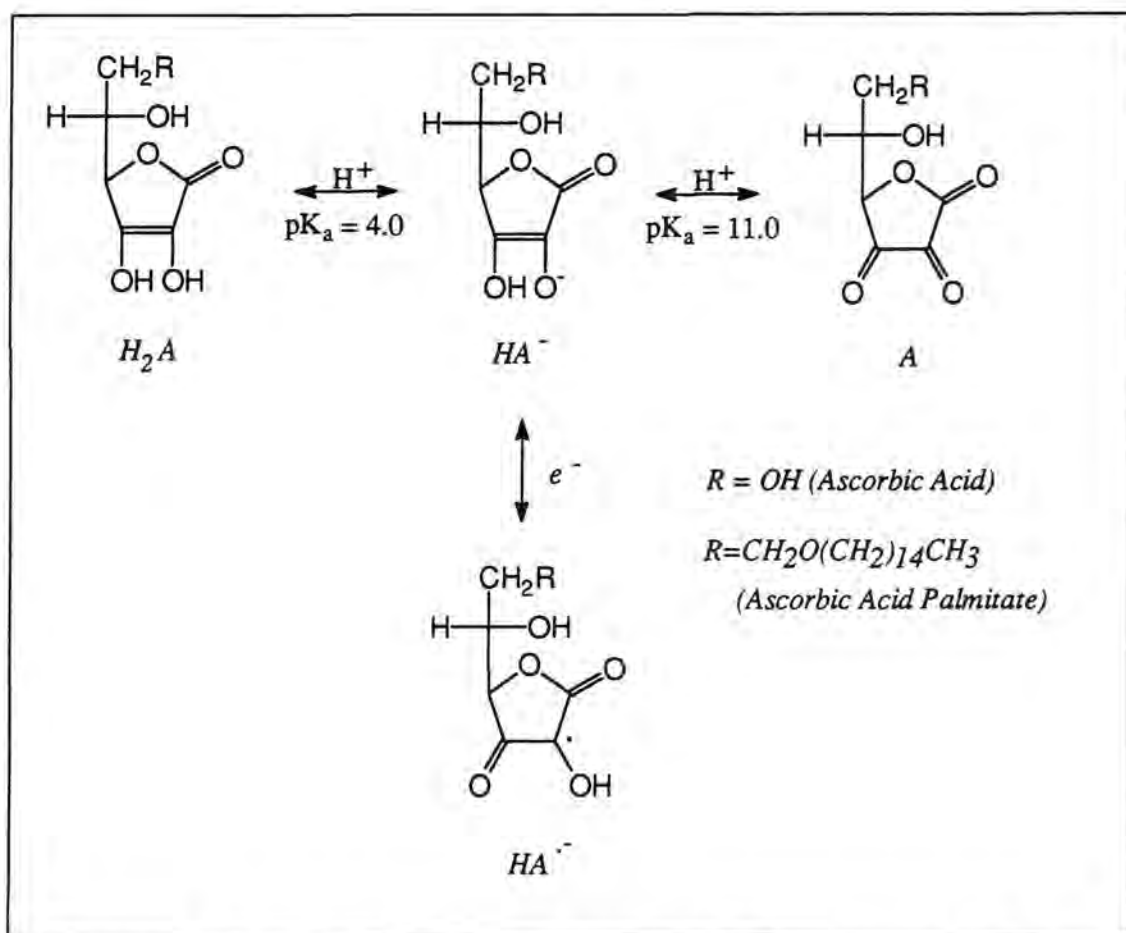
Figure 6.26. Equilibria of ascorbic acid (Palmitate) and redox couples at pH = 7.

Using equations 6.1, 6.2 and 6.3, theoretical values for the free energy change for reaction, ΔG, the activation free energy, $\Delta G^\#$ and the overall rate of electron transfer, k_Q, may be calculated ($k_d = 1.1 \times 10^{10}$ dm^3 mol^{-1} s^{-1} in MeOH). These results are displayed in Table 6.9. Excellent agreement between the predicted and measured triplet state quenching rates was obtained: however, due to errors in reduction potentials employed, the predicted value of k_Q may vary by several orders of magnitude. It may also be inferred that in a suitable solvent system, singlet state quenching should occur.

State	Energy /eV	ΔG /kJ mol^{-1}	$\Delta G^\#$ /kJ mol^{-1}	k_Q (Calc) /mol dm^3 s^{-1}	k_Q(Expt) /mol dm^3 s^{-1}
Singlet	1.83	-47.34	2.03	7×10^9	-
Triplet	1.13	20.3	24.4	1.98×10^6	$2 \pm 0.3 \times 10^6$

Table 6.9. Calculated quenching rates of $^tBu_4ZnPc^*$ by ascorbic acid in MeOH.

The measured value of triplet state quenching (2×10^6 dm^3 mol^{-1} s^{-1}) is significantly lower than would be expected for a diffusion controlled reaction. This implies that this process is activation controlled, i.e. k_a of Figure 6.2 is the rate determining step.

Another way of looking at this is that the efficiency of electron transfer is < 1 and hence k_Q may be expressed[77] as a function of k_d,

$$k_Q = \gamma k_d \qquad (6.15)$$

where k_d is the diffusion rate constant for the solvent under study and γ is the efficiency which may be expressed by Equation 6.16.

$$\gamma = \frac{k_a}{k_a + k_{-d} + \tau_F^{-1} + k_d\,[Q]} \qquad (6.16)$$

This equation is derived in Reference 77 and all rates terms are defined in Figure 6.2. In cases where $k_a < k_d$, the term $k_d[Q]$ may become significant, thus k_Q will vary with [Q] leading to Stern-Volmer plots with negative curvature such as the ones observed in this study. Using Equation 6.16 and a value of 1.1×10^{10} dm^3 mol^{-1} s^{-1} for the rate of diffusion in methanol, an efficiency of 1.8×10^{-4} may be estimated for this reaction. This is very low as a consequence of the endothermic nature (ΔG is positive) of electron transfer from triplet state zinc phthalocyanine to ascorbic acid.

Heterogeneous Solution

In micellar solution, AAP displayed a dramatic increase in the rate at which it reacted with triplet state phthalocyanine (Figure 6.27). k_Q increased by an order of magnitude from $1 \pm 0.1 \times 10^6$ dm^3 mol^{-1} s^{-1} for the quenching rate by ascorbic acid to $1.3 \pm 0.1 \times 10^7$ dm^3 mol^{-1} s^{-1} when AAP was employed as quencher. Since AAP is hydrophobic, it would be expected to locate within the lipid phase of the micelles. AA is water soluble and therefore remained in the aqueous phase. It can be assumed that $^tBu_4ZnPc$ is held inside the micelle, thus reaction with AAP occurred at a faster rate relative to that of AA due to its proximity to micelle bound phthalocyanine. It should also be noted that electron transfer between a hydrophobic sensitiser and hydrophilic quencher has been made possible through the use of a micellar solution, c.f. reaction between α-tocopherol and ascorbic acid[82]. As for TTF quenching, negatively curved plots were obtained. In this case, however, [TX] remained constant and it is likely that inefficient quenching ($k_a < k_d$) was responsible.
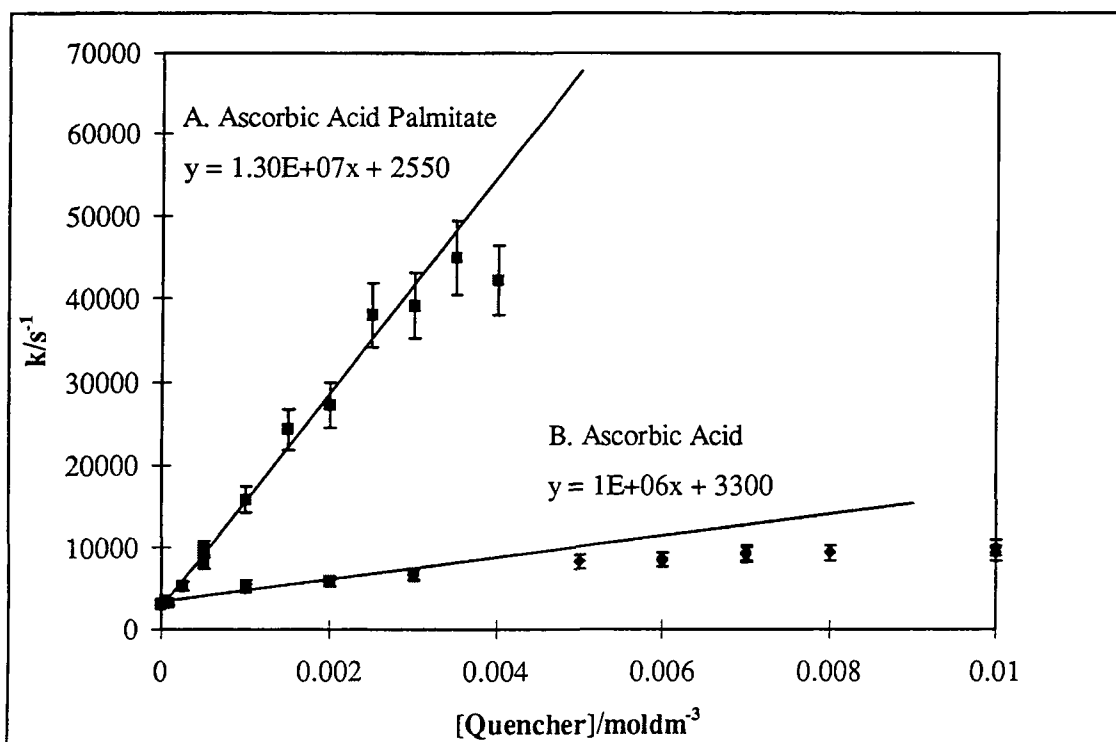
Figure 6.27. Comparison of $^tBu_4ZnPc$ triplet state quenching by a) ascorbic acid palmitate and b) ascorbic acid in 1% TX/H_2O solution.

The triplet state of sulfonated aluminium phthalocyanine by ascorbic acid in phosphate buffer saline has been reported by Ben-Hur[78] to quench triplet state species (k_Q = 5 x 10^{-8} dm^3 mol^{-1} s^{-1}) to produce a transient radical that absorbed at 572 nm and 620 nm. This corroborates the results above. It was also shown that the rate of photohaemolysis of red blood cells increased upon addition of ascorbic acid implying that photodamage to neoplastic tissue may occur via a Type I mechanism mediated by Vitamin C or that the protective effect of Vitamin C towards membrane damage[79] has been reduced.

6.4 Conclusion

It has been demonstrated that axial ligands may bind to zinc phthalocyanines causing changes in ground state absorption characteristics and excited singlet and triplet state properties. Cyanide ions have been shown to cause a significant red shift in the ground state absorption spectrum of $ZnPcS_2$. The equilibrium constant of binding was determined to be 800 dm^3 mol^{-1} in MeOH. Binding of THF to $ZnPc(CMe(CO_2Me)_2)_4$ induced an increase in the quantum yield and lifetime of triplet state species. It is likely that these changes were caused by a combination of decreased internal conversion pathways and increased intersystem crossing rates. It is suggested that *in vivo* ligand binding may account for shifts in reported action spectra of sensitisers relative to their *in vitro* absorption spectra.

Interaction of peripherally substituted zinc phthalocyanines with bovine serum albumin (BSA) has been investigated. No direct spectroscopic evidence for binding of hydrophobic sensitisers, $^tBu_4ZnPc$ or C10 was observed. $ZnPcS_2$ displayed clear changes in ground state absorption spectra recorded in PBS or 1% TX/PBS upon addition of BSA, however, no effect on its fluorescence, triplet state or singlet oxygen quantum yields was recorded. This implies that binding was weak, such that the electronic structure of the phthalocyanine was not perturbed. Fluorescence anisotropy measurements provided indirect evidence for binding. A significant increase in the steady state anisotropy of ZnPc's was recorded upon addition of BSA, suggesting an increase in the effective size of the fluorophore, i.e. binding to protein is implied. In contrast to literature reports, phthalocyanine triplet state quenching by oxygen was not decreased by the presence of BSA, however, some interaction between <u>oxidised</u> protein species and zinc phthalocyanine is suggested. Reasons for this behaviour are unclear and further work in this area is required. Evidence regarding binding of zinc phthalocyanines to BSA remains inconclusive.

It has been demonstrated that ZnPc's undergo electron transfer reactions with several electron donors, in particular with amine containing donor molecules. Reduced fluorescence yields of phthalocyanines with chemically bound tetrathiafulvalene ligands have been shown to be a result of intramolecular electron transfer quenching. In addition, it has been demonstrated that the nature of peripheral substituents may affect the propensity of a phthalocyanine to undergo Type I reactions. With respect to photodynamic therapy this may be important since the mechanism of cell destruction is still unclear. The significance of singlet oxygen as an intermediate has been largely accepted, however, there is still debate over the role of Type 1 reactions in causing cell necrosis. In addition, photodegradation of phthalocyanines which as observed *in vivo*[80] may be due to Type I reactions since it is known that in the main, phthalocyanines are stable to singlet oxygen[81]. The ability of a sensitiser to undergo electron transfer reactions with biological substrates such as proteins or DNA may, therefore, prove to be vital if we are to fully understand the processes involved in PDT. It has been found that Type I reactions with ascorbic acid may play an important role in the photodynamic process, however, electron transfer between zinc phthalocyanines and amino acids residues is unlikely to be significant.

6.5 References

[1]   Bishop S.M., Beeby A., Meunier H., Parker A.W., Foley M.S.C. and Phillips D., The photophysics of disulphonated metallophthalocyanines upon complexation with fluoride., *J. Chem. Soc. Faraday Trans.*, **92**, 2689, 1996.

[2]   Rosenthal I., Shafirovich V.Y., Geacintov N.E., Ben-Hur E. and Horowitz B., The photochemical properties of fluoroaluminum phthalocyanine., *Photochem. Photobiol.*, **60**, 215-220, 1994.

[3]   Foley M.S.C., The photophysics of sulphonated aluminium phthalocyanines for Photodynamic Therapy., *PhD Thesis*, Imperial College, London, 1994.

[4]   Ferraudi G.J. and Prasad D.R., Excited state redox properties of phthalocyanines: Influence of the axial ligand in the rates of relaxation and electron transfer quenching of the lowest excited $^3\pi\pi^*$ excited state., *J. Chem. Soc., Dalton Trans.*, 2137-2140, 1984.

[5]   Doeff M. and Sweigart D.A., Axial ligand substitution reactions of ruthenium II phthalocyanine., *Inorg. Chem.*, **20**, 1683-1687, 1981.

[6]   Nappa M. and Valentine J.S., The influence of axial ligands on metalloporphyrin visible absorption spectra: Complexes of tetraphenylporphyrinatozinc., *J. Am. Chem. Soc.*, **100**, 100-116, 1978.

[7]   Ben-Hur E., Hoe R.C., Ormondt H.V., Dubbelman T.M.A.R. and Steveninck J.V., Photodynamic inactivation of retroviruses by phthalocyanine: the effects of sulphonation, metal ligand and fluoride., *J. Photochem. Photobiol. B:Biol.*, **13**, 145-152, 1992.

[8]   Ben-Hur E., Malik. Z., Dubbelman T.M.A.R., Margaron P., Ali H. and Van Lier J.E., Phthalocyanine induced photohaemolysis: Structure activity relationship and the effect of fluoride., *Photochem. Photobiol.*, **58**, 351-355, 1993.

[9]   Ben-Hur E., Dubbelman T.M.A.R. and Steveninck J.V., The effect of fluoride on binding and photodynamic action of phthalocyanines with proteins., *Photochem. Photobiol.*, **54**, 703-707, 1991.

[10]   Reddi E., Transport modalities of photodynamic agents for tumours., *S.P.I.E.*, **2078**, 246, 1994.

[11]   Jori G., Beltramini M., Reddi E., Salvato B., Pagnan A., Ziron L., Tomio L. and Tsanov T., Evidence for a major role of plasma-lipoproteins as haematoporphyrin carriers *in vivo.*, *Cancer Lett.*, **24**, 291-297, 1984.

[12]   Carter D.C., He X.M., Munson S.H., Twigg P.D., Gernert K.M., Broom B.M. and Miller T.Y., 3-Dimensional structure of human serum albumin., *Science*, **244**, 1195, 1989.

[13]   Marcus R.A., Chemical and electrochemical electron transfer theory., *Ann. Rev. Phys. Chem.*, **15**, 155, 1964.

[14]   Marcus R.A., On the theory of oxidation-reduction reactions involving electron transfer. I*., *J. Chem. Phys.*, **24**, 965, 1956.

[15]   Gilbert A. and Baggot J., *Essentials of Molecular Photochemistry*, p184, Blackwell Scientific Publications, Oxford, 1991.

[16]   Rehm D. and Weller A., Kinetics of fluorescence quenching by electron and H-atom transfer., *Israel J. Chem.*, **8**, 259, 1970.

[17]   Darwent J.R., McCubbin I. and Porter G., Photoreduction of methyl viologen sensitised by sulphonated phthalocyanines in micellar solution., *J. Chem. Soc. Faraday Trans. 2*, **78**, 903-910, 1982.

[18]   Ohno T., Kato S. and Lichtin N.N., Electron transfer in the quenching of triplet states of zinc phthalocyanine and methylene blue by the use of Fe(III), Co(III) and organic oxidants., *Bull. Chem. Soc. Jpn.*, **55**, 2753, 1982.

[19]   Prasad D.R. and Ferraudi G., Electron transfer quenching vs exciplex-mediated quenching of the low-lying excited states in phthalocyanines., *Inorg. Chem.*, **22**, 1672-1674, 1983.

[20]   Aramendia P.F., Energy and charge transfer photosensitised by phthalocyanines in micelles., *EPA Newsletter*, **52**, 6-20, 1994.

[21]   Daraio M.E., Volker A., Aramendia P.F. and San Roman E., Reaction of zinc phthalocyanine excited states with amines in cationic micelles., *Langmuir*, **12**, 2932, 1996.

[22]   DeGraziano J.M., MacPherson A.N., Lidell P.A., Noss L., Sumida J.P., Seely G.R., Lewis J.E., Moore A.L., Moore T. A. and Gust D., Solvent dependence of photoinduced electron transfer in porphyrin dyads., *New J. Chem.*, **20**, 839, 1996.

[23]   Nyokong T., Gasyna Z and Stillman M., Phthalocyanine π cation radical species: Photochemical and electrochemical preparation of [ZnPc-1]$^{+\cdot}$ in solution., *Inorg. Chem.*, **26**, 548-553, 1987.

[24]   Ferraudi G., Oishi S. and Muraldiharan K., The photochemical properties of Rh(III) phthalocyanine cation radicals., *J. Phys. Chem.*, **88**, 5261-5264, 1984.

[25]   Ohno T., Kato S., Yamada A. and Tanno T., Electron transfer reactions of the photoexcited triplet state of chloroaluminium phthalocyanine with aromatic amines, benzoquinones and coordination compounds of iron(II) and iron(III)., *J. Phys. Chem.*, **87**, 775-781, 1983.

[26]   Ben-Hur E. and Rosenthal I., Photosensitisation of Chinese hamster cells by water soluble phthalocyanines., *Photochem. Photobiol.*, **43**, 615-619, 1986.

[27]   Ben-Hur E., Carmichael A., Riesz P. and Rosenthal I., Photochemical generation of superoxide radical and the cytotoxicity of phthalocyanines., *Int. J. Radiat. Biol.*, **48**, 837, 1985.

[28]   Cook M.J., Chambrier I., Cracknell S.J., Mayes D.A. and Russell D.A. Octa alkyl Zinc Phthalocyanines: Potential photosensitisers for use in the photodynamic therapy of cancer., *Photochem. Photobiol.*, **62**, 542-545, 1995.

[29]   Wang C., Bryce M.R., Batsanov A.S., Stanley C.F., Beeby A. and Howard J.A.K., Synthesis, spectroscopy and electrochemistry of phthalocyanine derivatives functionalised with four and eight peripheral tetrathiafulvalene units., *J. Chem. Soc., Perkin Trans.*, **2**, 1671, 1997.

[30]   Rossotti F. and Rossotti H., *The Determination of Stability Constants*, p277, McGraw Hill Book Company, New York, 1961.

[31]   Greenwood N.N. and Earnshaw A., *Chemistry of the Elements*, p1065, Pergamon Press, UK, 1984.

[32]   Phillips D., The photochemistry of sensitisers for photodynamic therapy., *Pure Appl. Chem.*, **67**, 117, 1995.

[33]   Gomer C.J., Doiron D.R., Rucker N., Razum N.J. and Fountain S.W., Action spectrum (620 - 640 nm) for hematoporphyrin derivative induced cell killing., *Photochem. Photobiol.*, **39**, 365, 1984.

[34]   Star W.M., *In vivo* action spectra, absorption and fluorescence excitation spectra of photosensitisers for photodynamic therapy., *J. Photochem. Photobiol. B:Biol.*, **28**, 101, 1995.

[35]   Cubeddu R., Canti G., Musolino M., Pifferi A., Taroni P. and Valentini G., *In vivo* absorption spectrum of disulphonated aluminium phthalocyanine in a murine tumour model., *J. Photochem. Photobiol. B:Biol.*, **34**, 229, 1996.

[36]   Davila J. and Harriman A., Photoreactions of macrocyclic dyes bound to human serum albumin., *Photochem. Photobiol.*, **51**, 9, 1990.

[37]   Foley M.S.C., Beeby A., Parker A.W., Bishop S.M. and Phillips D., Excited triplet state photophysics of the sulphonated aluminium phthalocyanines bound to human serum albumin., *J. Photochem. Photobiol. B:Biol.*, **38**, 10, 1997.

[38]   Doiron D.R. and Gomer C.J., *Porphyrin Localisation and Treatment of Tumours*, p373, Alan R Liss, New York, 1984.

[39]   Ambroz M., MacRobert A.J., Morgan J., Rumbles G., Foley M.S.C. and Phillips D., Time resolved fluorescence spectroscopy and intracellular imaging of disulphonated aluminium phthalocyanine., *Photochem. Photobiol. B:Biol.*, **22**, 105, 1994.

[40] Lang K., Wagnerova D.M., Engst P. and Kubat P., Quenching of the triplet state of metallocyanines by dioxygen in the presence of bovine serum albumin., *Zeit. Physik. Chem.*, **187**, 214, 1994.

[41] Reddi E., Lambert C.R., Jori G. and Rodgers M.A.J., Photokinetic and photophysical measurements of the sensitised photooxidation of the tryptophyl residue in N-Acetyl tryptophanamide and in HSA., *Photochem. Photobiol.*, **45**, 345-351, 1987.

[42] Creed D., The photophysics and photochemistry of the near UV absorbing amino acids - 1. Tryptophan and its simple derivatives., *Photochem. Photobiol.*, **39**, 537, 1984.

[43] Walrant P. and Santus R., N-Formylkynurenine, a tryptophan photooxidation product as a photodynamic sensitiser., *Photochem. Photobiol.*, **19**, 411, 1974.

[44] Reddi E., Rodgers M.A.J., Spikes J.D. and Jori G., The effect of medium polarity on the hematoporphyrin-sensitised photooxidation of L-tryptophan., *Photochem. Photobiol.*, **40**, 415, 1984.

[45] Rossi E., Van de Vorst A. and Jori G., Competition between the singlet oxygen and electron transfer mechanisms in the porphyrin-sensitised photooxidation of L-tryptophan in aqueous micellar media., *Photochem. Photobiol.*, **34**, 447, 1981.

[46] Langlois R., Brasseur N., Wagner J.R. and Van Lier J.E., Biological activities of phthalocyanines - IV. Type II sensitised photooxidation of L-tryptophan and cholesterol by sulfonated metallo phthalocyanines., *Photochem. Photobiol.*, **44**, 117, 1986.

[47] Mashiko S., Suzuki N., Koga S., Nakano M., Goto T., Ashino T., Mizumoto L. and Inaba H., Measurement of rate constants for quenching singlet oxygen with a cypridina luciferin analog (2-methyl-6-paramethoxyphenyl 3, 7 dihydroimidazole [1, 2-A] pyrazin-3-one) and sodium azide., *J. Biolum. Chemilum.*, **6**, 69, 1991.

[48] Vincent S.H. and Muller-Eberhard U., Effects of porphyrins on proteins of cytosol and plasma. In vitro photo-oxidation and cross-linking of proteins by naturally occurring and synthetic porphyrins., *J. Laboratory and Clinical Med.*, **110**, 475, 1987.

[49] Dubbelman T.M.A.R., De Goeij A.F.P.M. and Steveninck J.V., Photodynamic effects of protoporphyrin on human erythrocytes. Nature of the cross-linking of membrane proteins., *Biochim. Biophys. Acta.*, **511**, 141, 1978.

[50] Turro N.J., *Modern Molecular Photochemistry*, p246, University Science Books, California, 1991.

[51] Zeng H. and Durocher G., Analysis of fluorescence quenching in some antioxidants from non-linear Stern Volmer plots., *J. Lumin.*, **63**, 75, 1995.

[52]   Sung J., Shin K.J. and Lee S., Theory of diffusion influenced fluorescence quenching. Effects of static quenching on the Stern Volmer curve., *Chem. Phys.*, **167**, 17, 1992.

[53]   Keizer J., Nonlinear fluorescence quenching and the origin of positive curvature in Stern Volmer plots., *J. Am. Chem. Soc.*, **105**, 1494, 1983.

[54]   Stevens B., Application of a finite initial separation limit to the concentration gradient model of fluorescence quenching in liquids., *Chem. Phys. Lett.*, **134**, 519, 1987.

[55]   Stevens B., Biver III C.J. and McKeithan D.N., Parameterization of diffusion limited electron transfer quenching in the finite sink approximation., *Chem. Phys. Lett.*, **187**, 590, 1991.

[56]   Dr. A. Beeby, Unpublished Data.

[57]   Lakowitz J.R., *Topics in Fluorescence Spectroscopy*, **2**, p53, Plenum Press, New York, 1991.

[58]   Kalyansundarum K., *Photochemistry in microheterogeneous systems*, p56, Academic Press, London, 1987.

[59]   Kalyansundarum K., *Photochemistry in microheterogeneous systems*, p26, Academic Press, London, 1987.

[60]   Blatt E. and Sawyer W.H., Depth dependent fluorescent quenching in micelles and membranes., *Biochem. Biophys. Acta*, **822**, 43, 1985.

[61]   Atkins P.W., *Physical Chemistry*, p848, Edition 4, Oxford University Press, Oxford, UK., 1990.

[62]   Leznoff C.C. and Lever A.B.P., *Phthalocyanines. Properties and Applications.*, **1**, p305, VCH Publishers, New York, 1989.

[63]   Devonport W., Blower M.A., Bryce M.R. and Goldenberg L.M., A redox active tetrathiafulvalene 920 pseudorotaxane: spectrochemical and cyclic voltammetric studies of the highly reversible complexation/decomplexation process., *J. Org. Chem.*, **62**, 885, 1997.

[64]   Fox M.A. and Chanon M., *Photoinduced Electron Transfer, C: Photoinduced Electron Transfer Reactions. Organic Substrates*, p6, Elsevier, New York, 1988.

[65]   Mack J. and Stillman M., Photochemical formation of the anion-radical of zinc phthalocyanine and analysis of the absorption and magnetic circular-dichroism spectral data - assignment of the optical-spectrum of [ZnPc(-3)]⁻., *J. Am. Chem. Soc.*, **116**, 1292, 1994.

[66]   Zhu Q.Q., Schnabel W. and Jacques P., Photoreduction of thioxanthen-9-one and benzophenone by amines. Electrical conductivity and light emission studies., *J. Chem. Soc. Faraday Trans*, **87**, 1531, 1991.

[67]   Coyle J.D., Hill R.R., Roberts D.R., *Light,Chemical Change and Life: A Source Book in Photochemistry*, p364, Open University Press, Milton Keynes, 1982.

[68]   Zhang X.F. and Xu H.J., Mechanism of photosensitised oxidation of tyrosine by gallium or zinc phthalocyanine in homogeneous and heterogeneous media., *J. Photochem. Photobiol. B:Biol.*, **24**, 109-116, 1994.

[69]   Turro N.J., *Modern Molecular Photochemistry*, p138, University Science Books, California, 1991.

[70]   Marciniak B., Bobrowski K. and Hug G.L., Quenching of triplet states of aromatic ketones by sulphur containing aminoacid in solution. Evidence for electron transfer., *J. Phys. Chem.*, **97**, 11937, 1993.

[71]   Ferraudi G., Arguello G.A., Ali H. and Van Lier J.E., Type-I and Type-II sensitised photooxidation of amino-acid by phthalocyanines - a flash photochemical study., *Photochem. Photobiol.*, **47**, 657-660, 1988.

[72]   Berger T.M., Polidori M.C., Dabbagh A., Evans P.J., Halliwell B., Morrow J.D., Roberts II L.J. and Frei B., Antioxidant activity of vitamin C in iron overloaded human plasma., *J. Biol. Chem.*, **272**, 15656, 1997.

[73]   Clack D.W. and Yandle J.R., Electronic spectra of the negative ions of some metal phthalocyanines., *Inorg. Chem.*, **11**, 1738, 1972.

[74]   Minor P.C., Gouterman M. and Lever A.B.P., Electronic spectra of phthalocyanine anions and cations., *Inorg. Chem.*, **24**, 1894-1900, 1985.

[75]   Creutz C., The complexities of ascorbate as a reducing agent., *Inorg. Chem.*, **20**, 4449, 1981.

[76]   Tur'yan Y.I. and Kohen R., Formal redox potentials of the dehydro-L-ascorbic acid/L-ascorbic acid system., *J. Electroanal. Chem.*, **380**, 273, 1995.

[77]   Eftink M.R. and Ghiron C.A., Fluorescence quenching studies with proteins., *Anal. Biochem.*, **114**, 199, 1981.

[78]   Rosenthal I. and Ben-Hur E., Ascorbate assisted phthalocyanine sensitised photohaemolysis of human erythrocytes., *Int. J. Radiat. Biol.*, **62**, 481, 1992.

[79]   Bisby R.H. and Parker A.W., Reactions of the α tocopherol radical in micellar solutions studied by nanosecond laser flash photolysis., *Febs Lett.*, **290**, 205, 1991.

[80]   Ruck A., Beck G., Bactor R., Akgun N., Gschwend M.H. and Steiner R., Dynamic fluorescence changes during photodynamic therapy *in vivo* and in vitro of hydrophilic Al(III) phthalocyanine tetrasulphonate and lipophilic Zn(II) phthalocyanine administered in liposomes., *J. Photochem. Photobiol. B:Biol.*, **36**, 127, 1996.

[81]   Rotomskis R., Streckyte G. and Bagdonas S., Phototransformations of sensitisers. 1) Significance of the nature of the sensitiser in the photobleaching process

and photoproduct formation in aqueous solution., *J. Photochem. Photobiol. B:Biol.*, **39**, 167, 1997.

[82]   Bisby R.H. and Parker A.W., Reactions of the alpha-tocopheroxyl radical in micellar solutions studied by nanosecond laser flash photolysis., *Febs Lett.*, **290**, 205, 1991.

SUMMARY

♣ Two novel, β-tetra substituted zinc phthalocyanines have been synthesised. The photophysical properties of ZnPc were not significantly affected by the nature of the peripheral substituents.

♣ The fluorescence anisotropy of metal free and zinc phthalocyanines is dependent upon the exact experimental conditions, i.e. emission wavelength, excitation wavelength, solvent and temperature.

♣ The photophysical properties of zinc phthalocyanines were greatly affected by the nature of their environment.

   - The aggregation state of $ZnPc(CHMeCO_2H)_4$ displayed a remarkable sensitivity to the ionic strength of non-aqueous solution.

   - C10 aggregated at 77 K in EPA. The aggregate emitted fluorescence at 760 nm and generated triplet state species upon irradiation by 355 nm or 638 nm light. This is believed to be the first fluorescent phthalocyanine dimer bound solely by Van der Waals forces to be reported.

   - Low pH induced protonation of the azomethane bridges of the phthalocyanine ring. Protonated species, PcH_n^{n+}, displayed large changes in their photophysical properties with respect to the parent phthalocyanine including a dramatic reduction in their ability to generate singlet oxygen. Protonation of $ZnPcS_2$ occurred at physiologically important pH's and may have important implications for Photodynamic Therapy.

♣ Binding of bovine serum albumin to substituted zinc phthalocyanines has been investigated, however, results were inconclusive.

♣ Zinc phthalocyanines have been shown to act as electron acceptors in the presence of certain amine or sulphur based donors. Electron transfer reactions were shown to be important between ascorbic acid and phthalocyanine, however, reaction between aminoacids - tryptophan, tyrosine, methionine and cysteine - and the phthalocyanines was not observed.

APPENDIX A
A NOVEL SWITCH FOR SINGLET OXYGEN MEASUREMENTS

A.1 Introduction

Measurement and detection of singlet oxygen, $^1O_2$, has been important for many years. Singlet oxygen is a highly reactive species that is believed to be responsible for the destruction of biological media such as cells and tissues. In certain applications, for example, the photodynamic therapy of cancer (PDT), this is the required effect and production and reaction of $^1O_2$ must be optimised for maximum benefit. However, in other situations, e.g. skin sensitisation by pharmaceuticals, singlet oxygen is an undesirable side effect to be avoided. The ability to measure the properties of $^1O_2$, i.e. its quantum yield and lifetime, with precision and accuracy is therefore of great interest. There are two methods by which $^1O_2$ can be detected. Chemical trapping or quenching which involves an added acceptor species such as diphenylisobenzylfuran (DPBF) or β-Carotene respectively[1]. This is sometimes unsatisfactory since the added species may interfere with the chemistry in other ways. A second, more convenient and reliable method, was developed[2] around 1980. Direct detection of singlet oxygen phosphorescence at 1270 nm was made possible through the use of a highly sensitive germanium photodiode coupled to a transient digitiser. However, when certain sensitisers are investigated, in particular those with red shifted absorption and emission bands such as the phthalocyanines, measurement of $^1O_2$ emission still causes problems due to the presence of a large spike at the start of the observed transient emission decay[3-7]. It is thought that this phenemenon results from scattered laser light, sensitiser fluorescence and possibly some fluorescence from bandpass filters used to select 1270 nm light[8]. As a result, the traces recorded by the transient digitiser show the electronic effects and the $^1O_2$ signal can become distorted, preventing reliable measurements of τ_Δ and Φ_Δ by this technique. Previous attempts to minimise this effect include careful choice of solvent[5] and the use of interference filters to reduce unwanted emission wavelengths[6]. Neither solution is completely satisfactory.

In this study, it has been demonstrated that the observed effects are due to overloading of electronic circuits in the amplifier of a digital storage oscilloscope, DSO. The development of an electronic switch, based on a DG 403DJ analogue switch, which may be used to eliminate fluorescence contributions is also reported. Using a variable time gate to prevent the large spike due to fluorescence entering the DSO amplifier allows saturation of the oscilloscope amplifier to be avoided, thus $^1O_2$ detection is improved.

A.2 Materials and Methods

A.2.1 Materials

Several substances were used to test the performance of the switch. Rose Bengal (93 %) was purchased from Aldrich. Styryl 9 was purchased from Lambda Physik and AlPcS$_2$ was a gift from Imperial College, London. Solutions were prepared in Analar methanol.

A.2.2 Experimental

All experimental studies were performed at the Rutherford Appleton Laboratory Central Laser Facility.

Excitation of the sample was carried out using the 355 nm output of an excimer (Lumonix HE 460 (XeCl))) pumped dye laser (Lambda Physik FL3002) with a typical pulse duration of 10 ns and energy within the range 0.1-0.5 mJ per pulse. Light was delivered to the sample using a 5 mm diameter liquid light guide. The sample was held in a 10 mm pathlength quartz cuvette, and the absorbance was adjusted to 0.3 at the excitaton wavelength. The emission was collected at 90° to the excitation beam and 1270 nm radiation selected using an interference filter with a 20 nm bandpass (Infra-Red Engineering). Selected radiation was incident upon the cooled germanium photodiode/amplifier (NorthCoast EO-817P). In order to obtain the fastest response time from the detector it was operated in the high speed mode, "H" (t_{rise} ~ 200 ns, FWHM = 400 ns). Output of the detector was either transferred directly to a digital storage oscilloscope (Tektronics 2432A) or via the electronic switch box described below. Traces were the average of sixteen shots and were transferred to a computer for analysis by non-linear least squares methods.

Synchronisation of the firing of the laser and the oscilloscope was achieved using a Stanford digital signal generator (DG 535). The same generator was also used to provide a TTL pulse to operate the switching device (Figure A.1).

240
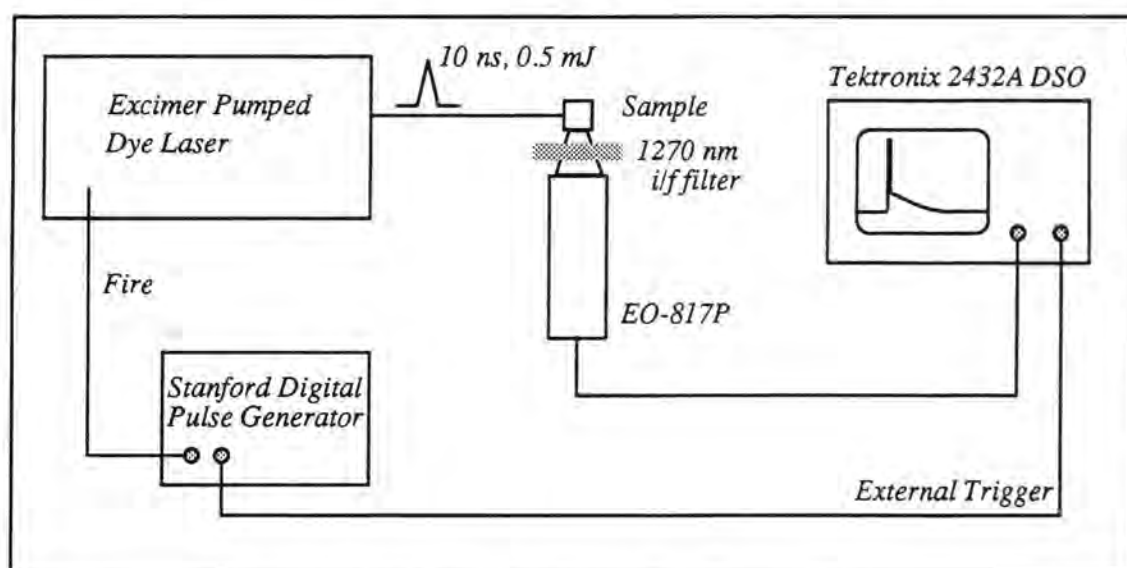
Figure A.1. Experimental arrangement.

A.2.3 The Switch

The device used to gate out the signal from the detector for the duration of the spike was based on an analogue switch and was controlled by a TTL signal from a Stanford signal generator. A block diagram of the circuit is shown in Figure A.2.
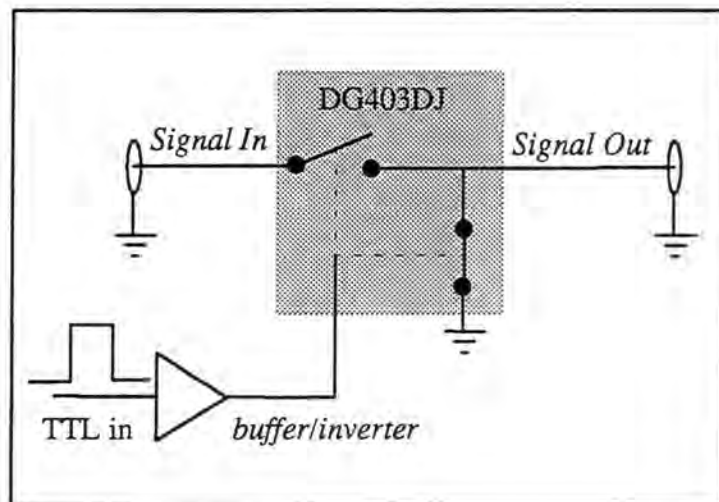
Figure A.2. Circuit diagram of switch.

When the TTL signal was at 0 V, the switch was in the 'closed' position allowing signals from the detector to pass to the input of the DSO. When the pulse was on, (+5 V) the switch opened, effectively isolating the detector. Additionally, the input of the DSO was shorted to ground by the use of a second switching element within the analogue switch chip.

241

A.3 Results and Discussion

A.3.1 Electrical properties

The first stage of the study was to investigate the electrical properties of the switch. It is important that switching the amplifier on in this way should not introduce any spurious signals that may influence the decay trace of $^1O_2$. As Figure A.3 shows, the switch does not perturb the baseline of the oscilloscope trace on a timescale over which the singlet oxygen decay may typically be observed. Furthermore, it was confirmed that radio frequency emission from the excimer laser HV discharge did not induce any signal in the measured background baseline.
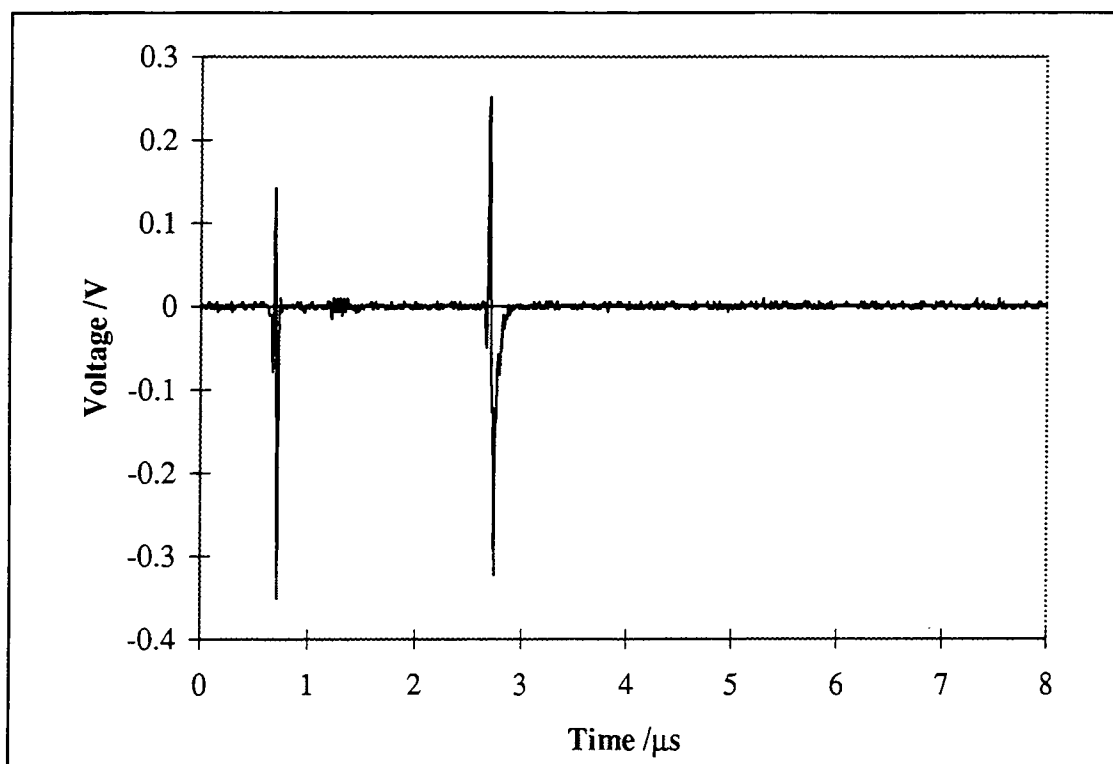
Figure A.3. Physical properties of the switch.

Large 'switching transients' can be observed. Subsequent examination of these on a faster timescale (200 ns/div) reveals that any distortions caused by switching signals are insignificant 1 μs after the amplifier is turned on. Hence they should cause little interference with the measurements of $^1O_2$. Figure A.4 shows the distortion and recovery of the baseline as the amplifier is switched off and again as it is turned on. The gate width is 400 ns. It can be clearly seen that ringing due to the switching has completely died away before distortions due to the 'on' signal begin.
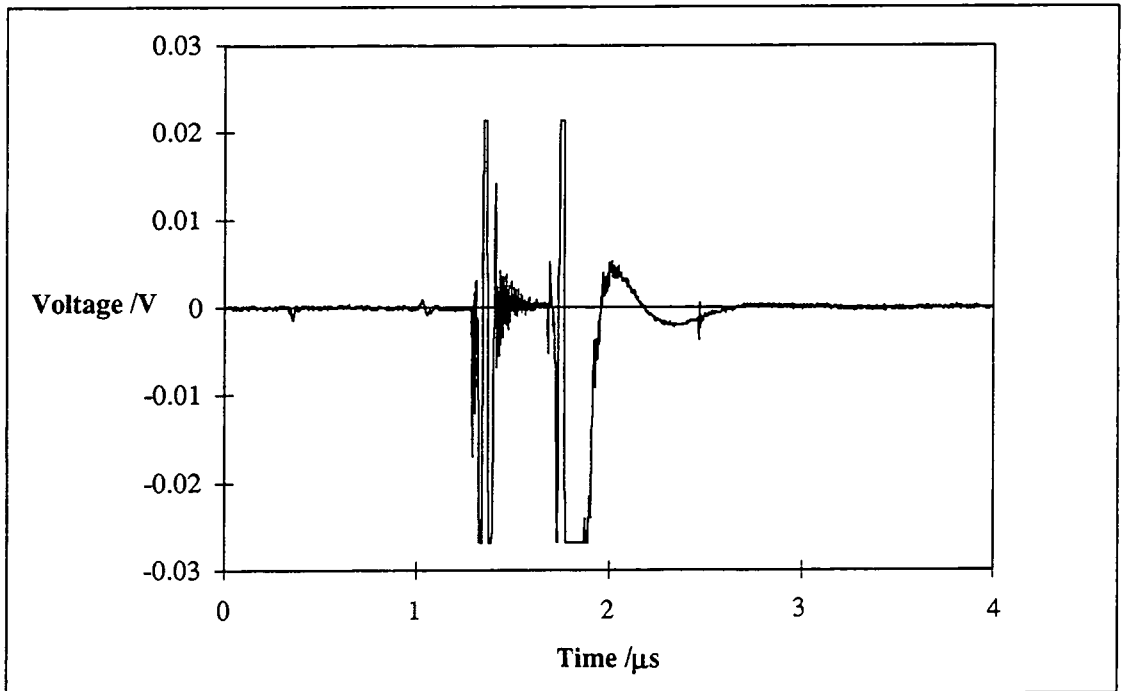
Figure A.4.

Decay trace of switching transient as the switch closes following a 400 ns gate.

A.3.2 Performance

Having shown that operation of the switch should not interfere with $^1O_2$ emission 1 µs after the gate is closed, its performance was investigated. A strong fluorescence signal at 1270 nm was generated by the excitation of a near infrared laser dye, Styryl-9 in methanol. The fluorescence lifetime of this dye is short (<10 ns) compared to the response of the Ge photodiode/amplifier (200 ns) and the dye does not sensitise singlet oxygen. Using a vertical scale of 0.5 V/div, the 4 V luminescence signal lies well within the range of the oscilloscope amplifier, saturation does not cause a problem and the trace is displayed in Figure A.5a.

However, when a more sensitive scale was used, such as that required to detect $^1O_2$ emission (1 mV/division), large amounts of ringing were observed and a negative offset was obtained (Figure A.5b) which recovered slowly over several milliseconds. This saturation occurred due to the 4 V peak of the pulse exceeding the 'overdrive' capacity of the front end amplifier of the DSO. Recovery of this amplifier occurred on a millisecond timescale.
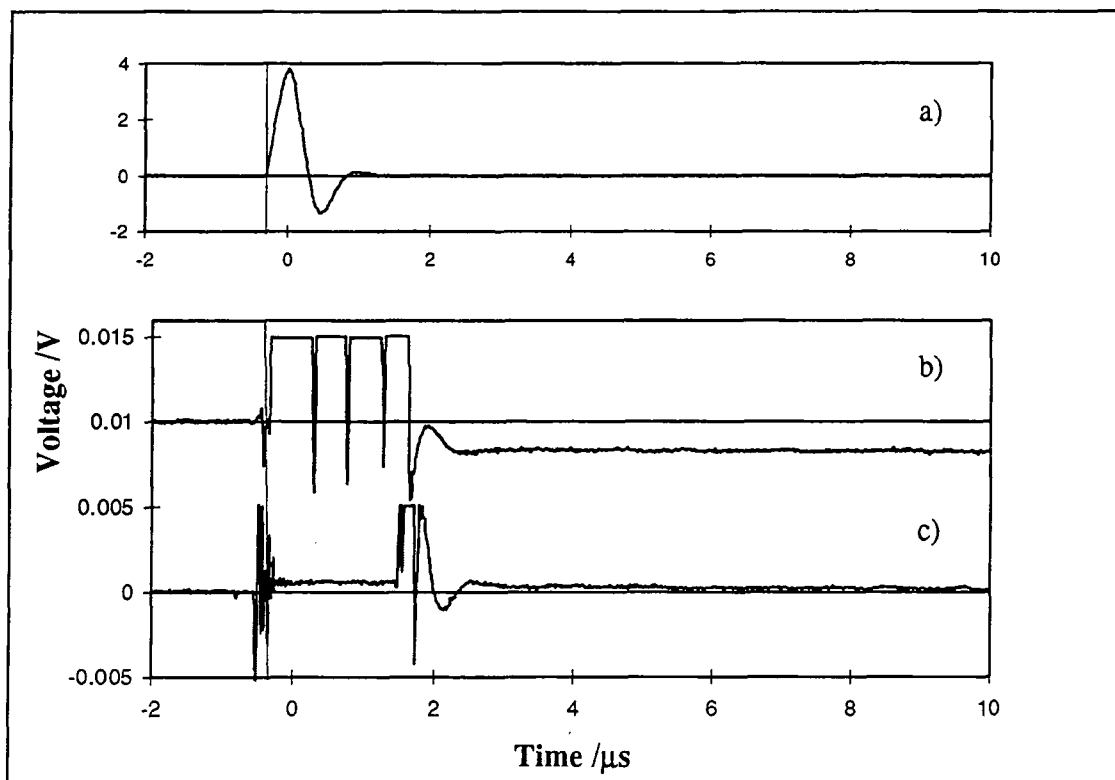
Figure A.5. a) Fluorescence recorded using 0.5 V/div. scale. b) Same reading on 1 mV/div. scale showing saturation of amplifier. c) Trace obtained using switch (1 mV/div.). Traces have been offset for clarity.

When the switch was introduced into the circuit, the amplifier was inactive throughout the majority of the fluorescence emission and saturation was avoided (Figure A.5c). The baseline should quickly recover to zero after distortions caused by the switching transient. In practise, however, a small decay with a lifetime of $\sim$ 7 μs was observed. The trace was repeated using a degassed solution and also one with sodium azide added to quench any $^1O_2$ present. Neither of these procedures had any effect on the decay indicating that it was not due to singlet oxygen produced by energy transfer from Styryl 9. Substitution of the sample cuvette for one made by a different manufacturer significantly reduced the yield of this transient. It is suggested that this trace was a result of emission from impurites inherent in quartz.

In order to demonstrate the benefits that can be achieved by eliminating amplifier saturation, a study was made of $^1O_2$ lifetimes obtained in methanol using various sensitiser solutions.
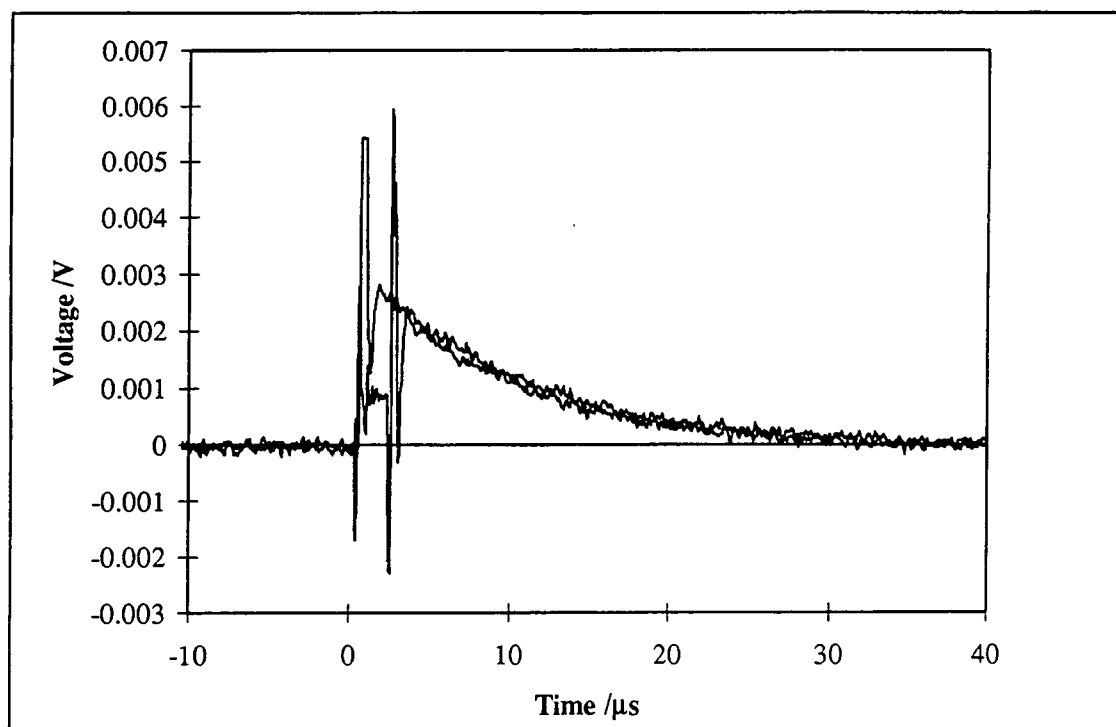
Figure A.6.

Overlap of $^1O_2$ decays sensitised by Rose Bengal with and without the switch.

Rose Bengal exhibits very little fluorescence leakage through the interference filter and has only a small spike at the start of the singlet oxygen decay, making it an ideal candidate to establish the effects of the switch on a singlet oxygen decay. Figure A.6 shows that use of the switch does not perturb measurement of either the yield of $^1O_2$ or the profile of the decay. Analysis of singlet oxygen decays obtained with variable gate times yielded a lifetime value of 9.8 ± 0.3 μs (Literature value = 10.4 μs)[9]. Quenching of the singlet oxygen by Rose Bengal has not been take into account for this data, (k_q = 4 ± 0.5 x 10^7 mol^{-1} dm^3 s^{-1}, unpublished data).

Phthalocyanines are known to have a large fluorescence spike at the start of their $^1O_2$ decay which interferes with any subsequent analysis. Use of the switch showed a significant improvement in both the profile and calculated lifetime of the singlet oxygen decay. With Styryl 9, a negative offset was obtained as a result of amplifier saturation when the detector was attached directly to the DSO. Analysis of the decay (singlet oxygen convolved with the amplifier recovery) revealed an average lifetime of 7.9 ± 0.4 μs - clearly different from the quoted literature value of 10.4 μs. Introduction of the switch removed the negative offset and significantly improved the lifetime value to 11.2 ± 0.4 μs. (Figure A.7).
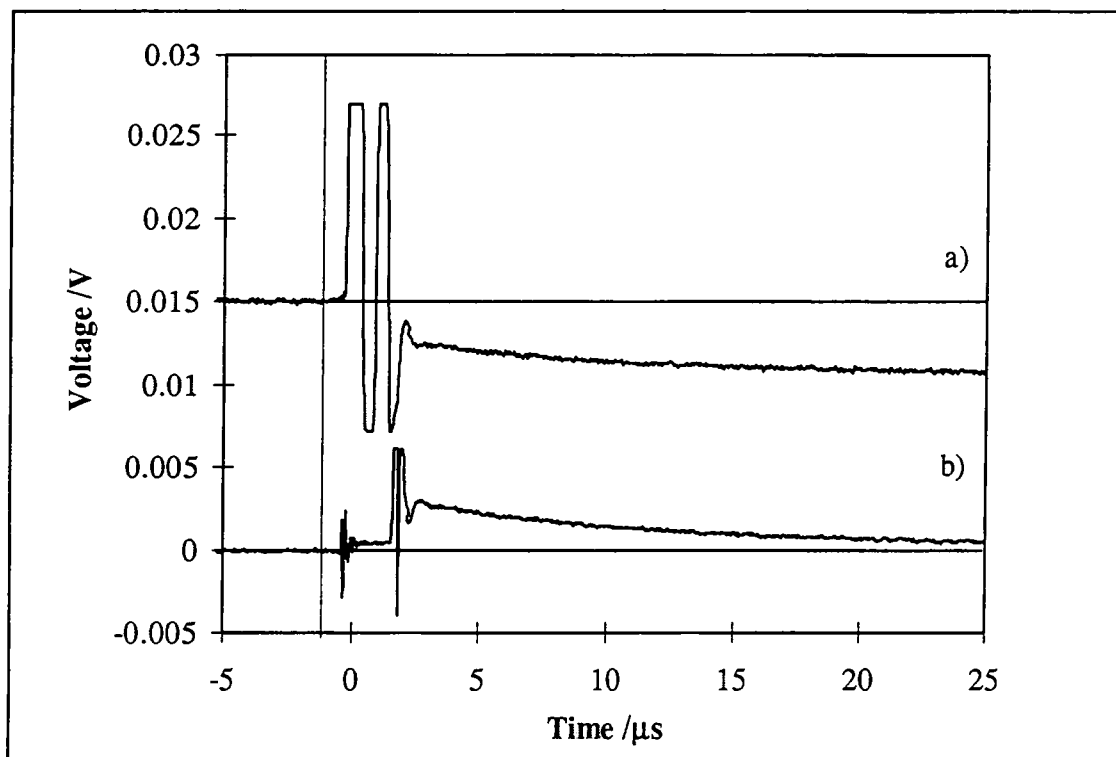
Figure A.7. $^1O_2$ *decay sensitised by phthalocyanine without (a) and with (b) the switch (offset for clarity).*

The most dramatic results were obtained when a mixture of Rose Bengal and Styryl 9 was used. Saturation of the amplifier occurred to such a degree that it was impossible to detect singlet oxygen (Figure A.8A(a)). Use of the switch allowed detection and analysis of singlet oxygen decays with the correct lifetime of 10.1 ± 0.2 µs (Figure A.8B).
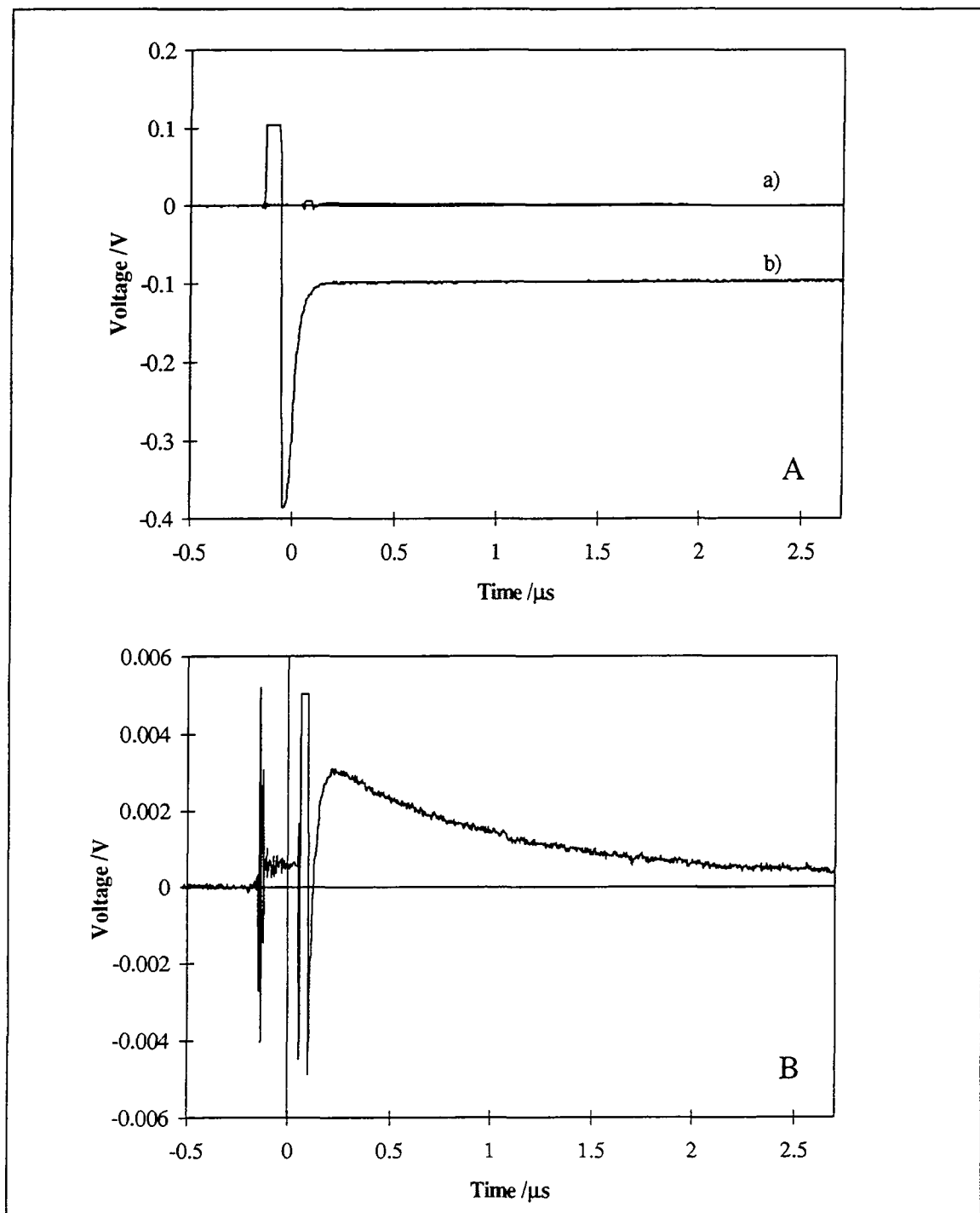
*Figure A.8. A) Signal produced by a mixture of Styryl 9 and Rose Bengal with (a)
and without (b) Switch.
B) Singlet oxygen decay viewed on correct scale (1 mV/div.).*

A.4 Conclusions

It has been shown that problems in detecting $^1O_2$ produced by certain sensitisers are caused by saturation of the input amplifier of the digital storage oscilloscope following intense fluorescence emission. A rapid switch has been developed to overcome the problem. Input to the oscilloscope input amplifier is controlled via a TTL pulse avoiding saturation as a result of large voltage spikes. Convolution with amplifier recovery due to saturation and decay of $^1O_2$ has been removed to allow calculation of lifetimes to within 10 % of established literature values.

A.5 References

[1]   Bensasson R.V., Land E.J. and Truscott T.G., *Excited States and Free Radicals in Biology and Medicine*, Oxford University Press, New York, pp118-142, 1993.

[2]   Byteva I.M. and Gurinovitch G.P., Sensitised luminescence of oxygen in solutions. *J. Lumin.* **21**, 17-20, 1979.

[3]   Bishop S., Preparation and properties of phthalocyanine photosensitisers for PDT. *PhD Thesis*, Imperial College, London, 1993.

[4]   Beeby A., Bishop S., Parker A.W., Simpson M.S.C. and Phillips D., Time resolved studies of singlet oxygen. *EPSRC Central Laser Facility Annual Report*, RAL-92-020, 227, 1992.

[5]   Ford W.E., Rihter B.D., Kenney M.E. and Rodgers M.A.J., Photoproperties of alkoxy-substituted phthalocyanines with deep red optical absorbance. *Photochem. Photobiol.* **50**, 277-282, 1989.

[6]   Michaeli A. and Feitelson J., Reactivity of singlet oxygen toward aminoacids and peptides., *Photochem. Photobiol.*, **59**, 284-289, 1994.

[7]   Nather D.U., Gilchrist J.R., Gensch T. and Roder B., Temporal and spectral separation of singlet oxygen luminescence from near infrared emitting photosensitisers., *Photochem. Photobiol.*, **57**, 1056, 1993.

[8]   Oldham T.C., Beeby A., Parker A.W., Stanley C.F., Telfer A., Barber A. and Phillips D., Improved Instrumentation For The Time-Resolved Detection Of Singlet Oxygen Luminesence., *CRC Rutherford Appleton Laboratory Annual Report*, RAL-TR-96-076, 126, 1995-1996.

[9]   Rodgers M.A.J., Solvent induced deactivation of singlet oxygen - additivity relationships in non-aromatic solvents. *J. Am. Chem. Soc.*, **105**, 6201, 1982.

K_1 - K_5 may be described as follows:

$$K_1 = \frac{[\,AlPcClF^-\,]}{[\,AlPcCl\,][\,F^-\,]}(\,a\,),\; K_2 = \frac{[\,AlPcF_2^-\,]}{[\,AlPcClF^-\,][\,F^-\,]}(\,b\,),\; K_3 = \frac{[\,(AlPcCl\,)_2\,F^-\,]}{[\,AlPcClF^-\,][\,AlPcCl\,]}(\,c\,)$$

$$K_4 = \frac{[\,(ClPcAl - F - AlPcF\,)^-\,]}{[\,AlPcClF^-\,][\,AlPcClF^-\,]}(\,d\,),\; K_5 = \frac{[\,(AlPcF\,)_2\,F^-\,]}{[\,AlPcF_2^-\,][\,AlPcClF^-\,]}(\,e\,)$$

$$(B.1)$$

If it is assumed that the absorption spectra of all monomeric species, i.e., AlPcCl, $AlPcF_2^-$ and $AlPcClF^-$, are equivalent (irrespective of the small shift observed), K_{obs} may be defined as

$$K_{obs} = \frac{[\,D\,]_{Total}}{[\,M\,]^2_{Total}} \qquad (B.2)$$

where $[M]_{Total} = [AlPcCl] + [AlPcClF^-] + [AlPcF_2^-]$ and $[D]_{Total} = [(AlPcCl)_2F^-] + [(ClPcAl\text{-}F\text{-}AlPcF)^-] + [(AlPcF)_2F^-]$

Hence,

$$K_{obs} = \frac{[\,(AlPcCl\,)_2\,F^-\,] + [\,(ClPcAl - F - AlPcF\,)^-\,] + [\,(AlPcF\,)_2^-\,]}{(\,[\,AlPcCl\,] + [\,AlPcClF^-\,] + [\,AlPcF_2^-\,]\,)(\,[\,AlPcCl\,] + [\,AlPcClF^-\,] + [\,AlPcF_2^-\,]\,)}$$

$$(B.3)$$

This may be split into component fractions, $K_{obs} = K_{obs}(A) + K_{obs}(B) + K_{obs}(C)$.

$$K_{obs}(A) = \frac{[\,(AlPcCl\,)_2\,F^-\,]}{(\,[\,AlPcCl\,] + [\,AlPcClF^-\,] + [\,AlPcF_2^-\,]\,)(\,[\,AlPcCl\,] + [\,AlPcClF^-\,] + [\,AlPcF_2^-\,]\,)}$$

$$(B.4)$$

$$K_{obs}(B) = \frac{[(ClPcAl-F-AlPcF)^-]}{([AlPcCl]+[AlPcClF^-]+[AlPcF_2^-])([AlPcCl]+[AlPcClF^-]+[AlPcF_2^-])}$$

(B.5)

$$K_{obs}(C) = \frac{[(AlPcF)_2^-]}{([AlPcCl]+[AlPcClF^-]+[AlPcF_2^-])([AlPcCl]+[AlPcClF^-]+[AlPcF_2^-])}$$

(B.6)

From Equations B.1a and B.1b, $K_{obs}(A)$ may be expressed as,

$$K_{obs}(A) = \frac{[(AlPcCl)_2 F^-]}{[AlPcCl](1+K_1[F^-]+K_1K_2[F^-]^2)[AlPcClF^-](\frac{1}{K_1[F^-]}+1+K_2[F^-])}$$

(B.7)

Rearranging,

$$K_{obs}(A) = \frac{[(AlPcCl)_2 F^-]K_1[F^-]}{[AlPcCl][AlPcClF^-](1+K_1[F^-]+K_1K_2[F^-]^2)^2}$$

(B.8)

Finally, substituting for Equation B.1c,

$$K_{obs}(A) = \frac{K_1K_3[F^-]}{(1+K_1[F^-]+K_1K_2[F^-]^2)^2}$$

(B.9)

Similarly, using Equation B.1a and b, $K_{obs}(B)$ may be expressed as

$$K_{obs}(B) = \frac{[(ClPcAl-F-AlPcF)^-]}{[AlPcClF^-]^2(\frac{1}{K_1[F^-]}+1+K_2[F^-])^2}$$

(B.10)

Rearranging and substituting for Equation B.1d gives

$$K_{obs}(B) = \frac{K_4 K_1{}^2 [F^-]^2}{(1 + K_1 [F^-] + K_1 K_2 [F^-]^2)^2} \qquad (B.11)$$

Finally $K_{obs}(C)$ may be defined as Equation B.12 by substituting for Equations B.1a and B.1b.

$$K_{obs}(C) = \frac{[(AlPcF)_2 F^-]}{[AlPcClF^-](\dfrac{1}{K_1 [F^-]} + 1 + K_2 [F^-])[AlPcF_2{}^-](\dfrac{1}{K_1 K_2 [F^-]^2} + \dfrac{1}{K_2 [F^-]} + 1)} \qquad (B.12)$$

Using Equation B.1e and rearranging gives

$$K_{obs}(C) = \frac{K_5 K_2 K_1{}^2 [F^-]^3}{(1 + K_1 [F^-] + K_1 K_2 [F^-]^2)^2} \qquad (B.11)$$

Recombining $K_{obs}(A)$, $K_{obs}(B)$ and $K_{obs}(C)$ yields Equation B.12, the desired expression.

$$K_{obs} = \frac{K_3 K_1 [F^-] + K_4 K_1{}^2 [F^-]^2 + K_5 K_2 K_1{}^2 [F^-]^3}{(1 + K_1 [F^-] + K_1 K_2 [F^-]^2)^2} \qquad (B.12)$$

Considering each protonation to be a separate step, the equilibrium may be expressed by Equation C.1.

$$Pc + H^+ \xleftarrow{\;K\;} PcH^+$$

(C.1)

where Pc = PcH_{n-1}^{n-1+} and PcH+ = PcH_n^{n+}.

Assuming conservation of mass, the total concentration of phthalocyanine species is given by Equation C.2 and the equilibrium constant, K by Equation C.3.

$$C_T = [Pc] + [PcH^+]$$

(C.2)

$$K = \frac{[PcH^+]}{[Pc][H^+]}$$

(C.3)

At any given wavelength, the absorbance, A(λ), will be due to both PcH_{n-1}^{n-1} and PcH_n^{n+} species, i.e.,

$$A = \varepsilon_{Pc}[Pc] + \varepsilon_{PcH^+}[PcH^+]$$

(C.4)

Substituting for Equation C.3 gives

$$A = \varepsilon_{Pc}(\frac{C_T}{1+K[H^+]}) + \varepsilon_{PcH^+}C_T - \frac{\varepsilon_{PcH^+}C_T}{1+K[H^+]}$$

(C.5)

Rearranging,

$$A = (\varepsilon_{Pc} - \varepsilon_{PcH^+})\frac{C_T}{1+K[H^+]} + \varepsilon_{PcH^+}C_T$$

(C.6)

Thus K may be calculated by non-linear fitting of Equation C.6 to a plot of A vs [H+].

PUBLICATIONS

1. Beeby A., Parker A.W. and Stanley C.F., Elimination of fluorescence contributions to singlet oxygen measurements using a novel electronic switch, *J. Photochem. Photobiol. B:Biol.*, **37**, 267, 1997.

2. Wang C., Bryce M.R., Batsanov A.S., Stanley C.F., Beeby A. and Howard J.A.K., Synthesis, spectroscopy and electrochemistry of phthalocyanine derivatives functionalised with four and eight peripheral tetrathiafulvalene units., Accepted by *J. Chem. Soc., Perkin Trans. 2*, 1997.

3. Oldham T.C., Beeby A., Parker A.W., Stanley C.F., Telfer A., Barber A. and Phillips D., Improved Instrumentation For The Time-Resolved Detection Of Singlet Oxygen Luminesence., *CRC Rutherford Appleton Laboratory Annual Report*, RAL-TR-96-076, 126, 1995-1996.

4. Stanley C.F. and Beeby A., Photophysical Properties of Zinc Phthalocyanines in Relation to their Use as Sensitisers for Photodynamic Therapy., *Aspects of Spectroscopy VII, Institute of Physics Spectroscopy Group.*, Durham, UK., August 21 - 22, 1997. - Oral Presentation.

5. Stanley C.F. and Beeby A., The Photophysical Properties of Phthalocyanine Dimers., *25th Annual Meeting, American Society for Photobiology.*, St. Louis, Missouri, July 5 - 10, 1997. - Poster Presentation.

6. Stanley C.F. and Beeby A., Photophysical Properties of Zinc Phthalocyanines at Low pH., *12th International Congress on Photobiology, ICP' 96.*, Vienna, Austria, September 1 - 6, 1996. - Poster Presentation.

CONFERENCES

1. Aspects of Spectroscopy VII, Institute of Physics Spectroscopy Group., Durham, UK., August 21 - 22, 1997. - Oral Presentation - <u>C. F. Stanley</u> and A. Beeby, Photophysical Properties of Zinc Phthalocyanines in Relation to their Use as Sensitisers for Photodynamic Therapy.

2. 25th Annual Meeting, American Society for Photobiology., St. Louis, Missouri, July 5 - 10, 1997. - Poster Presentation - <u>C. F. Stanley</u> and A. Beeby, The Photophysical Properties of Phthalocyanine Dimers.

3. 12th International Congress on Photobiology, ICP' 96., Vienna, Austria, September 1 - 6, 1996. - Poster Presentation - <u>C. F. Stanley</u> and A. Beeby, Photophysical Properties of Zinc Phthalocyanines at Low pH.

4. 6th Congress of the European Society for Photobiology., Cambridge, UK, September 3 - 8, 1995.

5. EPSRC Summer School in Laser Spectroscopy, University of East Anglia, UK, September 4 - 10, 1994.

6. North-Eastern Universities Graduate Symposia-
    University of Newcastle, 1997.
    University of Sunderland, 1996.
    University of Durham, 1995.

1996 - 1997

1. Professor G. Olah, *Crossing Conventional Lines in my Chemistry of the Elements*, Loker Hydrocarbon Research, USA.
2. Professor D. Knight, *The Purpose of Experiments - A Look at Davy and Faraday*, Durham University, Durham.
3. Professor D. Phillips, *A Little Light Relief*, Imperial College, London.
4. Professor Sir J. Black, *What I Learned as a Medicinal Chemist*, James Black Foundation.
5. Professor R. H. Grubbs, *Olefin Metathesis using Ruthenium Based Complexes*, Caltech, California.
6. Professor H. Ringsdorf, *Function Based on Organisation*, Johannes Gutenberg-Universitat, Mainz, Germany.
7. Dr. K. Reid, *Probing Dynamical Processes with Photoelectrons*, Nottingham University, Nottingham.
8. Professor J. Earnshaw, *Surface Light Scattering: Ripples and Relaxation*, Belfast University, Belfast.
9. Professor K. Muller-Dethlefs, *Chemical Application of Very High Resolution ZEKE Photoelectron Spectroscopy*, York University, York.
10. Dr. J. Clarke, *What We Can Learn From Polymer Movie Clips*, UMIST, Manchester.
11. Dr. T. Ryan, *Making Hairpins from Rings and Chains*, UMIST, Manchester.

1995 - 1996

1. Dr. D. M. Davies, *Chemical Reactions in Organised Systems: Peracid reactivity in Surfactant Micelles and Cyclodextrin Hosts*, University of Northumbria, Newcastle.
2. Professor B. Robinson, *Chemistry of Smart Fluids*, University of East Anglia, Norwich.
3. Professor I. Soutar, *A Water of Glass. Luminescence Studies of Water Soluble Polymers*, Lancaster University, Lancaster.
4. Professor J. Saykally, *Terahertz Laser Spectroscopy of Water Clusters; Towards a Genuine Molecular Model of the Liquid*, Berkeley, California.
5. Dr. J. Penfold, *Soft Soaps and Surfaces*, ISIS Facility, Rutherford Appleton Laboratory, Oxford.

6. Dr. Garry Rumbles, *Laser Cooling in the Condensed Phase: the Tale of a Novel Observation*, Imperial College, London.

7. Professor J. W. Emsley, *Liquid Crystals: More then Meets the Eye*, Southampton University, Southampton.

8. Professor E. W. Randall, *New Perspectives in NMR Imaging*, Queen Mary and Westfield College, London.

9. Professor V. Balzani, *Supramolecular Photochemistry*, University of Bologna, Italy.

1994 - 1995

1. Professor N. L. Owen, *Determining Molecular Structure - the INADEQUATE NMR Way*, Brigham Young University, Utah.

2. Professor N. Bartlett, *Some Aspects of Ag(II) and Ag(III) Chemistry*, University of California.

3. Dr. G. Rumbles, *Real or Imaginary 3rd Order Non-linear Optical Materials?* Imperial College, London.

4. Dr. T. Cosgrove, *Polymers Do it at Interfaces*, Bristol University, Bristol.

5. Dr. D. O'Hare, *Synthesis and Solid State Properties of Poly-, Oligo- and Multidecker Metallocenes*, Oxford University, Oxford.

6. Dr. M. Schroder, *Redox Active Macrocyclic Complexes: Rings, Stacks and Liquid Crystals*, University of Edinburgh, Edinburgh.

7. Professor R. Bonnett, *Chemical Aspects of PDT*, Queen Mary and Westfield College, London.

8. Dr. A. Beeby and Dr. A. Hughes, *Photochemistry: A Demonstration Lecture*, University of Durham, Durham.

9. Dr. P. G. Edwards, *The Manipulation of Electronic and Structural Diversity in Metal Complexes - New Ligands for New Properties*, University of Wales, Cardiff.